

# Effect of wave period on dune erosion



C. den Heijer



M.Sc. Thesis

January, 2005



WL | delft hydraulics





# Effect of wave period on dune erosion

C. den Heijer

M.Sc. Thesis

January, 2005

Graduation Committee:

Prof.dr.ir. M.J.F. Stive

TU Delft

Dr.ir. J. van de Graaff

TU Delft

Dr.ir. A.J.H.M. Reniers

TU Delft

Ir. J.H. de Vroeg

WL | Delft Hydraulics

Dr.ir. H.J. Steetzel

Alkyon

Ir. J.S.M. van Thiel de Vries

TU Delft



## Preface

This study has been carried out as my Master of Science Thesis work, the finishing touch of Civil Engineering at Delft University of Technology. This research lasted from January until August 2004 and is carried out at WL | Delft Hydraulics.

In November 2003 I started at WL | Delft Hydraulics as a trainee. Until January I was involved in physical model research on the effect of the wave period on the amount of dune erosion carried out in the Schelde flume. I had a very pleasant stay and became more and more interested in the subject. So, I am very grateful I got the opportunity to graduate on this subject at WL | Delft Hydraulics. During this research it appeared to be very handy to know the background of the measurement data and to know the people involved.

I would like to thank all the members of my graduation committee for their contribution to this research. Furthermore, I would like to thank Dirk-Jan Walstra, who was always willing to answer questions and gave tips about UNIBEST-TC. Last but not least I would like to thank my temporary colleagues at WL | Delft Hydraulics, especially from MCI, who were always helpful and interested and made my stay very pleasant.

Delft, January 2005

Kees den Heijer



# Contents

## List of Figures

## List of Tables

## List of Symbols

## Summary

|          |   |          |
|----------|---|----------|
| <b>1</b> | <b>Introduction .....</b>                 | <b>1</b> |
| 1.1      | Background .....                          | 1        |
| 1.2      | Problem definition .....                  | 1        |
| 1.3      | Objective.....                            | 2        |
| 1.4      | Boundary conditions and assumptions ..... | 2        |
| 1.5      | Research approach .....                   | 2        |
| 1.6      | Readers' guide .....                      | 3        |
| <b>2</b> | <b>Literature review .....</b>            | <b>5</b> |
| 2.1      | Dune erosion .....                        | 5        |
| 2.1.1    | Normal conditions.....                    | 5        |
| 2.1.2    | Severe storm surge.....                   | 5        |
| 2.1.3    | Definition of dune erosion .....          | 5        |
| 2.1.4    | Structural coastal erosion.....           | 6        |
| 2.1.5    | After storm.....                          | 6        |
| 2.1.6    | What is the problem? .....                | 6        |
| 2.2      | Wave period .....                         | 7        |
| 2.3      | Characteristic storm surge duration ..... | 7        |
| 2.4      | Description of DUROSTA .....              | 8        |

|         |  |    |
|---------|--|----|
| 2.4.1   | Wave propagation model .....                   | 9  |
| 2.4.1.1 | ENDEC.....                                     | 9  |
| 2.4.1.2 | Roller model.....                              | 10 |
| 2.4.2   | Cross-shore flow model.....                    | 11 |
| 2.4.3   | Sediment concentration model .....             | 13 |
| 2.4.4   | Nett cross-shore transport model .....         | 14 |
| 2.4.5   | Bed level change model.....                    | 15 |
| 2.4.6   | Extrapolation method for the dry profile ..... | 15 |
| 2.4.6.1 | Location transition point.....                 | 15 |
| 2.4.6.2 | Extrapolation method .....                     | 15 |
| 2.4.7   | Default settings .....                         | 16 |
| 2.5     | Description of UNIBEST-TC .....                | 16 |
| 2.5.1   | Wave propagation model .....                   | 17 |
| 2.5.1.1 | Roller model.....                              | 17 |
| 2.5.2   | Mean current profile model .....               | 18 |
| 2.5.3   | Wave orbital velocity model .....              | 19 |
| 2.5.4   | Sediment transport model .....                 | 20 |
| 2.5.4.1 | Bed load transport.....                        | 20 |
| 2.5.4.2 | Suspended load transport.....                  | 21 |
| 2.5.4.3 | Time averaged concentration profile.....       | 22 |
| 2.5.5   | Bed level change model.....                    | 23 |
| 2.5.6   | Extrapolation method for dry profile .....     | 23 |
| 2.5.6.1 | Location transition point.....                 | 23 |
| 2.5.6.2 | Extrapolation method .....                     | 24 |
| 2.5.7   | Settings .....                                 | 24 |
| 2.6     | Comparison DUROSTA and UNIBEST-TC .....        | 25 |

|          |   |           |
|----------|---|-----------|
| 2.6.1    | Similarities .....  | 25        |
| 2.6.2    | Differences .....   | 25        |
| <b>3</b> | <b>Analysis of physical model research .....</b>                  | <b>27</b> |
| 3.1      | Background .....  | 27        |
| 3.1.1    | Scale choice .....  | 27        |
| 3.1.2    | Test program .....  | 28        |
| 3.2      | Measurements .....  | 28        |
| 3.2.1    | Profiles and erosion volumes .....                                | 28        |
| 3.2.2    | Waves .....   | 29        |
| 3.2.2.1  | Locations .....   | 29        |
| 3.2.2.2  | Re-analysis of measurements .....                                 | 30        |
| 3.2.2.3  | Wave period .....   | 30        |
| 3.2.3    | Flow velocity .....   | 31        |
| 3.2.4    | Sediment concentration .....                                      | 32        |
| 3.2.5    | Grain size .....  | 32        |
| 3.2.6    | Water temperature .....   | 32        |
| 3.2.7    | Fall velocity .....   | 32        |
| 3.3      | Results for separate series .....                                 | 32        |
| 3.3.1    | A-series .....  | 32        |
| 3.3.2    | Comparison with earlier research .....                            | 33        |
| 3.3.3    | B-series .....  | 33        |
| 3.4      | Results after combining two test series .....                     | 34        |
| 3.4.1    | Formation of continuous series .....                              | 34        |
| 3.4.2    | Relative increase of erosion with respect to reference case ..... | 35        |
| <b>4</b> | <b>DUROSTA computations .....</b>                                 | <b>37</b> |
| 4.1      | Computation set up .....  | 37        |

|         |  |    |
|---------|--|----|
| 4.1.1   | Grid .....   | 37 |
| 4.1.2   | Initial profile .....  | 37 |
| 4.2     | Simulations .....  | 38 |
| 4.2.1   | Tuning near wave board .....   | 38 |
| 4.2.1.1 | Wave propagation .....   | 38 |
| 4.2.1.2 | Erosion development .....  | 39 |
| 4.2.1.3 | Cross-shore profiles .....   | 39 |
| 4.2.2   | Tuning at NAP - 5 m .....  | 40 |
| 4.2.2.1 | Wave propagation .....   | 40 |
| 4.2.2.2 | Erosion development .....  | 40 |
| 4.2.3   | Tuning over whole profile by gamma .....                                   | 41 |
| 4.2.3.1 | Wave propagation .....   | 41 |
| 4.2.3.2 | Erosion development .....  | 41 |
| 4.2.4   | Tuning over the whole profile with compensation for changed<br>gamma ..... | 42 |
| 4.2.4.1 | Erosion development .....  | 42 |
| 4.3     | Sediment concentration and flow velocity .....                             | 42 |
| 4.3.1   | Sediment concentration verticals .....                                     | 43 |
| 4.3.2   | Flow velocity .....  | 43 |
| 4.3.3   | Remarks .....  | 44 |
| 4.4     | Sensitivity analysis .....   | 44 |
| 4.4.1   | Reduced or extended profile .....  | 44 |
| 4.4.2   | Initial profile schematisation .....                                       | 45 |
| 4.4.3   | Grid .....   | 45 |
| 4.4.4   | Grain properties .....   | 46 |
| 4.4.5   | Wave height .....  | 46 |
| 4.4.5.1 | Varying wave height in time .....  | 46 |

|          |   |           |
|----------|---|-----------|
| 4.5      | Prototype computations .....                                      | 46        |
| 4.5.1    | Set up.....   | 47        |
| 4.5.2    | Erosion volume.....   | 47        |
| 4.6      | Conclusions .....   | 47        |
| <b>5</b> | <b>UNIBEST-TC computations.....</b>                               | <b>49</b> |
| 5.1      | Computation set-up.....   | 49        |
| 5.1.1    | Settings .....  | 49        |
| 5.2      | Simulations .....   | 50        |
| 5.2.1    | Tuning near wave board .....                                      | 50        |
| 5.2.2    | Tuning over whole profile by gamma .....                          | 50        |
| 5.3      | Sediment concentration and flow velocity.....                     | 50        |
| 5.3.1    | Sediment concentration .....                                      | 51        |
| 5.3.2    | Flow velocity.....  | 51        |
| 5.4      | Concluding remarks .....  | 51        |
| <b>6</b> | <b>Discussion .....</b>   | <b>53</b> |
| 6.1      | Wave conditions tests.....  | 53        |
| 6.2      | Wave tuning .....   | 53        |
| 6.3      | Comparison DUROSTA and UNIBEST-TC computations .....              | 54        |
| 6.4      | Sediment concentration and velocity verticals.....                | 54        |
| <b>7</b> | <b>Conclusions and recommendations .....</b>                      | <b>55</b> |
| 7.1      | Conclusions .....   | 55        |
| 7.2      | Recommendations.....  | 56        |
| 7.2.1    | General .....   | 56        |
| 7.2.2    | Practical recommendations for further physical model research.... | 56        |

## References

## Tables

**Figures**

**Appendices**

**A Re-analysis of wave measurement data ..... A-1**

**B Input file DUROSTA..... B-1**

**C Input file UNIBEST-TC ..... C-1**

## List of Figures

- Figure 1.1 Schematised coastal profile, prototype reference profile; Averaged profile along the Dutch coast
- Figure 2.1 Principle of dune erosion
- Figure 2.2 Overview cross-shore profiles in Schelde flume; Qualitative effect of longer wave period after 6 hours (A-series) or 3 hours (B-series) of severe wave attack
- Figure 2.3 Assumed naturally varying deep water wave conditions and water level during a storm; Peak wave period research boundaries
- Figure 2.4 Overview of DUROSTA sub-models
- Figure 2.5 Overview of UNIBEST-TC sub-models
- Figure 3.1 Desired initial cross-shore profile for A-series
- Figure 3.2 Desired initial cross-shore profile for B-series
- Figure 3.3 Wave height for separate time intervals compared with averaged signal over whole test; T01
- Figure 3.4 Development of measured peak wave period in space, A-series
- Figure 3.5 Development of measured wave period ( $T_{m-l,0}$ ) in space, A-series
- Figure 3.6 Development of measured peak wave period in space, B-series
- Figure 3.7 Development of measured wave period ( $T_{m-l,0}$ ) in space, B-series
- Figure 3.8 Development of measured erosion; A-series
- Figure 3.9 Relative measured erosion w.r.t. test T03; A-series
- Figure 3.10 Comparison H4265 with M1819-I; Development of measured erosion volumes in time
- Figure 3.11 Development of measured erosion; B-series
- Figure 3.12 Relative measured erosion w.r.t. test T11; B-series
- Figure 3.13 Development of measured erosion in time
- Figure 3.14 Development of measured erosion volumes in time; B-series translated into depth scale 30
- Figure 3.15 Relative erosion with respect to basic case  $T_p = 12$  s for different moments of model time; B-series translated into depth scale 30
- Figure 4.1 Comparison computed initial and final cross-shore profile and corresponding wave propagation; T01
- Figure 4.2 DUROSTA; Wave propagation; Default settings; Tuned at  $x = 9.39$ ; A-series
- Figure 4.3 DUROSTA; Erosion development in time; Default settings; Tuned at  $x = 9.39$ ; A-series
- Figure 4.4 Comparison computed and measured profiles at the end of each test; A-series
- Figure 4.5 DUROSTA; Wave propagation; Default settings; Tuned at  $x = 3.00$ ; B-series
- Figure 4.6 DUROSTA; Erosion development in time; Default settings; Tuned at  $x = 3.00$ ; B-series

- Figure 4.7 Comparison computed and measured profiles at the end of each test; B-series
- Figure 4.8 DUROSTA; Wave propagation; Default settings; Tuned at  $x = 31.99$ ; A-series
- Figure 4.9 DUROSTA; Erosion development in time; Default settings; Tuned at  $x = 31.99$ ; A-series
- Figure 4.10 DUROSTA; Wave propagation; Default settings; Tuned at  $x = 34.82$ ; B-series
- Figure 4.11 DUROSTA; Erosion development in time; Default settings; Tuned at  $x = 34.82$ ; B-series
- Figure 4.12 DUROSTA; Wave propagation; Tuning by breaker index  $\gamma$ ; A-series
- Figure 4.13 DUROSTA; Erosion development in time; Tuning by breaker index  $\gamma$ ; A-series
- Figure 4.14 DUROSTA; Wave propagation; Tuning by breaker index  $\gamma$ ; B-series
- Figure 4.15 DUROSTA; Erosion development in time; Tuning by breaker index  $\gamma$ ; B-series
- Figure 4.16 DUROSTA; Erosion development in time; Tuning by breaker index  $\gamma$ ;  $\gamma$ -dependent parameter compensation; A-series
- Figure 4.17 DUROSTA; Erosion development in time; Tuning by breaker index  $\gamma$ ;  $\gamma$ -dependent parameter compensation; B-series
- Figure 4.18 Comparison sediment concentration computation and measurements Schelde flume,  $x = 39.13$ , T02
- Figure 4.19 Comparison sediment concentration computation and measurements Schelde flume,  $x = 40.52$ , T02
- Figure 4.20 Comparison sediment concentration computation and measurements Schelde flume,  $x = 41.91$ , T02
- Figure 4.21 Comparison sediment concentration computation and measurements Schelde flume,  $x = 39.13$ , T03
- Figure 4.22 Comparison sediment concentration computation and measurements Schelde flume,  $x = 40.52$ , T03
- Figure 4.23 Comparison sediment concentration computation and measurements Schelde flume,  $x = 41.91$ , T03
- Figure 4.24 Comparison sediment concentration computation and measurements Schelde flume,  $x = 43.30$ , T03
- Figure 4.25 Comparison computed velocities and measurements Schelde flume,  $x = 39.13$ , T02
- Figure 4.26 Comparison computed velocities and measurements Schelde flume,  $x = 40.52$ , T02
- Figure 4.27 Comparison computed velocities and measurements Schelde flume,  $x = 41.91$ , T02
- Figure 4.28 Comparison computed velocities and measurements Schelde flume,  $x = 39.13$ , T03
- Figure 4.29 Comparison computed velocities and measurements Schelde flume,  $x = 40.52$ , T03

- Figure 4.30 Comparison computed velocities and measurements Schelde flume,  $x = 41.91$ , T03
- Figure 4.31 Comparison computed velocities and measurements Schelde flume,  $x = 43.30$ , T03
- Figure 4.32 Overview of cross-shore profiles
- Figure 4.33 Sensitivity of erosion volume for slightly different cross-shore profile; For each set of wave conditions computations with 4 different initial profiles
- Figure 4.34 Relative erosion volume w.r.t. prototype  $T_p = 12$  s after 3.5 h model time (19 h prot.) of wave attack
- Figure 5.1 UNIBEST-TC; Erosion development in time; Tuned near wave board
- Figure 5.2 UNIBEST-TC; Erosion development in time; Tuned by breaker index  $\gamma$



## List of Tables

|           |   |
|-----------|---|
| Table 2.1 | Overview of default settings of DUROSTA obtained from Steetzel (1993) and from the help function in the program               |
| Table 2.2 | Overview of input parameters of UNIBEST-TC  |
| Table 3.1 | Overview of test program with desired wave conditions and water level (Coeveld and De Vroeg, 2004)                            |
| Table 3.2 | Overview of the wave heights $H_{m0}$ which have been derived from the spectra between the boundaries $f_{min}$ and $f_{max}$ |
| Table 3.3 | Some characteristic values out of the grain size measurements   |
| Table 3.4 | Measured water temperatures   |
| Table 4.1 | Sensitivity of erosion volume for wave height according to DUROSTA  |



## List of Symbols

| Symbol    | Units     | Meaning  |
|-----------|-----------|--|
| $a$       | m         | thickness of bed load layer  |
| $a_m$     | m         | amplitude in orbital velocity formulation  |
| $a_n$     | m         | amplitude in orbital velocity formulation  |
| $A$       | $m^2$     | area of a roller   |
| $A$       | $m^3/m^1$ | (cumulative) dune erosion quantity above the maximum storm surge level   |
| $B_j$     | m/s       | amplitude in orbital velocity formulation  |
| $c$       | $kg/m^3$  | time and space averaged sediment concentration   |
| $c$       | m/s       | wave celerity  |
| $c_a$     | $kg/m^3$  | reference sediment concentration (at level $z = a$ )   |
| $c_g$     | m/s       | wave group velocity  |
| $c_0$     | $kg/m^3$  | maximum concentration  |
| $C$       | $kg/m^3$  | sediment concentration   |
| $C_r$     | -         | correlation coefficient between wave envelope and long wave surface variation in orbital velocity formulation            |
| $C_0$     | $kg/m^3$  | reference sediment concentration (at level $z = 0$ )   |
| $d$       | m         | water depth (to mean surface level)  |
| $d_t$     | m         | water depth below mean wave trough level   |
| $D$       | m         | grain size, diameter   |
| $D$       | $W/m^2$   | wave energy dissipation rate   |
| $D_b$     | $W/m^2$   | wave energy dissipation rate due to breaking   |
| $D_f$     | $W/m^2$   | wave energy dissipation rate due to bottom friction  |
| $D_{iss}$ | $W/m^2$   | dissipation of roller energy   |
| $D_t$     | $W/m^2$   | turbulent energy dissipation rate  |
| $D^*$     | -         | dimensionless particle parameter   |
| $D_{10}$  | m         | grain size diameter such that 10 % of the grains by mass are smaller than $D = D_{10}$                                   |
| $D_{50}$  | m         | geometric mean sediment diameter; grain size diameter such that 50 % of the grains by mass are smaller than $D = D_{50}$ |
| $D_{90}$  | m         | grain size diameter such that 90 % of the grains by mass are smaller than $D = D_{90}$                                   |
| $E$       | $J/m^2$   | wave energy per unit area  |
| $E_r$     | $J/m^2$   | roller energy  |
| $f$       | Hz        | frequency  |
| $f'_{cw}$ | -         | weighted friction factor, accounting for both wave and current friction  |
| $f_C$     | -         | distribution function of suspended sediment  |

| Symbol          | Units                                    | Meaning   |
|-----------------|--|---|
| $f_w$           | -  | bottom friction factor  |
| $F_D$           | -  | dimensionless function related to the sediment diameter   |
| $F_k$           | -  | function which describes the effect of the way the waves break  |
| $g$             | m/s <sup>2</sup>                         | gravitational constant  |
| $G_{nm}$        | -  | transfer function in orbital velocity formulation   |
| $H$             | m  | wave height   |
| $H_0$           | m  | wave height at deep water   |
| $H_m$           | m  | maximum wave height in energy dissipation formulation   |
| $H_{m0}$        | m  | spectral 'significant wave height', $H_{m0} = 4\sqrt{m_0}$  |
| $H_{rms}$       | m  | root mean square wave height  |
| $H_{rms,0}$     | m  | root mean square wave height at seaward boundary of model   |
| $H_s$           | m  | significant wave height   |
| $I_0$           | m  | basic constant in mass flux computation   |
| $I_1$           | m  | basic constant in sediment load function  |
| $I_2$           | m <sup>2</sup>                           | basic constant in nett transport computation  |
| $I_3$           | m  | basic constant in nett transport computation  |
| $j$             | -  | counter in orbital velocity formulation   |
| $k$             | m <sup>-1</sup>                          | wave number   |
| $\bar{K}$       | J/kg =<br>m <sup>2</sup> /s <sup>2</sup> | depth-averaged, turbulent energy per unit of mass   |
| $K_c$           | -  | dimensionless constant in reference concentration formulation   |
| $K_{lin}$       | s <sup>-1</sup>                          | constant in secondary flow equation related to linear contribution to $u(z)$  |
| $K_{log}$       | m/s                                      | constant in secondary flow equation related to logarithmic contribution to $u(z)$                                     |
| $K_{opt}$       | -  | constant in wave run up formulation   |
| $K_r$           | -  | dimensionless constant in roller area formulation   |
| $K_1$           | -  | additional constant   |
| $K_2$           | -  | additional constant   |
| $K_\varepsilon$ | -  | constant in reference mixing formulation  |
| $K_\mu$         | -  | constant in mixing gradient formulation   |
| $L$             | m  | length of a roller; characteristic length scale   |
| $L$             | m  | wavelength  |
| $m$             | kg/m/s                                   | landward directed mass flux above mean wave trough level  |
| $m$             | -  | number of waves in one wave group in orbital velocity formulation   |
| $m_0$           | m <sup>2</sup>                           | zeroth spectral moment (area under the spectral curve); variance of the surface elevation, which is total wave energy |
| $m_n$           |  | n-th moment of the frequency spectrum   |
| $n$             | -  | number in orbital velocity formulation  |

| Symbol        | Units                 | Meaning  |
|---------------|-----------------------|--|
| $n$           | -                     | scale factor $\left( = \frac{X_{\text{prot}}}{X_{\text{model}}} \right)$   |
| $n$           | -                     | ratio of wave group and phase velocity ( $=c_g/c$ )  |
| $n_A$         | -                     | erosion volume scale factor  |
| $n_d$         | -                     | depth scale factor   |
| $n_H$         | -                     | wave height scale factor   |
| $n_l$         | -                     | length scale factor  |
| $n_L$         | -                     | wavelength scale factor  |
| $n_{Sf}$      | -                     | profile steepness scale factor   |
| $n_T$         | -                     | wave period scale factor   |
| $n_w$         | -                     | fall velocity scale factor   |
| $p$           | -                     | porosity of sediment   |
| $P_{br}$      | -                     | portion of breaking waves  |
| $P_t$         | J/s/m                 | turbulent energy flux ( $=\bar{E}c_g$ )  |
| $q_b$         | m <sup>3</sup> /s/m   | bed load transport rate including pores  |
| $q_{bot+sus}$ | m <sup>3</sup> /s/m   | combined bed load and suspended transport rate including pores   |
| $q_s$         | kg/s/m                | suspended sediment transport rate  |
| $q_{s,c}$     | m <sup>3</sup> /s/m   | current related suspended sediment transport including pores   |
| $q_{s,c}$     | kg/s/m                | current related suspended sediment transport   |
| $q_{s,w}$     | kg/s/m                | wave related suspended sediment transport  |
| $Q_b$         | -                     | fraction of breaking waves in energy dissipation formulation   |
| $S$           | m <sup>2</sup> /Hz    | energy density   |
| $S$           | kg/s/m                | (time-averaged) depth-integrated sediment transport per unit width   |
| $S^*$         | m <sup>3</sup> /s/m   | (time-averaged) depth-integrated sediment transport per unit width in the most landward computing point            |
| $S_l$         | kg/s/m                | contribution of zone below wave trough to $S$  |
| $S_{max}$     | -                     | maximum wave steepness   |
| $S_u$         | kg/s/m                | contribution of zone above wave trough to $S$  |
| $S_x$         | m <sup>3</sup> /s/m   | sediment transport per unit width in cross-shore direction   |
| $S(x)$        | m <sup>3</sup> /s/m   | transport landward from the last computing point   |
| $S_{xx}$      | J/m <sup>2</sup> =N/m | radiation stress in x-direction through x-plane  |
| $t$           | s                     | time   |
| $T$           | -                     | dimensionless bed shear stress parameter   |
| $T$           | s                     | wave period  |
| $T_{m-1,0}$   | s                     | wave period based on zeroth ( $m_0$ ) and first negative ( $m_{-1}$ ) moment                                       |
| $T_p$         | s                     | peak wave period, defined as the period in a arbitrary wave spectrum with a global maximum of the spectral density |
| $u$           | m/s                   | time-averaged value of horizontal component of velocity field (overbar omitted)                                    |
| $u_b$         | m/s                   | near bottom velocity in bed load transport formulation   |

| Symbol          | Units     | Meaning  |
|-----------------|-----------|--|
| $u_i$           | m/s       | horizontal component of velocity in $i$ -direction with $i = x$ or $y$                           |
| $u_{orb}$       | m/s       | amplitude of wave orbital velocity   |
| $u_{rms}$       | m/s       | root mean square orbital velocity  |
| $u_0$           | m/s       | (virtual) velocity at reference level (bottom)   |
| $U_1$           | m/s       | orbital velocity   |
| $U_2$           | m/s       | orbital velocity   |
| $U_2'$          | m/s       | orbital velocity   |
| $U_3$           | m/s       | orbital velocity   |
| $U_4$           | m/s       | orbital velocity   |
| $v$             | m/s       | time and space averaged fluid velocity   |
| $V$             | m/s       | local instantaneous fluid velocity   |
| $w_s$           | m/s       | fall velocity of sediment with grain size $D = D_{50}$ , in stagnant water                       |
| $w_{s,m}$       | m/s       | fall velocity of suspended sediment in a fluid sediment mixture                                  |
| $x$             | m         | horizontal cross-shore coordinate  |
| $z$             | m         | vertical coordinate (positive upward)  |
| $z$             | m         | wave run up level in the dry profile extrapolation formulation                                   |
| $z_b$           | m         | vertical coordinate of the bed profile with respect to the reference level                       |
| $z_s$           | m         | significant wave run up level above mean water level   |
| $\alpha$        | $m/s^2$   | constant in shear stress equation $\left( \frac{d\bar{\tau}/dz}{\rho} \right)$                   |
| $\alpha$        | -         | dissipation coefficient  |
| $\alpha$        | -         | exponent in scale relation   |
| $\alpha_D$      | -         | power in $F_D$ -function   |
| $\alpha_k$      | -         | constant in penetration depth formulation  |
| $\beta$         | $m^2/s^2$ | constant in shear stress equation $\left( \frac{\tau_0}{\rho} \right)$                           |
| $\beta$         | -         | exponent in scale relation   |
| $\beta$         | -         | slope of the face of the wave in roller dissipation equation                                     |
| $\beta$         | -         | average beach slope in wave run up formulation   |
| $\beta_s$       | -         | slope factor   |
| $\gamma$        | -         | breaker index  |
| $\gamma$        | -         | numerical smoothing factor in bottom scheme  |
| $\Delta$        | -         | relative density of sediment with respect to water $\left( = \frac{\rho_s - \rho}{\rho} \right)$ |
| $\varepsilon$   | -         | term in orbital velocity formulation   |
| $\varepsilon_0$ | $m^2/s$   | reference mixing coefficient at level $z = 0$  |

| Symbol               | Units                  | Meaning   |
|----------------------|------------------------|---|
| $\varepsilon_{s,c}$  | $\text{m}^2/\text{s}$  | current related mixing coefficient  |
| $\varepsilon_{s,cw}$ | $\text{m}^2/\text{s}$  | sediment mixing coefficient for combined current and waves  |
| $\varepsilon_{s,w}$  | $\text{m}^2/\text{s}$  | wave related mixing coefficient   |
| $\eta$               | m                      | water surface elevation   |
| $\bar{\eta}$         | m                      | (time averaged) mean elevation of the water level above the mean level $h$ due to wave set-up or set-down |
| $\theta$             | rad                    | angle of wave attack with respect to shore normal   |
| $\theta'$            | -                      | dimensionless effective shear stress  |
| $\theta_{cr}$        | -                      | dimensionless critical shear stress   |
| $\Theta_{cr}$        | -                      | critical Shields parameter  |
| $\mu$                | m/s                    | vertical mixing gradient  |
| $\nu_t$              | $\text{m}^2/\text{s}$  | turbulent viscosity   |
| $\xi_a$              | m                      | amplitude in orbital velocity formulation   |
| $\rho$               | $\text{kg}/\text{m}^3$ | mass density of fluid (water) (subscript f omitted)   |
| $\rho_s$             | $\text{kg}/\text{m}^3$ | mass density of sediment  |
| $\sigma$             | -                      | relative height above bottom ( $z/d$ )  |
| $\bar{\tau}_{b,cr}$  | $\text{N}/\text{m}^2$  | time averaged critical bed shear stress according to Shields  |
| $\bar{\tau}'_{b,cw}$ | $\text{N}/\text{m}^2$  | time averaged effective bed shear stress  |
| $\tau_{cr}$          | $\text{N}/\text{m}^2$  | critical shear stress   |
| $\tau_i$             | $\text{N}/\text{m}^2$  | shear stress in $i$ -direction with $i = x$ or $y$  |
| $\tau_{s,wave}$      | $\text{N}/\text{m}^2$  | shear stress in direction of wave propagation, introduced by surface roller                               |
| $\varphi$            | rad                    | phase difference between bound wave and short wave in orbital velocity formulation                        |
| $\varphi$            | rad                    | angle of repose of the sediment   |
| $\Phi_{bd}$          | -                      | non-dimensional bed load transport vector   |
| $\varphi_d$          | -                      | damping factor dependent on the concentration   |
| $\omega$             | rad/s                  | angular frequency ( $=2\pi/T$ )   |
| $\Delta\omega$       | rad/s                  | term in orbital velocity formulation  |



## Summary

For the judgement of the safety of the Dutch dune coast use is made of a method to compute for given design conditions, the amount of dune erosion. The core of the method is the so-called DUROS-model. This model does not take into account the effect of the wave period on the amount of dune erosion and was developed for the at that time supposed reach of wave periods for the Dutch coast ( $T_p \leq 12.0$  s).

According to present understanding one has to take account of longer wave periods ( $T_p$  up to 16 or 18 s). In addition, preliminary explorations supposed the dune erosion process to be dependent on the wave period. However, the used model was not validated for these high wave periods.

Recently, a series of small scale physical model tests have been carried out by WL | Delft Hydraulics in the Schelde flume. According to that research dune erosion is clearly dependent on the wave period.

In this research these tests are analysed and they are simulated as good as possible to verify the models DUROSTA and UNIBEST-TC with respect to the wave period influence.

The most important conclusions are:

- Assuming the applied scale relations and a relatively long storm duration, from the small scale physical model tests an increase of dune erosion volume above storm surge level of 25 – 35 % is found for a prototype peak wave period of  $T_p = 18.4$  s compared to  $T_p = 12$  s.
- In DUROSTA the breaker index  $\gamma$ , used by ENDEC, is set constant (default  $\gamma = 0.85$ ). Application of DUROSTA with this breaker index results for the larger prototype wave periods in less accurate computed wave height development (with respect to the measurements).
- In case of imposing the measured wave height near the wave board, then DUROSTA reproduces the measured relative effect of the wave period on the amount of dune erosion rather good. However, in that case the larger amount of dune erosion for a longer wave period is mainly caused by a larger (over-estimated w.r.t. measurements) wave height near the dune. Remark must be made that this near dune measured wave height is including reflection and long waves.
- In all DUROSTA computations the erosion volumes are under-estimated with respect to the measurements.
- The erosion volumes computed by UNIBEST-TC are much lower compared to the measurements. However, the possibility to compute dune erosion with UNIBEST-TC is just recently included and is still in development. In addition, UNIBEST-TC has not yet been calibrated for these kind of dune erosion tests.
- In both models a longer wave period does only cause consistently more dune erosion if the wave height near the dune is larger. This in contrast to the measurements of the B-series where, although approximately equal wave heights near the dune (including reflection and long waves), the effect of the wave period is clearly visible.

The most important recommendation is to carry out large scale physical model research and based on that, further desk study.



# I Introduction

## I.1 Background

For the judgement of the safety of the Dutch dune coast a computation model is used that, for given design conditions, determines the amount of dune erosion. The core of this model is the so-called DUROS-model (TAW, 1984).

The model uses particular computation values for normative hydraulic conditions. The so-called boundary conditions book (In Dutch: Randvoorwaardenboek, RWS, 2002) contains these values. Nowadays as normative wave period, expressed as peak wave period, the value  $T_p = 12.0$  s is used for the Dutch Wadden coast and the coast of (South- and North-) Holland. For the most southern part of the coast of South-Holland and the islands of Zeeland  $T_p = 8.0$  s is used. Given the available information at that time and the expected reach of wave periods at the Dutch coast ( $T_p \leq 12.0$  s), during development of the DUROS-model the shape of the erosion profile was assumed to be independent of the wave period.

According to present understanding one has to take a much longer wave period into account, compared to formerly, during design conditions (De Ronde et al., 1995; Roskam and Hoekema, 1996). This increase varies between 30 % (south) to 60 % (north) compared to today used 12.0 s (peak wave period). According to recently carried out research (Steezel, 2002) the wave period has an effect on the shape of the erosion profile. It is also computed, that the amount of dune erosion could increase significantly. Nevertheless, the used methods to carry out this computation are applied outside the validated range.

End 2003 WL | Delft Hydraulics (Coeveld and De Vroeg, 2004) carried out physical model tests (small scale guide tests, depth scale 30 and 40) commissioned by the Road and Hydraulic Engineering Institute (DWW). These tests showed a clear positive relation between wave period and dune erosion volume. Still there is the intention to do large-scale physical model tests (depth scale 5 to 7.5). This all is necessary to generate data to improve the tool for the judgement of the safety of dunes as water defence.

## I.2 Problem definition

Given the above called recent understanding about the normative wave conditions for the Dutch dune coast and the fact that the presently used DUROS-model contains no wave period dependency it is necessary to make an estimate of the consequences. If the increase of dune erosion is significant for these renewed design conditions the priority to improve the judgement method also increases.

The time dependent cross-shore transport models DUROSTA (Steezel, 1993) and UNIBEST-TC (UNiform BEach Sediment Transport – Time dependent Cross-shore; Bosboom et al., 2000) are both able to compute dune erosion taking into account the wave period. However, these models are not validated for these long wave periods ( $T_p > 12.0$  s).

Comparison of test results (wave period varied) with each other and with corresponding computations can give insight in the quality of these models concerning the wave period dependency. Sufficient agreement of tests (in general) and computations can facilitate the choice for a judgement method based on one of these more present-day time dependent models. On the other hand insufficient agreement asks for more research and improvement of existing models or even (in the ‘worst’ case) development of new models.

### 1.3 Objective

The objective of this research is to verify the models DUROSTA and UNIBEST-TC concerning the wave period influence (based on recent small scale tests).

Sufficient agreement of one or both of the models with the tests can support an estimate of the relative increase of dune erosion by applying renewed conditions compared to the conditions as presently used. Insufficient agreement will lead to pointing out as good as possible the module or modules which ask for improvement.

In both cases it is very important to keep in mind that this research is mainly based on just small scale model data. To get more insight and to make a better estimate of the effects large scale physical model research is recommended. The necessity of further research will be argued from a technical point of view.

### 1.4 Boundary conditions and assumptions

- This research is mainly based on the recent physical model tests carried out by WL | Delft Hydraulics (Coeveld and De Vroeg, 2004).
- The cross-shore profiles which are used for this research are based on a reference cross-shore profile represented in Figure 1.1 (averaged profile along the Dutch coast).
- A constant storm surge level and constant wave conditions during the whole test are applied.
- The tests were 2D, so perpendicular incoming waves and no longshore current.

### 1.5 Research approach

The study can be divided into three parts. At first a literature review is carried out. Following aspects will come up:

- General information about dune erosion
- Wave period
- Characteristic storm duration
- Description of DUROSTA
- Description of UNIBEST-TC

In the second part the physical model research comes up (Coeveld and De Vroeg, 2004). The test results will be analysed. For practical reasons the test series were split up into two parts with different scale factors (A-series depth scale 30; B-series depth scale 40). These two series will first be considered separately. In order to overview the whole tested range of prototype wave periods ( $10 \text{ s} < T_p < 19 \text{ s}$ ) the results of the B-series (depth scale 40) are converted into depth scale 30. With that more or less continuous series it is possible to

compare the test results with the basic case. With basic case is meant the up to now normative wave period for the Dutch coast ( $T_p = 12.0$  s).

The last part of the research consists of numerical modelling. The tests are simulated on model scale to enable direct comparison with the measurements. The simulations have been carried out in different ways, for example by imposing the measured wave heights near the wave board in the computation models and by using the measured wave heights closer to the dune as input in the models. These approaches led to different results because of the fact that the wave module did not fully reproduce the measured wave heights over the whole cross-shore profile.

## **1.6 Readers' guide**

A summary of the entire study, list of figures, list of tables and list of symbols are added at the beginning of this document. At the end references, tables, (most of the) figures and appendices will be found. If figures are among the text, which occurs occasionally, then that is mentioned.

The composition of the chapters roughly follows the research process. In Chapter 2 some general aspects about dune erosion and the used models are described. Chapter 3 is about the physical model data which were the basis of this research. In Chapter 4 a number of DUROSTA computations are described. The computations with UNIBEST-TC are presented in Chapter 5. In Chapter 6 some topics have been discussed which are important to be aware of for considering this research and for the set-up of further research. Chapter 7 contains the conclusions and recommendations.



## 2 Literature review

This chapter deals first with dune erosion in general. After that wave period and storm duration come up briefly. And at last both used models, DUROSTA and UNIBEST-TC, will be briefly outlined.

### 2.1 Dune erosion

In this section the situation of a dune coast during normal conditions is mentioned and on the other hand the situation during a severe storm surge, which can cause dune erosion. In addition, the definition of dune erosion is given and the difference with structural erosion. In spite of the fact that after a storm normal conditions can reverse the dune erosion process, in a natural way, still in some cases problems are possible. These problems are mentioned finally.

#### 2.1.1 Normal conditions

During normal conditions the water level fluctuates just in the normal tidal range. Furthermore, moderate wave conditions and with that moderate sediment transport rates occur. This situation leads to a general shape of a cross-shore profile that is considered in some kind of dynamic equilibrium. In case of an unstable coast this dynamic equilibrium profile moves on the longer term.

#### 2.1.2 Severe storm surge

During severe storm surge the water level is much higher, sometimes even above the dune foot. In addition, the waves generated by the storm are much higher and longer than normal. The principle of profile formation is the same: nature strives to a new dynamic equilibrium cross-shore profile. However, in this case two properties are more extreme:

- The present cross-shore profile (normal conditions equilibrium) is far out of equilibrium
- The severe conditions enable a (relatively) high adaptation speed

One can imagine that the latter is intensified by the first which makes it possible to reshape the cross-shore profile relatively fast. During the storm the profile will transform more and more to a new equilibrium shape as a result of which the processes will slow down with time.

#### 2.1.3 Definition of dune erosion

Dune erosion is a relatively fast developing cross-shore transport process which occurs during severe wave attack combined with high water levels. Large quantities of sand coming from the dunes are transported seaward. If no seaward or lateral losses occur, the sand balance will be closed in cross-shore direction. The principle is sketched in Figure 2.1 (text). The eroded sand will deposit on the beach and foreshore in such a way that a so-called erosion profile appears. Research turned out that when this erosion profile is formed, the erosion process advances just relatively slow in time (WL | Delft Hydraulics, 1982).

In stable coast compartments the eroded dune sand will in the years after de storm surge (nearly) completely be transported back to the dunes (reversible process) in a natural way.

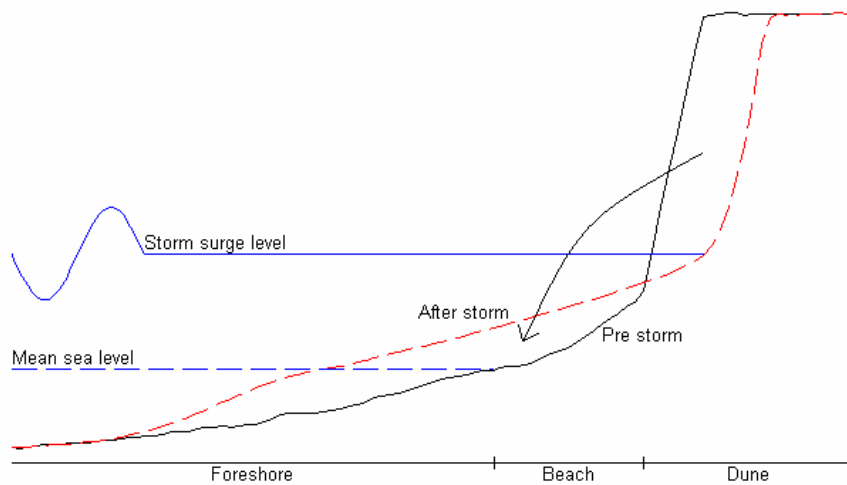


Figure 2.1 Principle of dune erosion

#### 2.1.4 Structural coastal erosion

Structural coastal erosion caused by waves and currents is a gradual sand loss from the coastal profile. This sand loss can be cross-shore (seaward) as well as longshore (neighbouring profiles). The gradual sand loss results in a landward shift of the coastline.

In coast compartments with structural erosion the dune erosion process is (partly) irreversible. By waves and currents a gradual sideward loss of eroded dune sand can take place, so a permanent loss of dune volume occurs.

#### 2.1.5 After storm

After a storm or storm season, a period with again more normal conditions begins. As becomes clear from Figure 2.1 (text) the after storm profile is far out of equilibrium for normal conditions (assuming the pre storm profile as equilibrium).

By wind sand will gradually be transported from the dry beach back to the dunes. Assuming no structural erosion, waves and tidal movement will deposit sand from the foreshore to the beach from where the wind on its turn can transport it back to the dunes.

This is in a nutshell the reverse of the dune erosion process.

#### 2.1.6 What is the problem?

As described above the dune erosion process is in principle reversible and so would cause no problems. However, in general two cases can surely cause problems:

- If the erosion and with that the retreat of the dune face is that large that the dune disappears, the hinterland will inundate.

- As a result of less severe storm events (hinterland does not inundate) buildings which are on the dunes can be damaged.

## 2.2 Wave period

Steetzel did in commission of the Road and Hydraulic Engineering Institute (DWW) an exploration about the effect of more severe wave conditions to the dune coast. In that report (Steetzel, 2002) some qualitative conclusions came up about the effect of a longer wave period based on earlier small scale tests done in the Schelde flume of WL | Delft Hydraulics (1982), viz.:

- A 'landward' shift of the front of the deposit.
- A higher located deposit.
- A milder slope of the erosion profile around the waterline (storm surge level).
- A higher located dune foot (transition swash dominated beach profile to steep dune front)
- A more 'landward' located dune front.

The overall conclusion was that all these effects together lead to a relative increase of the amount of dune erosion.

Steetzel (2002) presented these effects qualitatively with arrows in some graphs with different test results (WL | Delft Hydraulics, 1982). In Figure 2.2 the same arrows are drawn for both test series of the results of Coeveld and De Vroeg (2004). The above mentioned effects are in the latter results visible as well. In series B the effects are slightly less clear, possibly because of shorter test duration and relative less wave period increase.

Steetzel (2004) mentioned that a relative longer wave period results in less decrease of the significant wave height towards the coast and so (for a given position in the cross-shore profile) to more severe wave attack.

## 2.3 Characteristic storm surge duration

In Figure 2.3 an overview is given of the assumed naturally varying hydraulic conditions during a storm. The equations behind these graphs are obtained from Steetzel (1993). For the wave conditions only the maximum values are shown on the vertical axes. This is because the used equations and/or parameter settings are not by definition also valid for these much higher maximum values. So, the two upper plots are meant qualitative.

In the tests and computations which come up in this research use is made of an idealized situation with a constant water level and constant wave conditions. According to Vellinga (1986) the erosion volume after a storm with naturally varying water level and wave conditions can be compared with a 5 hours storm with maximum storm surge level and accompanying wave conditions. This characteristic storm duration is in the model with depth scale  $n_d = 30$  approximately 1 hour.

It is also not by definition true that this characteristic storm duration of 5 hours is also valid for the maximum hydraulic conditions in this research ( $T_p = 19$  s and  $H_s = 9$  m). However, for the time being it is assumed that the same characteristic storm duration is applicable for all used conditions.

## 2.4 Description of DUROSTA

In this section a brief outline of the model DUROSTA is presented. The English-language variant is called UNIBEST-DE (UNIform Beach Sediment Transport – Dune Erosion). For this study DUROSTA version 1.20 is used.

The model DUROSTA computes the resulting cross-shore transport due to wave action as the depth-integrated product of time-averaged velocities and time-averaged concentrations. This approach results from the fact that during severe storm conditions, when large amounts of sediment are in the vertical, the transport is to a large extent dependent on the average velocities. The contribution of the fluctuations, the so-called correlation contribution, is assumed to be relatively small.

This approach is considered acceptable inside the breaker zone, because of the (rather strong) undertow. Outside the breaker zone this is likely not true because of the increasing correlation between the fluctuating water movement and sediment concentration.

The model can be subdivided in five sub-models:

- Wave propagation model
- Cross-shore flow model
- Sediment concentration model
- Nett cross-shore transport model
- Bed level change model

Figure 2.4 visualizes set-up of the model and the correspondence between the sub-models.

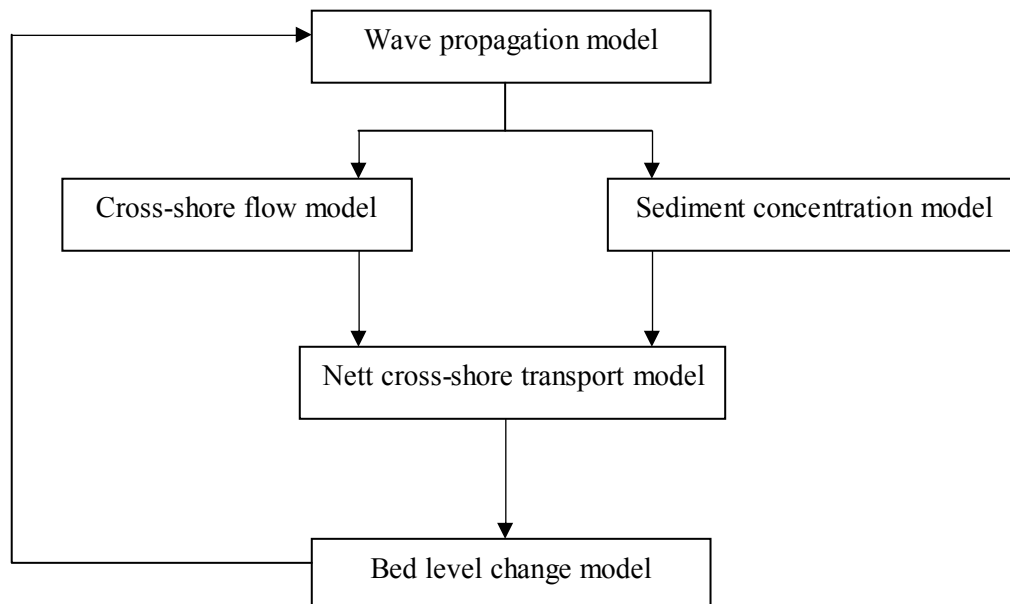


Figure 2.4 Overview of DUROSTA sub-models

The brief description given below was mainly obtained from Steetzel (1993). Remark must be made that the formulations for longshore transport are left out of consideration because it is not used in this research.

## 2.4.1 Wave propagation model

For each time step, the momentary wave height decay is computed using ENDEC (Battjes and Janssen, 1978) starting from the seaward boundary.

### 2.4.1.1 ENDEC

The basic equations describing this wave height decay while taking account of the wave-induced cross-shore water level set-up are the wave action equation and the cross-shore momentum equation.

The first differential equation, for perpendicular incoming waves, is described by:

$$\frac{dEc_g}{dx} + D_b + D_f = 0 \quad (2.1)$$

in which:

|        |                     |   |
|--------|---------------------|---|
| $Ec_g$ | W/m                 | energy flux   |
| $E$    | J/m <sup>2</sup>    | wave energy per unit area                           |
| $c_g$  | m/s                 | wave group velocity                                 |
| $D_b$  | J/m <sup>2</sup> /s | wave energy dissipation rate due to breaking        |
| $D_f$  | J/m <sup>2</sup> /s | wave energy dissipation rate due to bottom friction |
| $x$    | m                   | horizontal cross-shore coordinate                   |

Where the wave energy:

$$E = \frac{1}{8} \rho g H_{rms}^2 \quad (2.2)$$

in which:

|           |                   |                              |
|-----------|-------------------|------------------------------|
| $\rho$    | kg/m <sup>3</sup> | mass density of water        |
| $g$       | m/s <sup>2</sup>  | gravitational constant       |
| $H_{rms}$ | m                 | root mean square wave height |

The wave energy dissipation rate due to breaking is described by:

$$D_b = \frac{1}{4} \rho g \alpha Q_b (\omega / 2\pi) H_m^2 \quad (2.3)$$

in which:

|          |       |                            |
|----------|-------|----------------------------|
| $\alpha$ | -     | dissipation coefficient    |
| $Q_b$    | -     | fraction of breaking waves |
| $\omega$ | rad/s | angular frequency (=2π/T)  |
| $T$      | s     | wave period                |
| $H_m$    | m     | maximum wave height        |

It is assumed that waves which are higher than  $H_m$  will break and smaller non-broken waves obey a Rayleigh distribution. This maximum wave height is described by:

$$H_m = \left( \frac{0.88}{k} \right) \tanh \left( \frac{\gamma kd}{0.88} \right) \quad (2.4)$$

in which:

|          |                 |                                     |
|----------|-----------------|-------------------------------------|
| $k$      | $\text{m}^{-1}$ | wave number                         |
| $\gamma$ | -               | breaker index                       |
| $d$      | m               | water depth (to mean surface level) |

The fraction of breaking waves is described by:

$$\frac{1 - Q_b}{-\ln Q_b} \left( \frac{H_{rms}}{H_m} \right)^2 \quad (2.5)$$

The wave energy dissipation rate due to bottom friction is described by:

$$D_f = \frac{1}{8} \rho f_w \pi^{-\frac{1}{2}} \left( \omega H_{rms} / \sinh(kd) \right)^3 \quad (2.6)$$

in which:

|       |   |                        |
|-------|---|------------------------|
| $f_w$ | - | bottom friction factor |
|-------|---|------------------------|

The second equation, the cross-shore momentum equation, accounts for the change in mean water level due to the radiation stress effect and is described by:

$$\frac{dS_{xx}}{dx} + \rho g (d + \bar{\eta}) \frac{d\bar{\eta}}{dx} = 0 \quad (2.7)$$

in which:

|              |                             |   |
|--------------|-----------------------------|---|
| $S_{xx}$     | $\text{J/m}^2 = \text{N/m}$ | radiation stress in x-direction through x-plane   |
| $\bar{\eta}$ | m                           | (time averaged) mean elevation of the water level above the mean level $d$ due to wave set-up or set-down |

The radiation stress is described by:

$$S_{xx} = \left( 2n - \frac{1}{2} \right) E \quad (2.8)$$

in which:

|     |   |   |
|-----|---|---|
| $n$ | - | ratio of wave group and phase velocity ( $=c_g/c$ ) |
|-----|---|---|

### 2.4.1.2 Roller model

A roller model is applied because of the fact that the start of the wave set-up was predicted too far seaward. Instead of being dissipated immediately after the breakpoint, organized wave energy is converted into turbulent kinetic energy first (which can be seen from the development of a roller at the face of a breaking wave), before being dissipated ultimately via the production of turbulence. In this way the dissipation process is delayed, hence shifting the region of wave set-up in shoreward direction.

In the dissipation term  $D_b$ , an additional differential equation is included to make a distinction between the dissipation source term in the wave energy balance equation ( $D_b$ ) due to wave breaking and the dissipation of the turbulent kinetic energy ( $D_t$ ).

$$\frac{dP_t}{dx} + D_t = D_b \quad (2.9)$$

in which:

|       |                  |                                   |
|-------|------------------|-----------------------------------|
| $P_t$ | J/s/m            | turbulent energy flux             |
| $D_t$ | W/m <sup>2</sup> | turbulent energy dissipation rate |

The turbulent dissipation  $D_t$  is described by (Launder and Spalding, 1972):

$$D_t = \rho \overline{K}^3 \quad (2.10)$$

in which:

|                |  |   |
|----------------|--|---|
| $\overline{K}$ | J/kg =<br>m <sup>2</sup> /s <sup>2</sup> | depth-averaged, turbulent energy per unit of mass |
|----------------|--|---|

The mean turbulent energy flux  $P_t$  is computed from:

$$\frac{dP_t}{dx} = \rho \frac{d}{dx} (cd\overline{K}) \quad (2.11)$$

in which:

|     |     |               |
|-----|-----|---------------|
| $c$ | m/s | wave celerity |
|-----|-----|---------------|

Combination of former equations and successive elaboration in an iterative computational procedure yields a cross-shore distribution of the turbulent dissipation term. More details about this can be found in (Steetzel, 1990; Roelvink and Stive, 1989).

#### 2.4.2 Cross-shore flow model

The time-averaged velocity profile below the wave trough is based on the vertical distribution of the time-averaged shear stress. The velocity profile is described by:

$$u(z) = u_0 + K_{lin}z + K_{log} \ln \left( 1 + \frac{\mu z}{\varepsilon_0} \right) \quad (2.12)$$

in which:

|                 |                   |  |
|-----------------|-------------------|--|
| $z$             | m                 | vertical coordinate (positive upward)                  |
| $u_0$           | m/s               | (virtual) velocity at reference level (bottom)         |
| $K_{lin}$       | s <sup>-1</sup>   | constant related to linear contribution to $u(z)$      |
| $K_{log}$       | m/s               | constant related to logarithmic contribution to $u(z)$ |
| $\mu$           | m/s               | vertical mixing gradient                               |
| $\varepsilon_0$ | m <sup>2</sup> /s | reference mixing coefficient at level $z = 0$          |

The constants  $K_{lin}$  and  $K_{log}$  are described by respectively:

$$K_{lin} = \frac{\alpha}{\mu} \quad (2.13)$$

$$K_{log} = \frac{1}{\mu} \left( \beta - \frac{\alpha}{\mu} \varepsilon_0 \right) \quad (2.14)$$

in which:

$$\begin{aligned} \alpha & \quad \text{m/s}^2 & \quad \text{constant } \left( \left( d\bar{\tau} / dz \right) / \rho \right) \\ \beta & \quad \text{m}^2/\text{s}^2 & \quad \text{constant } \left( \tau_0 / \rho \right) \end{aligned}$$

The reference mixing coefficient and the mixing gradient are described by respectively:

$$\varepsilon_0 = K_\varepsilon D_{50} u_{rms} \gamma \quad (2.15)$$

$$\mu = K_\mu c / \gamma \quad (2.16)$$

in which:

$$\begin{aligned} K_\varepsilon & \quad - & \quad \text{constant in reference mixing formulation} \\ D_{50} & \quad \text{m} & \quad \text{geometric mean sediment diameter; grain size diameter such that} \\ & & \quad \text{50 \% of the grains by mass are smaller than } D = D_{50} \\ u_{rms} & \quad \text{m/s} & \quad \text{root mean square orbital velocity} \\ \gamma & \quad - & \quad \text{breaker index} \\ K_\mu & \quad - & \quad \text{constant in mixing gradient formulation} \end{aligned}$$

The mass flux  $m$  which occurs above the mean trough level directed to the shore is described by:

$$m = \frac{E}{c} + P_{br} K_r \rho \frac{H_{rms}^2}{T_p} \quad (2.17)$$

in which:

$$\begin{aligned} m & \quad \text{kg/m/s} & \quad \text{landward directed mass flux above mean wave trough level} \\ P_{br} & \quad - & \quad \text{portion of breaking waves} \\ K_r & \quad - & \quad \text{dimensionless quotient of roller area and } H_{rms}^2 \\ T_p & \quad \text{s} & \quad \text{peak wave period} \end{aligned}$$

Since in the case of a secondary current (in a two-dimensional case) no nett transport of water is present by definition, the same mass flux  $m$  has to occur below the wave trough in the opposite direction. By application of this continuity condition the following equation can be derived:

$$-\frac{m}{\rho} = u_0 d_t + \frac{1}{2} K_{lin} d_t^2 + K_{log} I_0 \quad (2.18)$$

in which:

$$\begin{aligned} u_0 & \quad \text{m/s} & \quad \text{(virtual) velocity at reference level (bottom)} \\ d_t & \quad \text{m} & \quad \text{water depth below mean wave trough level} \\ I_0 & \quad \text{m} & \quad \text{constant} \end{aligned}$$

Constant  $I_0$  is described by:

$$I_0 = \frac{\varepsilon_0}{\mu} \left[ \left( 1 + \frac{\mu d_t}{\varepsilon_0} \right) \left[ \ln \left( 1 + \frac{\mu d_t}{\varepsilon_0} \right) - 1 \right] + 1 \right] \quad (2.19)$$

### 2.4.3 Sediment concentration model

In DUROSTA the bottom transport is neglected and only the suspended transport is taken into account to compute the cross-shore transport. The amount of suspended sediment is determined by the concentration vertical which is described by:

$$C(z) = C_0 \left[ 1 + \frac{\mu z}{\varepsilon_0} \right]^{(-w_s/\mu)} \quad (2.20)$$

in which:

|       |                   |  |
|-------|-------------------|--|
| $C_0$ | kg/m <sup>3</sup> | reference sediment concentration (at level $z = 0$ )                       |
| $w_s$ | m/s               | fall velocity of sediment with grain size $D = D_{50}$ , in stagnant water |

For breaking waves, the amount of suspension and thus the reference concentration is mainly related to the turbulence level generated from breaking waves.

Due to the wave breaking process a certain amount of turbulent kinetic energy is released from the upper zone. Depending on the way of breaking a specific fraction of this energy reaches the bottom and causes an increase in the near bottom sediment suspension quantity. Finally, the amount of suspension has to be related to both the intensity of wave breaking and the way individual waves break.

The reference concentration is related to both the intensity of breaking and the way of breaking according to:

$$C_0 = \rho_s K_c F_D \left( \frac{\rho}{\tau_{cr}} \right)^{\frac{3}{2}} F_k^{\frac{3}{2}} \left( \frac{D_t}{\rho} \right) \quad (2.21)$$

in which:

|               |                   |  |
|---------------|-------------------|--|
| $\rho_s$      | kg/m <sup>3</sup> | mass density of sediment   |
| $K_c$         | -                 | constant   |
| $F_D$         | -                 | dimensionless function related to the sediment diameter, $F_D = \left( \frac{0.000225}{D_{50}} \right)^{\alpha_D}$   |
| $\alpha_D$    | -                 | constant   |
| $\tau_{cr}$   | N/m <sup>2</sup>  | critical shear stress, $\tau_{cr} = \Theta_{cr} (\rho_s - \rho) g D_{50}$  |
| $\Theta_{cr}$ | -                 | critical Shields parameter   |
| $F_k$         | -                 | function which describes the effect of the way the waves break, $F_k = \left[ \alpha_k \gamma \left( \exp \left( \frac{1}{\alpha_k \gamma} \right) - 1 \right) \right]^{-1}$ |
| $\alpha_k$    | -                 | constant   |

#### 2.4.4 Nett cross-shore transport model

The cross-shore transport is computed from the depth-integrated product of the time-averaged velocity profile and the time-averaged sediment concentration profile. The sediment transport is distributed in two parts, one above the wave trough landward directed  $S_u$  and another below the wave trough seaward directed  $S_l$ :

$$S = S_l + S_u \quad (2.22)$$

in which:

|       |        |  |
|-------|--------|--|
| $S$   | kg/s/m | (time-averaged) depth-integrated sediment transport per unit width |
| $S_l$ | kg/s/m | contribution of zone below wave trough to $S$                      |
| $S_u$ | kg/s/m | contribution of zone above wave trough to $S$                      |

where the lower contribution  $S_l$  is described by:

$$S_l = C_0 (u_0 I_1 + K_{lin} I_2 + K_{log} I_3) \quad (2.23)$$

in which three basic parameters  $I_1$  (expressed in m),  $I_2$  (in m<sup>2</sup>) and  $I_3$  (in m) according to respectively:

$$I_1 = \frac{\varepsilon_0}{\mu} \frac{1}{K_1} (K_2^{K_1} - 1) \quad (2.24)$$

$$I_2 = \frac{\varepsilon_0}{\mu} \frac{1}{K_1} \left( K_2^{K_1} \left( d_t - \frac{\varepsilon_0}{\mu} \frac{1}{K_1 + 1} \right) + \frac{\varepsilon_0}{\mu} \frac{1}{K_1 + 1} \right) \quad (2.25)$$

$$I_3 = \frac{\varepsilon_0}{\mu} \frac{1}{(K_1)^2} (K_2^{K_1} (K_1 \ln(K_1) - 1) + 1) \quad (2.26)$$

in which two additional, dimensionless constants  $K_1$  and  $K_2$  are defined as:

$$K_1 = 1 - \frac{w_s}{\mu} \quad (2.27)$$

$$K_2 = 1 + \frac{\mu}{\varepsilon_0} d_t \quad (2.28)$$

The upper contribution  $S_u$  is described by:

$$S_u = -C_0 f_C(d) \left[ u_0 d_t + \frac{1}{2} K_{lin} d_t^2 + K_{log} I_0 \right] \quad (2.29)$$

in which:

$$f_C(d) = \left( 1 + \frac{\mu d}{\varepsilon_0} \right)^{\left( \frac{-w_s}{\mu} \right)} \quad (2.30)$$

$f_C(d)$  is the relative concentration at mean water level. This implies in the computation a constant concentration above the wave trough.

The total nett sediment transport can be written as:

$$S = C_0 \left[ u_0 (I_1 - f_C(d) d_t) + K_{lin} \left( I_2 - f_C(d) \frac{1}{2} d_t^2 \right) + K_{log} (I_3 - f_C(d) I_0) \right] \quad (2.31)$$

### 2.4.5 Bed level change model

Bottom changes are computed using the conservation equation of sediment mass, according to:

$$\frac{dz_b(x)}{dt} = \frac{-1}{(1-p)} \left( \frac{dS_x(x)}{dx} \right) \quad (2.32)$$

in which:

|       |                     |   |
|-------|---------------------|---|
| $z_b$ | m                   | vertical coordinate of the bed profile with respect to the reference level      |
| $p$   | -                   | porosity  |
| $S_x$ | m <sup>3</sup> /s/m | sediment transport per unit width in cross-shore direction (=S/ρ <sub>s</sub> ) |
| $S$   | kg/s/m              | (time-averaged) depth-integrated sediment transport per unit width              |

### 2.4.6 Extrapolation method for the dry profile

Around the waterline not modelled and not yet understood physical processes take place. For this reason landward from a more or less arbitrary transition point an extrapolation method is applied in stead of the cross-shore transport concept.

#### 2.4.6.1 Location transition point

The location of this transition point was chosen at a quarter of the local wavelength seaward from the waterline. This implies that for a longer wave period (larger wavelength) the location of the transition point is more seaward.

During a dune erosion computation, with constant wave conditions and water level, the location of the transition point will shift in time by two mechanisms. The wavelength at the original location will reduce due to bottom changes (reduced water depth). The transition point has to move landward to be again at a quarter of the local wavelength from the waterline. In addition, the waterline itself will move landward due to the erosion process.

#### 2.4.6.2 Extrapolation method

The transport landward from the transition point is described by the transport in that point  $S^*$  times a wave run up related reduction factor.

$$S(x) = S^* \left[ \exp\left(-2 \frac{z^2}{z_s^2}\right) - \sqrt{\frac{\pi}{2}} \left( \sqrt{2} \frac{z}{z_s} \right) \left( 1 - \frac{2}{\pi} \int_0^{\sqrt{2} \frac{z}{z_s}} \exp(-x^2) dx \right) \right] \quad (2.33)$$

in which:

|       |                                   |   |
|-------|-----------------------------------|---|
| $S^*$ | m <sup>3</sup> /m <sup>1</sup> /s | (time-averaged) depth-integrated sediment transport per unit width in the most landward computing point |
| $z_s$ | m                                 | significant wave run up above the mean water level  |

$$z_s = 0.5T_p \sqrt{gH_s} \tan \beta \quad (2.34)$$

See also Walstra and Steetzel (2003).

### 2.4.7 Default settings

Table 2.1 gives an overview of the default parameter settings of DUROSTA. Since the model among others was calibrated on this kind of tests there is at first no reason to change the settings.

## 2.5 Description of UNIBEST-TC

This section describes the UNIBEST-TC model. UNIBEST-TC stands for UNIFORM Beach Sediment Transport – Time dependent Cross-shore. For this study version 2.04 is used with the wave run up module of version 2.10. Furthermore, for the location of the transition point the DUROSTA approach, a quarter of the local wave length from the waterline, is implemented and applied (see Section 2.5.6).

The model consists of five sub-models:

- Wave propagation model
- Mean current profile model
- Wave orbital velocity model
- Bed load and suspended load transport model
- Bed level change model

Figure 2.5 visualizes the set-up of the model and the correspondence between the sub-models.

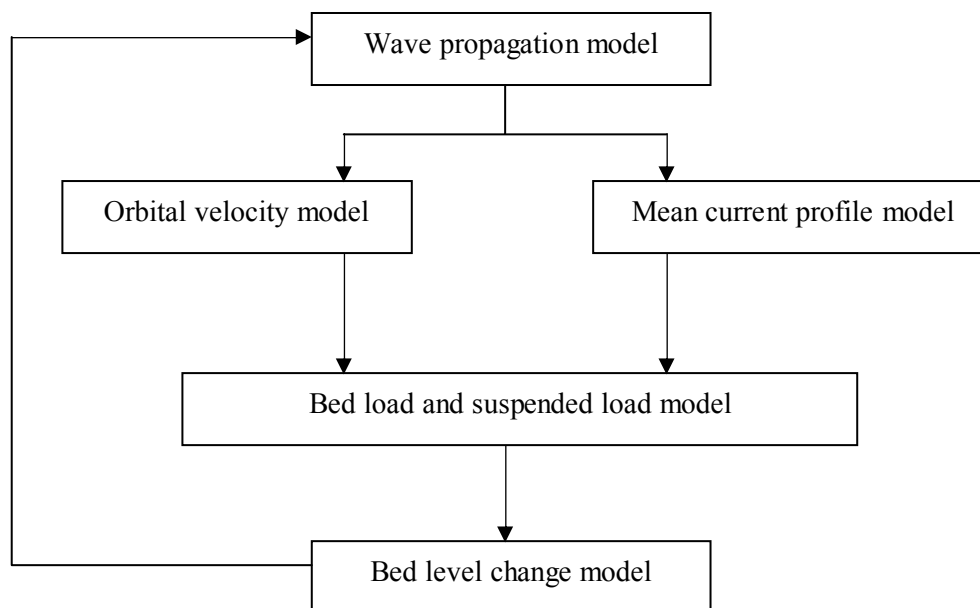


Figure 2.5 Overview of UNIBEST-TC sub-models

The brief description of the modules was mainly obtained from Bosboom et al. (2000). Remark must be made that formulations for longshore transport in general are left out of consideration because these are not used in this research.

## 2.5.1 Wave propagation model

Similar to DUROSTA, in UNIBEST-TC the wave height decay model ENDEC is used. A description is given in Section 2.4.1.1. However, in this case another roller model is applied.

### 2.5.1.1 Roller model

A roller model is applied because of the fact that the start of the wave set-up was predicted too far seaward. Instead of being dissipated immediately after the breakpoint, organized wave energy is converted into turbulent kinetic energy first (which can be seen from the development of a roller at the face of a breaking wave), before being dissipated ultimately via the production of turbulence. In this way the dissipation process is delayed, hence shifting the region of wave set-up in shoreward direction. The roller model according to Nairn et al. (1990) is applied:

$$\frac{\partial}{\partial x}(2E_r c \cos \theta) = D_b - Diss \quad (2.35)$$

in which:

|          |                  |   |
|----------|------------------|---|
| $x$      | m                | horizontal cross-shore coordinate                 |
| $E_r$    | J/m <sup>2</sup> | roller energy                                     |
| $c$      | m/s              | wave celerity                                     |
| $\theta$ | rad              | angle of wave attack with respect to shore normal |
| $D_b$    | W/m <sup>2</sup> | wave energy dissipation rate due to breaking      |
| $Diss$   | W/m <sup>2</sup> | dissipation of roller energy                      |

For perpendicular incoming waves  $\cos \theta = 1$ .

The roller energy  $E_r$  represents the amount of kinetic energy in a roller with area  $A$  and length  $L$ , and is defined as

$$E_r = \frac{1}{2} \rho c^2 \frac{A}{L} \quad (2.36)$$

in which:

|     |                |                    |
|-----|----------------|--------------------|
| $A$ | m <sup>2</sup> | area of a roller   |
| $L$ | m              | length of a roller |

The roller energy balance is closed by modelling the dissipation  $Diss$  of roller energy as the power per unit length performed by the shear stress between roller and water surface:

$$Diss = \beta \rho g c \frac{A}{L} = 2\beta g \frac{E_r}{c} \quad (2.37)$$

in which:

|         |                   |                               |
|---------|-------------------|-------------------------------|
| $\beta$ | -                 | slope of the face of the wave |
| $\rho$  | kg/m <sup>3</sup> | mass density of water         |
| $g$     | m/s <sup>2</sup>  | gravitational constant        |

The formulation for the radiation stress in case of perpendicular incoming waves becomes:

$$S_{xx} = \left(2n - \frac{1}{2}\right) E + 2E_r \quad (2.38)$$

in which:

|          |             |   |
|----------|-------------|---|
| $S_{xx}$ | $J/m^2=N/m$ | radiation stress in x-direction through x-plane                   |
| $n$      | -           | ratio of wave group velocity and wave phase velocity ( $=c_g/c$ ) |
| $E$      | $J/m^2$     | wave energy per unit area   |

## 2.5.2 Mean current profile model

The modelling of the mean current profile is done according to Roelvink and Reniers (1994) who use a quasi-3D model in which the effects of wind stress, breaking-induced forcing, surface slope and the wave boundary layer are taken into account. The quasi-3D model is a direct descendant of the model according to De Vriend and Stive (1987) who identify three layers:

- The surface or trough-to-crest layer, which is represented by boundary conditions on the middle layer;
- The middle layer, from the top of the bottom (wave) boundary layer to the mean water level;
- The bottom boundary layer.

The velocity profile is obtained by integrating the following relation for the shear stress:

$$\tau_i = \frac{\rho v_t}{d} \frac{\partial u_i}{\partial \sigma} \quad (2.39)$$

in which:

|          |         |   |
|----------|---------|---|
| $\tau_i$ | $N/m^2$ | shear stress in i-direction with $i = x$ or $y$                     |
| $v_t$    | $m^2/s$ | turbulent viscosity   |
| $u_i$    | $m/s$   | horizontal component of velocity in i-direction with $i = x$ or $y$ |
| $\sigma$ | -       | relative height above bottom ( $z/d$ )                              |

The wave-induced shear stress translates the momentum decay of the surface layer due to wave breaking to the lower layers and provides the boundary condition for the middle layer. The shear stress in the direction of wave propagation, introduced by the surface roller, is given by:

$$\tau_{s,wave} = \frac{Diss}{c} \quad (2.40)$$

|                 |         |   |
|-----------------|---------|---|
| $\tau_{s,wave}$ | $N/m^2$ | shear stress in direction of wave propagation, introduced by surface roller |
|-----------------|---------|---|

The mass flux  $m$  is taken into account as:

$$m = \frac{E + 2E_r}{c} \quad (2.41)$$

The cross-shore depth-mean velocity in the lower layers, necessary for the computation of the cross-shore current profile, must compensate for the mass flux in the surface layer and is therefore given by:

$$\bar{u}_x = -\frac{m}{d} \quad (2.42)$$

### 2.5.3 Wave orbital velocity model

The model of the time-variation of the near-bed velocity (orbital motion) due to non-linear short waves and long waves related to wave groups is based on the concept described in Roelvink and Stive (1989). In short, this model consists of two parts:

- A contribution due to wave asymmetry which is computed using Rienecker and Fenton's (1981) method for monochromatic waves, where the mean wave energy and peak period are used as input for the case of random waves.
- A contribution due to bound long waves based on Sand (1982), and an empirical relationship for the phase of the bound long wave relative to the short wave envelope.

Starting point is a time series of the near-bed velocity in case of regular waves (including wave asymmetry), based on the Rienecker and Fenton model:

$$U_1(t) = \sum_{j=1}^n B_j \cos(j\omega t) \quad (2.43)$$

in which:

$B_j$             m/s            amplitude, such that the difference between the maximum and minimum velocity of asymmetric waves equals the difference in case of monochromatic waves

Next a second velocity time series which is slightly out of phase with  $U_1(t)$  is added, the amplitude modulation on the time scale of a wave group is introduced yielding a time series  $U_2(t)$ :

$$U_2(t) = \sum_{j=1}^n \cos(j\omega t) \varepsilon^j = \sum_{j=1}^n \cos(j\omega t) \left[ \frac{1}{2} (1 + \cos(\Delta\omega \cdot t)) \right]^j \quad (2.44)$$

where:

$$\Delta\omega = \frac{\omega}{m} \quad (2.45)$$

in which:

$m$             -            number of waves in one wave group (set to 7 by default)

The magnitude of  $U_2$  is corrected to  $U'_2$  in such a way, that the third moment of  $U'_2$  equals the third moment of  $U_1$ :

$$U'_2(t) = \left( \frac{\frac{1}{T} \int_0^T U_1^3 dt}{\frac{1}{mT} \int_0^{mT} U_2^3 dt} \right)^{1/3} U_2(t) \quad (2.46)$$

The long wave velocity  $U_3$  is computed according to Roelvink and Stive (1989) such that the wave group related features of a random wave field are represented by a bichromatic wave train and a bound long wave with amplitude  $\xi_a$ :

The second step implies the modelling of a bound long wave. In case of a random wave field the grouping of the short waves will generate bound long waves. The long wave velocity  $U_3$  is computed according to Roelvink and Stive (1989) who assume that the wave-group related features of a random wave field may be represented by a bichromatic wave train with equal amplitudes  $a_m$  and  $a_n$  respectively, and an accompanying bound long wave with amplitude  $\xi_a$ .

$$U_3(t) = \xi_a \frac{\sqrt{gd}}{d} \cos\left(\frac{\omega}{m}t + \varphi\right) \quad (2.47)$$

where:

$$\xi_a = -G_{nm} \frac{a_n a_m}{d} \quad (2.48)$$

$$m_0 \cong \frac{1}{8} H_{rms}^2 = \frac{1}{2} a_n^2 + \frac{1}{2} a_m^2 + \frac{1}{2} \xi_a^2 \quad (2.49)$$

in which:

|            |                |   |
|------------|----------------|---|
| $\xi_a$    | m              | long wave amplitude                                 |
| $\varphi$  | rad            | phase difference between bound wave and short wave  |
| $G_{nm}$   | -              | transfer function according to Sand (1982)          |
| $a_m, a_n$ | m              | amplitude of the bichromatic wave train $a_m = a_n$ |
| $m_0$      | m <sup>2</sup> | variance of the surface elevation                   |

The phase shift  $\varphi$  is calculated according to an empirical expression by Roelvink and Stive (1989):

$$\cos(\varphi) = C_r \left[ 1 - 2 \left( \frac{H_{rms}}{H_{rms,0}} \right)^2 \right] \quad (2.50)$$

in which:

|             |   |   |
|-------------|---|---|
| $C_r$       | - | correlation coefficient between wave envelope and long wave surface variation |
| $H_{rms,0}$ | m | root mean square wave height at seaward boundary of model                     |

Final step is the computation of the time series  $U_4(t)$  of the total orbital velocity, by simply adding the effects due to the short wave envelope and the bound long wave:

$$U_4(t) = U_2'(t) + U_3(t) \quad (2.51)$$

## 2.5.4 Sediment transport model

Separate transport formulations are used for bed load transport, bed load being that part of the load which is in more or less continuous contact with the bed, and suspended transport.

### 2.5.4.1 Bed load transport

By correlation of various non dimensional parameters using a range of datasets of sediment transport in oscillatory flow over horizontal beds, a generalized bed load transport formula

has been obtained by Ribberink (see Van Rijn et al., 1995). This formulation is used supplemented with corrections to account for slope effects on the transport.

The non-dimensional bed load transport vector  $\Phi_{bd}$  is given by:

$$\Phi_{bd}(t) = \frac{q_b(t)}{\sqrt{\Delta g D_{50}^3}} = 9.1 \frac{\beta_s}{(1-p)} \left\{ |\theta'(t)| - \theta_{cr} \right\}^{1.8} \frac{\theta'(t)}{|\theta'(t)|} \quad (2.52)$$

in which:

|               |                     |   |
|---------------|---------------------|---|
| $q_b$         | m <sup>3</sup> /s/m | bed load transport rate including pores |
| $p$           | -                   | porosity of sediment                    |
| $\theta'$     | -                   | dimensionless effective shear stress    |
| $\theta_{cr}$ | -                   | dimensionless critical shear stress     |
| $\beta_s$     | -                   | slope factor                            |

The instantaneous dimensionless effective shear stress  $\theta'$  is due to current and waves and only represents the sediment forcing, as a ratio of the flow drag-force on the grains and the under water weight of grains, and not the form drag (induced by bed forms).

$$\theta'(t) = \frac{1/2 \rho f'_{cw} |u_b(t)| u_b(t)}{(\rho_s - \rho) g D_{50}} \quad (2.53)$$

|           |     |   |
|-----------|-----|---|
| $f'_{cw}$ | -   | weighted friction factor, accounting for both wave and current friction |
| $u_b$     | m/s | near bottom velocity (at top of bottom layer)                           |

The parameter  $\theta_{cr}$  is the non dimensional critical shear stress, representing the threshold of motion of sand grains. This threshold parameter is calculated according to the classical Shields curve as modelled by Van Rijn (1993) as a function of the non dimensional grain size  $D^*$ .

The slope factor  $\beta_s$  increases the transport rates in the case of down-slope transport and decreases the transport rates for up-slope transports:

$$\beta_s = \frac{\tan \varphi}{\tan \varphi + \frac{dz_b}{ds}} \quad (2.54)$$

|                   |     |                                 |
|-------------------|-----|---------------------------------|
| $\varphi$         | rad | angle of repose of the sediment |
| $\frac{dz_b}{ds}$ | -   | bottom slope                    |

#### 2.5.4.2 Suspended load transport

The suspended sediment transport rate  $q_s$  can be computed from the vertical distribution of fluid velocities and sediment concentrations:

$$q_s = \int_a^{d+\eta} VCdz \quad (2.55)$$

in which velocity  $V$  and concentration  $C$  can be divided in an averaged and a fluctuating component:

$$V = v + \tilde{v} \text{ and } C = c + \tilde{c} \quad (2.56)$$

in which:

|             |                   |                                     |
|-------------|-------------------|-------------------------------------|
| $q_s$       | kg/s/m            | suspended sediment transport rate   |
| $\tilde{v}$ | m/s               | fluctuating velocity component      |
| $\tilde{c}$ | kg/m <sup>3</sup> | fluctuating concentration component |

Substituting Eq. (2.56) in Eq. (2.55) and averaging over time and space yields:

$$\bar{q}_s = \int_a^d vcdz + \int_a^d \tilde{v}\tilde{c}dz = \bar{q}_{s,c} + \bar{q}_{s,w} \quad (2.57)$$

in which:

|           |        |  |
|-----------|--------|--|
| $q_{s,c}$ | kg/s/m | current related suspended sediment transport |
| $q_{s,w}$ | kg/s/m | wave related suspended sediment transport    |

The wave related suspended sediment transport is assumed to be small as compared to the current related suspended sediment transport. The suspended load transport in volume per unit time and width inclusive pores is therefore computed as:

$$q_{s,c} = \frac{\int_a^h vcdz}{(1-p)\rho_s} \quad (2.58)$$

### 2.5.4.3 Time averaged concentration profile

Usually, the time averaged convection diffusion equation is applied to compute the equilibrium concentration profile in steady flow, but here it is assumed that it is also valid for wave related mixing. This equation reads:

$$w_{s,m}c + \varphi_d \mathcal{E}_{s,cw} \frac{dc}{dz} = 0 \quad (2.59)$$

in which:

|                      |                   |   |
|----------------------|-------------------|---|
| $w_{s,m}$            | m/s               | fall velocity of suspended sediment in a fluid sediment mixture |
| $\varphi_d$          | -                 | damping factor dependent on the concentration                   |
| $\mathcal{E}_{s,cw}$ | m <sup>2</sup> /s | sediment mixing coefficient for combined current and waves      |

For combined current and wave conditions the sediment mixing coefficient is modelled as:

$$\mathcal{E}_{s,cw} = \sqrt{(\mathcal{E}_{s,w})^2 + (\mathcal{E}_{s,c})^2} \quad (2.60)$$

in which:

|                     |                   |                                    |
|---------------------|-------------------|------------------------------------|
| $\mathcal{E}_{s,c}$ | m <sup>2</sup> /s | current related mixing coefficient |
| $\mathcal{E}_{s,w}$ | m <sup>2</sup> /s | wave related mixing coefficient    |

The convection diffusion equation is solved by numerical integration from a near bed reference level  $a$  to the water surface. The reference concentration  $c_a$  is given by:

$$c_a = 0.015 \rho_s \frac{D_{50}}{a} \frac{T^{1.5}}{D_*^{0.3}} \quad (2.61)$$

in which:

|       |   |  |
|-------|---|--|
| $T$   | - | dimensionless bed shear stress parameter |
| $D_*$ | - | dimensionless particle parameter         |

The bed shear stress parameter is defined as follows:

$$T = \frac{\tau'_{b,cw} - \tau_{b,cr}}{\tau_{b,cr}} \quad (2.62)$$

in which:

|                |                |  |
|----------------|----------------|--|
| $\tau_{b,cr}$  | $\text{N/m}^2$ | time averaged critical bed shear stress according to Shields |
| $\tau'_{b,cw}$ | $\text{N/m}^2$ | time averaged effective bed shear stress                     |
| $\tau_{cr}$    | $\text{N/m}^2$ | critical shear stress  |

## 2.5.5 Bed level change model

After the computation of the transport rates along the profile, the bed level changes are computed from the depth integrated mass balance:

$$\frac{\partial z}{\partial t} + \frac{\partial q_{bot+sus}}{\partial x} = 0 \quad (2.63)$$

in which:

|               |                                |  |
|---------------|--------------------------------|--|
| $q_{bot+sus}$ | $\text{m}^3/\text{s}/\text{m}$ | combined bed load and suspended transport rate including pores |
|---------------|--------------------------------|--|

## 2.5.6 Extrapolation method for dry profile

Around the waterline not modelled and not yet understood physical processes take place. For this reason is landward from a more or less arbitrary last transition point an extrapolation method applied in stead of the cross-shore transport concept.

### 2.5.6.1 Location transition point

The formulation of the location of the transition point has been changed during this study.

Originally, the location of this transition point was described by a minimum depth:

$$h_{\min} = g \left( \frac{T_p}{T_{dry}} \right)^2 \quad (2.64)$$

The constant  $T_{dry}$  has to be specified by the user. This implies for constant  $T_{dry}$ ,  $h_{\min}$  is dependent on  $T_p$ . For mild bed slopes, the location of the transition point will be strongly

dependent on  $T_p$ . A larger  $T_p$  implies a larger  $h_{min}$ , which means a more seaward transition point with lower transport rates. Extrapolation from this more seaward point appeared to cancel out the effect of the higher  $T_p$ , so all peak wave periods had approximately equal erosion volumes.

During a dune erosion computation, with constant wave conditions and water level, the location of the transition point will shift in time. Due to bottom change (reduced water depth) the point has to shift seaward to obtain again the minimum depth  $h_{min}$ .

Mainly because of the strong dependency of the location of the transition point on the  $T_p$  is chosen to set, similar to DUROSTA, that location to a quarter of the local wavelength from the waterline. Also according this method the location is dependent on the wave period, but not as strong as in the above mentioned method.

Similar to DUROSTA (see Section 2.4.6.1), during a computation, the transition point will shift landward by two mechanisms.

### 2.5.6.2 Extrapolation method

The transport landward from the transition point is, similar to DUROSTA, described by the transport in that point  $S^*$  times a wave run up related reduction factor.

$$S(x) = S^* \left[ \exp\left(-2 \frac{z^2}{z_s^2}\right) - \sqrt{\frac{\pi}{2}} \left(\sqrt{2} \frac{z}{z_s}\right) \left(1 - \frac{2}{\pi} \int_0^{\sqrt{2} \frac{z}{z_s}} \exp(-x^2) dx\right) \right] \quad (2.65)$$

in which:

|       |                                  |   |
|-------|----------------------------------|---|
| $S$   | $\text{m}^3/\text{m}^1/\text{s}$ | (time-averaged) depth-integrated sediment transport per unit width                                      |
| $S^*$ | $\text{m}^3/\text{m}^1/\text{s}$ | (time-averaged) depth-integrated sediment transport per unit width in the most landward computing point |
| $z_s$ | m                                | significant wave run up level above mean water level  |

The significant wave run up level is defined as:

$$z_s = 0.5T_p \sqrt{gH_s} \tan \beta \quad (2.66)$$

See also Walstra and Steetzel (2003).

### 2.5.7 Settings

The model UNIBEST-TC is not only meant for dune erosion cases and so a number of parameters have to be set based on this particular situation. Most of the settings which differ from the default settings are described in Section 5.1.1, but a few are very basic and so also included here. The extrapolation method is set to: 'Vertical + wave run up' which means the extrapolation as described in Section 2.5.6. Furthermore is the parameter OPTDRY set to 2 which is meant to compute the transition point at a quarter of the local wave length seaward from the waterline.

## 2.6 Comparison DUROSTA and UNIBEST-TC

Looking to the theoretical backgrounds of the models DUROSTA and UNIBEST-TC, as described in Sections 2.4 and 2.5, a number of similarities and differences can be called. This section gives a brief overview of the most outstanding characteristics of both models.

### 2.6.1 Similarities

- In both models, ENDEC is applied to compute the wave height decay.
- The suspended transport is in both models described by the depth integrated product of time-averaged velocities and time-averaged sediment concentrations.
- The extrapolation over the dry profile is, with the *used settings* of UNIBEST-TC, equal for both models.
- The location of the transition point is, with the *used version* of UNIBEST-TC, equal for both models.

### 2.6.2 Differences

- DUROSTA computes the cross-shore transport based on only suspended transport. This implies that the (often landward directed) bottom transport is neglected. For the breaker zone and short time scales this neglect is considered acceptable, but outside the breaker zone it is not, which implies an under-estimate of the landward directed contribution of the cross-shore transport. UNIBEST-TC takes both suspended and bottom transport into account. Inside the breaker zone the bottom transport takes a minor role with respect to the suspended transport, but outside the breaker zone it is an important contribution.
- In DUROSTA a varying time step is used. With a maximum time step and profile change the time step is adapted to the present profile change. UNIBEST-TC makes use of a constant time step. This time step has to be sufficiently small to keep the computation stable during the fastest profile change. However, during (big) parts of the simulation the process is slower and a bigger time step would be sufficient. Because of this a UNIBEST-TC computation takes (much) more time with respect to a comparable DUROSTA computation.



## 3 Analysis of physical model research

This chapter is about the physical model data which are used for this research. Central is the research carried out by WL | Delft Hydraulics in the end of 2003 which was primary focussed on the effect of the wave period on the amount of dune erosion. These small scale guide tests were meant to verify the wave period effect and to create a purposeful strategy for necessity and set up of further (physical) research at larger scale ( $n_d = 5$  to 7.5).

First the main conclusions of the physical model research are presented. After that the scale choice comes up briefly. Then the measurements are described. Finally the test results are presented and considered. For practical reasons the test series was split up in two series with different scales. These two series are considered separately as well as related to each other.

### 3.1 Background

The above called research was done in the Schelde flume of WL | Delft Hydraulics and in Dutch reported by Coeveld and De Vroeg (2004). The test program was based on a desk study of Steetzel and Van de Graaff (2003).

Seven tests were carried out (including one extra repeat test) using two different depth scales. Most important conclusion was that the test with the longest peak wave period showed the biggest dune erosion volume. In the tests with depth scale  $n_d = 30$ , the peak wave period increased with 42 % from  $T_p = 10.0$  s (prototype) up to  $T_p = 14.2$  s and the erosion volume, after six hours model time, with approximately 25 %. In the tests with depth scale  $n_d = 40$ , the peak wave period increased with 34 % from  $T_p = 14.2$  s (prototype) up to  $T_p = 19.0$  s and the erosion volume, after three hours model time, with approximately 18 %.

#### 3.1.1 Scale choice

An important assumption of the research was to refer (and partly repeat, to confirm) to earlier research which was also done by WL | Delft Hydraulics (1982) in the Schelde flume. The recent research was carried out in a new Schelde flume with the same dimensions (length  $\approx 50$  m, width = 1.0 m and depth = 1.2 m). The problem arose that in 1982 they used a scale factor as small as possible, so the hydraulic conditions in the facilities were optimally utilised. Now the aim was to create more severe conditions which only could be done on a smaller scale. The limiting factor was the wave generator which could not create that long waves (Steetzel and Van de Graaff, 2003) on the original scale.

As a consequence it was decided to split up the research in two series of tests with two different scales. First series of three tests (series A, depth scale factor  $n_d = 30$ ) to verify the earlier research and extend to the present limits of the facilities. Second series of another three tests on smaller scale (series B, depth scale factor  $n_d = 40$ ) to extend to the desired range of wave periods. For both series a distortion of 1.68 w.r.t. to the prototype reference profile was applied.

The test with the longest waves on scale  $n_d = 30$  was carried out with approximately the same prototype conditions as the one with the shortest waves on scale  $n_d = 40$ . This was done to be able to link these two series to each other.

The both used profiles are represented in Figure 3.1 and 3.2. The slopes are given in rounded values.

### 3.1.2 Test program

An overview of the program with the desired wave conditions is given in Table 3.1. This table is based on Steetzel and van de Graaff (2003). Remarkable are the desired wave heights at the wave board for the tests on scale 40 (T11, T12 and T13) which are equal to the deep water values. According to the computations of Steetzel and van de Graaff (2003) these wave heights (at the wave board) were hardly different from the deep water values which was reason to set them equal.

After carrying out all the tests the used sediment seemed to contain less mud. To check a possible effect of this 'cleaner' sediment on the amount of dune erosion test T02a, which is a repeat of T02, was carried out at the end. Test T02a was carried out with the same wave conditions as T02 but with profile measurements at only two moments in time. The comparable erosion volumes showed reasonable similarity. For the sake of clarity (to prevent confusion) test T02a is in general not dealt with in this report.

The tests of both series were divided in time intervals with increasing duration:

- A 0 to 0.1 h (6 minutes)
- B 0.1 to 0.3 h (12 minutes)
- C 0.3 to 1.0 h (42 minutes)
- D 1.0 to 3.0 h
- E 3.0 to 6.0 h

For test T12 and T13 interval E was not carried out so these tests had a duration of 3 hours.

## 3.2 Measurements

This section gives a brief description of the following measurements:

- The profile
- The wave conditions
- The flow velocities of the water
- The sediment concentrations
- The grain size distribution of the sediment
- The temperature of the water
- The fall velocity of the sediment in water

For these measurements the method and/or important remarks are described. Furthermore is given which measurements or values are assumed as representative to use as input (or reference). In addition, it will be given which measurements are assumed as representative to compare with results of computations.

For a more detailed description of measurement methods and results is referred to Coeveld and De Vroeg (2004).

### 3.2.1 Profiles and erosion volumes

At the start of each test the initial profile is measured. Next the profile is measured after each time interval (see Section 3.1.2).

The profile measurements were carried out with three profile followers driving simultaneously from the dune to the wave board (up to down). As a representative profile is assumed, following Coeveld and De Vroeg (2004), the average of the three measured profiles. This implies that possible crosswise non-uniformity is neglected. In the present study some attention was paid to possible consequences. Comparing the three separate profiles, differences are visible. In most cases two profiles are approximately equal and one side profile is a little lower. This could be due to measurement inaccuracy. It is not proved that there was a structural crosswise non-uniformity. Erosion volumes derived from each profile separate are slightly different from each other but there is no consistent relation found between the vertical position of the profile and the erosion volume. Generally spoken there is no good reason found to suppose that another assumption, than the average of the three profiles, gives more accurate results.

Looking to the cross-shore sediment balance over the whole flume with respect to the initial profile of that particular test, in all cases a surplus is found (varying from 15 to 35 % of the erosion volume). The balance between the erosion volume and the near shore depositing zone results however still in deficiency (varying from 10 to 75 % of the erosion volume). For the sediment surplus over the whole flume some possible explanations are: rough sample interval further off-shore, ripples (difficult to measure) and non-uniform crosswise profile. In addition, sand brought in suspension (over the entire profile) deposits probably less densely (profilers made tracks in the bed). Another reason could be a denser dune than the deposited sand in the recent tests due to the use of needle vibrators. Furthermore, in the tests sometimes a lean-over of the dune originated which could not be measured exactly with the applied method. However, by extra profile measurements, after taking away the lean-over at the end of the test, it is still not possible to close the balance (only a reduction of the surplus of about 1 or 2 % is found).

For test T01 the sediment balance of each of the three profiles a measurement has been considered. The slightly different profiles give slightly different sediment surpluses but it is not clearly consistent to the vertical position of the profile.

The real erosion volume (above storm surge level) is assumed as representative and not the deposit volume. The most important reason is that in the erosion zone above the water level were no ripples, which increases the accuracy of the profile follower. In addition, the deposit zone is less clear to define and introduces more inaccuracies.

Summarizing, as profile measurement the average of the three simultaneous profile measurements is taken into account and the erosion volumes will be used as presented in Coeveld and De Vroeg (2004). The extra erosion volumes which are measured after taking away the lean-over for some tests are not taken into account among other things because it was not done for all tests and if done, only for the end measurement.

### **3.2.2 Waves**

#### **3.2.2.1 Locations**

The water surface elevation was measured at six locations. For each interval in each test a separate surface elevation signal is measured.

Three of the wave height meters were located close together near the wave board. These are meant to derive the incident wave characteristics. The other three wave height meters are located at approximately 13 m, 10 m and 8.4 m prototype water depth (with respect to water level NAP + 5 m). For detailed information about the locations of the wave height meters is referred to Coeveld and De Vroeg (2004).

### 3.2.2.2 Re-analysis of measurements

For each time interval of each test (see Section 3.1.2) a separate signal was measured and from that the wave characteristics were derived. These different measurements show variations in time. Near the wave board, the (incident) wave characteristics vary in a limited range. However, more near the dune, a clear decreasing wave height in time is visible, due to bottom changes.

To derive representative wave characteristics a sufficient number of waves is required, preferably at least 1000. However, the first short periods contain much less than 1000 waves. Furthermore, it is desirable (from a practical point of view) to simulate the tests with constant wave conditions, and with that the question arise which of the four or five measurements per test are representative for the whole test.

To solve this problem the measured signals are pasted behind each other which results for each test in one wave signal (for each location). The wave characteristics, which have been derived from these signals, are a sort of time-averaged over the whole test. Figure 3.3 shows for two locations of test T01 the original (each time interval separate) and the combined wave heights (averaged over whole test). This figure is only meant as an example. In addition, the represented measurement locations are the locations which have been used as tuning target for the simulations presented in the following chapters. The wave heights as derived from the surface elevation signal of the entire tests are presented in Table 3.2. In addition, the accompanying frequency boundaries are presented.

The computations with DUROSTA and UNIBEST-TC are based on these time-averaged wave characteristics. In the next chapter some reasons for neglecting the time varying wave conditions come up.

In Appendix A a brief description is given of the applied method to combine the successive wave signals and to re-analyse these by AUKE-PC.

### 3.2.2.3 Wave period

Considering the (not presented) energy density spectra of the different wave height measurements, is visible that for measurements closer to the dune a peak is less clear visible in the spectra. This is due to deformation of the spectrum as a consequence of breaking waves.

In Figures 3.4 and 3.6 the measured peak wave period  $T_p$  over the cross-shore profile is represented for both test series. In all cases an increasing  $T_p$  going landward is visible. One can imagine that the short (relatively) high waves (high frequencies) break first and so energy is transported from high to lower frequencies which implies an increasing wave period. Going to the dune, the peak of the spectrum becomes lower due to energy dissipation. In addition, a second low frequent peak originates (surf beat). In the most landward measurement point of the tests T13 and T12 (Figure 3.6), this low frequent peak prevails the higher frequent peak. That is the reason that these peak wave periods are 'suddenly' extremely high.

One can conclude that the peak wave period is not a good measure to describe the development of ‘the’ wave period in shallow water.

Another (spectral) measure for the wave period is  $T_{m-1,0}$ , defined as:

$$T_{m-1,0} = \frac{m_{-1}}{m_0} \quad (3.1)$$

in which the  $n^{\text{th}}$  moment of the frequency spectrum:

$$m_n = \int_{f_{\min}}^{f_{\max}} f^n S(f) df \quad (3.2)$$

|                      |                        |  |
|----------------------|------------------------|--|
| $T_{m-1,0}$          | s                      | wave period based on zeroth ( $m_0$ ) and first negative ( $m_{-1}$ ) moment |
| $f$                  | Hz                     | frequency  |
| $S$                  | $\text{m}^2/\text{Hz}$ | energy density   |
| $f_{\min}, f_{\max}$ | Hz                     | frequency boundaries   |

The frequency boundaries are presented in Table 3.2.

Figures 3.5 and 3.7 show the measured  $T_{m-1,0}$  in space for both test series. Especially for the longer (prototype) wave periods the increase of the  $T_{m-1,0}$  going landward is less extreme/more stable compared to  $T_p$ .

The incident wave characteristics (A-series  $x = 9.39$  m and B-series  $x = 3.00$  m) show the best estimate of the desired peak wave periods (Table 3.1). In ENDEC (used by DUROSTA and UNIBEST-TC) a changing peak wave period in space is not taken into account.

For the computations the peak wave period  $T_p$  of the incident wave signal (combination of three near wave board measurements) is used as input. For this are three reasons:

- The wave period of the incident measured wave signal was considered as target for the wave period tuning in the physical model.
- Near the wave board the spectrum is still not deformed and so a clear peak is visible in the spectrum at that point.
- The increasing wave period in space is not simulated by the wave module ENDEC. If this phenomenon has a measurable effect on dune erosion then it is likely that this was taken into account by the calibration of the entire model DUROSTA. This means in fact that the model is not meant to impose a near shore wave period. Important is in this case to keep in mind for which wave periods the model DUROSTA was calibrated (mostly for prototype  $T_p = 12$  s).

### 3.2.3 Flow velocity

Flow velocities were electromagnetically measured at different locations, varying both in cross-shore as in vertical position. Measurements were carried out at two cross-shore locations simultaneously.

Each measured velocity vertical consists out of three points. First the velocity at 2 cm above the bed was measured, next just below the approximated wave trough and finally in between. Each measurement lasted 10 minutes, so the complete vertical covers about half an hour time.

For further information is referred to Coeveld and De Vroeg (2004).

### 3.2.4 Sediment concentration

To measure the sediment concentration the method of transverse suction was applied. Based on the amount of sediment water mixture and the sediment volume in that particular sample the concentration was derived using calibration factors.

For locations and description of the method of sediment measurements is referred to Coeveld and De Vroeg (2004), for detailed information about the determination of the used calibration factors is also referred to Den Heijer (2004).

### 3.2.5 Grain size

For all tests the same sediment is used. At different locations and specific points of time in total 64 sediment samples were taken and sieved. For each sieved sample the characteristic values  $D_{10}$ ,  $D_{50}$  and  $D_{90}$  are derived. According to Coeveld and De Vroeg (2004) no clear dependency of time or space is visible. That supports the assumption to handle with the average  $D_{10}$ ,  $D_{50}$  and  $D_{90}$  of all these measurements as being representative for the used sediment. Table 3.3 summarizes the measurements.

### 3.2.6 Water temperature

For all tests the water temperature is measured every period. The average temperature per test is given in Table 3.4.

### 3.2.7 Fall velocity

From seven bottom sediment samples the fall velocity in water was measured. For each sample the fall velocity  $w_s$  ( $w_{s50}$ ) of the sediment is derived. The average value of those seven numbers is taken as representative fall velocity:  $w_s = 0.0061$  m/s.

## 3.3 Results for separate series

Although for the systematic research the whole range of (prototype) wave periods is most interesting, still the series separate can give insight in the effect of the wave period and comparison is more straightforward.

### 3.3.1 A-series

In Figure 3.8 the erosion volumes of the A-series (test T01 – T03,  $n_d = 30$ ) are represented in two different ways.

Looking to the top subplot, where the measured erosion volumes are plotted as function of model time, one can see that from 1 hour model time and upwards the erosion volumes are clearly increasing with increasing peak wave period. The measure points at 0.1 h and 0.3 h show that relation less convincingly. An explanation can be that the erosion in the physical model takes place by shelves, possibly because of cohesion. As a consequence of this sort of step by step erosion it makes difference whether the profile measurement takes place just before or just after the erosion of a shelf. Because of the high erosion rate and short measurement intervals in the first hour of the test these effects can play an important role.

Later on the erosion rate is much smaller, and the longer measurement intervals enable more averaging.

In the bottom subplot of Figure 3.8, the measured erosion volumes are plotted as function of the number of (incident) waves. The tests with longer wave periods contain, for a constant test duration, fewer waves. From this point of view the lines are more diverging, compared to the top subplot.

Figure 3.9 shows the relative erosion volumes of the tests of the A-series with respect to the test with the shortest wave period (test T03; prototype  $T_p = 10.2$  s). These plots are, similar to Figure 3.8, as function of time and as function of number of waves represented.

Figure 3.9 also makes clear that from 1 hour and upwards the erosion volumes are clearly increasing with increasing wave period. Furthermore is visible that the relative erosion volumes as function of the number of waves give much higher values compared to the top subplot.

### 3.3.2 Comparison with earlier research

Test T01 (A-series) can be compared with T04, T15 and T20 of M1819-I (WL | Delft Hydraulics, 1982). The erosion volume development of these four tests is plotted in Figure 3.10. The plot makes clear that the development of the erosion volumes is different but the final results are rather close together. This is another indication of decreasing spreading with longer test duration. A remark could be made that from hearsay it is known that the lean-over of the dunes in the M1819 tests was redistributed to vertical by hand. By doing this, no erosion volume is neglected which results in larger measured erosion. In addition, in fact the dune foot is replaced seaward, which enables more wave attack. These can be reasons for high erosion volumes at the beginning of the tests when the lean-over most occurs.

### 3.3.3 B-series

Figures 3.11 and 3.12 represent the erosion development of the B-series (test T11 – T13,  $n_d = 40$ ) in two different ways, similar to Figures 3.8 and 3.9.

The top subplots show more or less the same behaviour like the A-series: the further in time, the more clearly the positive wave period dependency. In this case it is even visible that around the measure points 0.1 h and 0.3 h there is a negative relation between wave period and erosion volume. Furthermore the point at 1 h model time does not give a consistent relation between wave period and erosion volume. So in this series, which apart from test T11 is carried out for only 3 hours a test, only the measurement points at 3 h show a more or less consistent relation between wave period and erosion volume.

Considering the wave conditions of series B, the wave periods in the model are in fact not much longer but the wave heights are lower compared to series A, obviously because of the smaller scale. This results in smaller erosion volumes and as a consequence smaller differences between the tests. Assuming approximately equal absolute accuracy implies lower relative accuracy.

Remarkable is that the erosion volumes at 0.1 h and 0.3 h are (absolute) equal or even bigger than the corresponding points of the A-series.

### 3.4 Results after combining two test series

Because up to now a peak wave period  $T_p = 12.0$  s is used as normative, it is useful to know the influence of the wave period with respect to the reference case  $T_p = 12.0$  s. Since there is only for depth scale  $n_d = 30$  such a reference test available, scale translation is necessary to give an overview of the complete tested wave period range.

#### 3.4.1 Formation of continuous series

Figure 3.13 gives an overview of the erosion volumes of both test series in one plot as a function of model time. The erosion volumes in the tests with depth scale  $n_d = 40$  are smaller due to the smaller scale and so also in absolute sense less severe wave attack.

According to Vellinga (1986) the results of model tests, like erosion volume  $A$  profile steepness  $S_f$  (distortion) and time  $t$ , can be converted to prototype values with following relations:

$$n_A = n_t n_d = n_d^2 \left( \frac{n_d}{n_w^2} \right)^\alpha \quad (3.3)$$

$$n_{Sf} = \left( \frac{n_d}{n_w^2} \right)^{-\alpha} \quad (3.4)$$

$$n_t = n_d^\beta \quad (3.5)$$

with  $\alpha = 0.28$  and  $\beta = 0.5$ .

All of the tests, so both of the depth scales, were carried out with a model distortion of 1.68. However, according to the following relation obtained from Vellinga (1986) the distortion is dependent on depth scale  $n_d$  and grain size scale  $n_w$ .

$$\frac{n_t}{n_d} = \left( \frac{n_d}{n_w^2} \right)^\alpha \quad (3.6)$$

This means with the same grain size, which was the case, the profile with depth scale  $n_d = 40$  should be more distorted, so steeper, than the one with  $n_d = 30$ . Because the absolute distortion was equal, depth scale  $n_d = 30$  was relatively more distorted than  $n_d = 40$ .

A relatively more distorted profile results in more erosion for two reasons (Steetzel, 1996):

- For pure geometrical consideration a steeper cross-shore profile gives more erosion
- Furthermore a steeper cross-shore profile will result in relatively more severe wave attack in the zone where the erosion profile will be formed

After applying Eq. (3.3) and (3.5) to the B-series, the erosion development of all tests is plotted in Figure 3.14. The translated tests are marked with a '\*'. This graph shows especially from 3 hours model time and upwards that test T11\* is closer to T01 than to T02, although the opposite should be true. Possibly the erosion volumes of the converted B-series are too low because the relative steepness difference is not taken into account. Still, for the time being the scale factor of Eq. (3.3) will be used to convert the erosion volumes of the B-series into depth scale 30.

Up to one hour model time and even, but to a less extent, one hour itself T11\* gives too high erosion volumes compared to T02. This is a logical result of multiplying equal or even higher erosion volumes (see Section 3.3.3) by a scale factor bigger than one.

### 3.4.2 Relative increase of erosion with respect to reference case

With the more or less continuous series from Section 3.4.1 it is possible to make a rough estimate of the relative dune erosion volume with respect to the basic case: prototype  $T_p = 12$  s.

Figure 3.15 gives a visualisation of the relative increase of erosion volume. In this case for a number of moments in time (storm durations), the relative increase is obtained by linear interpolation of Figure 3.14 (at that particular moment of model time). The reference erosion (model  $T_p = 2.19$  s) is for each point of time obtained by linear interpolation of test T01 ( $T_p = 2.27$  s) and T03 ( $T_p = 1.87$  s). Figure 3.15 shows very clear the increasing consistency with increasing model time. Apart from test T11\*, the points of 2.6 h and 3.5 h in Figure 3.12 are very regular positioned.

From a prototype point of view, it is desirable to know something about the increase of the erosion volume around the characteristic storm duration (approximately 1 hour model time). Taking account of the scale effects (especially in the first part of the tests) and the uncertainties it is not advisable to pay too much attention to first part of the tests. Based on Figure 3.15 a rough estimate of the increase of the erosion volume above storm surge level for  $T_p = 18.4$  s with respect to  $T_p = 12$  s is 25 to 35%.



## 4 DUROSTA computations

For a short description of the model itself reference is made to Section 2.4, for a more complete description and background of the model is referred to Steetzel (1993).

In this section the computations with DUROSTA are described. The physical model tests of WL | Delft Hydraulics (Coeveld and De Vroeg, 2004) are simulated. The differences and similarities with the model tests are the central issue.

To make a proper comparison between DUROSTA and the physical model tests it is necessary to generate model input which represents as good as possible the actual situation in the flume. Assuming a certain grid, which is described first, for each test an initial profile can be generated based on the profile measurements. With these cross-shore profiles, simulations have been carried out in different ways. First all tests are simulated by imposing the measured wave height near the wave board (A-series:  $x = 9.39$  m; B-series:  $x = 3.00$  m). With default settings of DUROSTA this approach resulted especially for the tests with a longer wave period in an overestimate of the wave height near the dune compared with the measurements.

In the next series of computations the measured wave height closer to the dune (A-series:  $x = 31.99$  m; B-series:  $x = 34.82$  m) is used as a tuning target. With this approach in most cases the wave propagation over the profile is complete different.

Finally, computations are carried out with for each test a specific breaker index to fit the computed wave propagation at the wave board as well as near the dune.

These approaches lead to different results and different conclusions on how the model responds to varying wave periods.

### 4.1 Computation set up

In this section the grid and initial profile realization comes up which have been applied for all the computations presented in Section 4.2.

#### 4.1.1 Grid

The grid has to be sufficiently fine for wave propagation over the profile as well as for the profile development. This leads to a grid with decreasing space step going to the dune, taking into account the maximum allowed number of 250 steps. For all computations the same grid is applied with space steps of 0.5 m (seaward boundary) decreasing to 0.1 m (near dune).

#### 4.1.2 Initial profile

The dataset of the measured (initial) profiles consists of 4500 points which is much more than the number of computational grid points. To generate the input initial profile for each test that particular measured profile is converted to the computational grid. In order to do this, only the measurement points which corresponded with computational grid points have

been taken into account. As a consequence small scale irregularities are smoothed but the bigger scale shape of the measured profile is still present.

## 4.2 Simulations

In this section, for different approaches of imposing the wave heights, simulations of the tests are presented. For each simulation the wave propagation and the computed erosion is discussed, with respect to the measurements. With these different approaches the behaviour of DUROSTA for varying wave periods is illustrated.

An example of an input file is presented in Appendix B.

### 4.2.1 Tuning near wave board

In the below presented simulation the wave heights are tuned to the measured incident waves. That means at location  $x = 9.39$  m for the A-series and at  $x = 3.00$  m for the B-series. DUROSTA is applied with default settings.

#### 4.2.1.1 Wave propagation

Due to the changing of the cross-shore profile during the test, the wave propagation is affected. However, as becomes clear from Figure 4.1, in the model this change of the wave propagation occurs mainly landward from the most landward wave height meter. So, with constant wave conditions the computed wave propagation will not significantly change in time for at least the measurement locations. Among others, this is also a reason to use the wave characteristics of the whole tests (see Section 3.2.2.2) to compare with.

In Figure 4.2 the wave propagation for the three tests, with different wave periods, of the A-series is presented. From now on the computed wave height developments are plotted for  $t = 0$  and measurement points are based on the wave signal of the whole tests. The cross-shore profile is the desired initial profile. The wave height at the seaward boundary is for each of the three tests chosen to impose the measured wave height at location  $x = 9.39$  m. At the other measurement locations, differences are visible between the measured and the corresponding computed wave heights. The line for T01 (prototype  $T_p = 12.4$  s) shows the best reproduction of the corresponding measurements points. Near the dune for T02 (prototype  $T_p = 14.9$  s) an over-estimation and for T03 (prototype  $T_p = 10.2$  s) is under-estimation is visible for the computed wave height compared to the corresponding measurements. Generally spoken, the measured wave heights (for the different wave periods) converge more, going landward, compared to the computed wave propagation.

Figure 4.5 shows the wave propagation for the B-series. The set up of this figure is similar to Figure 4.2. Again the wave heights are imposed to fit the measurements near the wave board ( $x = 3.00$  m). In this case test T11 (prototype  $T_p = 14.2$  s) gives also near the dune a good reproduction of the measurements. However, for the other two tests (prototype  $T_p = 16.2$  s and 18.4 s) the wave heights near the dune are overestimated with respect to the measurements.

### 4.2.1.2 Erosion development

With the wave conditions as represented in Figure 4.2, the resulting dune erosion volume as a function of time is showed in Figure 4.3. In the top subplot the basic computation result is multiplied by 1.12, which is a correction for a systematic under-estimation, among others due to porosity difference between the erosion and deposition zone, determined by Steetzel (1993). In the research of Coeveld and De Vroeg (2004) the sediment balance over the whole flume resulted in a surplus (see also Section 3.2.1). However, the balance over the erosion and deposition zone resulted in a deficiency, in most cases even (far) more than 12 % (of the measured erosion volume). Nevertheless, the computed erosion volumes times 1.12 is dealt with as ‘the’ DUROSTA result.

In the bottom subplot of Figure 4.3 shows the measured erosion volumes and for each test a fit of the computed erosion. To fit these lines the above used factor 1.12 is replaced by another so-called fit factor. These fits are based on the erosion volumes after 3 and 6 h model time. The first few points (0.1, 0.3 and 1 h) are left out of consideration in this method, among others because these points are less reliable than the last few points. The fact that in most cases the first few points show good correspondence with the fitted line is promising. The fit factor is used as a measure for the under-estimation for that particular simulation with respect to the accompanying test.

Considering Figure 4.3, a number of aspects are visible. First of all, the top subplot shows clearly an increasing computed dune erosion with an increasing wave period. Furthermore, the fit factors in the bottom subplot are all larger than 1.12, which means under-estimation with respect to the measured erosion volumes. Although not all of the fit factors are equal to each other, no clear trend is visible.

The set up of Figure 4.6 is similar to Figure 4.3 but in this case the B-series is represented. Because the duration of test T12 and T13 was only 3 h, the fits in the bottom subplot are in these cases based on the erosion volume at  $t = 3$  h. In the top subplot the lines of T11 (prototype  $T_p = 14.2$  s) and T13 (prototype  $T_p = 16.2$  s) are close together, which in the bottom subplot turns out in a higher fit factor for T13. Differences in fit factors also occur for the B-series but again, no clear trend is visible. Remarkable is that the over-estimation of the wave height near the dune for tests T12 and T13 does not result in a significant over-estimation (or less under-estimation) of the erosion volume.

### 4.2.1.3 Cross-shore profiles

Figure 4.4 shows for the three tests of the A-series parts of the initial profiles, combined with the final computed as well as measured profiles. Here the basic computational result is showed, so the additional 12 % erosion volume is not taken into account.

In all of the plots of Figure 4.4 the under-estimated erosion volume with respect to the measurements is visible. The computed final slope of the dune front is approximately equal to the initial slope. This in contrast to the almost vertical (or even leaned over) measured final slope. Also differences occur between the computed and measured deposition zones. In the case of test T01 the measured deposition zone is best reproduced by the computation.

Similar to Figure 4.4 in Figure 4.7 the profiles of the B-series are showed. Roughly the same remarks can be made about these plots. A difference is that in this case the sediment balance for the measured profiles is far out of equilibrium (much more erosion than sedimentation).

However, large amounts of eroded sediment are transported further offshore, which is outside the range of these plots.

## 4.2.2 Tuning at NAP - 5 m

By imposing the wave height near the wave board, as presented in Section 4.2.1, in most cases the computed wave heights differ from the measurements near the dune. Although the erosion results of previous simulation were not that bad, maybe an improvement (different view) can be reached by tuning the wave heights more near the dune.

In case of special coastline shapes it can be impossible to define the seaward boundary of a 2D cross-shore profile at deep water. To use DUROSTA in that case a more landward boundary has to be defined. In that case input wave conditions have to be obtained from a more sophisticated model.

For these reasons in this simulation the wave heights are tuned to the wave height measurement point at the NAP - 5 m (prototype) bottom line. In the model that depth line was at  $x = 31.99$  m (A-series) and  $x = 34.82$  m (B-series). The settings are still kept at the default values.

### 4.2.2.1 Wave propagation

The graphs of the wave propagation for this simulation are presented in Figure 4.8 (A-series) and 4.10 (B-series). The set up of these figures is similar to Figures 4.2 and 4.5.

Considering these wave propagation plots with respect to the previous simulation a number of things are conspicuous. First of all a relatively high change of the wave height input at the boundary turns out in only a small change near the dune. This has of course to do with wave breaking. In addition, in a sense linked to the previous point, the wave heights of the tests are not any more in the same order over the whole profile.

For test T01 and T03 the input at the wave board must be much higher to reach a slight higher value at  $x = 31.99$  m, on the other hand for test T02 the input at the wave board must be much lower to reach the desired wave height at that point.

For all tests of the B-series the input at the wave board has to be (much) lower than applied in the previous simulation. This turns out in a complete opposite order of the wave heights for the biggest part of the profile.

### 4.2.2.2 Erosion development

The graphs of the erosion development in time of this simulation are presented in Figure 4.9 (A-series) and 4.11 (B-series). These figures are similar to Figures 4.3 and 4.6.

Also the erosion volumes can be considered with respect to the previous simulation.

For test T01 and T03 the higher wave inputs turn out in higher erosion volumes (derivable from the smaller fit factors). The other way around for test T02 the lower wave height results in less erosion. In spite of that the erosion development of the three tests is still in the expected order (at least the biggest time), but differences are not quite regular. With expected order, in this context, is meant: the longer the (peak) wave period the larger the erosion rate.

Also for the B-series the changed wave heights, with respect to the previous simulation, result in different erosion volumes. The erosion of T11 is a little smaller but for T12 and T13

the erosion is much smaller. Considering the three tests together the expected order is no longer visible.

### 4.2.3 Tuning over whole profile by gamma

The two previous simulations showed that in case of default settings, or near wave board or near dune, tuning is possible, but not both together. Furthermore it is visible that tuning near the dune only is reached by complete different input and wave propagation. In addition, it does not result in better outcomes with respect to the measured erosion volumes.

The below presented simulation is carried out with for each test a different breaker index  $\gamma$ . The input wave height at the boundary is varied to match to the incident wave measurement and the breaker index  $\gamma$  is varied to match as good as possible to the two most near dune wave height measure points. Apart from the breaker index  $\gamma$  no settings have been changed.

#### 4.2.3.1 Wave propagation

The graphs of the wave propagation for this simulation are presented in Figure 4.12 (A-series) and 4.14 (B-series). The set up of these figures is similar to Figures 4.2 and 4.5. From the graphs it becomes clear that in this way for the whole profile the wave propagation can match approximately, for values of  $\gamma$  in a range of 0.77 to 0.89. Furthermore it is visible that a higher wave period needs a smaller breaker index  $\gamma$  to give these results. Remark must be made that the default  $\gamma$ -value for DUROSTA is 0.85.

According to Battjes and Stive (1985) the breaker index  $\gamma$  is dependent on the deep water wave steepness  $s_0$ :

$$\gamma = 0.5 + 0.4 \tanh(33s_0) \quad (4.1)$$

Applying Eq. (4.1) also a decreasing breaker index is found with increasing wave period. Using the desired prototype wave height of  $H_s = 9.0$  m at depth contour NAP – 20 m, the breaker index would range from 0.70 to 0.88 ( $T_p$  from 18.4 s to 10.2 s).

Although the above found breaker indexes do not exactly match with the computed values, still the dependency and the order of magnitude is corresponding. This makes it quite plausible to use a smaller breaker index for a case with smaller wave steepness (longer wave period).

#### 4.2.3.2 Erosion development

The graphs of the erosion development in time of this simulation are presented in Figure 4.13 (A-series) and 4.15 (B-series). These figures are similar to Figures 4.3 and 4.6.

Looking to the fit factors a trend is visible of increasing fit factors with increasing wave period. This means that the measured effect of the wave period on the amount of dune erosion is not sufficiently good reproduced by the model. For the A-series the expected order is not present in the top subplot and for the B-series the order is opposite.

So, although in this simulation the computed wave propagation is matching better with the measurements than in the previous simulations, still the measured effect of the wave period on the amount of dune erosion is not computed.

#### 4.2.4 Tuning over the whole profile with compensation for changed gamma

In Section 4.2.3 is showed that although good matching wave propagation still results in quite different erosion volumes with respect to the measurements. However, this is not surprising since the breaker index  $\gamma$  is not only used for the wave propagation but also for the following three sediment transport related variables.

$$F_k = \left[ \alpha_k \gamma \left( \exp \left( \frac{1}{\alpha_k \gamma} \right) - 1 \right) \right]^{-1} \quad (4.2)$$

$$\varepsilon_0 = K_\varepsilon D_{50} u_{rms} \gamma \quad (4.3)$$

$$\mu = K_\mu c / \gamma \quad (4.4)$$

$F_k$  is a variable in the formula for the reference concentration  $C_0$ , and  $\varepsilon_0$  and  $\mu$  describe the sediment mixing. Each of these three formulas contains a constant ( $\alpha_k$ ,  $K_\varepsilon$  and  $K_\mu$ ) which is able to compensate a changed breaker index. For every value of  $\gamma$ , different from the default 0.85, the three constants can be changed from their default value so that  $F_k$ ,  $\varepsilon_0$  and  $\mu$  are equal to a case with complete default settings. With this is assumed that the default settings of these constants are the best possible settings.

Above described method is some kind of a trick to consider the behaviour of DUROSTA with as good as possible wave propagation (with respect to the measurements).

By applying this method the wave propagation is equal to the simulation which is showed in Figures 4.12 and 4.14 and described in Section 4.2.3.1.

##### 4.2.4.1 Erosion development

The graphs of the erosion development in time of this simulation are presented in Figure 4.16 (A-series) and 4.17 (B-series). These figures are similar to Figures 4.3 and 4.6.

The trend of increasing fit factors with increasing wave period is still there but it is less strong with respect to previous simulation. The computed erosion volumes for the A-series are approximately equal to the ‘Tuning near dune’ case (Section 4.2.2). Also the B-series results are comparable to the ‘Tuning near dune’ case, but to a less extent.

Apparently the wave height near the dune is the most important deciding factor to compute the dune erosion rate in the DUROSTA approach.

### 4.3 Sediment concentration and flow velocity

Since the sediment transport is computed from the depth integrated product of the time averaged velocities and time averaged concentrations it is useful to compare the computed verticals with the measurements. However, in the used version (1.20) of DUROSTA, there is no possibility to generate complete concentration and velocity verticals. The first developed version(s), which still had such an output possibility, appeared to be not available anymore. Version 1.20 is only able to generate reference values of concentration and velocity ( $C_0$  and  $u_0$ ).

Based on the reference concentration output combined with a number of other outputs it is possible to compute verticals afterwards. In principle, a comparable method must be also applicable for the velocity verticals. However, this appeared to be much more complicated and so the choice is made to plot only the reference values of the velocity.

### 4.3.1 Sediment concentration verticals

The concentration vertical is in DUROSTA described by:

$$C(z) = C_0 \left[ 1 + \frac{\mu z}{\varepsilon_0} \right]^{(-w_s/\mu)} \quad (4.5)$$

in which:

$$\varepsilon_0 = K_\varepsilon D_{50} u_{rms} \gamma \quad (4.6)$$

$$\mu = K_\mu c / \gamma \quad (4.7)$$

By assuming  $c = \sqrt{gd}$  it is possible to compute  $C(z)$ . For a particular point of time the X-functions  $C_0$ ,  $d$ ,  $u_{rms}$  are the only varying parameters to compute the concentration verticals according to above called formulations.

Figures 4.18 through 4.24 show some of the concentration verticals of test T02 (prototype  $T_p = 14.9$  s) and T03 (prototype  $T_p = 10.2$  s) for the case of Section 4.2.1 (tuning near wave board). Choice has been made to compare these tests because these give the biggest difference in wave period within one scale ( $n_d = 30$ ). Each figure represents at one particular  $x$ -location the measured and two computed verticals (DUROSTA and UNIBEST-TC). All of the computed verticals are at time  $t = 0$ . At that time no profile change has taken place which enables better comparison. The measurements are the first available ones in time at that particular location; the mentioned time is the middle of the measurement interval. These are assumed to be comparable with the computations because the measured concentration verticals appeared to be hardly dependent of time (see Coeveld and De Vroeg, 2004).

In this section only the DUROSTA verticals combined with the measured ones are considered. The UNIBEST-TC verticals come up in the next chapter.

About these figures a number of remarks can be made:

- All of the computed concentrations are lower compared to the measured verticals. In general the differences range from a factor 2 up to about 40 or 50, but for a few measurement points the difference factors are even around or more than 100.
- For locations closer to the dune the difference between the measured and computed verticals turns out to be smaller.
- The computed verticals are hardly curved, in contrast to the two most seaward measured verticals (T02 Figure 4.18 and 4.19; T03 Figure 4.21 and 4.22).
- The computed concentrations of test T02 (higher  $T_p$ ) are all higher compared to test T03 (smaller  $T_p$ ).

### 4.3.2 Flow velocity

Figures 4.25 through 4.31 show some of the measured velocity verticals combined with the DUROSTA bottom velocity and the UNIBEST-TC verticals, again for test T02 and T03 (case of Section 4.2.1, tuning near wave board). The mentioned times of the measurements are the start times of the first measurement points (lowest points, see Section 3.2.3).

Although only the bottom velocity gives limited information, it is still possible to make a few remarks:

- The computed velocities become higher going to the dune.

- The computed velocities of T02 (higher  $T_p$ ) are higher compared to T03 (smaller  $T_p$ ).
- Except Figure 4.26, most of the computed bottom velocities are approximately equal to the smallest measured velocities of the verticals.

### 4.3.3 Remarks

The computed concentrations and velocities are smaller compared to the measurements, especially further seaward. Despite the in a number of cases large differences between measurements and computations, still the computed erosion is only about 30-40 % smaller compared to the measurements. A possible reason is, that at the most landward measurement location, which is around the transition point for the extrapolation of the dry profile, the differences are relatively small.

## 4.4 Sensitivity analysis

Since in this study physical model tests are simulated, the input for the computations is based on measured values and the results are compared with measured values. However, these measurements have a certain inaccuracy. In order to get a feeling for the effects of these inaccuracies on the computation results, a number of important parameters have been varied.

### 4.4.1 Reduced or extended profile

The applied wave conditions in the physical model tests were based on prototype conditions at depth contour NAP – 20 m. Application of the scale factor and distortion on the prototype profile of Figure 1.1 would for the A-series result in the situation visualised in the top subplot of Figure 4.32. This so-called extended profile until prototype depth contour NAP – 20 m did not fit with the dimensions of the flume. Although the smaller scale in case of the B-series, also in that case the profile did not fit. Since it is not possible to put sediment just in front of the wave board, as represented in the middle subplot of Figure 4.32, the so-called reduced profile has been applied (bottom subplot).

Using the three profiles of Figure 4.32 (and similar situations for the B-series), sensitivity computations have been carried out. The results, which are not presented, show that for the erosion volumes in general the effect is negligible, only in a few cases a slight difference is visible.

The wave propagation on the other hand is clearly different. The steep part at the toe of the reduced profile, which is meant to cut of the profile, induces in the wave model ENDEC shoaling which not occurs with the extended profile. Later on, more near shore, the waves are again approximately of the same height. So, the waves near the dune are nearly equal and that results in practically the same erosion volume.

To simulate the tests as best as possible the here presented computations are all carried out with the reduced profile.

#### 4.4.2 Initial profile schematisation

In the predictions done by Steetzel (2004) is the profile schematised with straight lines between some characteristic points.

As expected the real profile applied in the physical model was not as smooth as schematised and slightly different for each test. The differences are visualised by Coeveld and De Vroeg (2004) in charts. By analysing the measurement data in detail, it can be concluded that the profiles of all tests are averagely above the desired line. Computations with this more realistic profile resulted all in smaller erosion volumes. Explanation is found in more damping of the waves because of the roughness and an on average slight higher profile. The latter had in general the biggest influence.

Figure 4.33 shows the by DUROSTA computed erosion volumes after six hours of wave attack using different initial profiles. For each measured initial profile the wave conditions of all the tests of that particular series have been applied. In addition, computations with the desired profile have been carried out. Figure 4.33 makes clear there is influence of the initial profile but the effect of the wave period is stronger. Also is visible that in all cases, but especially in the A-series, the computations with the desired profile result in the most erosion.

The points of the computations using the measured initial profile of test T13 are conspicuous in Figure 4.33. These are all clearly below the other points of the corresponding wave periods. From consideration of the measured initial profiles of the B-series in detail, the initial profile of test T13 appeared to be clearly above the desired profile (more than profile T11 and T12) in the sedimentation area. For this reason less erosion is necessary to create an equilibrium profile and from the beginning of the simulation the wave attack near the dune is slight less severe.

#### 4.4.3 Grid

In order to carry out the sensitivity for the grid size, five different grids have been applied to simulate again all of the tests for the case of Section 4.2.1 (tuning near wave board).

With these different grids the computed erosion volume after six hours of wave attack has been related, for each test, to the computed erosion for the corresponding test using the general applied grid (see Section 4.1.1). The under laying computations for these computations are not presented.

The erosion volumes, using a constant grid size of 0.2 m (rather coarse), turned out to be 6-11 % larger compared to the results with the general applied grid. Using another grid with size decreasing from 0.4 m at the wave board to 0.05 m near the dune, the erosion volumes turned out to be 6-8 % smaller compared to the general applied grid.

In general can be concluded that the finer the grid (near the dune) the smaller the computed erosion volume.

The difference between +11 % more and -8 % less erosion is very large. However, in case of a different grid, the computed erosion volumes of all tests change with a certain percentage and a small spreading around that. Apart from the above mentioned rather coarse grid (constant grid size 0.2 m), in the other cases the spreading was less than 2 %.

Because in this study most attention is paid to the relative increase of dune erosion with increasing wave period and the results appeared to be rather sensitive to different grid sizes, has been chosen to apply the same grid for both test series.

#### 4.4.4 Grain properties

Because of the fact that the used grain properties ( $D_{50} = 93 \mu\text{m}$ ;  $w_s = 0.0061 \text{ m/s}$ ) are based on a limited number of samples it is important to know something about the sensitivity for this input. In the predictions of Steetzel (2004) the measured sediment properties ( $D_{50} = 100 \mu\text{m}$ ;  $w_s = 0.008 \text{ m/s}$ ) of the M1819-I research (WL | Delft Hydraulics, 1982) were used.

Again the case of Section 4.2.1 is used for this comparison. By increasing both sediment properties ( $D_{50} + 7.5 \%$ ;  $w_s + 31 \%$ ) the erosion volumes after 6 hours model time (for all tests) decrease with approximately 3 %.

With this result it is unlikely that the differences in erosion volume between measurements and computations can be explained by inaccurate grain properties input.

#### 4.4.5 Wave height

Although this research is focussed on varying wave period, wave height is still important. The limited flume length was reason for the application of a reduced cross-shore profile. With this more near shore (seaward) boundary also a reduced wave height, with respect to deep water, was applied.

The sensitivity for the wave height can be illustrated by comparing the computations of Section 4.2.2 with Section 4.2.1. Table 4.1 shows this comparison. The relative change of erosion volume after 6 hours model time varies from  $\frac{1}{3}$  to approximately  $\frac{1}{2}$  of the relative wave height change. Taking also into account the peak wave period, a slight increase of sensitivity seems visible for increasing peak wave period.

##### 4.4.5.1 Varying wave height in time

For all the above presented computations constant wave conditions in time have been used. However, most of the measured wave heights were decreasing in time, especially for locations near the dune, due to the change of the cross-shore profile. To take into account these varying conditions, the computations of Section 4.2 have also been carried out with varying wave heights (not presented). The first three wave measurement intervals (time period A, B and C; together 1 h) were combined (Appendix A) to have a measurement with more than 1000 waves. Using this, the tests have been simulated with three different wave conditions (first hour, following two hours and last three hours). Differences with the computations of Section 4.2 were negligible in most cases. In addition, if a difference was found, this would not lead to different conclusions about the behaviour of DUROSTA for varying wave periods.

Because of the negligible influence of varying wave conditions and the fact that the computed wave height only landward of the most landward wave height meter changes in time, due to profile change (see Figure 4.1), have been chosen to simulate all the tests with constant ('averaged') wave conditions.

#### 4.5 Prototype computations

To control the behaviour of DUROSTA on prototype scale with respect to the test scale two series of corresponding computations are presented. The computations are carried out for a

peak period range of 10 to 20 s with steps of 2 s. In addition, corresponding computations are carried out at depth scale  $n_d = 30$ .

#### 4.5.1 Set up

The seaward boundary is put at depth line NAP – 20 m which means for used design conditions 25 m water depth. The schematised cross-shore profile (Figure 1.1), which also was the basis for the profile in the model tests, is used as input. Wave height is set to 9.0 m (deep water). For the computations on scale  $n_d = 30$  the same grid as the above presented computations is used and for the prototype computations relatively the same grid is used. For the prototype computations a grain size of  $D_{50} = 225 \mu\text{m}$  and a fall velocity of  $w_s = 0.0269 \text{ m/s}$  is used. The prototype computations are carried out with an undistorted profile. For the computations on scale  $n_d = 30$  the same distortion ( $n_l/n_d = 1.68$ ) as in the tests has been applied. The computations are carried out with default settings.

#### 4.5.2 Erosion volume

In Figure 4.34 the measured relative erosion after 3.5 hours model time is showed with respect to  $T_p = 12 \text{ s}$  in the same way like Figure 3.15. To express all these erosion volumes in scale  $n_d = 30$  the results of the B-series have been converted (see Section 3.4).

The computed erosion on scale  $n_d = 30$  (also after 3.5 h) corresponds very good with the measurements. The computed prototype erosion after 19 hours ( $= 3.5 \text{ h} * \sqrt{30}$ ) gives a slight steeper curve.

### 4.6 Conclusions

From the computations which are presented in this chapter and the sensitivity analysis it is possible to conclude a number of things.

- In DUROSTA the breaker index  $\gamma$ , used by ENDEC, is set constant (default  $\gamma = 0.85$ ). Application of DUROSTA with this breaker index results for the larger prototype wave periods in less accurate computed wave height development (with respect to the measurements).
- In the first computations with DUROSTA, in which the measured wave height has been imposed near the wave board (Section 4.2.1), the measured relative effect of the wave period on the amount of dune erosion is good reproduced. However, in that case the larger amount of dune erosion for a longer wave period is mainly caused by a larger (over-estimated w.r.t. measurements) wave height near the dune. Remark must be made that this near dune measured wave height is including reflection and long waves.
- Using for each test a specific breaker index, it is possible to fit the computed wave height near the wave board as well as near the dune with the measurements. In that case a decreasing breaker index with increasing wave period is found, which is in accordance with Battjes and Stive (1985).
- In case of imposing the measured wave heights (including reflection and long waves) near the dune, the measured effect of the wave period on the amount of dune erosion is not fully reproduced any more. Especially for the B-series (test series on scale 40) this can result in a decreasing computed dune erosion with increasing wave period (opposite to the test results).

- The considered sediment concentration and velocity profiles show, especially further seaward, much difference with the measurements.
- The sensitivity for a slight different grid size is conspicuous.

## 5 UNIBEST-TC computations

For a short description of the model itself is referred to Section 2.5, for a more complete description and background of the model is referred to Bosboom et al. (2000).

With respect to the in the previous chapter considered DUROSTA computations, in this chapter the UNIBEST-TC computations come up less extensive.

From the, in the previous chapter described, DUROSTA computations the measured influence of the wave period on the amount of dune erosion appeared to be reproducible in case of imposing the wave height near the wave board. On the other hand by imposing the measured wave height near the dune this influence was hardly visible anymore.

These two approaches are also applied for the UNIBEST-TC computations to whether a comparable behaviour like DUROSTA is found or not.

### 5.1 Computation set-up

In order to apply the same approaches for the UNIBEST-TC computations as which have been applied for DUROSTA, most of the input parameters can be straight taken from the DUROSTA input.

The grid and initial profile are generated as described in Section 4.1. Since in UNIBEST-TC the root mean square wave height is  $H_{rms}$  used, the significant wave height  $H_{m0}$ , which is used in DUROSTA, has been converted according to:

$$H_{rms} = \frac{H_{m0}}{\sqrt{2}} \quad (5.1)$$

An example of an input file is presented in Appendix C.

#### 5.1.1 Settings

Table 2.2 gives an overview of the default run parameters and the chosen values. The parameters which differ from default are described below.

- The time step is much smaller compared to the default value. Because of the fine grid and the relatively fast profile change, a small time step is necessary to assure a stable computation. The number of time steps depends logical on the test duration and time step.
- Output frequency is set to 10. Because of the large number of small time steps it is not necessary to generate output every time step.
- The breaker index  $\gamma$  is at first set to the default value of DUROSTA. With these settings it is possible to obtain the wave input from the DUROSTA computations and to compare the results with equal wave development. With the default value of 0.00 ENDEC will be applied with breaker index according to Battjes and Stive (1985):

$$\gamma = 0.5 + 0.4 \tanh(33s_0) \quad (5.2)$$

- Breaker delay is switched off because no banks were present in the test profile.

- TANPHI1 and TANPHI2 are both set to 0.6 which means that slope effects are negligible.
- Grain sizes  $D_{50}$  and  $D_{90}$  are obtained from the measurements and  $D_{ss}$  is set to  $0.85 \cdot D_{50}$  in accordance with the recommendations in the manual.
- RKVAL and RC are both halved because of the fine sediment.
- The temperature of the water is obtained from the measurements (see Table 3.3)

The extrapolation method is set to: ‘Vertical + wave runup’ which means the extrapolation as described in Section 2.5.6. Furthermore is the parameter OPTDRY set to 2 which is meant to compute the transition point at a quarter of the local wave length seaward from the waterline.

## 5.2 Simulations

To give an impression of the behaviour of UNIBEST-TC, two conspicuous DUROSTA simulations are selected to compute with UNIBEST-TC as well. Firstly is taken the one with wave tuning near the wave board and secondly the one with tuning by the breaker index  $\gamma$ . For the first DUROSTA gave good results but for the second, despite the good (with respect to the measurements) wave height development, the effect of the wave period was not corresponding the physical model research.

### 5.2.1 Tuning near wave board

The wave propagation is not dealt with here because it is equal to the DUROSTA computations (see Section 4.2.1.1 and Figures 4.2 and 4.5).

The erosion development in time is for both series represented in Figure 5.1. At first sight a few things stand out. The lines are almost linear which means that the decreasing erosion rate during the test is not present. The erosion volumes are very small, for example the measured erosion after 6 hours of test T02 is about 10 times the computed value.

### 5.2.2 Tuning over whole profile by gamma

Again for the wave propagation is referred to the previous chapter (Section 4.2.3.1 and Figures 4.12 and 4.14).

The corresponding erosion graphs are represented in Figure 5.2. The lines of the A-series are still almost linear, for the B-series a slightly curved shape is visible. Furthermore, the computed erosion of test T01 (prot.  $T_p = 12.4$  s; A-series) is larger compared to test T02 (prot.  $T_p = 14.9$  s). In the B-series the two tests with the largest wave periods show approximately the same erosion development. The erosion volumes are even lower with respect to previous simulation, especially for the B-series.

## 5.3 Sediment concentration and flow velocity

In UNIBEST-TC it is possible to generate concentration and velocity verticals as output. To enable comparison with DUROSTA also the ‘tuning near wave board’-case from Section 5.2.1 is used here.

### 5.3.1 Sediment concentration

The concentration verticals of UNIBEST-TC are also plotted in Figures 4.18 through 4.24. About these lines a number of remarks can be made:

- All of the computed concentrations are lower compared to the measurements and largely lower compared to the DUROSTA verticals.
- The computed concentrations are slight higher going closer to the dune.
- All of the computed verticals are more curved compared to the DUROSTA verticals.
- The computed concentrations of test T02 (larger  $T_p$ ) are slight higher compared to test T03 (smaller  $T_p$ ).

### 5.3.2 Flow velocity

The velocity verticals are plotted in Figures 4.25 through 4.31. Some remarks can be made about these graphs:

- The computed velocities become higher going to the dune.
- The computed velocities of T02 (larger  $T_p$ ) are higher compared to T03 (smaller  $T_p$ ).
- Except Figure 4.25 and 4.26, most of the measure points are reasonably around the computed verticals.

## 5.4 Concluding remarks

Based on the carried out computations with UNIBEST-TC a number of remarks can be made.

- Qualitatively considered, the two simulations which are described above give more or less comparable results with DUROSTA. By imposing the measured wave height near the wave board, a positive relation is found between wave period and dune erosion volume. On the other hand, by tuning to the measured wave height near the dune, a consistent relation between wave period and dune erosion volume is no longer visible. However, this last simulation shows relatively more differences in erosion volume between the different tests than in the comparable DUROSTA simulation.
- The erosion development in time is with the used settings approximately linear. Some other computations, which are not presented here, indicated that a shift of the transition point closer to the dune will result in a more realistic curved shape of the erosion development in time.
- The computed erosion volumes are very low compared to the measurements.
- Linked with this, the concentration verticals are much lower.
- The velocity verticals are of the same order as the measurements.

Concerning the above mentioned remarks, one has to keep in mind that UNIBEST-TC not has been developed to compute dune erosion. This in contrast to DUROSTA, which was developed to compute dune erosion and has been calibrated with a lot of physical model tests on different scales. Gootjes (2000) implemented an extrapolation method for the dry profile in UNIBEST-TC to make it possible to compute dune erosion. Later on, Walstra and Steetzel (2003) implemented the same extrapolation method for the dry profile as is used in DUROSTA. Walstra and Steetzel (2003) also showed that UNIBEST-TC could give rather good results with respect to large scale physical model tests.

Generally spoken, the possibility to compute dune erosion with UNIBEST-TC is just recently included and it is still in development. More research to improve UNIBEST-TC, concerning dune erosion, is recommended.

## 6 Discussion

In this chapter some critical notes come up about this research (or used physical model data) and some choices which have been made. In case of further desk study and in case of preparation of further (large scale) physical model research it is recommended to keep these remarks in mind.

### 6.1 Wave conditions tests

The aim of the physical model research (Coeveld and De Vroeg, 2004) was to focus on the effect of the wave period on dune erosion. However, because of the scale choice (see Section 3.1.1) it was not possible to create the complete cross-shore profile until depth contour NAP – 20 m in the flume (see Figure 4.32). For that reason it was necessary to base the desired wave conditions (Table 3.1) at the wave board on wave height decay computations. This implies that the results of the tests are also dependent on the quality of these computations. In addition, the desired (which is computed) wave conditions were not fully realised.

The combination of the uncertainty in the desired wave conditions and the fact that these desired conditions are not realised makes it very difficult to derive the deep water wave conditions which are in fact applied in the tests. It is certainly not impossible that the different tests represent different deep water (depth contour NAP – 20 m) wave heights. In that case it is also not known which part of the erosion difference (between different tests) is due to wave height difference and which part is due to wave period difference.

In this research are the above mentioned uncertainties in fact ignored and it is assumed that the measured difference in erosion volume between the tests is fully due to the wave period difference.

For further research (large scale physical model) it is very important to be aware of this and therefore choose the scale and wave conditions so that it is possible to make a distinction between wave height and wave period related effects.

### 6.2 Wave tuning

In this study it has been chosen to tune the wave heights to the measurements at certain points in the cross-shore profile.

The fact that near the wave board the incident wave conditions have been derived makes that measurement point very useful to tune the wave height in the model. However, a disadvantage is that this measurement point was positioned around the (steep) toe of the cross-shore profile. This toe induced in the wave model ENDEC some increase of wave height which was not noticeable in the physical model.

The measurement point at prototype NAP - 5 m has been used as tuning target as well. Only a single wave height meter was used at that point which means that the measured wave height consists of incident and reflected waves. In addition, the derived wave height  $H_{m0}$  is including the long wave part of the spectrum (see Table 3.2). Both reflection and long waves are not included in the wave model ENDEC which makes this way of tuning less reliable. However, from these computations it can still be derived that a decreasing breaker index

with increasing wave period, which is in accordance with Battjes and Stive (1985), gives better wave development results but worse erosion volume results.

### 6.3 Comparison DUROSTA and UNIBEST-TC computations

This research has been focussed on the behaviour of DUROSTA. First, the model has been applied with default settings, and later on a number of computations have been presented with adapted boundary conditions or settings (breaker index  $\gamma$ ).

For the UNIBEST-TC part of this research, which is much less extensive, mainly the same simulation set-up has been applied as in the DUROSTA computations. However, this means that no simulations are presented with complete default settings of UNIBEST-TC. Actually, it would be 'more fair' to compare both models by using default settings and tuning the wave height for instance to the incident wave measurement near the wave board. In that case UNIBEST-TC uses the breaker index according to Battjes and Stive (1985) which likely results in more realistic wave height development.

### 6.4 Sediment concentration and velocity verticals

The represented computed concentration verticals show in all cases an under-estimation of the measured verticals. A possible reason can be that the moments of time of the measurements and the computations do not correspond. This implies that the bottom shape of the computed and measured situation does not correspond as well.

Some (not presented) output of the verticals at a moment closer to the measurement time gave (at least for DUROSTA) somewhat better results. However, in this case the computed verticals are based on the computed bottom profile at that time (starting from  $t = 0$  with the measured initial profile). Considering the fact that the computed erosion is less than measured, in this case still no comparison is made between situations with the same cross-shore profile.

A probably more realistic comparison is possible by imposing the cross-shore profile (in the computation) which was present in the flume at the moment of the concentration measurement. However, at the moments of the concentration measurements no profile measurements are available. So, the best approximation of the present profile (in the flume) can be achieved by starting the computation from the last available profile measurement in time before the considered concentration measurement.

## 7 Conclusions and recommendations

### 7.1 Conclusions

- From the analysis of the test results (physical model) appears a clear influence of the wave period on the amount of dune erosion. For loads of equal duration, a longer wave period causes more dune erosion. Comparing loads of equal number of waves, the effect is even stronger.
- Around the characteristic storm duration of approximately 1 hour model time the test results (small scale) show less consistent wave period influence than after longer model time.
- Assuming the scale translation as applied in Section 3.4 and at least the characteristic storm duration, an increase of dune erosion volume above storm surge level of 25 – 35 % is found for a prototype peak wave period of  $T_p = 18.4$  s with respect to  $T_p = 12$  s.
- The accuracy of the tests with the highest (prototype) wave periods, which were carried out on the smallest scale, is supposed less than those with the lower periods. So, just the interest zone seems less accurate than the already validated zone.
- In DUROSTA the breaker index  $\gamma$ , used by ENDEC, is set constant (default  $\gamma = 0.85$ ). Application of DUROSTA with this breaker index results for the larger prototype wave periods in less accurate computed wave height development (with respect to the measurements).
- In all DUROSTA computations the erosion volumes are underestimated with respect to the measurements.
- In the first computations with DUROSTA (default settings), in which the measured wave height has been imposed near the wave board (Section 4.2.1), the measured relative effect of the wave period on the amount of dune erosion is good reproduced. However, in that case the larger amount of dune erosion for a longer wave period is mainly caused by a larger (over-estimated w.r.t. measurements) wave height near the dune. Remark must be made that this near dune measured wave height is including reflection and long waves.
- In case of imposing the measured wave heights near the dune, the measured effect of the wave period on the amount of dune erosion is not fully reproduced any more. Especially for the B-series (test series on scale 40) this can result in a decreasing computed dune erosion with increasing wave period (opposite to the test results).
- The erosion volumes computed by UNIBEST-TC are much lower compared to the measurements. However, the possibility to compute dune erosion with UNIBEST-TC is just recently included and is still in development. In addition, UNIBEST-TC has not yet been calibrated for these kind of dune erosion tests.
- In both models a longer wave period does only cause consistently more dune erosion if the wave height near the dune is bigger. This in contrast to the measurements of the B-series where, although approximately equal wave heights near the dune (including reflection and long waves), the effect of the wave period is clearly visible.

## 7.2 Recommendations

### 7.2.1 General

- It is strongly recommended to carry out large scale physical model research as soon as possible for a number of reasons:
  - From the results of the small scale research it becomes clear that the wave period has significant influence on the amount of dune erosion.
  - Due to some scale effects in the small-scale model (lean-over), larger scale verification is required.
  - According to this research it is not proved that the models DUROSTA and UNIBEST-TC are able to simulate the dune erosion process sufficiently good for varying peak wave periods. Large scale measurements can confirm that doubt or can on the other hand prove that large scale tests are sufficiently good reproducible.
  - Check in more detail how sensitive the dune erosion process is for wave period, separate from wave propagation effects.
- It is advisable to use a more stable parameter than the  $T_p$  as a measure for the wave period. Research is necessary to determine a measure for the wave period which is especially suitable for dune erosion ( $T_{m-1,0}$  or other). With that the used models have to be adapted.
- A landward shift of the transition point in UNIBEST-TC can possibly improve the results (for dune erosion cases). It is recommended to optimise the location of that point.
- To use UNIBEST-TC for dune erosion, which is a relatively fast developing process, a smaller time unit (e.g. hours instead of days) would be easier to use. A possibility in the user interface to choose the time unit is possibly easy to implement and will increase the user friendliness. In addition, a dynamic time step would reduce the computation time significantly.

### 7.2.2 Practical recommendations for further physical model research

During the analysis of the physical model research sometimes problems came up which could be solved much more easy if it was known before. In this section some recommendations are given to prevent as much as possible this kind of problems in future dune erosion research. The recommendations can origin from bad but also from good experiences.

- Analysis and straightforward conclusions are much easier in case all of the tests are carried out with the same scale factor.
- By choosing wave conditions and scale factor so that at the wave board the wave height for all tests is equal and only the wave period varies, will make it possible to focus purely on the effect of the wave period on dune erosion.
- It is recommended to make some kind of reference for the profile measurement at the profile toe as well as at the dune top.
- With a simple computer program it is possible to calculate right after each profile measurement the sand volume in the flume, the difference in sand volume with previous tests and possibly present eye-catching differences in the profile (with respect to previous tests).

- It is recommended to measure also near dune the incident wave height (e.g. at the NAP - 5 m depth contour).



## References

- Battjes, J.A., and J.P.F.M. Janssen, 1978**, Energy loss and set-up due to breaking in random waves. Proc. 16<sup>th</sup> Int. Conf. on Coastal Eng., ASCE, pp. 569-587.
- Battjes, J.A. and M.J.F. Stive, 1985**, *Calibration and Verification of a Dissipation Model for Random Breaking Waves*. Journal of Geophysical Research, Vol. 90, No. 5C, pp 9159-9167, September 1985.
- Bosboom, J., S.G.J. Aarninkhof, A.J.H.M. Reniers, J.A. Roelvink, D.J.R. Walstra, 2000**, *Unibest-TC 2.0x, Overview of model formulations*. WL | Delft Hydraulics report H2305.42, January 2000.
- Coeveld, E.M. and J.H. de Vroeg, 2004**, *Modelonderzoek duinafslag, Meetverslag kleinschalige gidsproeven (Research dune erosion, Measure report small-scale guide tests)*. WL | Delft Hydraulics report H4265 (in Dutch), March 2004.
- Gootjes, G. 2000**, Dunes as source of sediment for Delft3D-MOR. WL | Delft Hydraulics report Z2534, March 2000.
- Heijer, C. den, 2004**, *Concentratiemeting door dwarse afzuiging (Concentration measurement by transverse suction)*. WL | Delft Hydraulics internal report H4265 (in Dutch), March 2004.
- Lauder, B.E. and D.B. Spalding, 1972**, *Mathematical models of turbulence*. Academic Press, San Diego, California.
- Nairn, R.B., J.A. Roelvink and H.N. Southgate, 1990**, *Transition zone width and implications for modelling surfzone hydrodynamics*. Proc. Int. Conf. on Coastal Eng., Delft, The Netherlands, pp. 68-82.
- Rienecker, M.M. and J.D. Fenton, 1981**, *A Fourier approximation method for steady water waves*. J. Fluid Mech., Vol. 104, pp. 119-137.
- Rijkswaterstaat / RWS, 2002**, *Hydraulische randvoorwaarden voor primaire waterkeringen (Hydraulic boundary conditions for primary water defences)*. (in Dutch).
- Rijn, L.C. van, 1993**, *Principles of sediment transport in rivers, estuaries and coastal seas*. Amsterdam: Aqua Publications – II1, ISBN 90-800356-2-9.
- Rijn, L.C. van et al., 1995**, *Yearly-averaged sand transport at the 20 m and 8 m NAP depth contours of the JARKUS-profiles 14, 40, 76 and 103*. WL | Delft Hydraulics Report H1887.
- Roelvink, J.A. and A.J.H.M. Reniers, 1994**, *Upgrading of a quasi-3D hydrodynamic model*. Abstracts-in-depth, MAST G8-M overall workshop, Gregynog.
- Roelvink, J.A. and M.J.F. Stive, 1989**, *Bar generating cross-shore flow mechanism on a beach*. Journal of Geophysical Research, Vol. 94, No. C4, pp. 4785-4800.

- Ronde, J.G. de, J.G.A. van Marle, A.P. Roskam, J.H. Andorka Gal., 1995**, *Golfrandvoorwaarden langs de Nederlandse kust op relatief diep water (Wave boundary conditions along the Dutch coast at relatively deep water)*. Rijkswaterstaat, Rijksinstituut voor Kust en Zee / RIKZ, Report RIKZ-95.024 (in Dutch), December 1995.
- Roskam, A.P. and J. Hoekema, 1996**, *Randvoorwaarden voor golfperioden langs de Nederlandse kust (Boundary conditions for wave periods along the Dutch coast)*. Rijksinstituut voor Kust en Zee / RIKZ, Report RIKZ-96.019 (in Dutch), July 1996.
- Sand, S.E., 1982**, *Long wave problems in laboratory models*. J. Waterw. Port Coastal Ocean Div. Am. Soc. Civ. Eng., 108, pp. 492-503.
- Steezel, H.J., 1990**, *DUROSTA, Tijdsafhankelijk dwarstransportmodel voor extreme condities (DUROSTA, dynamical cross-shore transport model for extreme conditions)*. Research report WL | Delft Hydraulics H298 part III (in Dutch).
- Steezel, H.J., 1993**, *Cross-shore Transport during Storm Surges*. Ph.D. Thesis Delft University of Technology, ISBN 90-9006345-5.
- Steezel, H.J., 1996**, *Schaalrelaties, Nadere analyse schaalrelaties dwarstransport via formulering pragmatisch transportmodel (Scale relations, elaborated analysis scale relations cross-shore transport by formulating pragmatic transport model)*. (in Dutch), WL | Delft Hydraulics report H2167, June 1996.
- Steezel, H.J., 2002**, *Effect van zwaardere golfcondities op duinenkust. Verkenning effect grotere golfhoogte en langere golfperiode op mate duinafslag en veiligheid duinenkust (Effect of more severe wave conditions on dune coast. Exploration effect larger wave height and longer wave period to the amount of dune erosion and safety dune coast)*. Report desk study, Alkyon report A963R1 (in Dutch), September 2002.
- Steezel, H.J. and J. van de Graaff, 2003**, *Modelonderzoek duinafslag, Definitie proevenprogramma (Model research dune erosion. Definition test program)*. Report desk study, Alkyon report A1112R1, September 2003.
- Steezel, H.J., 2004**, *Modelonderzoek duinafslag, Nadere specificatie gidsproeven en voorspellende berekeningen (Research dune erosion, More accurate specification pilot tests and predicting computations)*. Report desk study, Alkyon report A1112R2, January 2004.
- Technische Adviescommissie voor de Waterkeringen (Technical Advisory Committee on Water Defences) / TAW, 1984**, *Leidraad voor de beoordeling van de veiligheid van duinen als waterkering (Guide to assessment of the safety of dunes as a sea defence)*.
- Technische Adviescommissie voor de Waterkeringen (Technical Advisory Committee on Water Defences) / TAW, 1995**, *Basisrapport zandige kust (Base report sandy coast)*. ISBN 90 36 93 704 3 (in Dutch).
- Vellinga, P., 1986**, *Beach and dune erosion during storm surges*. Ph.D. Thesis, Delft University of Technology; also: Publication No.372 WL | Delft Hydraulics, December 1986.
- Vriend, H.J. de and M.J.F. Stive, 1987**, *Quasi-3D modelling of nearshore currents*. Coastal Eng., Vol. 11, pp. 565-601.

**Walstra, D.J.R. and H.J. Steetzel, 2003**, *Description of improvements in the UNIBEST-TC model. Upgrade of UNIBEST-TC Version 2.04 to 2.10*. WL | Delft Hydraulics report Z3412, July 2003.

**WL | Delft Hydraulics, 1982**, *Systematisch onderzoek naar kenmerkende factoren voor duinafslag (Systematic investigation of parameters relevant for dune erosion)*. Research report M1819 part I (in Dutch), December 1982.

**Webpages:**

[http://www.minvenw.nl/rws/perspectief/archief/per325/per325\\_images/PER-325-ZV-duinafslag.jpg](http://www.minvenw.nl/rws/perspectief/archief/per325/per325_images/PER-325-ZV-duinafslag.jpg)



# Tables

|               | Symbol          | Description                                     | Value               | Unit |
|---------------|-----------------|---|---------------------|------|
| Wave          | $\alpha$        | Factor in breaker index dissipation formulation | 1.0                 | -    |
|               | $\gamma$        | Maximum breaker index                           | 0.85                | -    |
|               | $c_f$           | Friction factor bottom friction dissipation     | 0.01                | -    |
| Mixing        | $K_\varepsilon$ | Coefficient in $\varepsilon_0$ -relation        | 21.9                | -    |
|               | $K_\mu$         | Coefficient in $\varepsilon(z)$ -relation       | $8.5 \cdot 10^{-3}$ | -    |
| Concentration | $K_c$           | Coefficient in $C_0$ -formulation               | $1.2 \cdot 10^{-6}$ | -    |
|               | $\alpha_k$      | Coefficient in penetration depth dissipation    | 0.5                 | -    |
|               | $\alpha_D$      | Power in grain size function                    | 1.2                 | -    |
| Flux          | $K_r$           | Dimensionless roller area                       | 0.9                 | -    |
|               | -               | Dimensionless averaging distance                | 1.0                 | -    |
| X-transport   | $K_{cor}$       | Transport correction factor                     | 1.6                 | -    |
|               | $K_{sl}$        | Coefficient in slope transport                  | 4.0                 | -    |
|               | $K_{sw}$        | Coefficient in swash modelling                  | 2.0                 | -    |
| Y-transport   | -               | Friction in longshore flow modelling            | 0.1                 | m    |
| Runup         | $K_{opt}$       | Factor in wave runup formulation                | 1.25                | -    |

**Table 2.1 Overview of default settings of DUROSTA obtained from Steetzel (1993) and from the help function in the program**

| Run parameter | Symbol     | Description   | Default value        | Chosen value         | Unit              |
|---------------|------------|---|----------------------|----------------------|-------------------|
| 'DT'          | $dt$       | Time step   | 2.0                  | 0.0002               | days              |
| 'NT'          | $Nt$       | number of time steps  | 5                    | 1250                 | -                 |
| 'USTRA'       |            | User defined transport rate at the last computational grid point  | 0                    | 0                    | m <sup>3</sup> /h |
| 'JFR'         |            | Frequency of output (JFR = 10 means once per 10 time steps)   | 1                    | 10                   | -                 |
| 'IBOD'        |            | Morphodynamic switch  | 1                    | 1                    | -                 |
| 'ALFAC'       | $\alpha$   | Wave breaking parameter for use in dissipation formulation according to Battjes & Janssen (1978)  | 1.0                  | 1.0                  | -                 |
| 'GAMMA'       | $\gamma$   | Wave breaking parameter to determine maximum local wave height  | 0.00                 | 0.85                 | -                 |
| 'BETD'        |            | Roller parameter according to Nairn et al. (1990), expressing the steepness of the wave front   | 0.1                  | 0.1                  | -                 |
| 'FWEE'        | $f_w$      | Friction factor for wave dissipation due to bottom friction. The default value is obtained from Delta Flume experiments   | 0.01                 | 0.01                 | -                 |
| 'K_IJL'       |            | Breaker delay switch  | 1                    | 0                    | -                 |
| 'TANPHI1'     |            | Internal friction angle at location XF1; computed bed load transport rates are corrected for the local bottom slope, as a function the local angle of internal friction $\varphi$ | 0.03                 | 0.6                  | -                 |
| 'TANPHI2'     |            | Internal friction angle at location XF2   | 0.10                 | 0.6                  | -                 |
| 'XF1'         |            | Reference location for TANPHI1 (most seaward)   | 500.0                | 500.0                | m                 |
| 'XF2'         |            | Reference location for TANPHI2 (most shoreward)   | 1200.0               | 1200.0               | m                 |
| 'D50'         | $D_{50}$   | grain size of bed material  | $0.20 \cdot 10^{-3}$ | $0.93 \cdot 10^{-4}$ | m                 |
| 'D90'         | $D_{90}$   | grain size of bed material  | $0.30 \cdot 10^{-3}$ | $1.22 \cdot 10^{-4}$ | m                 |
| 'DSS'         |            | $D_{50}$ of suspended sediment  | $0.17 \cdot 10^{-3}$ | $0.80 \cdot 10^{-4}$ | m                 |
| 'DVAR'        |            | Cross-shore varying grain size switch: linearly varying sediment sizes cross-shore, according to the diameter multiplication factors FDIA# at reference depths HDIA#              | 0                    | 0                    | -                 |
| 'FCVISC'      | $\alpha_w$ | Viscosity coefficient of vertical velocity profile  | 0.1                  | 0.1                  | -                 |

| Run parameter | Symbol | Description   | Default value | Chosen value               | Unit |
|---------------|--------|---|---------------|----------------------------|------|
| 'RKVAL'       |        | Friction factor for mean current computation  | 0.01          | 0.005                      | m    |
| 'DIEPV'       |        | Reference depth for tidal velocity  | 5.0           | 5.0                        | m    |
| 'REMLG'       |        | Layer over which the sediment transport is reduced to zero in case of a fixed bed   | 0.10          | 0.10                       | m    |
| 'RC'          |        | Current related roughness for sediment transport computation, the default value is obtained from Delta Flume experiments        | 0.01          | 0.005                      | m    |
| 'RW'          |        | Wave related roughness for sediment transport computation, the default value equals RC  | 0.01          | 0.01                       | m    |
| 'TEMP'        |        | Temperature of the water  | 10.0          | 13.7 to 15.9 <sup>1)</sup> | °C   |
| 'SALIN'       |        | Salinity of the water   | 0.0           | 0.0                        | ‰    |
| 'C_R'         |        | Correlation coefficient between wave envelope and bound long waves; varies from -C_R at deep water up to +C_R at the shore line | 0.25          | 0.25                       | -    |

**Table 2.2 Overview of input parameters of UNIBEST-TC. Values which differ from default are considered in Section 5.1.1.**

---

<sup>1)</sup> Dependent on measurements (see Table 3.3)

| Test | Prototype  |              | Model     |                           |            |              |                 |                            |                            |
|------|------------|--------------|-----------|---------------------------|------------|--------------|-----------------|----------------------------|----------------------------|
|      | deep water |              | scale     | water depth <sup>1)</sup> | deep water |              | near wave board |                            | WHM 5 <sup>2)</sup>        |
|      | $T_p$ (s)  | $H_{m0}$ (m) | $n_d$ (-) | (m)                       | $T_p$ (s)  | $H_{m0}$ (m) | $T_p$ (s)       | $H_{m0}$ (m) <sup>3)</sup> | $H_{m0}$ (m) <sup>3)</sup> |
| T01  | 12.0       | 9.00         | 30        | 0.700                     | 2.19       | 0.300        | 2.19            | 0.280                      | 0.186                      |
| T02  | 14.2       | 9.00         |           |                           | 2.59       | 0.300        | 2.59            | 0.290                      | 0.199                      |
| T02a | 14.2       | 9.00         |           |                           | 2.59       | 0.300        | 2.59            | 0.290                      | 0.199                      |
| T03  | 10.0       | 9.00         |           |                           | 1.83       | 0.300        | 1.83            | 0.255                      | 0.170                      |
| T11  | 14.2       | 9.00         | 40        | 0.700                     | 2.25       | 0.225        | 2.25            | 0.225                      | 0.149                      |
| T12  | 19.0       | 9.00         |           |                           | 3.00       | 0.225        | 3.00            | 0.225                      | 0.163                      |
| T13  | 16.4       | 9.00         |           |                           | 2.59       | 0.225        | 2.59            | 0.225                      | 0.157                      |

**Table 3.1 Overview of test program with desired wave conditions and water level (Coeveld and De Vroeg, 2004)**

<sup>1)</sup> Near wave board

<sup>2)</sup> WHM 5 stands for a wave height meter at the location with a prototype water depth of 10 m

<sup>3)</sup> These values for  $H_{m0}$  are based on Steetzel (2004)

|                                  |                         |              |              |              |
|----------------------------------|-------------------------|--------------|--------------|--------------|
| <b>T03</b>                       | WHM 1,2,3 <sup>1)</sup> | WHM 4        | WHM 5        | WHM 6        |
| <b><math>x</math> (m)</b>        | <b>9.39</b>             | <b>21.28</b> | <b>31.99</b> | <b>37.63</b> |
| <b><math>H_{m0}</math> (m)</b>   | 0.211                   | 0.194        | 0.171        | 0.157        |
| <b><math>f_{min}</math> (Hz)</b> | 0.085                   | 0.012        | 0.012        | 0.012        |
| <b><math>f_{max}</math> (Hz)</b> | 1.880                   | 1.733        | 2.075        | 2.258        |
|                                  |                         |              |              |              |
| <b>T01</b>                       |                         |              |              |              |
| <b><math>x</math> (m)</b>        | <b>9.39</b>             | <b>21.28</b> | <b>31.99</b> | <b>37.63</b> |
| <b><math>H_{m0}</math> (m)</b>   | 0.241                   | 0.217        | 0.185        | 0.164        |
| <b><math>f_{min}</math> (Hz)</b> | 0.085                   | 0.012        | 0.012        | 0.012        |
| <b><math>f_{max}</math> (Hz)</b> | 1.880                   | 1.819        | 2.112        | 2.380        |
|                                  |                         |              |              |              |
| <b>T02</b>                       |                         |              |              |              |
| <b><math>x</math> (m)</b>        | <b>9.39</b>             | <b>21.28</b> | <b>31.99</b> | <b>37.63</b> |
| <b><math>H_{m0}</math> (m)</b>   | 0.262                   | 0.228        | 0.193        | 0.167        |
| <b><math>f_{min}</math> (Hz)</b> | 0.085                   | 0.012        | 0.012        | 0.012        |
| <b><math>f_{max}</math> (Hz)</b> | 1.819                   | 1.624        | 2.063        | 2.344        |
|                                  |                         |              |              |              |
| <b>T11</b>                       |                         |              |              |              |
| <b><math>x</math> (m)</b>        | <b>3.00</b>             | <b>26.79</b> | <b>34.82</b> | <b>39.02</b> |
| <b><math>H_{m0}</math> (m)</b>   | 0.218                   | 0.173        | 0.144        | 0.127        |
| <b><math>f_{min}</math> (Hz)</b> | 0.073                   | 0.012        | 0.012        | 0.012        |
| <b><math>f_{max}</math> (Hz)</b> | 1.624                   | 2.026        | 2.551        | 2.795        |
|                                  |                         |              |              |              |
| <b>T13</b>                       |                         |              |              |              |
| <b><math>x</math> (m)</b>        | <b>3.00</b>             | <b>26.79</b> | <b>34.82</b> | <b>39.02</b> |
| <b><math>H_{m0}</math> (m)</b>   | 0.223                   | 0.180        | 0.148        | 0.130        |
| <b><math>f_{min}</math> (Hz)</b> | 0.073                   | 0.012        | 0.012        | 0.012        |
| <b><math>f_{max}</math> (Hz)</b> | 1.624                   | 1.965        | 2.417        | 2.515        |
|                                  |                         |              |              |              |
| <b>T12</b>                       |                         |              |              |              |
| <b><math>x</math> (m)</b>        | <b>3.00</b>             | <b>26.79</b> | <b>34.82</b> | <b>39.02</b> |
| <b><math>H_{m0}</math> (m)</b>   | 0.224                   | 0.181        | 0.148        | 0.128        |
| <b><math>f_{min}</math> (Hz)</b> | 0.073                   | 0.012        | 0.012        | 0.012        |
| <b><math>f_{max}</math> (Hz)</b> | 1.257                   | 1.929        | 2.429        | 2.515        |

**Table 3.2 Overview of the wave heights  $H_{m0}$  which have been derived from the spectra between the boundaries  $f_{min}$  and  $f_{max}$ .**

<sup>1)</sup> Incident wave derived from three wave height meters (WHM)

|                | <i>D</i> <sub>10</sub> (μm) | <i>D</i> <sub>50</sub> (μm) | <i>D</i> <sub>90</sub> (μm) |
|----------------|-----------------------------|-----------------------------|-----------------------------|
| <b>minimum</b> | 51                          | 82                          | 115                         |
| <b>average</b> | 65                          | 93                          | 122                         |
| <b>maximum</b> | 76                          | 109                         | 148                         |

**Table 3.3** Some characteristic values out of the grain size

| <b>Test</b> | <b>Average temperature (°C)</b> |
|-------------|---------------------------------|
| T01         | 15.9                            |
| T02         | 15.9                            |
| T03         | 15.7                            |
| T11         | 13.7                            |
| T12         | 14.1                            |
| T13         | 14.0                            |

**Table 3.4 Measured water temperatures**

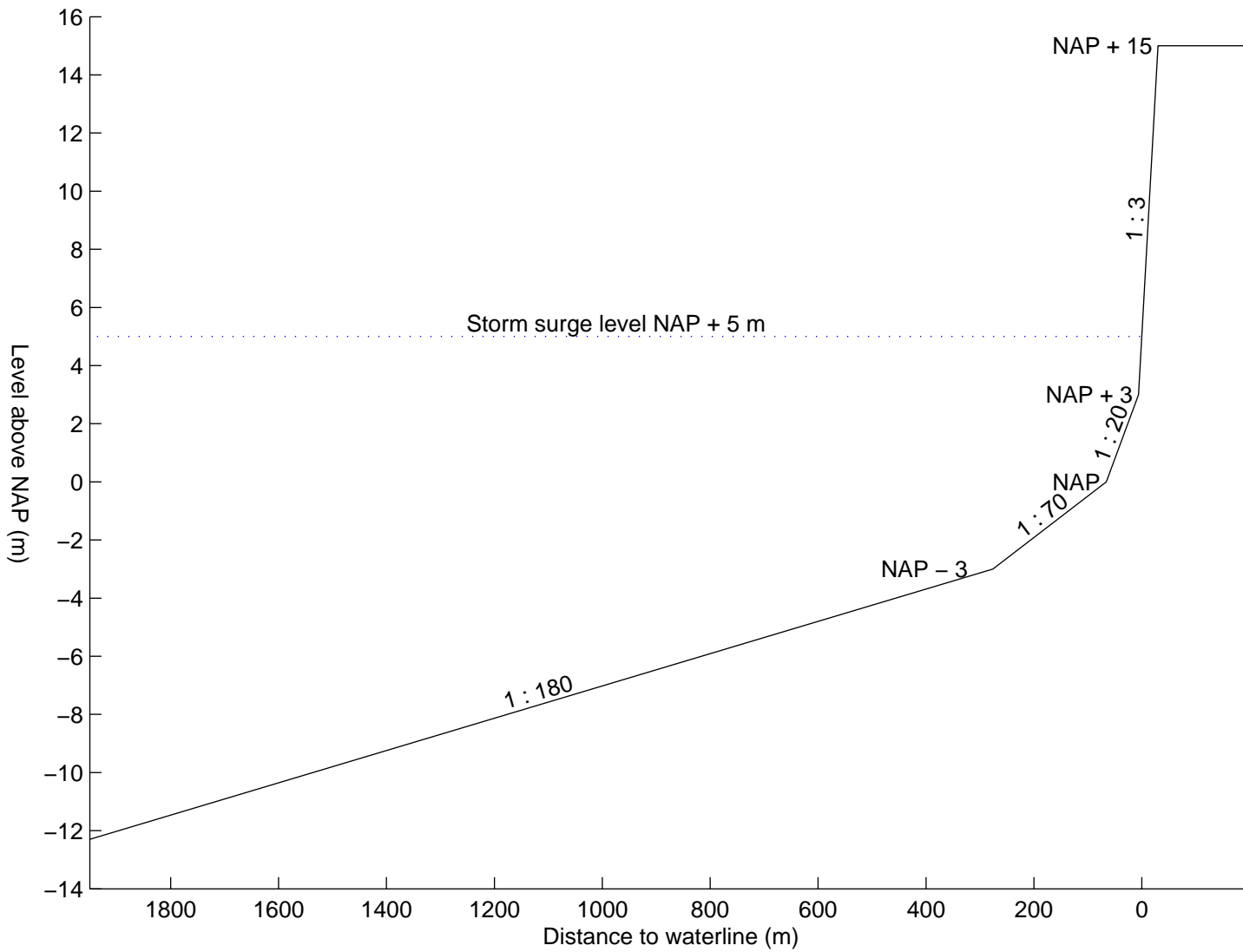
| Test | Peak wave period $T_p$<br>(s) | Wave height input (%) | Erosion volume change<br>(%) |
|------|-------------------------------|-----------------------|------------------------------|
| T03  | 1.87                          | -12%                  | -4%                          |
| T01  | 2.27                          | -11%                  | -4%                          |
| T02  | 2.72                          | +16%                  | +6%                          |
| T11  | 2.24                          | +13%                  | +4%                          |
| T13  | 2.57                          | +23%                  | +9%                          |
| T12  | 2.92                          | +33%                  | +15%                         |

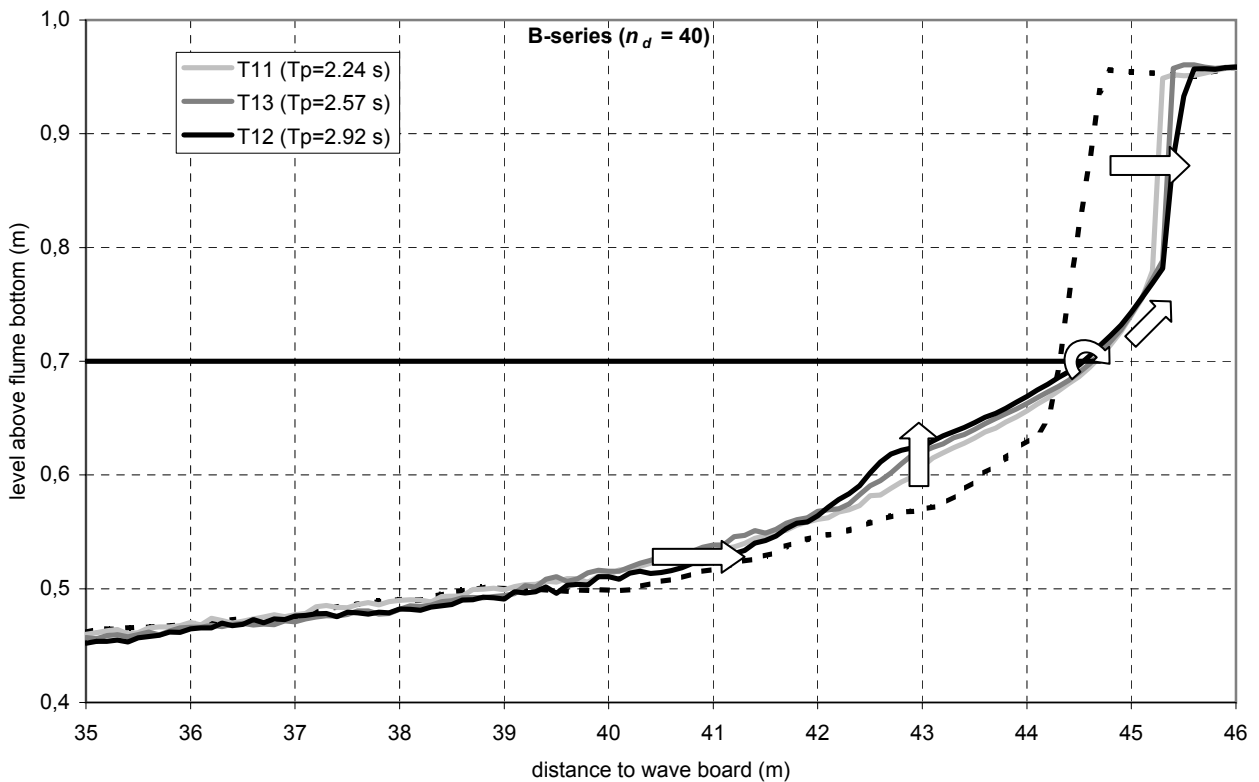
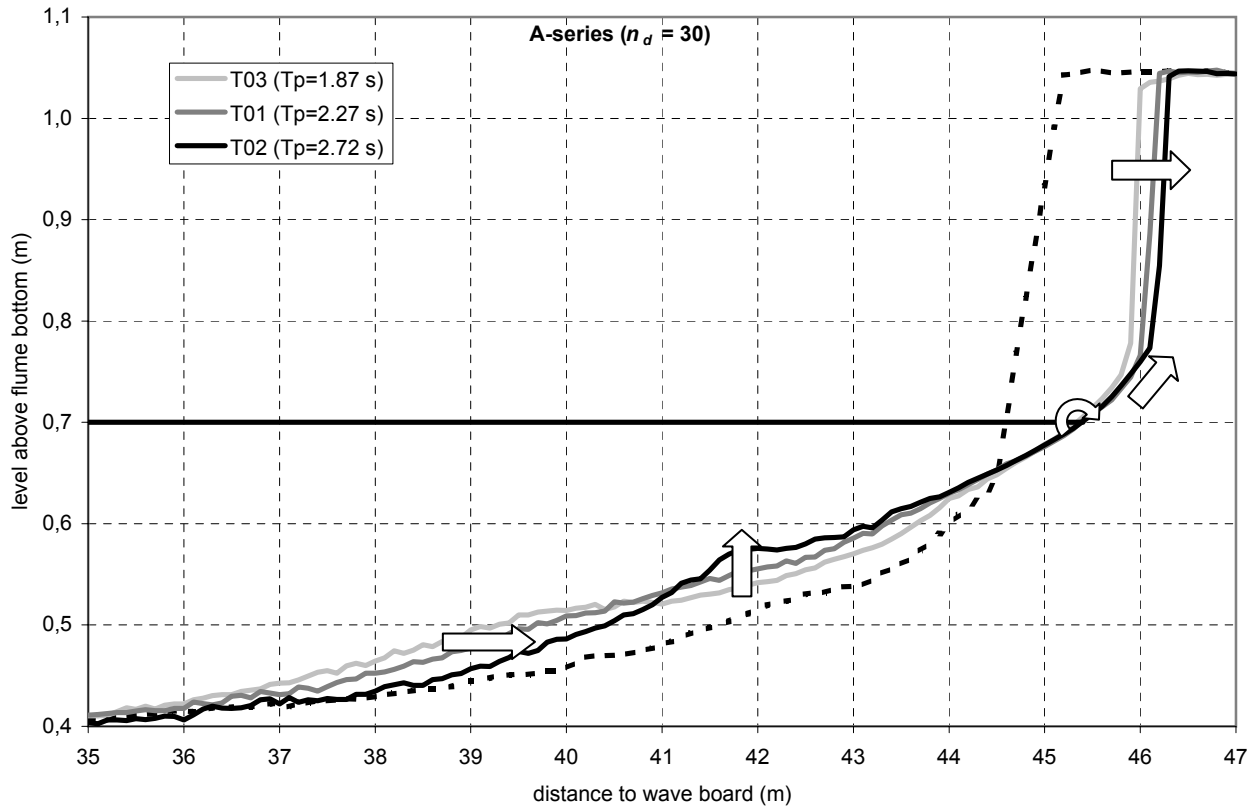
**Table 4.1 Sensitivity of erosion volume for wave height according to DUROSTA (default settings). ‘Tuning near dune’ computations (Section 4.2.2) with respect to ‘Tuning near wave board’ (Section 4.2.1).**



# Figures

Schematised coastal profile, prototype reference profile  
Averaged profile along the Dutch coast





Overview cross-shore profiles in Schelde flume

2004

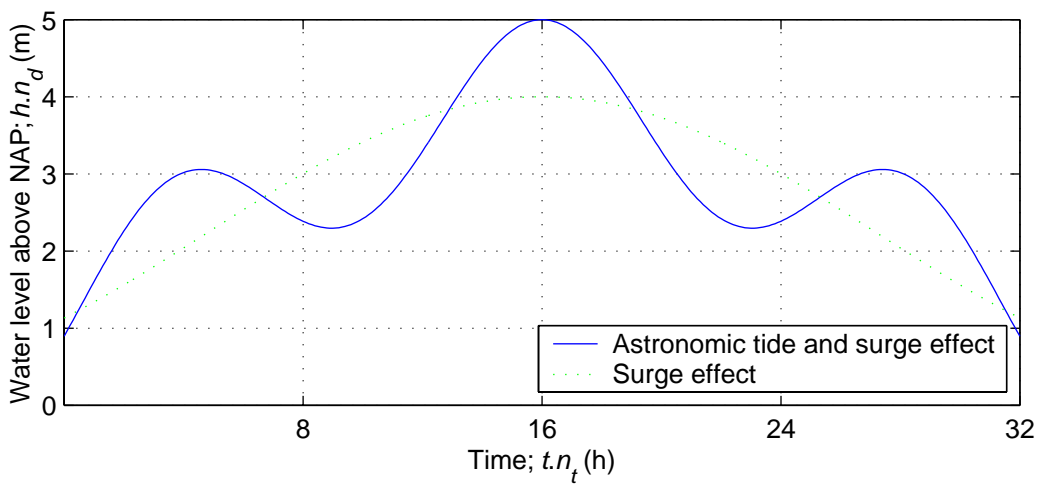
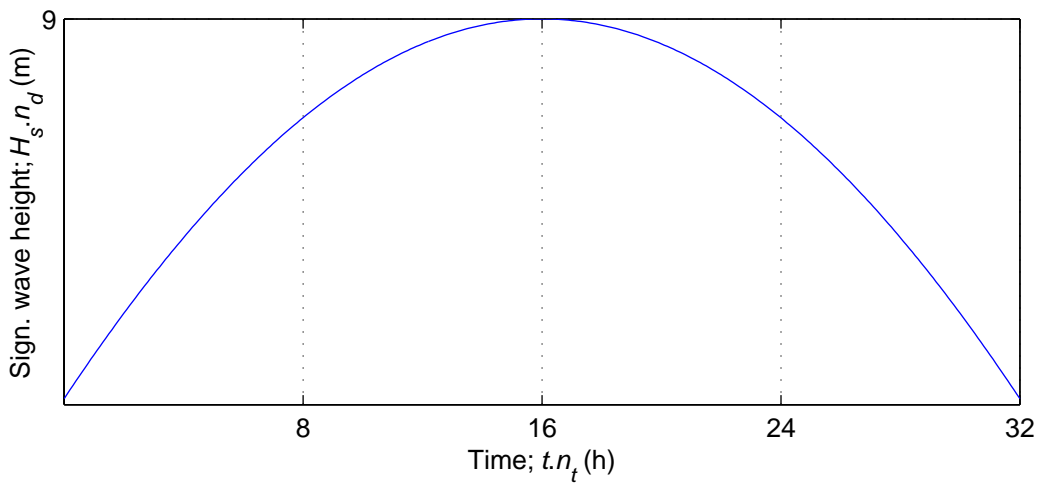
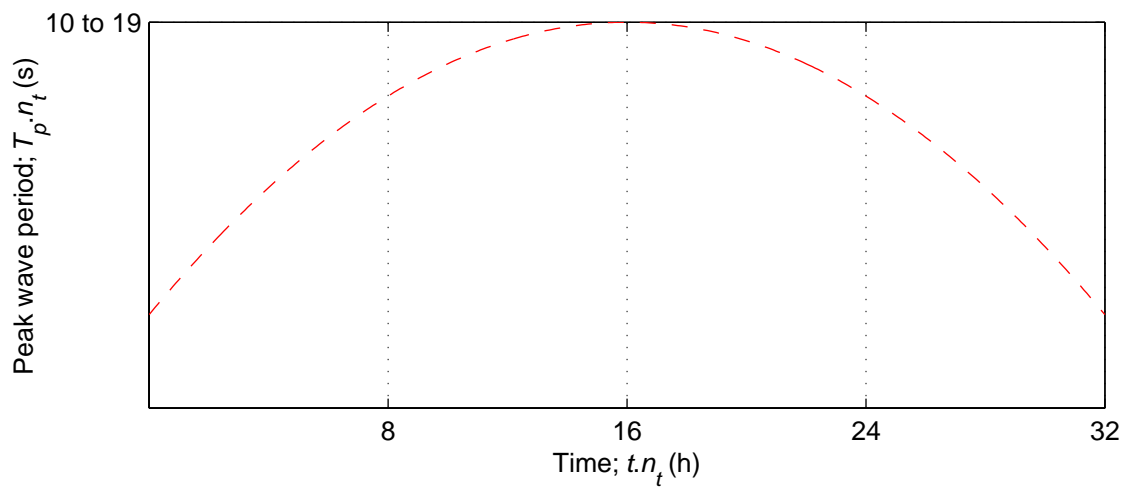
Qualitative effect of longer wave period after 6 hours (A-series) or 3 hours (B-series) of severe wave attack

T01/T03 and T11/T13

WL | Delft Hydraulics

H4265

Fig. 2 . 2



Assumed naturally varying deep water wave conditions  
and water level during a storm;  
Peak wave period research boundaries

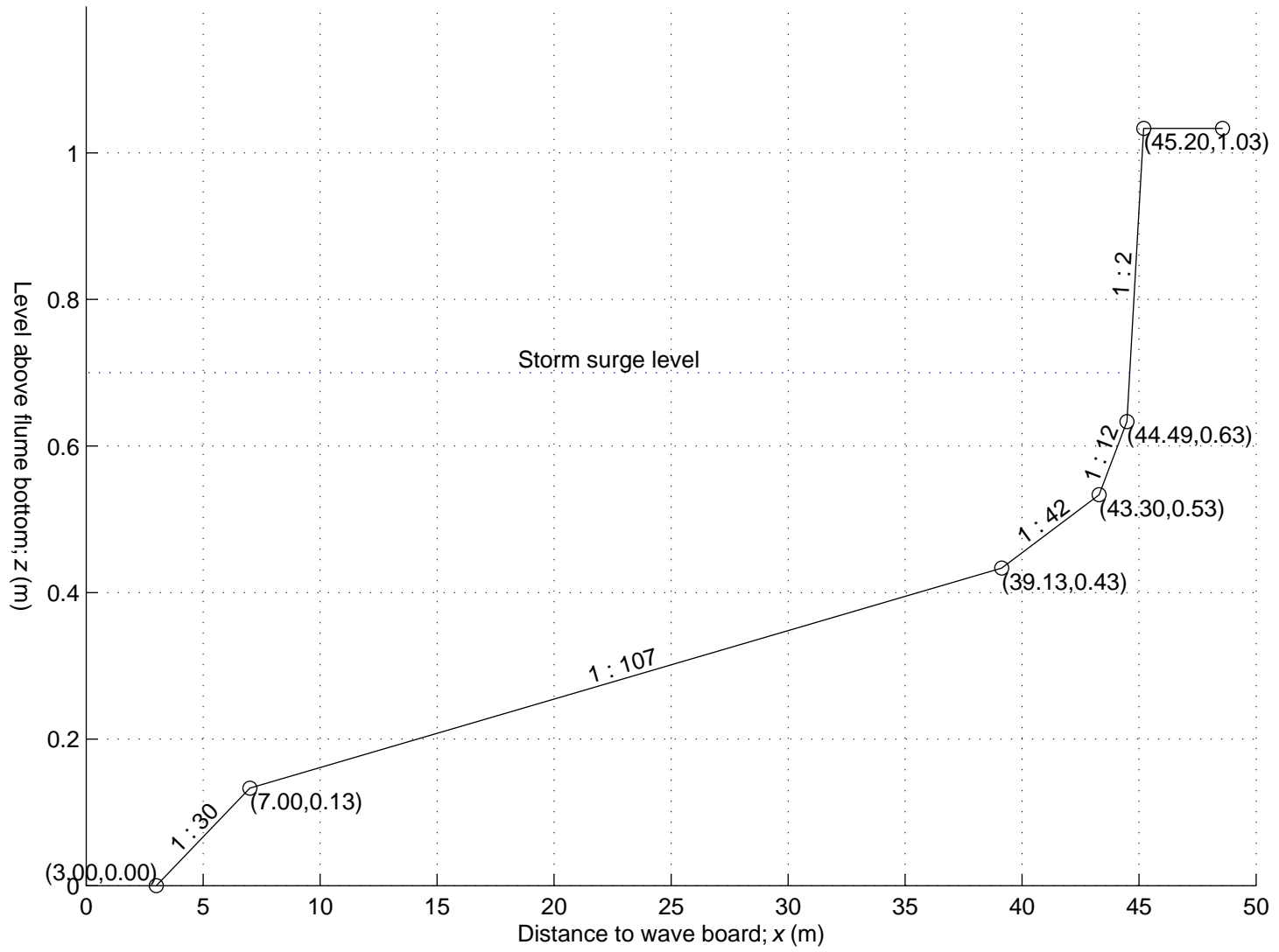
$$(n_t = \sqrt{n_d})$$

Desired initial cross-shore profile for A-series

$(n_d = 30)$

2004

Distortion = 1.68



WL | DELFT HYDRAULICS

Desired initial cross-shore profile for B-series

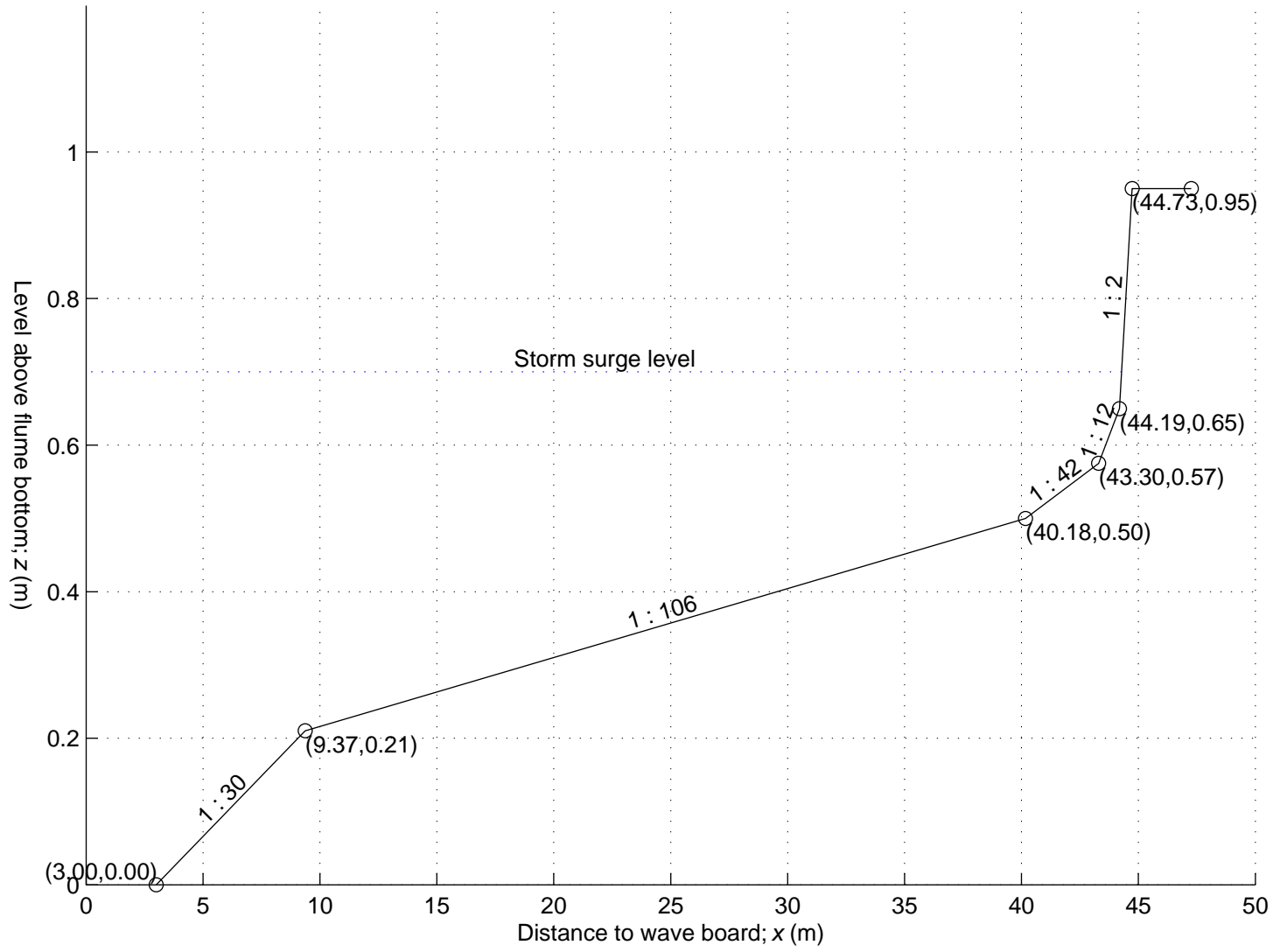
$(n_d = 40)$

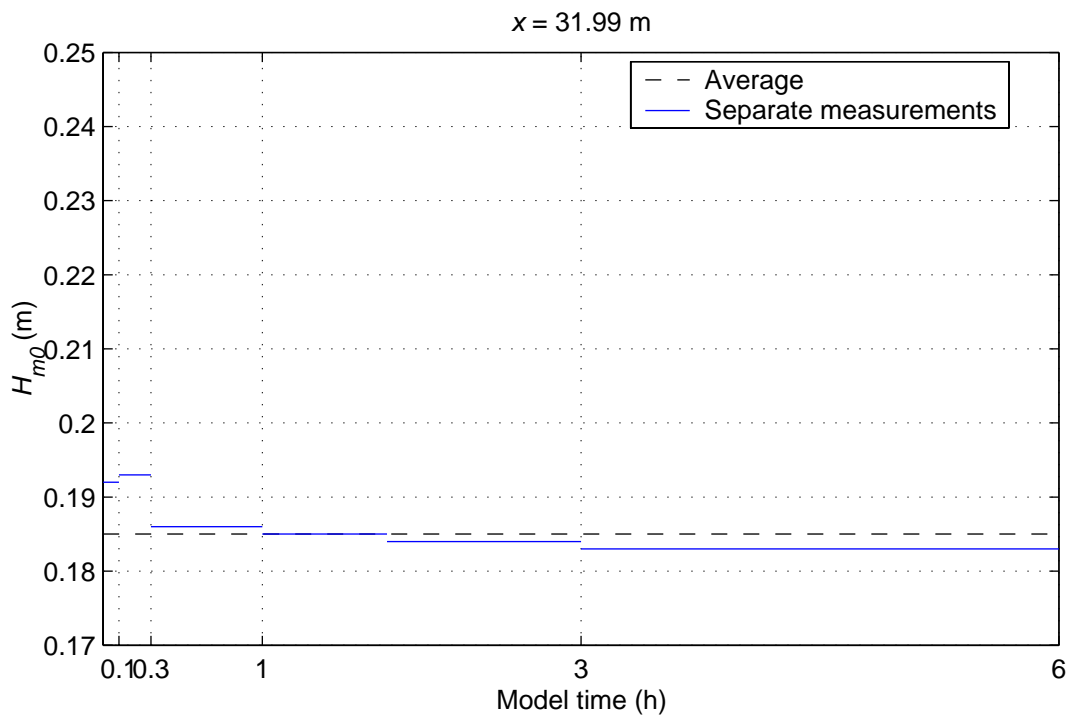
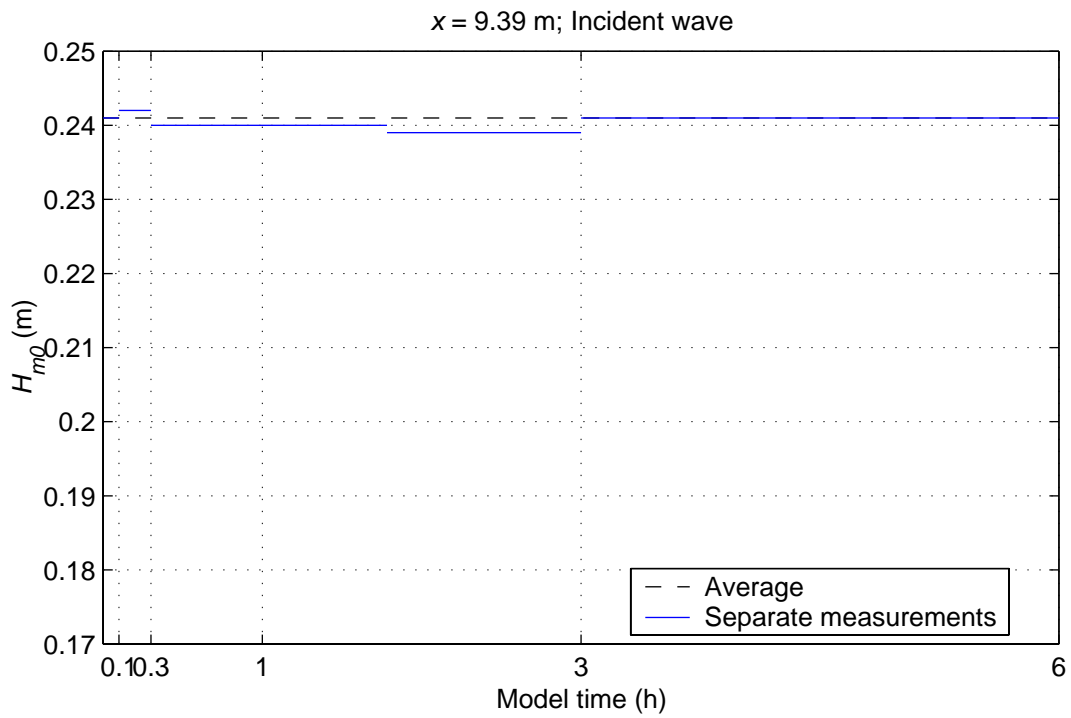
2004

Distortion = 1.68

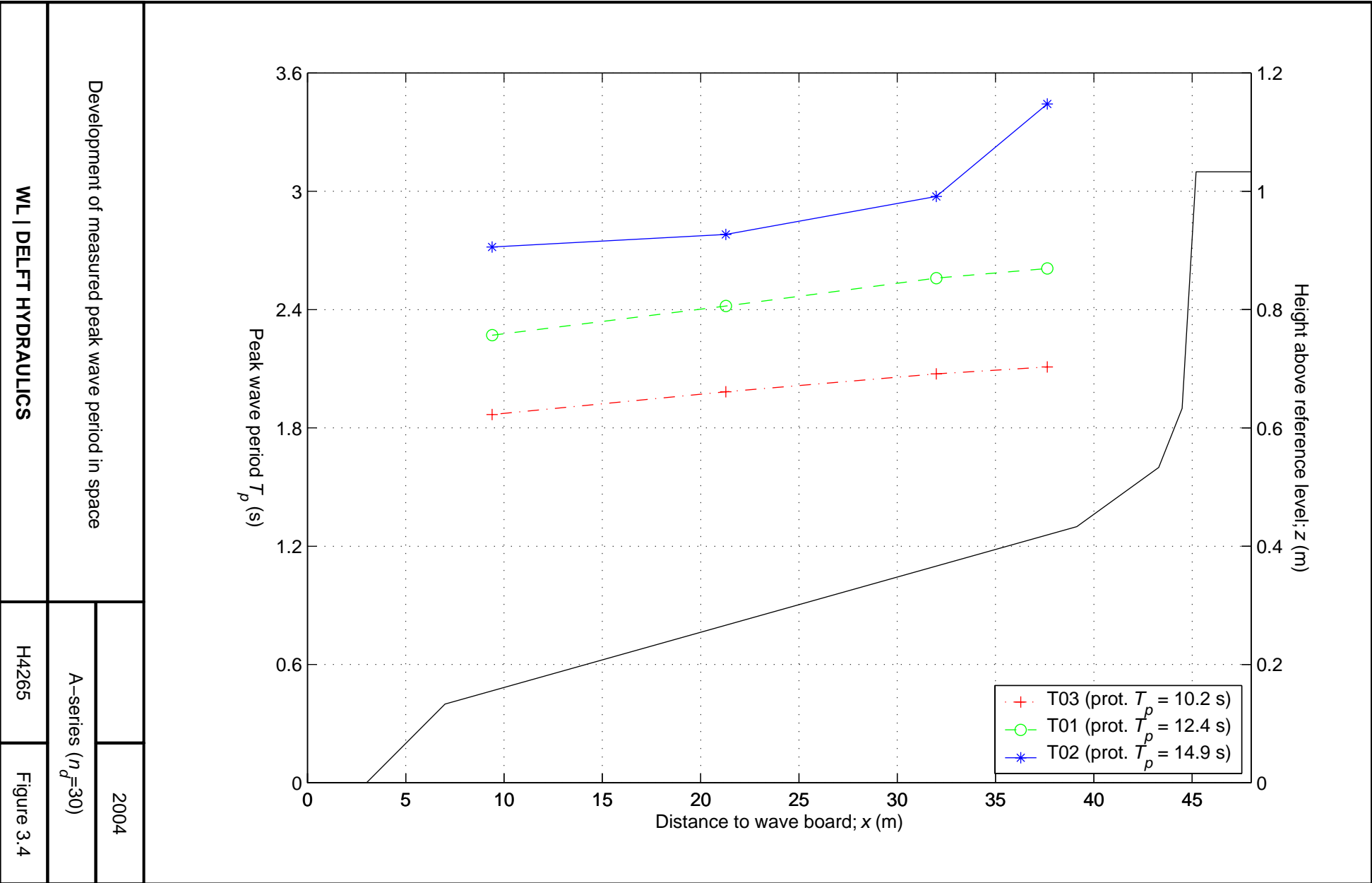
H4265

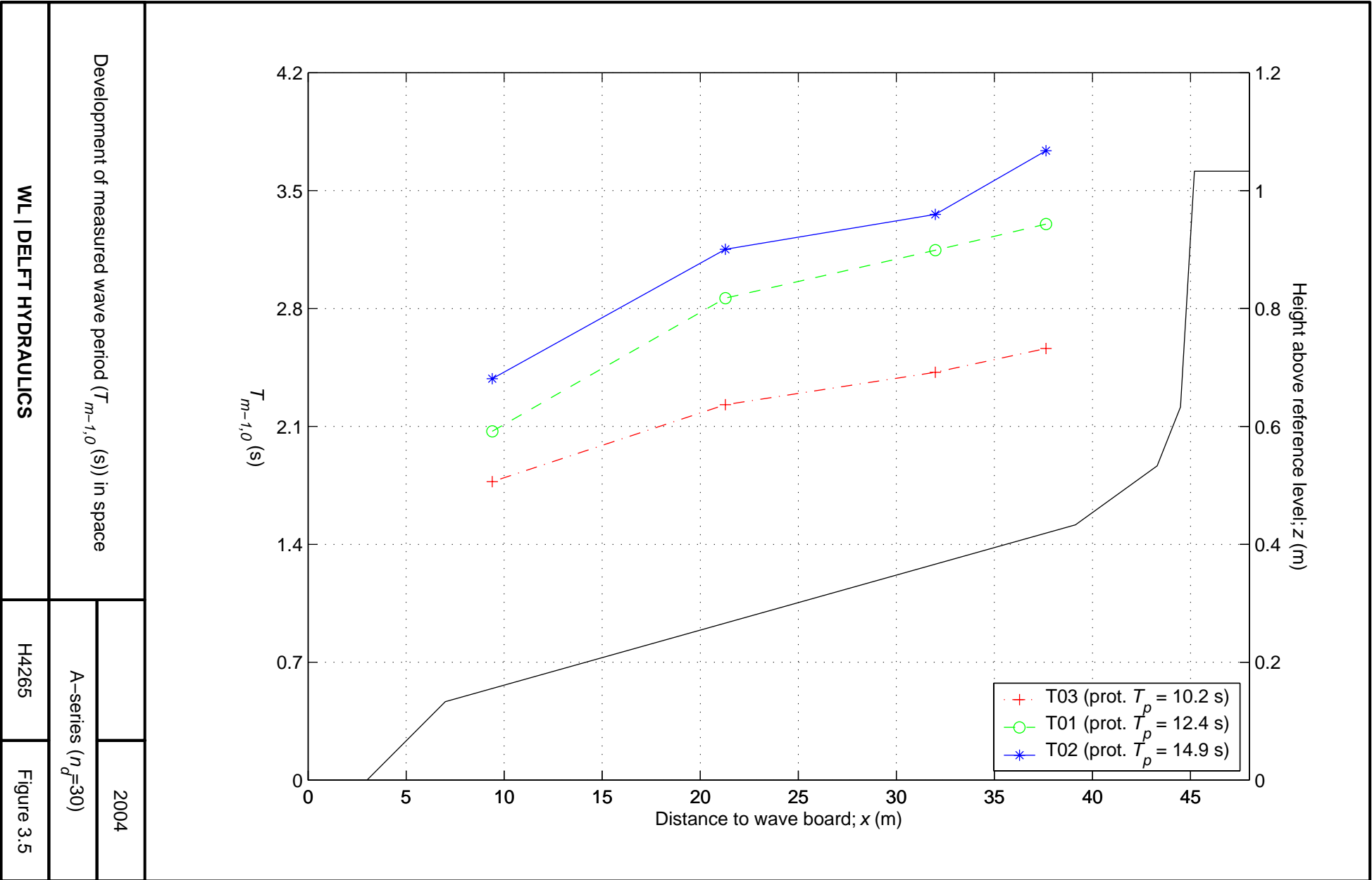
Figure 3.2

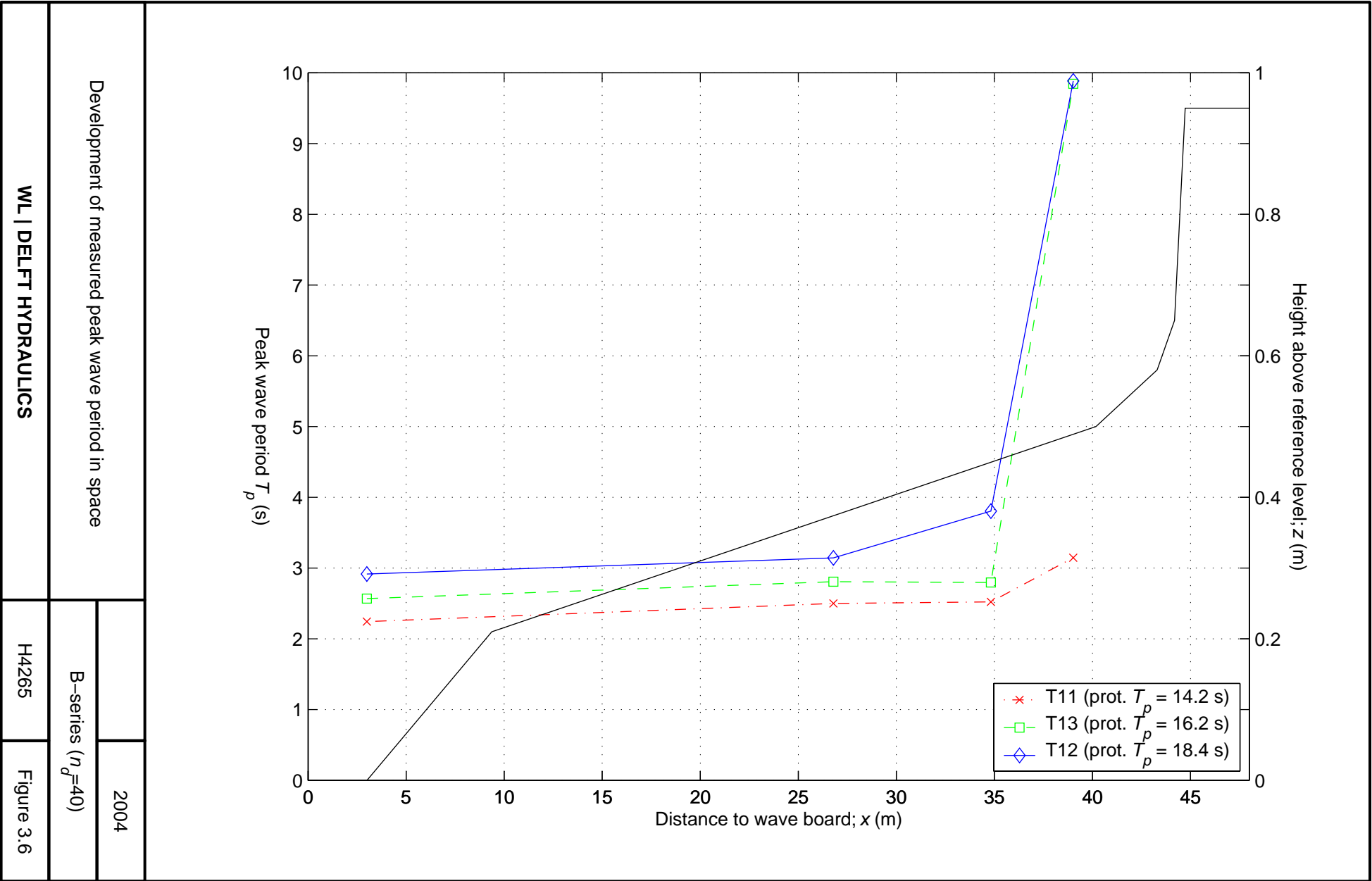


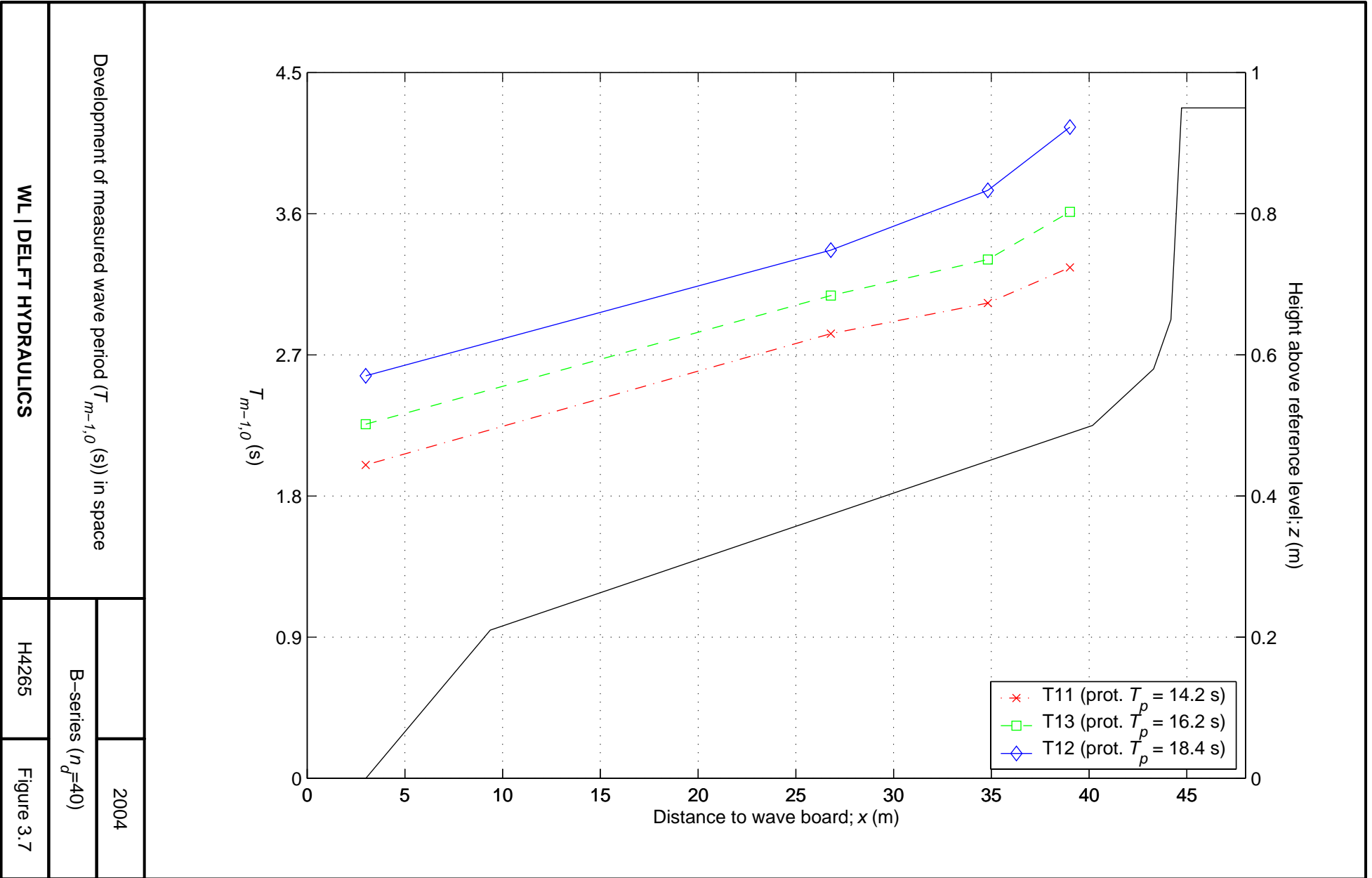


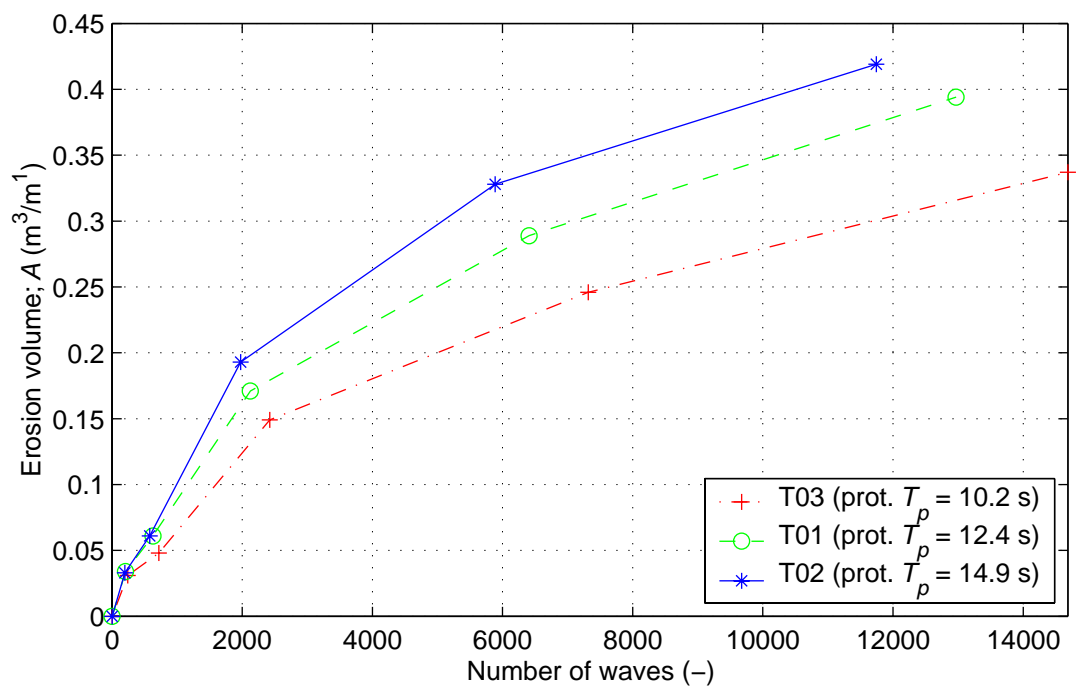
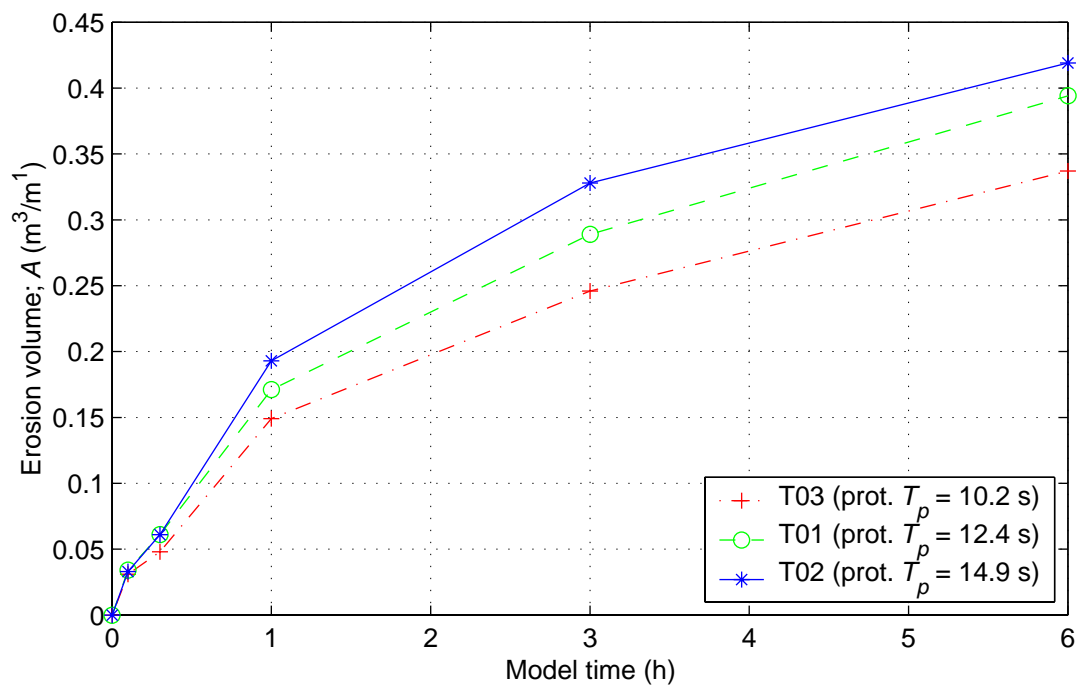
|   |                         |
|---|-------------------------|
| Wave height for separate time intervals compared with averaged signal over whole test | T01                     |
|   | A-series ( $n_d = 30$ ) |
| <b>WL   DELFT HYDRAULICS</b>  | Figure 3.3              |



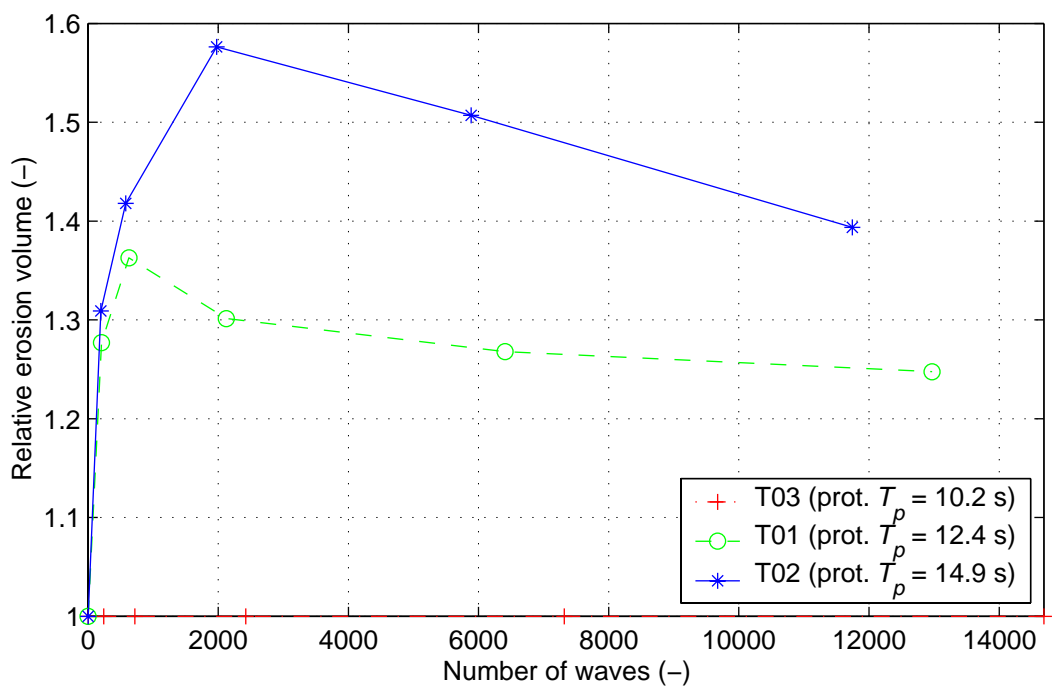
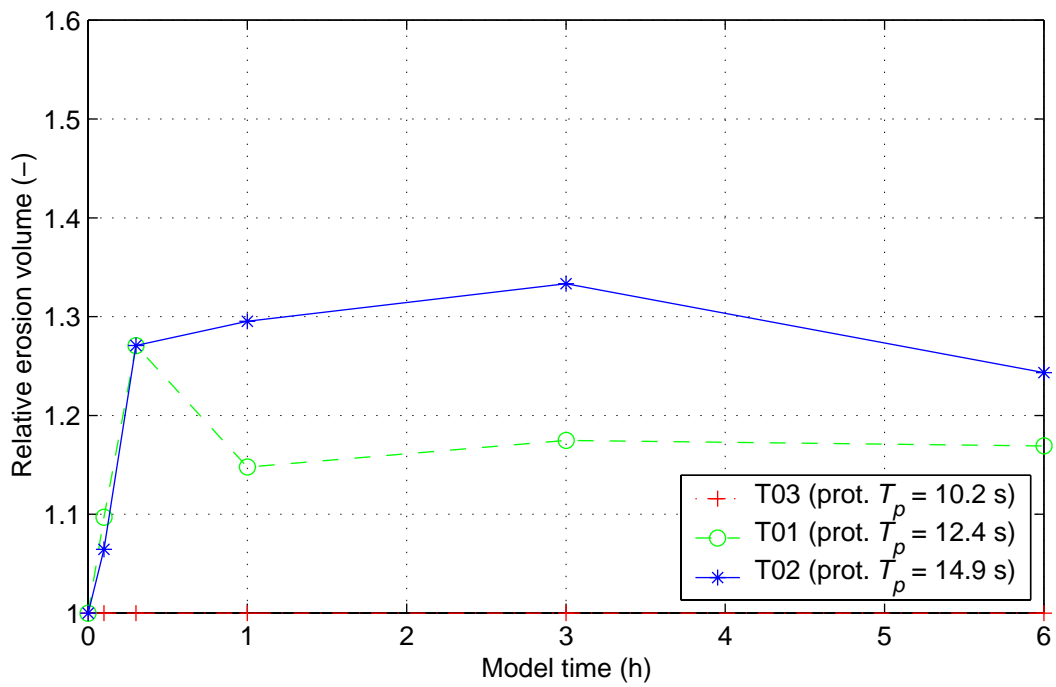




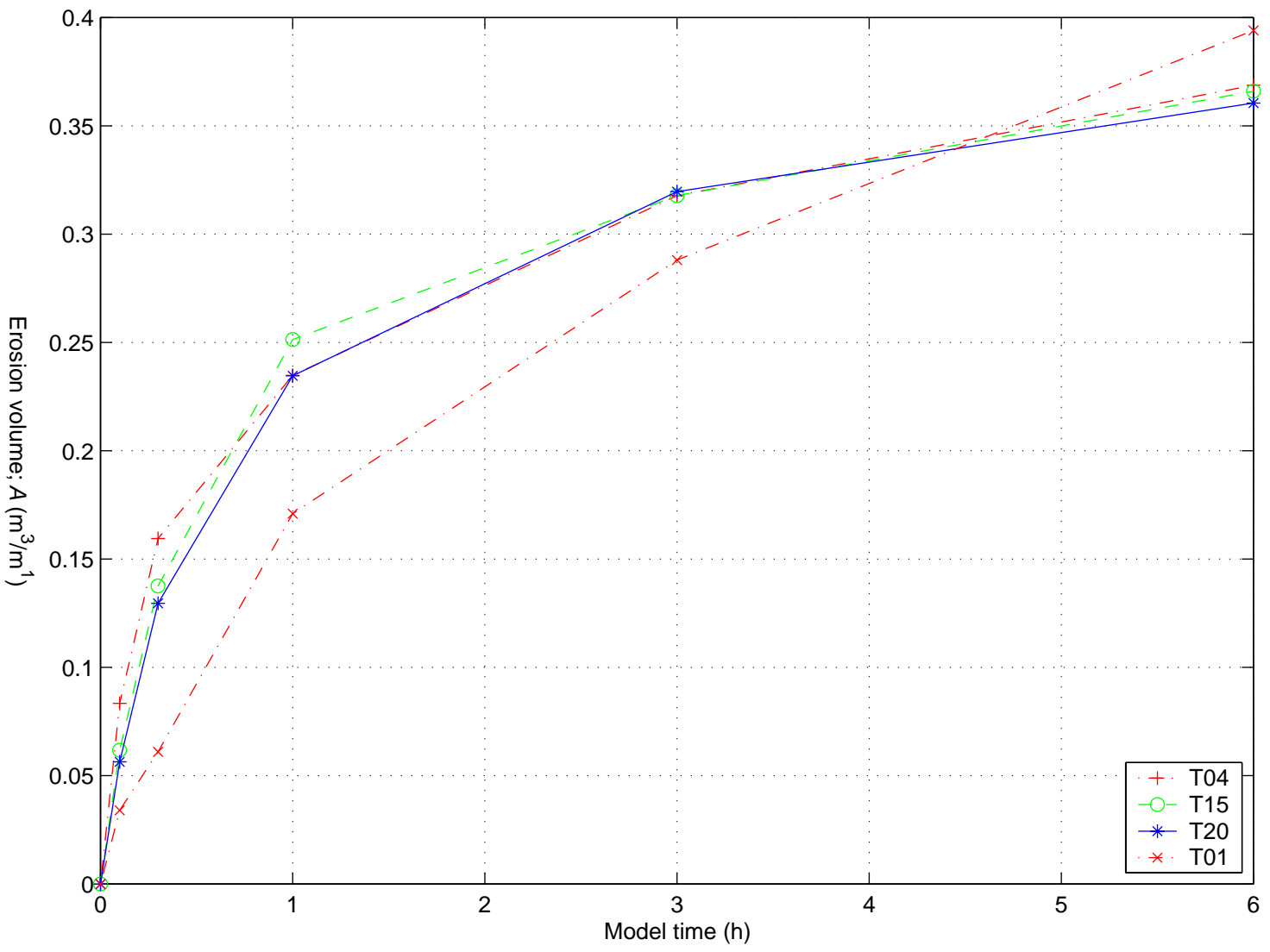




|                                 |                         |            |
|---------------------------------|-------------------------|------------|
| Development of measured erosion |                         | 2004       |
|                                 | A-series ( $n_d = 30$ ) |            |
| <b>WL   DELFT HYDRAULICS</b>    | H4265                   | Figure 3.8 |



|   |                         |
|---|-------------------------|
| Relative measured erosion w.r.t. test T03 | 2004                    |
|   | A-series ( $n_d = 30$ ) |
| <b>WL   DELFT HYDRAULICS</b>              | H4265      Figure 3.9   |



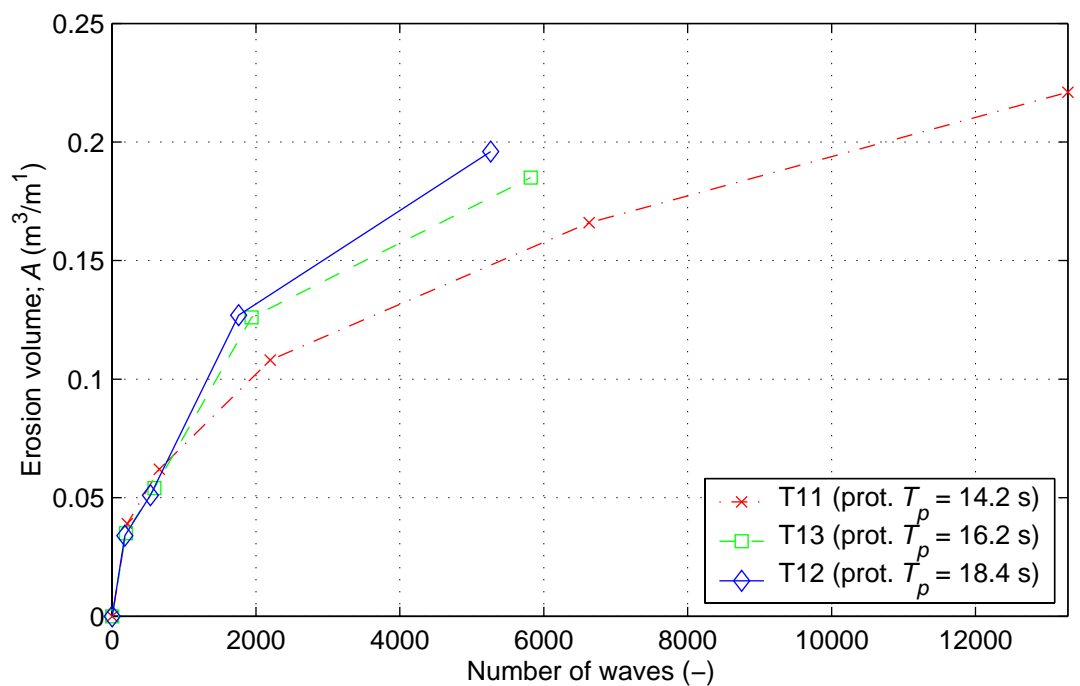
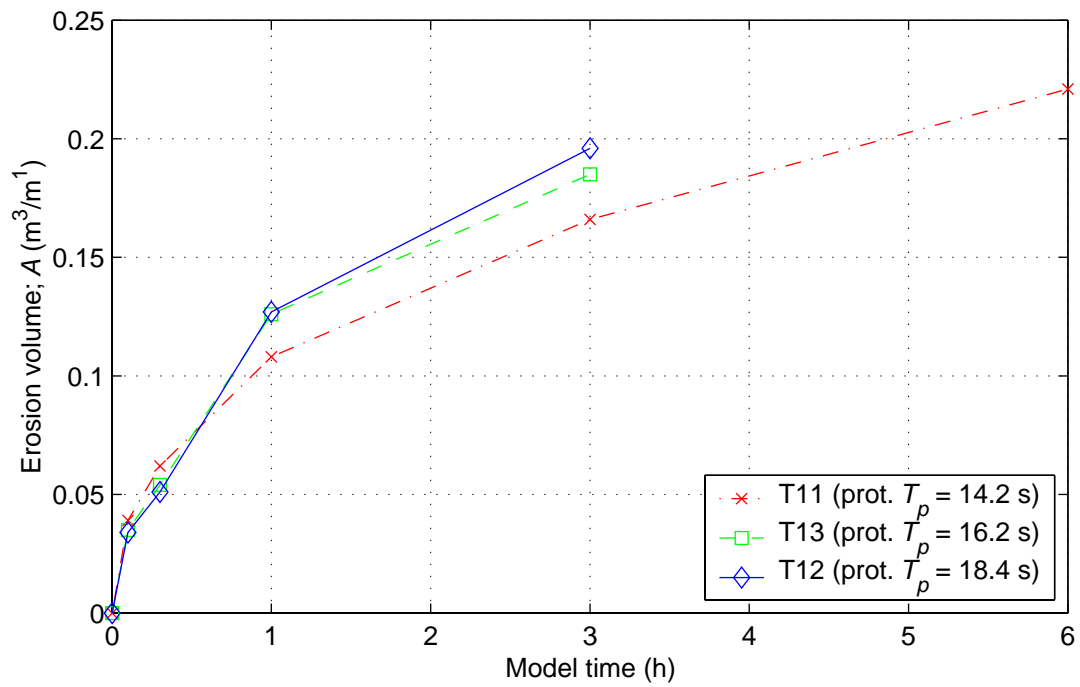
Comparison H4265 (T01) with M1819-I (T04, T15 and T20)  
 Development of measured erosion volumes in time

H4265 (2004)

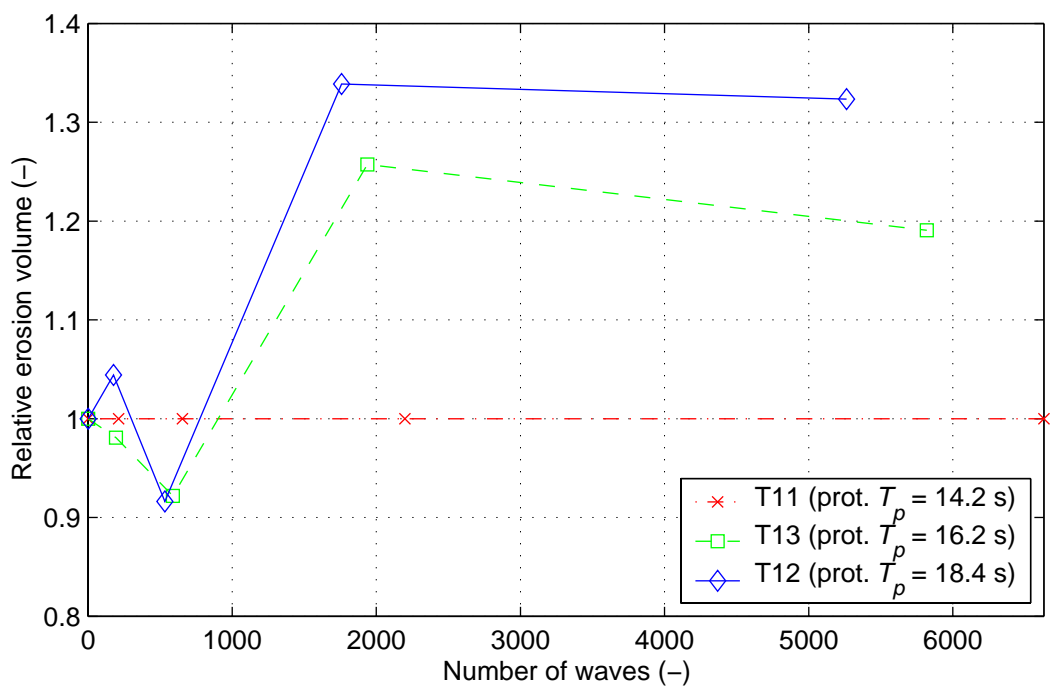
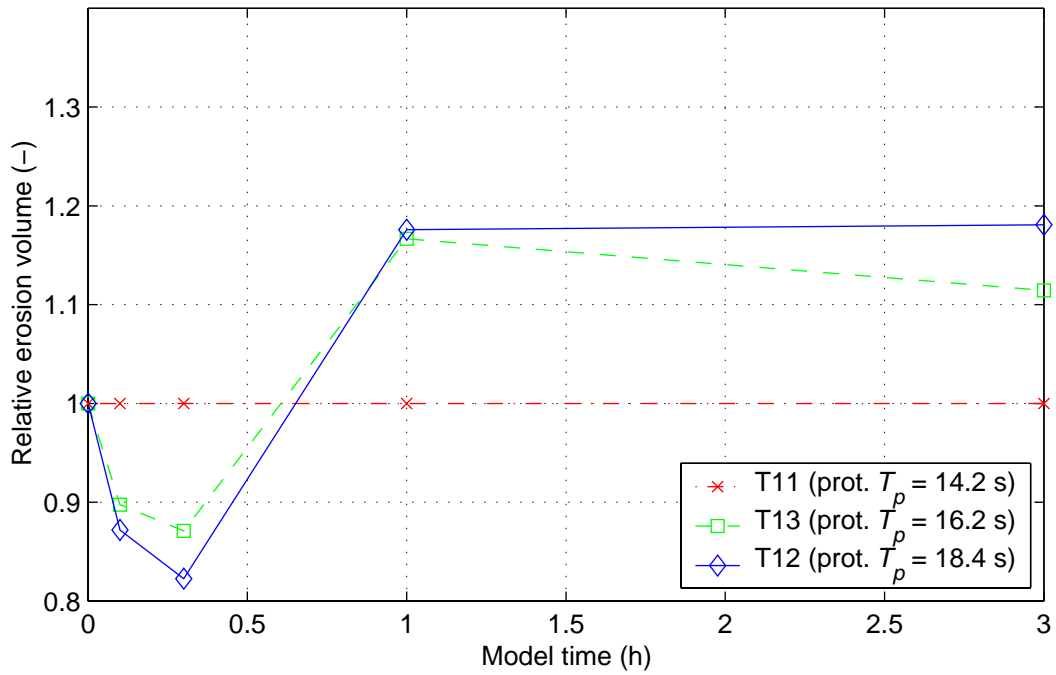
M1819-I (1982)

WL | DELFT HYDRAULICS

Figure 3.10



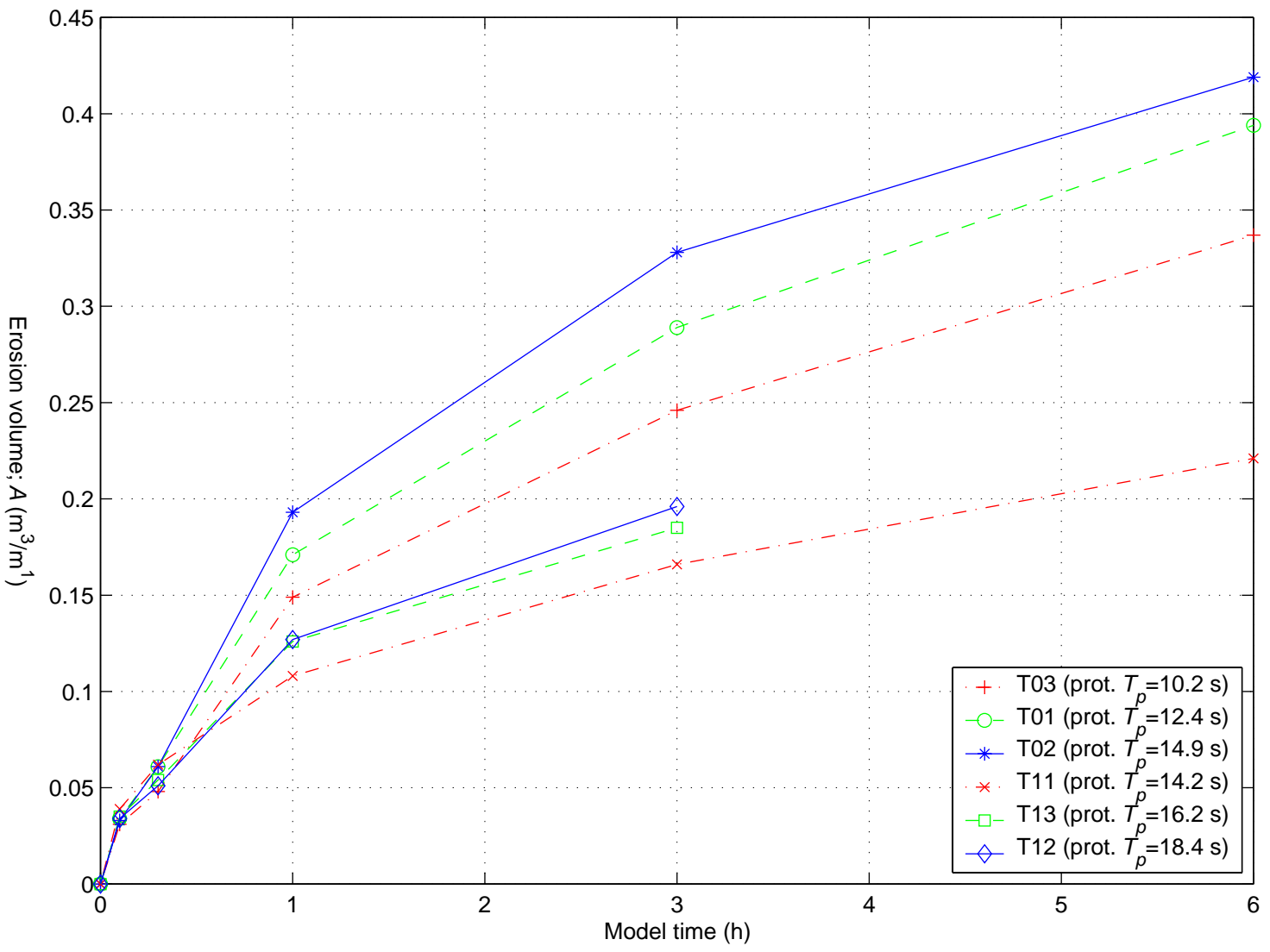
|                                 |                         |             |
|---------------------------------|-------------------------|-------------|
| Development of measured erosion |                         | 2004        |
|                                 | B-series ( $n_d = 40$ ) |             |
| <b>WL   DELFT HYDRAULICS</b>    | H4265                   | Figure 3.11 |



|   |                         |             |
|---|-------------------------|-------------|
| Relative measured erosion w.r.t. test T11 |                         | 2004        |
|   | B-series ( $n_d = 40$ ) |             |
| <b>WL   DELFT HYDRAULICS</b>              | H4265                   | Figure 3.12 |

Development of measured erosion volumes in time

2004



\* B-series translated into depth scale  $\eta_{\rho}^2=30$

Development of measured erosion volumes in time

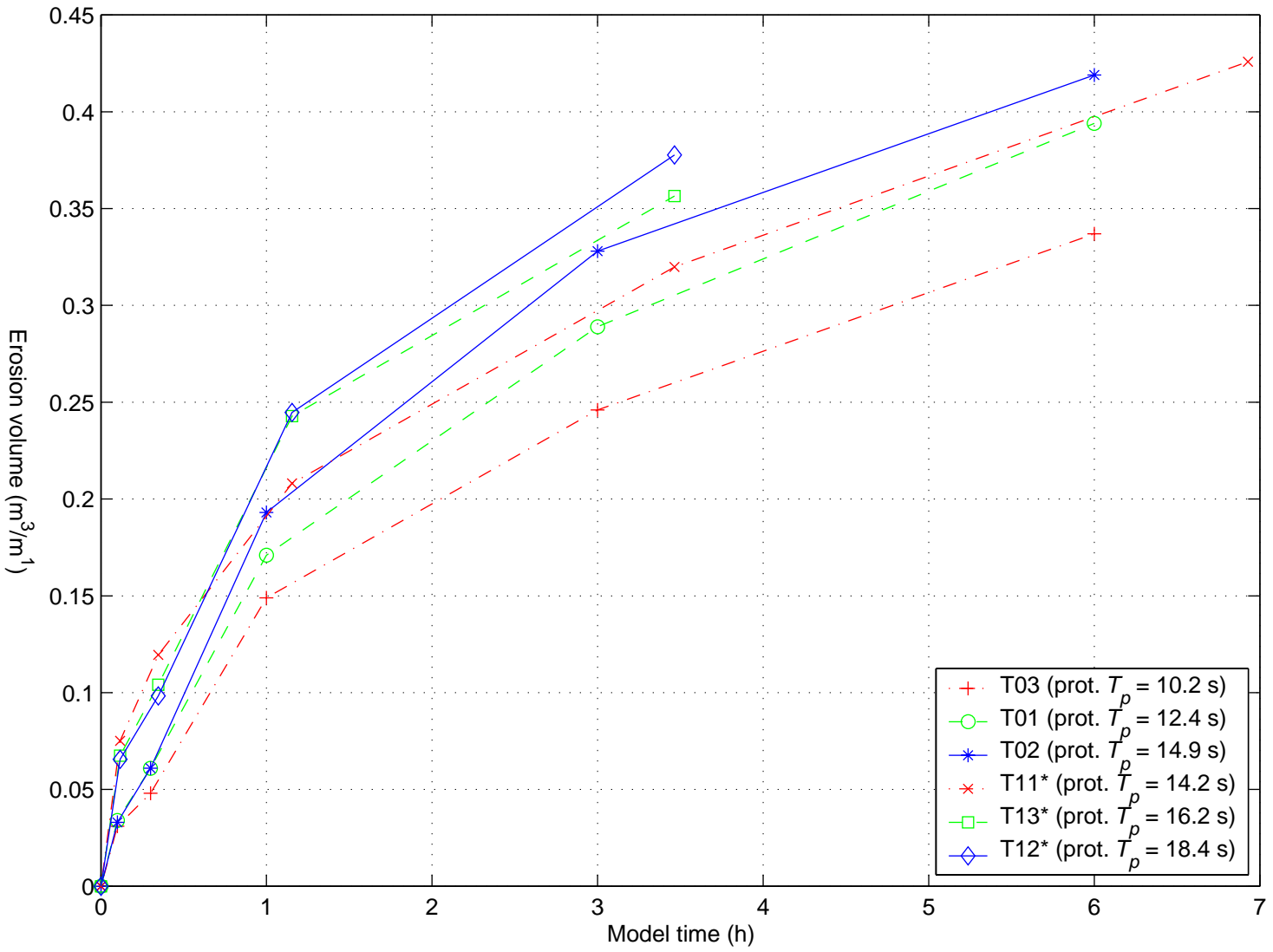
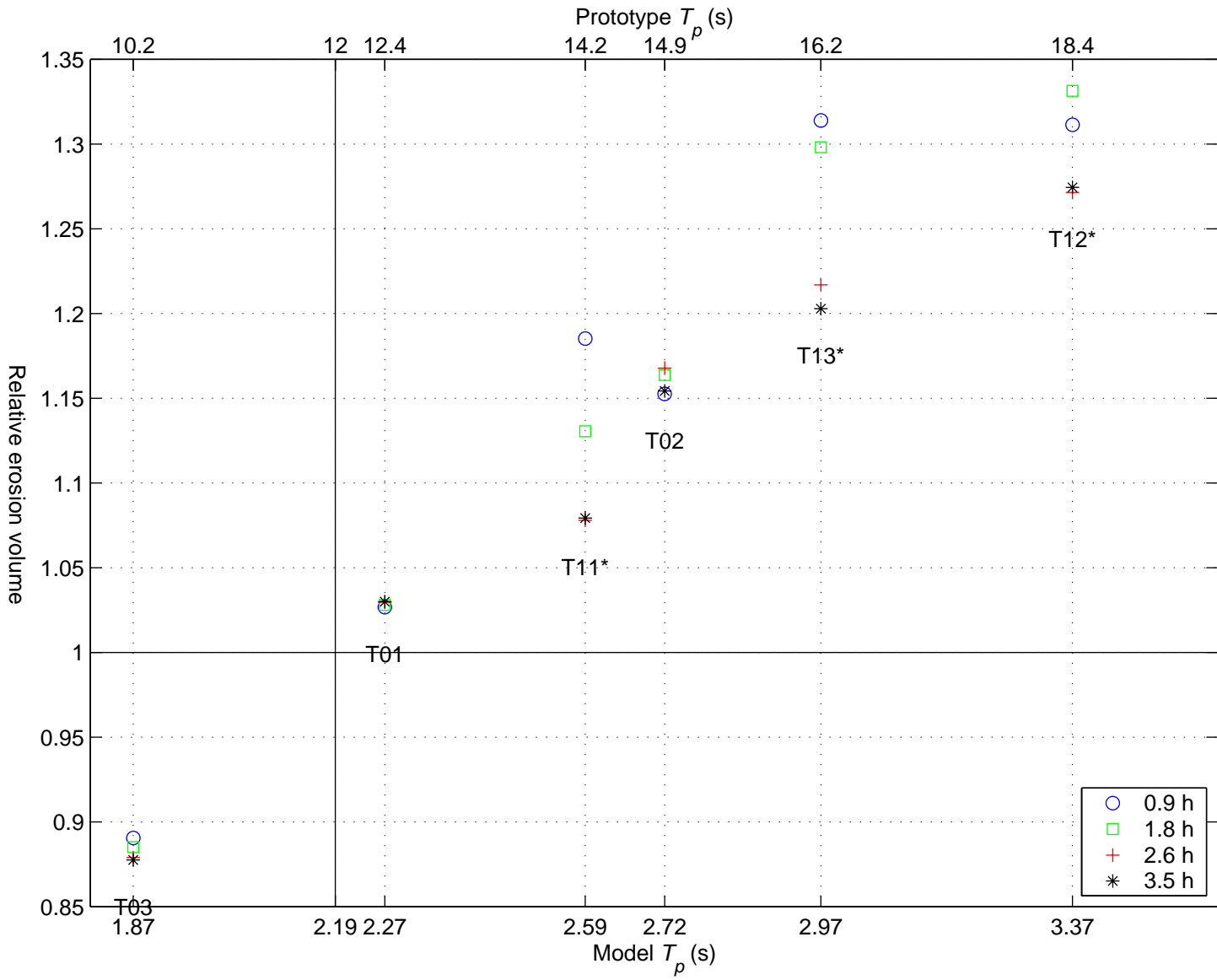
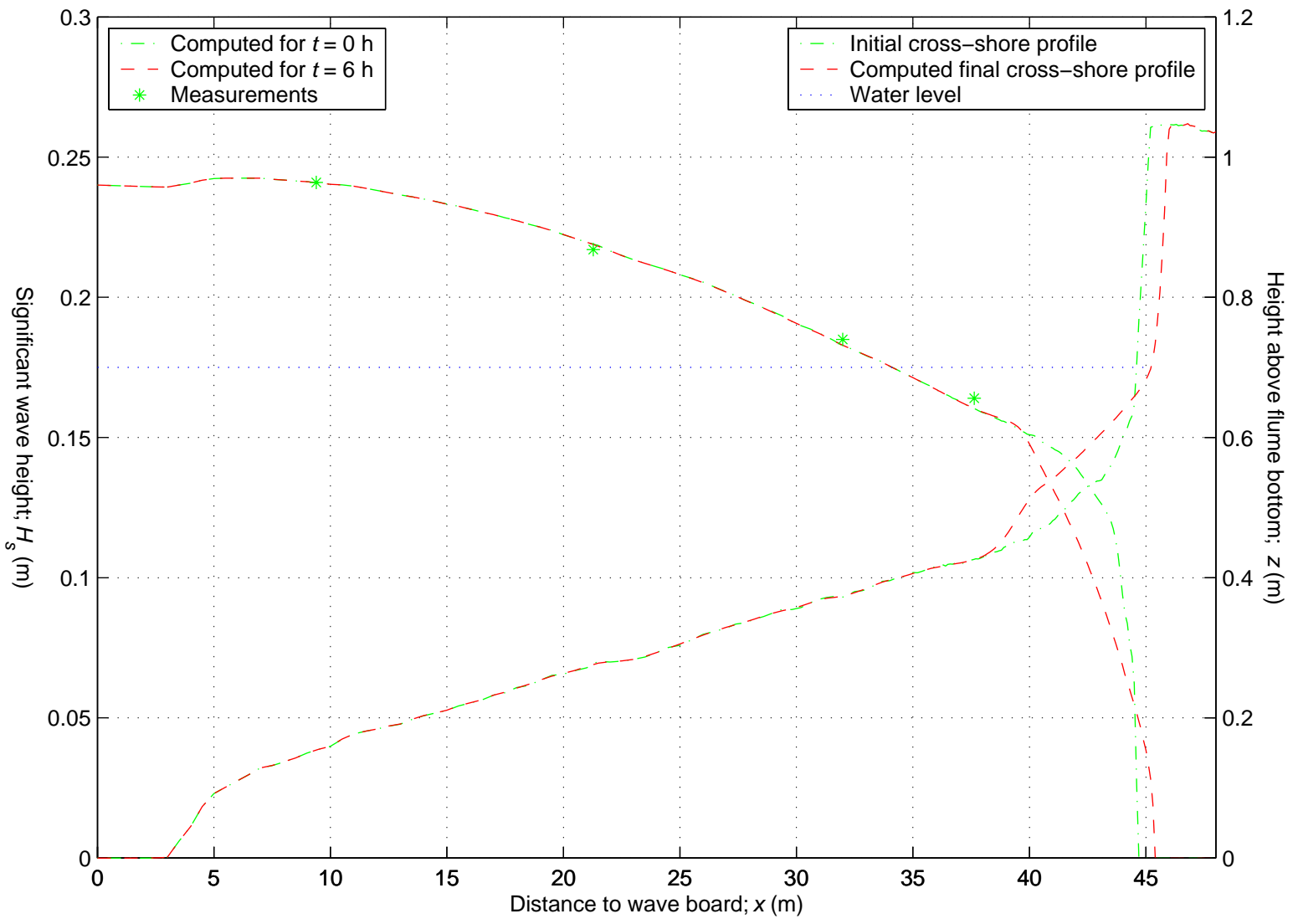


Figure 3.14

Relative erosion with respect to basic case  $T_p = 12$  s  
 for different moments of model time  
 \* B-series translated into depth scale  $n_d=30$





Comparison computed initial and final cross-shore profile and corresponding wave propagation

DUROSTA T01 ( $T_p=2.27$  s)

A-series ( $n_p=30$ )

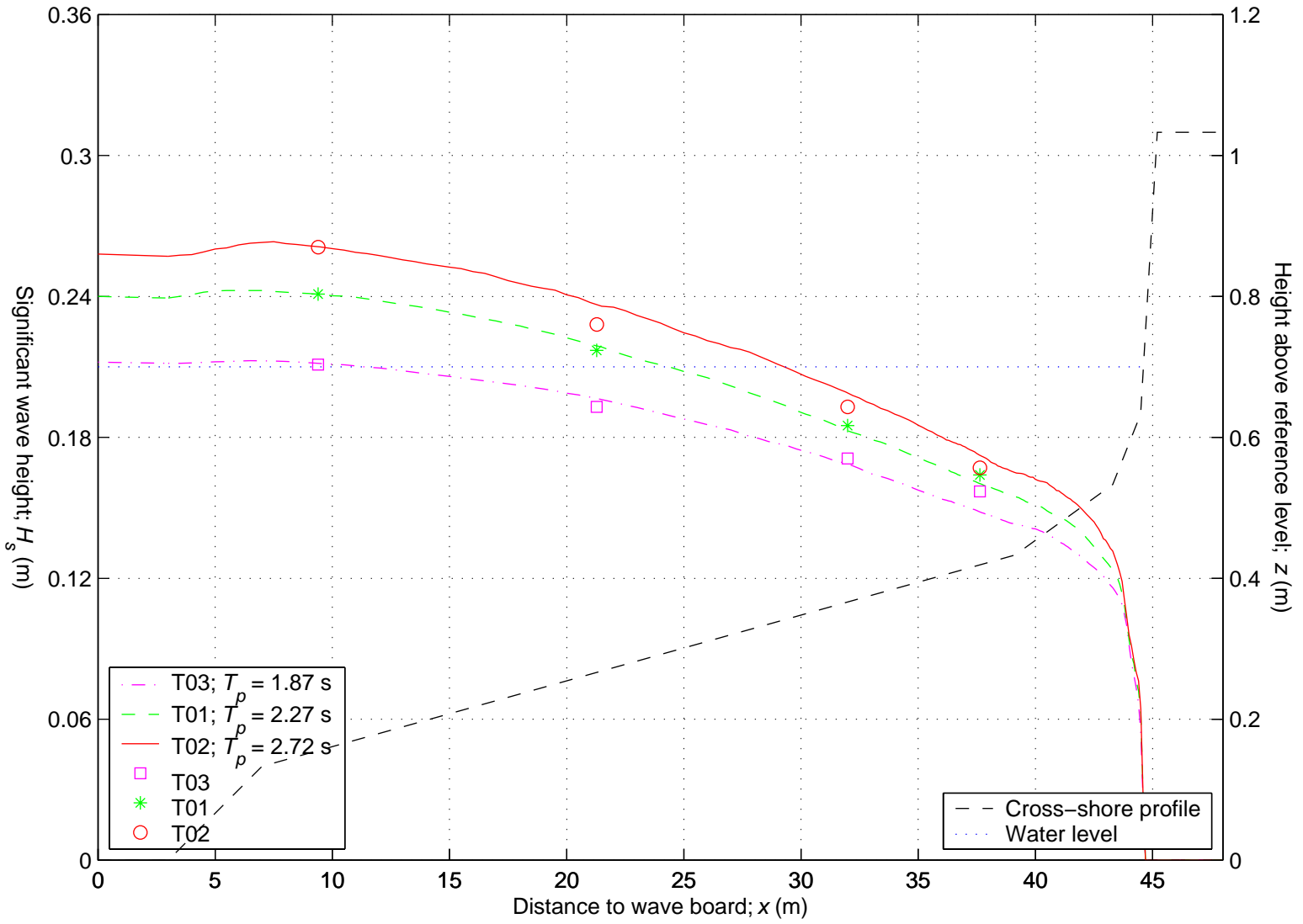
WL | DELFT HYDRAULICS

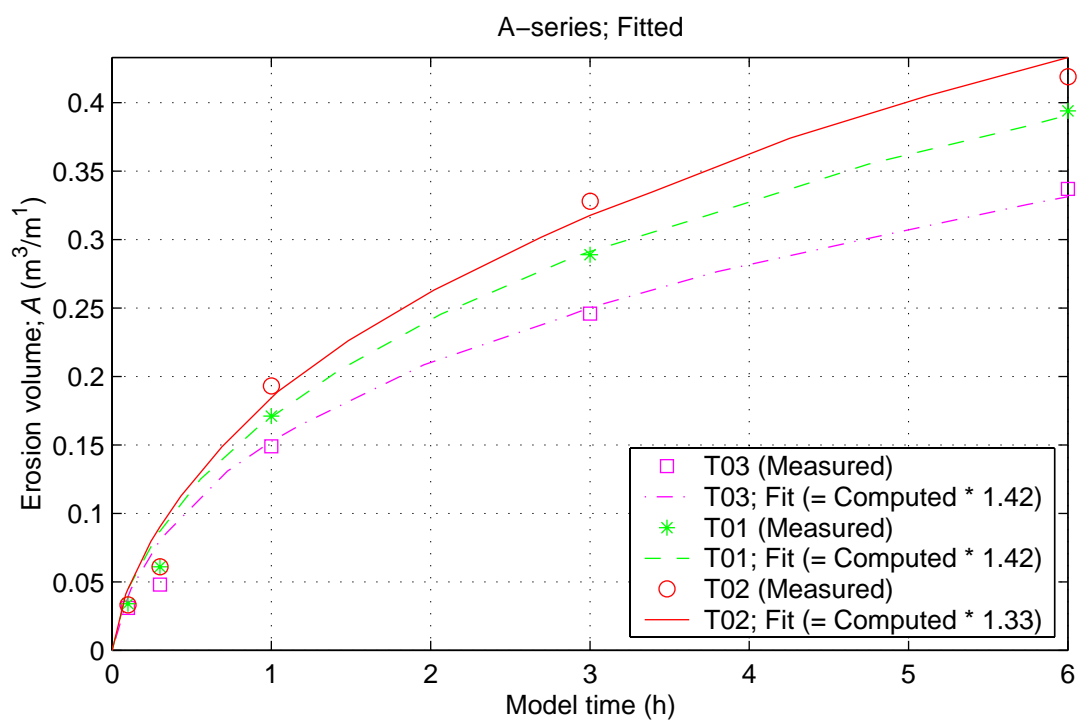
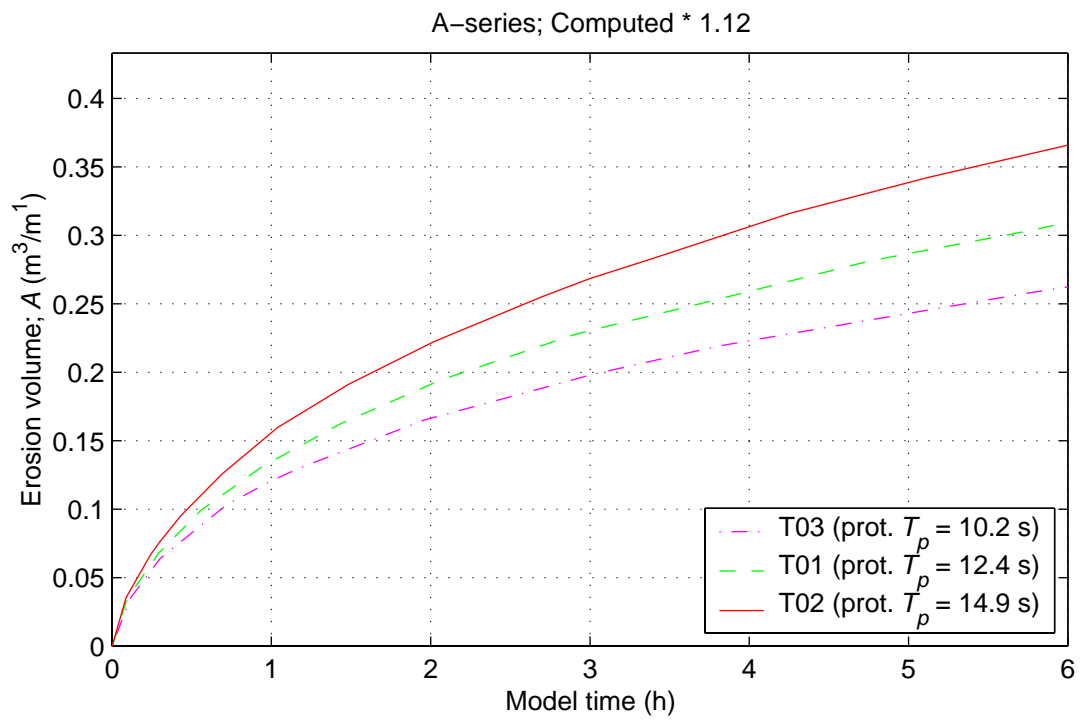
Figure 4.1

Wave propagation;  
Default settings; Tuned at  $x = 9.39$  m

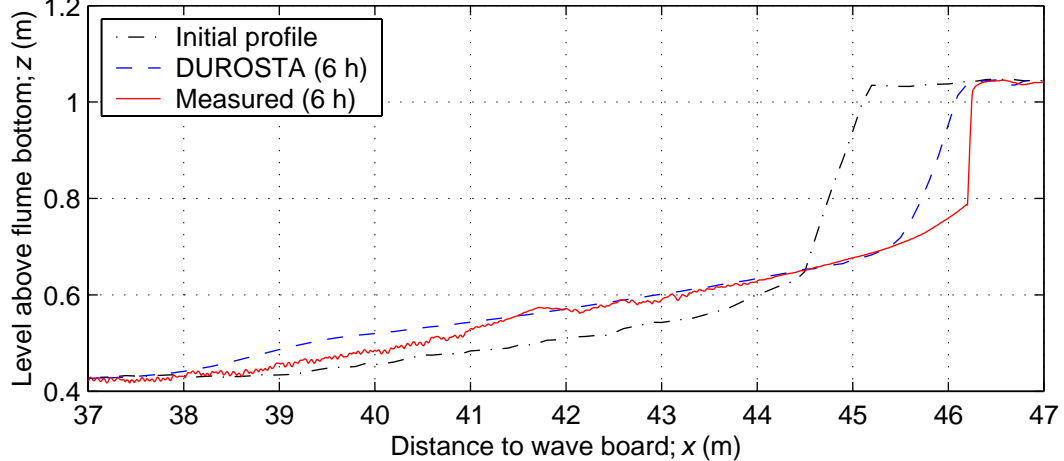
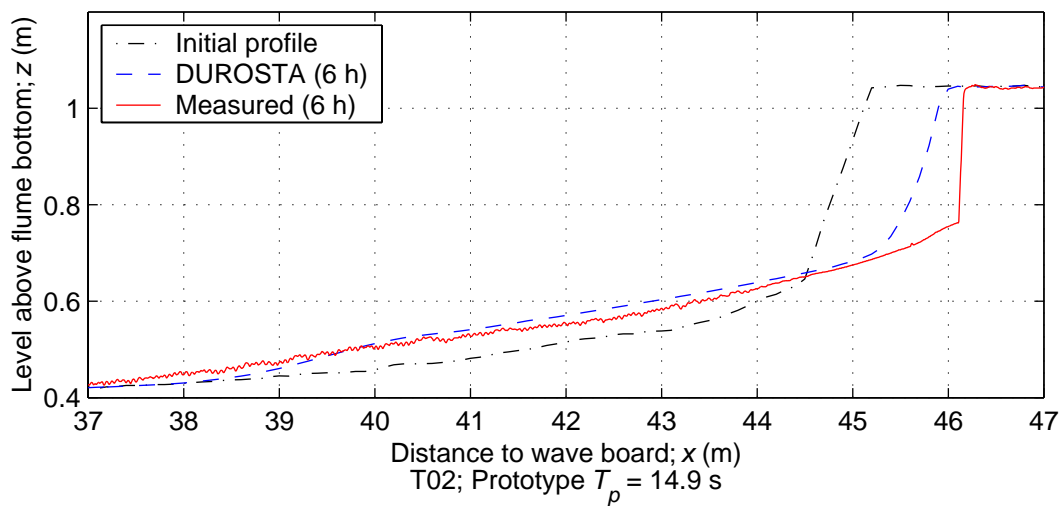
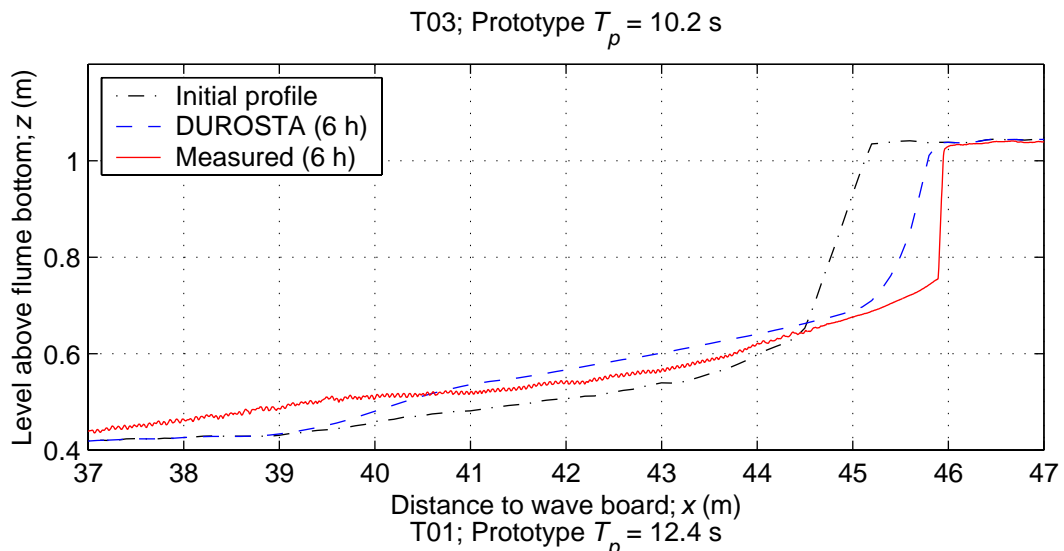
DUROSTA

A-series ( $n_d = 30$ )





|  |                         |
|--|-------------------------|
| Erosion volume development in time; Default settings;<br>Tuned at $x = 9.39$ m | DUROSTA                 |
|  | A-series ( $n_d = 30$ ) |
| <b>WL   DELFT HYDRAULICS</b>   | Figure 4.3              |

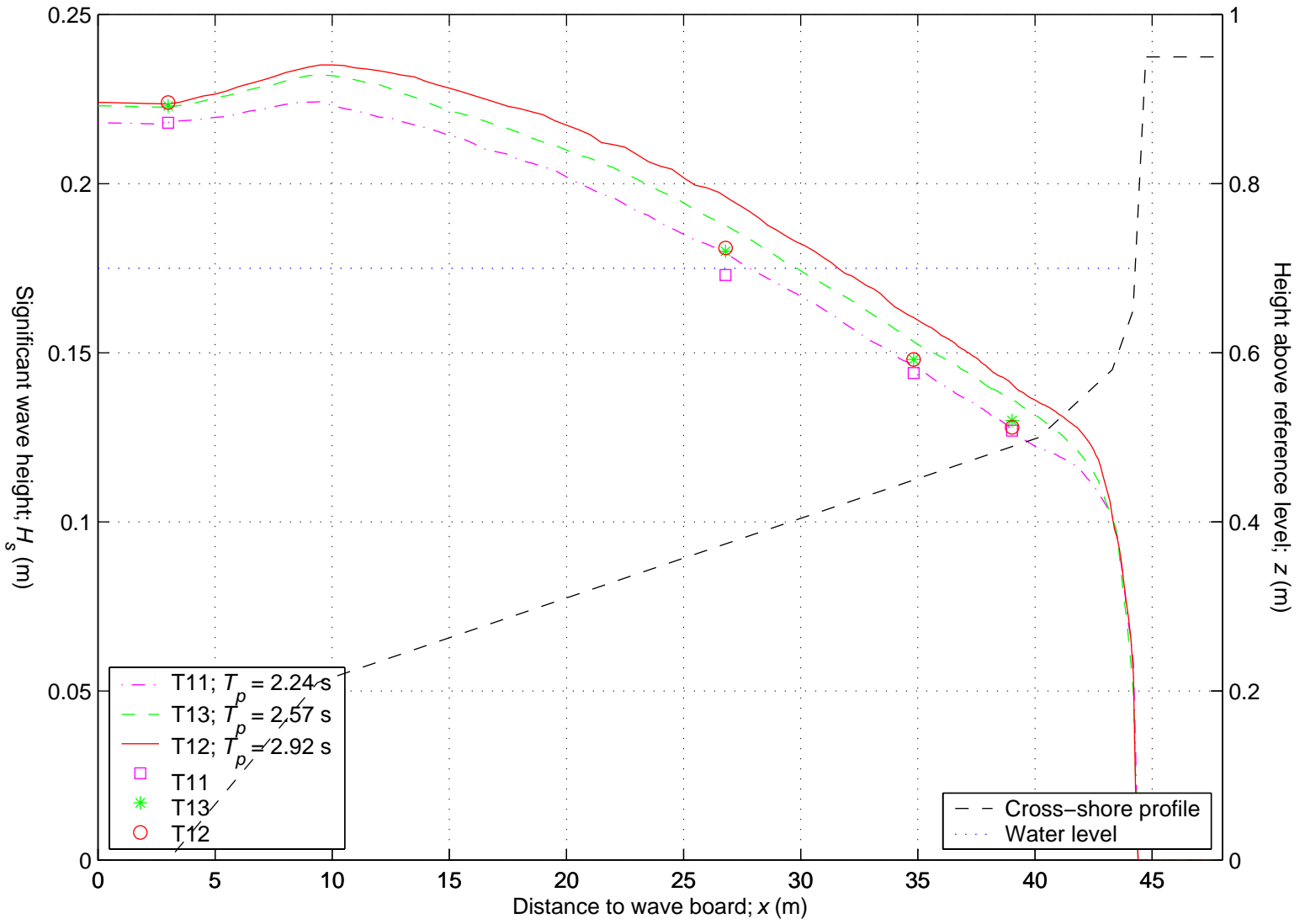


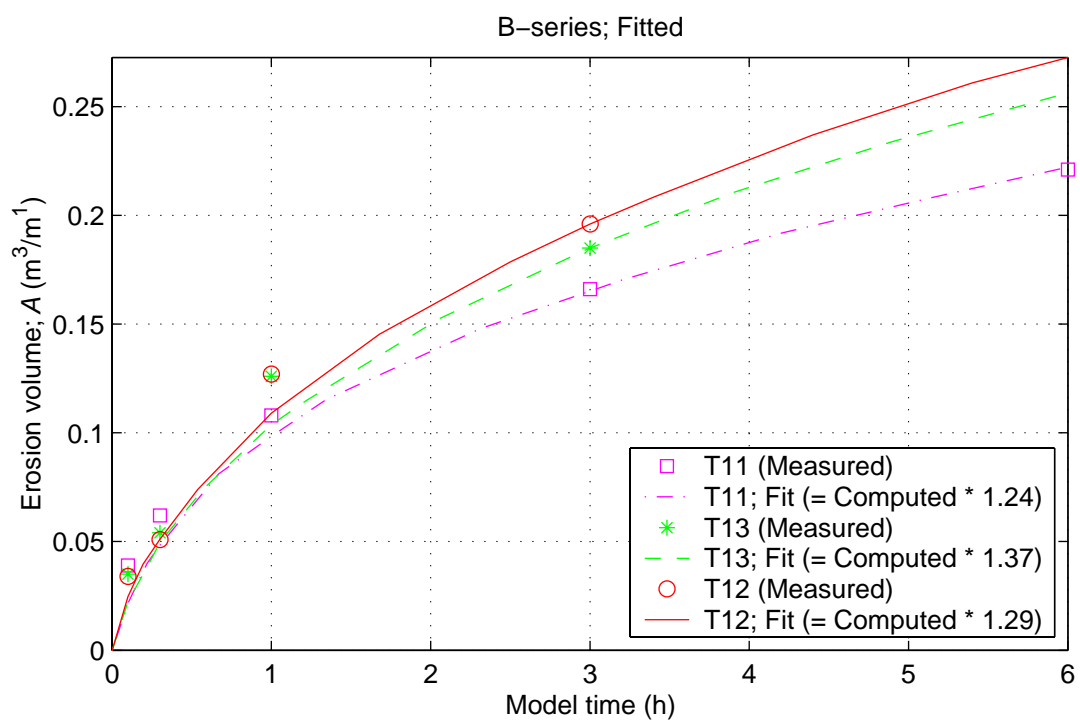
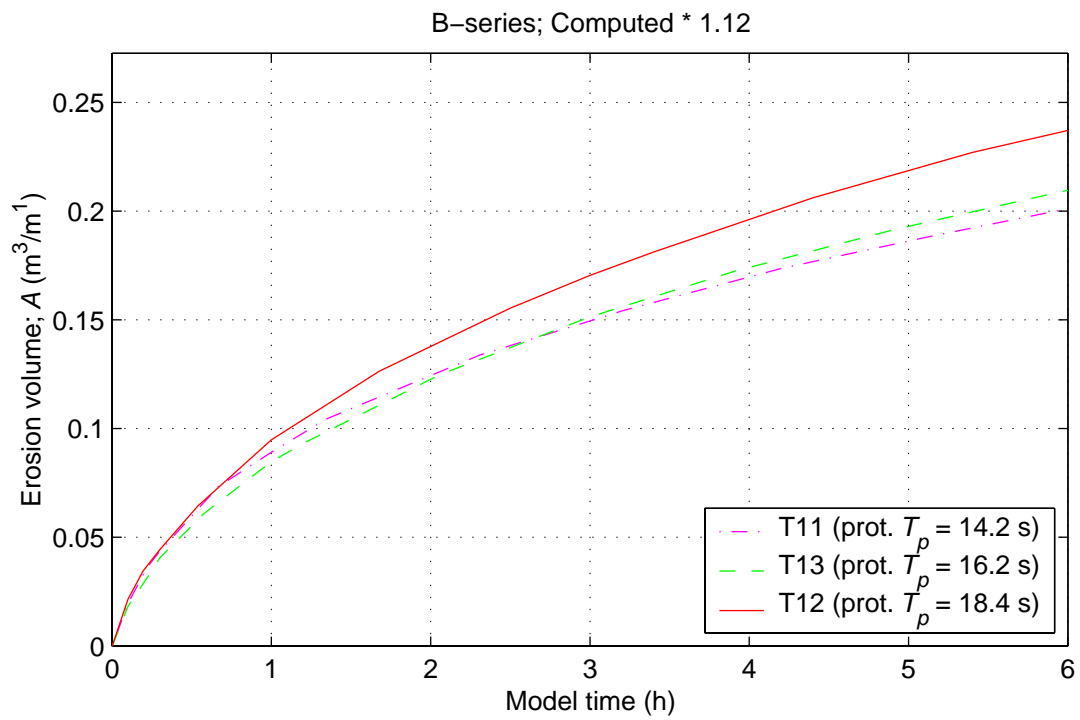
|   |                         |            |
|---|-------------------------|------------|
| Comparison computed and measured profiles at the end of each test | DUROSTA                 |            |
|   | A-series ( $n_d = 30$ ) |            |
| <b>WL   DELFT HYDRAULICS</b>                                      |                         | Figure 4.4 |

Wave propagation;  
Default settings; Tuned at  $x = 3.00$  m

DUROSTA

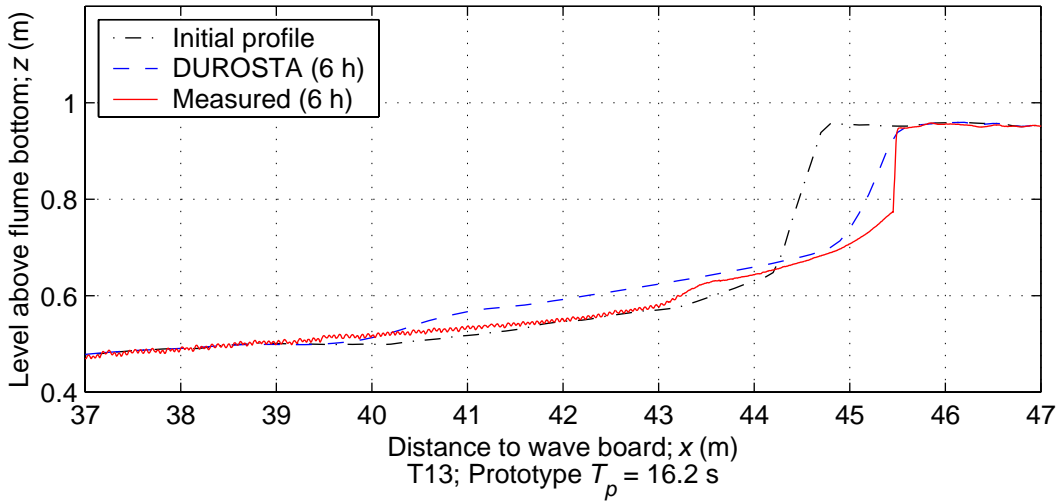
B-series ( $n_d = 40$ )



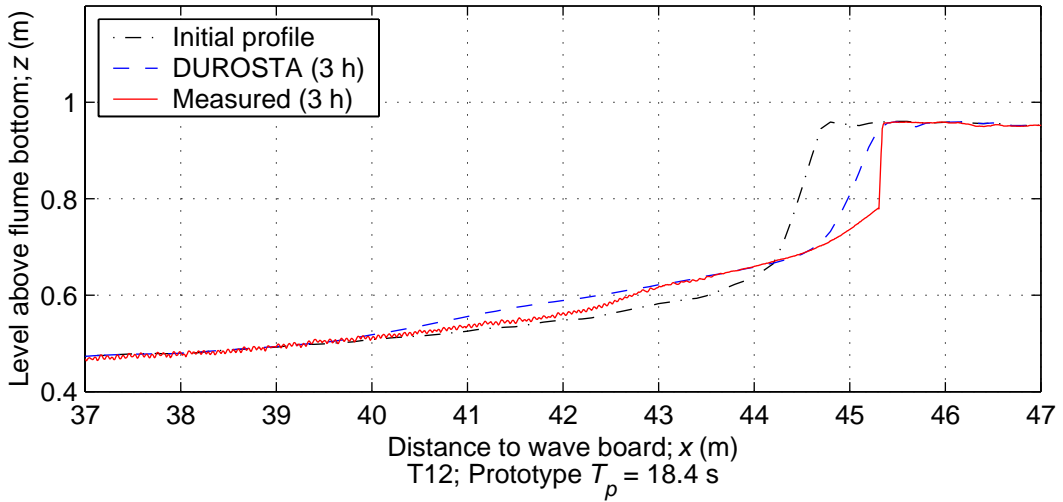


|  |                         |            |
|--|-------------------------|------------|
| Erosion volume development in time; Default settings;<br>Tuned at $x = 3.00$ m | DUROSTA                 |            |
|  | B-series ( $n_d = 40$ ) |            |
| <b>WL   DELFT HYDRAULICS</b>   |                         | Figure 4.6 |

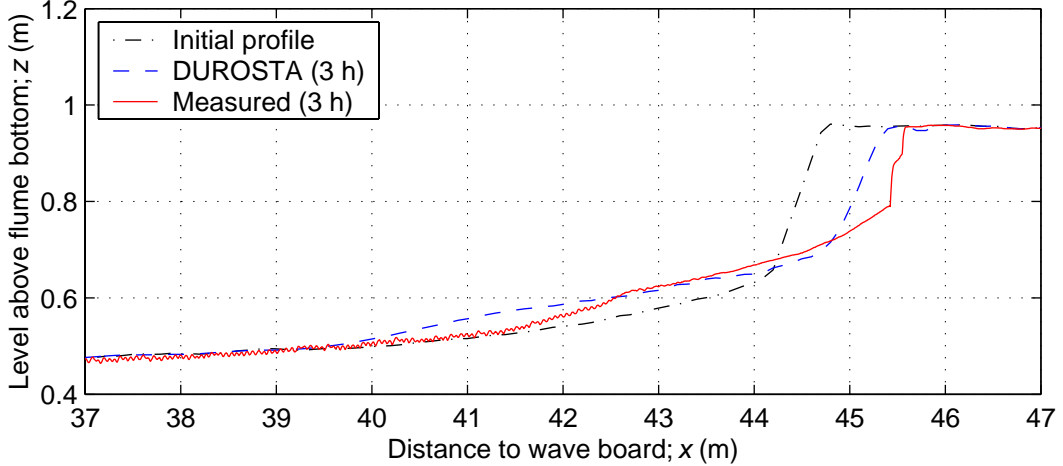
T11; Prototype  $T_p = 14.2$  s



T13; Prototype  $T_p = 16.2$  s



T12; Prototype  $T_p = 18.4$  s



Comparison computed and measured profiles at the end of each test

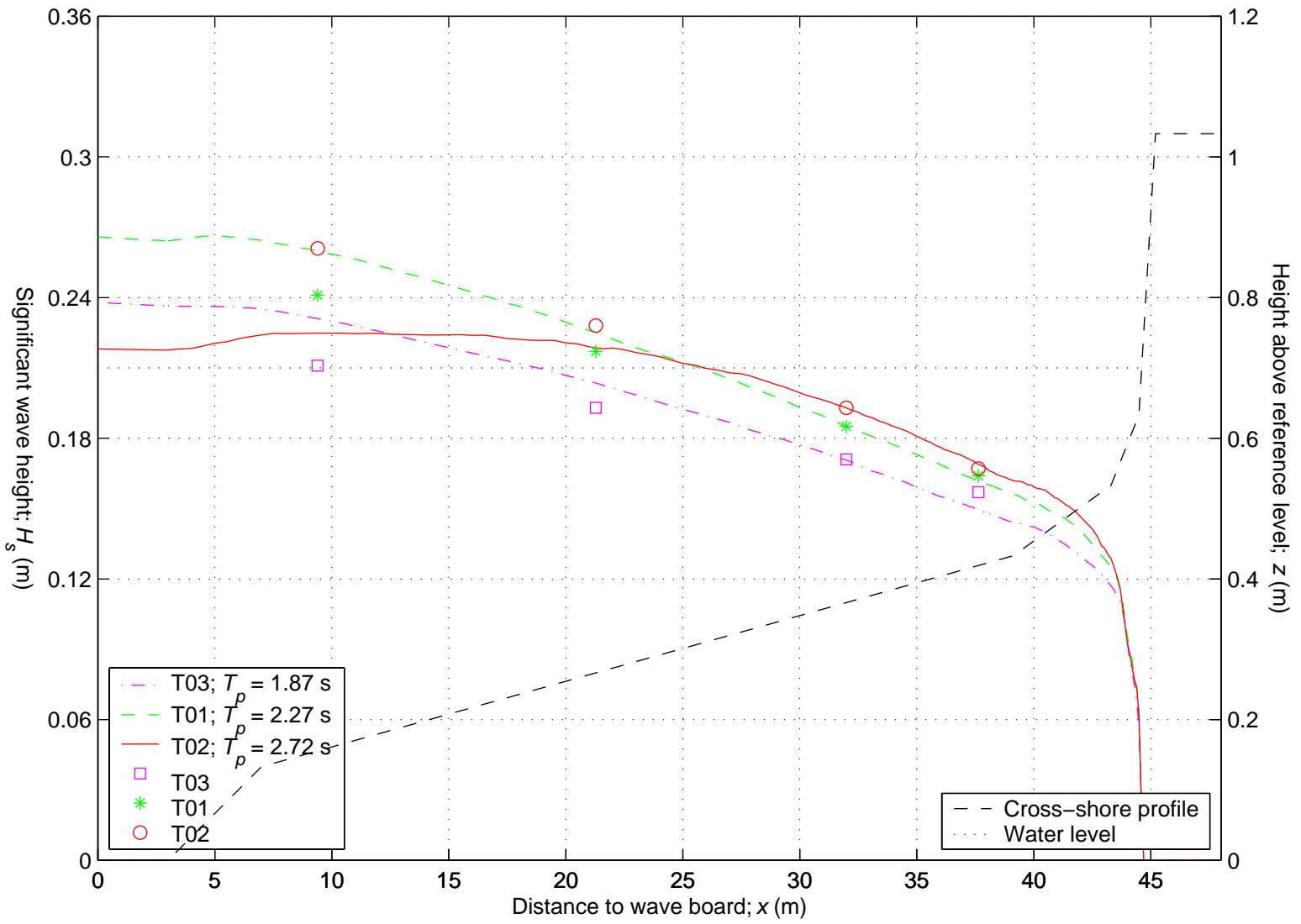
DUROSTA

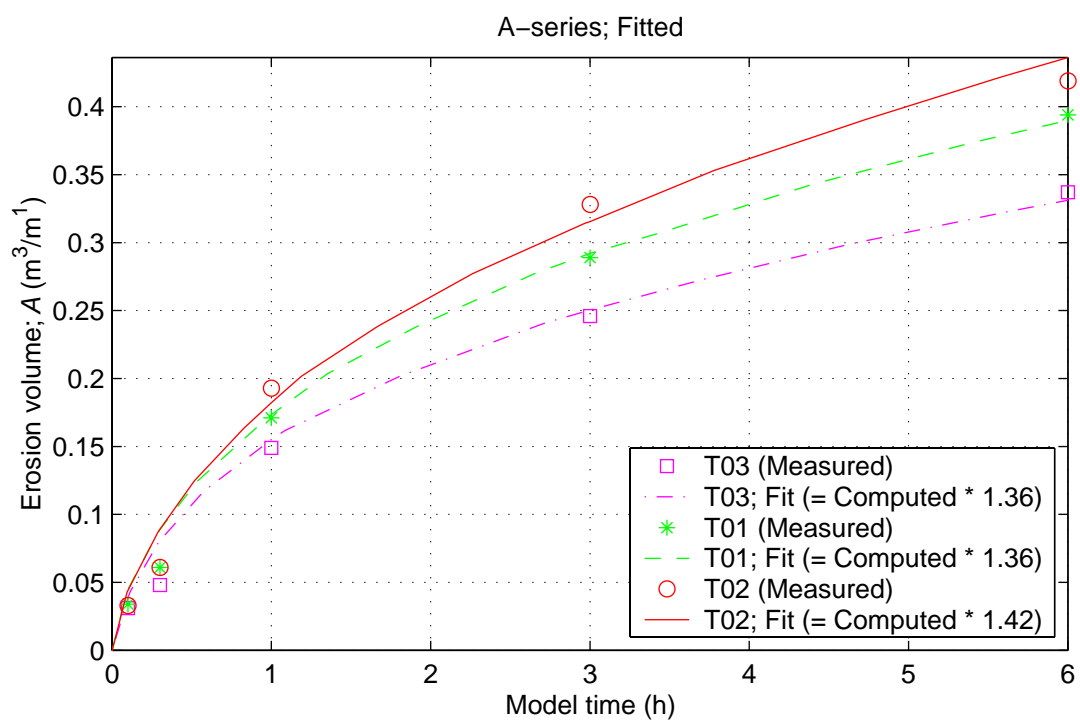
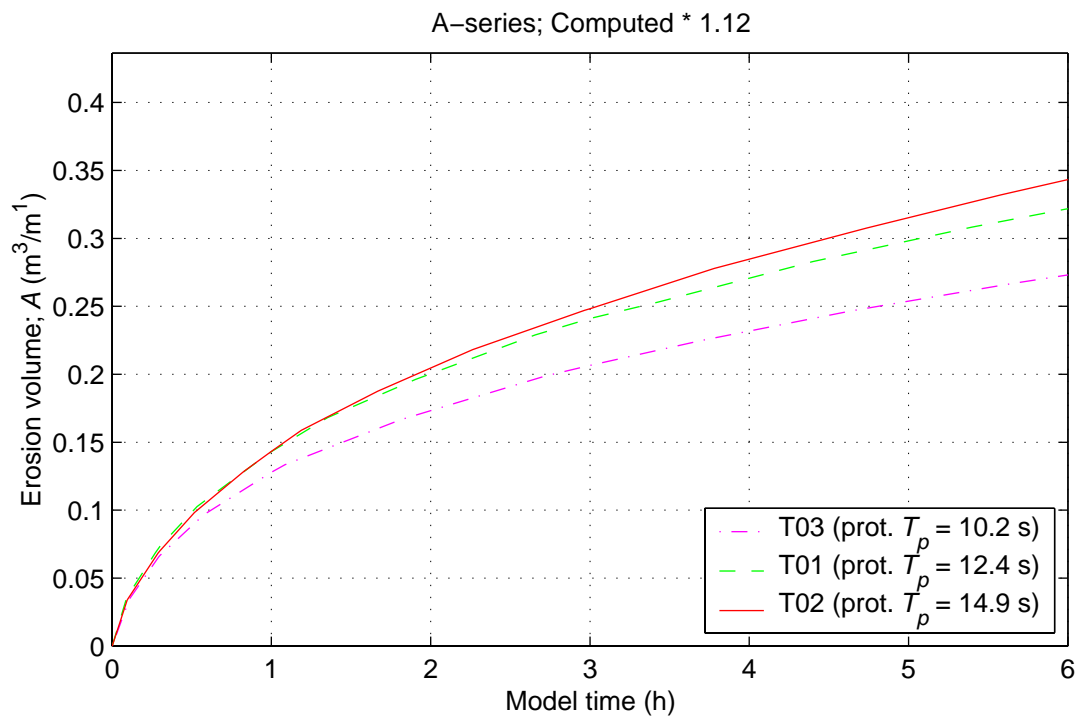
B-series ( $n_d = 40$ )

Wave propagation;  
Default settings; Tuned at  $x = 31.99$  m

DUROSTA

A-series ( $n_d = 30$ )



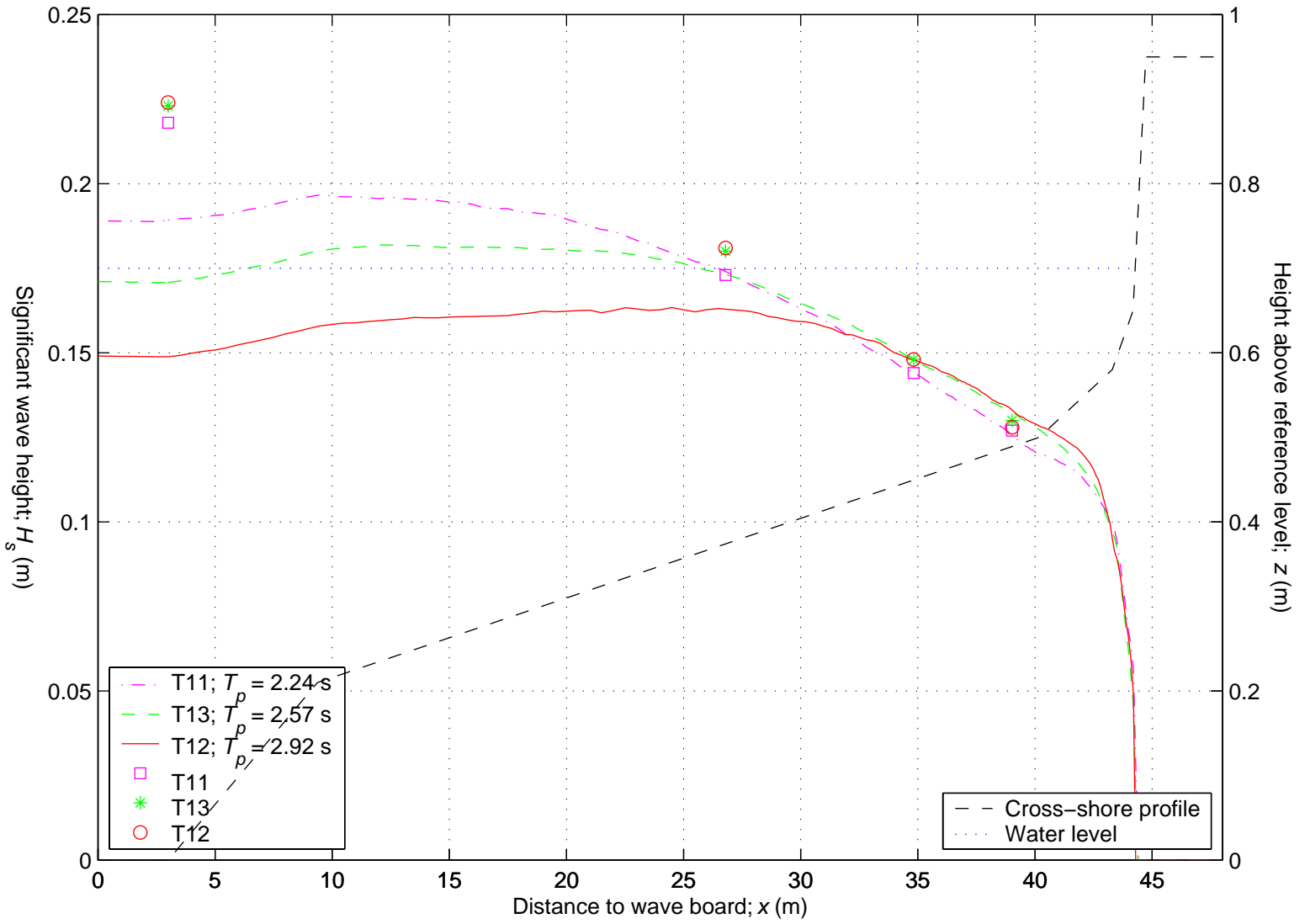


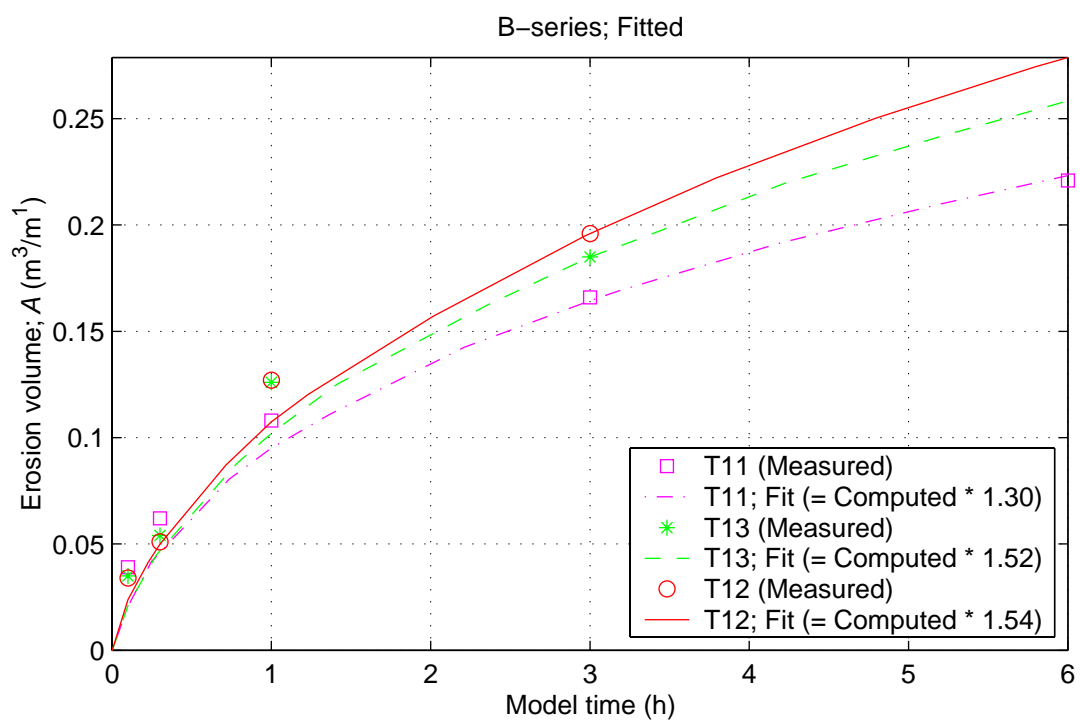
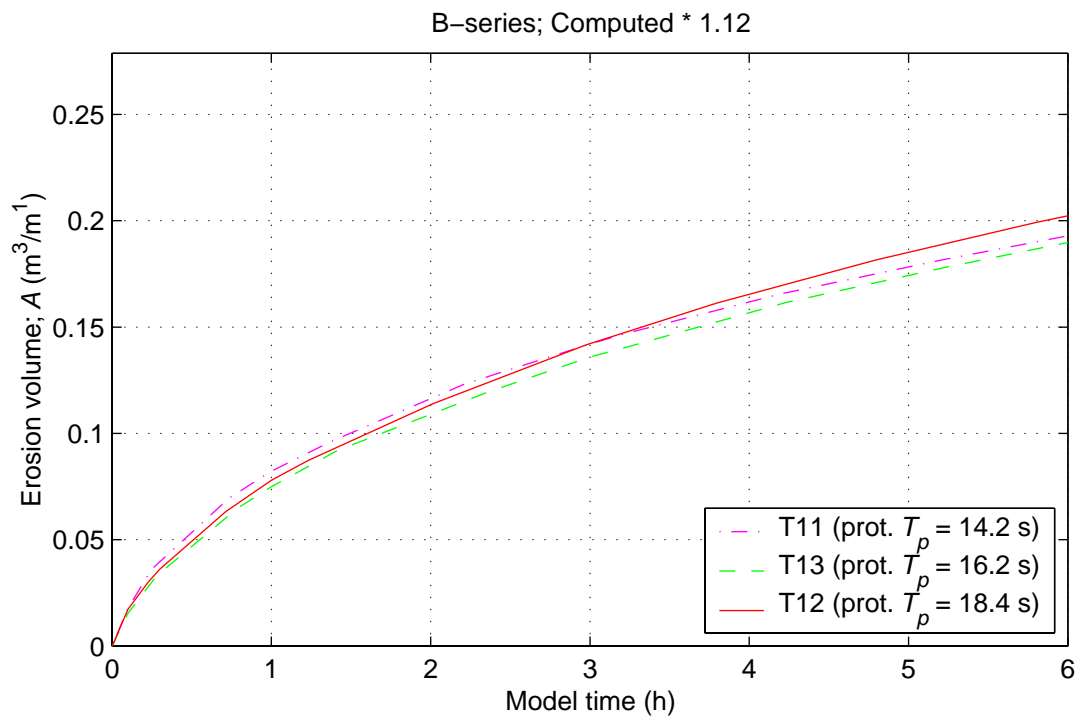
|   |                         |
|---|-------------------------|
| Erosion volume development in time; Default settings;<br>Tuned at $x = 31.99$ m | DUROSTA                 |
|   | A-series ( $n_d = 30$ ) |
| <b>WL   DELFT HYDRAULICS</b>  | Figure 4.9              |

Wave propagation;  
Default settings; Tuned at  $x = 34.82$  m

DUROSTA

B-series ( $n_d = 40$ )

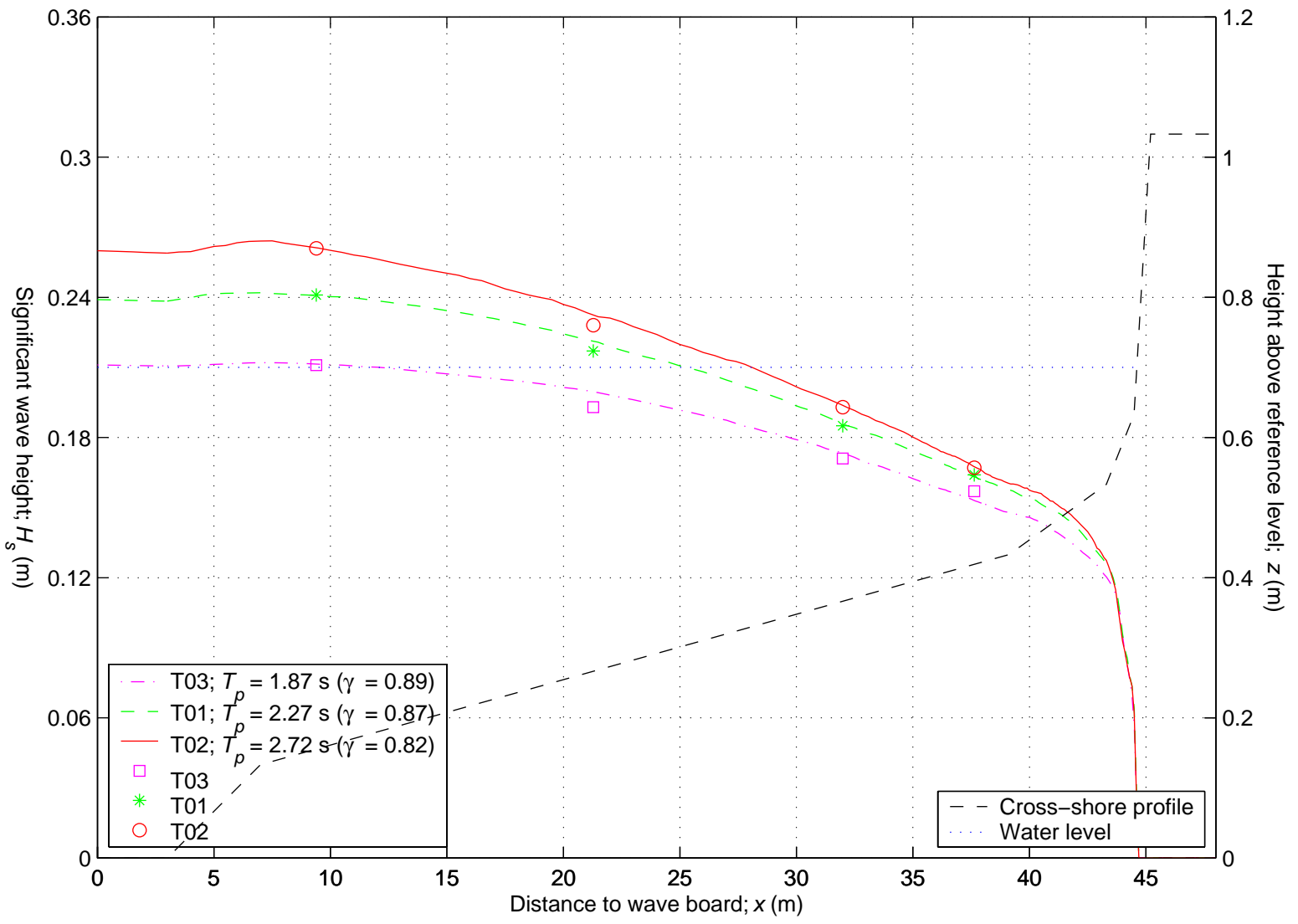


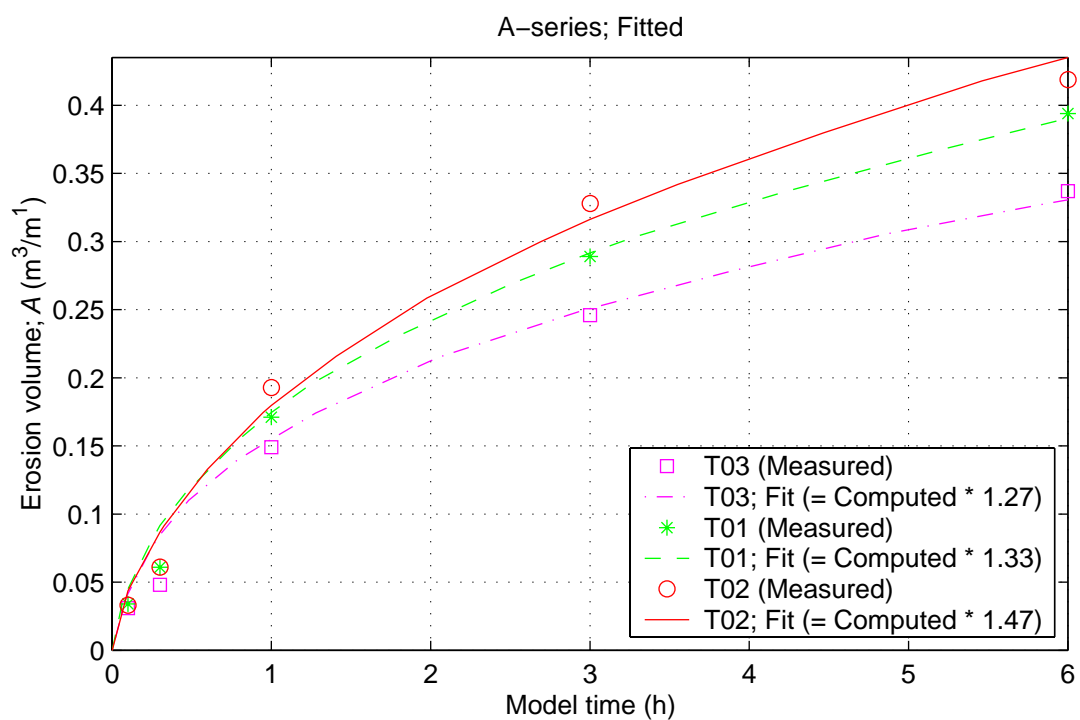
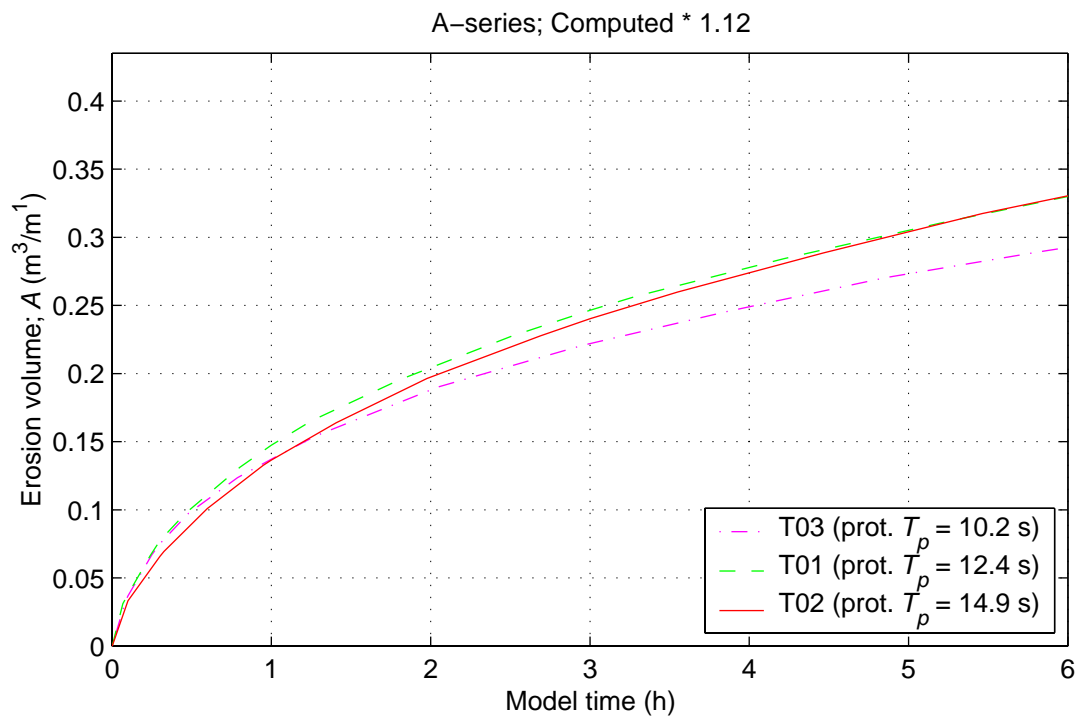


Erosion volume development in time; Default settings;  
Tuned at  $x = 34.82$  m

DUROSTA

B-series ( $n_d = 40$ )



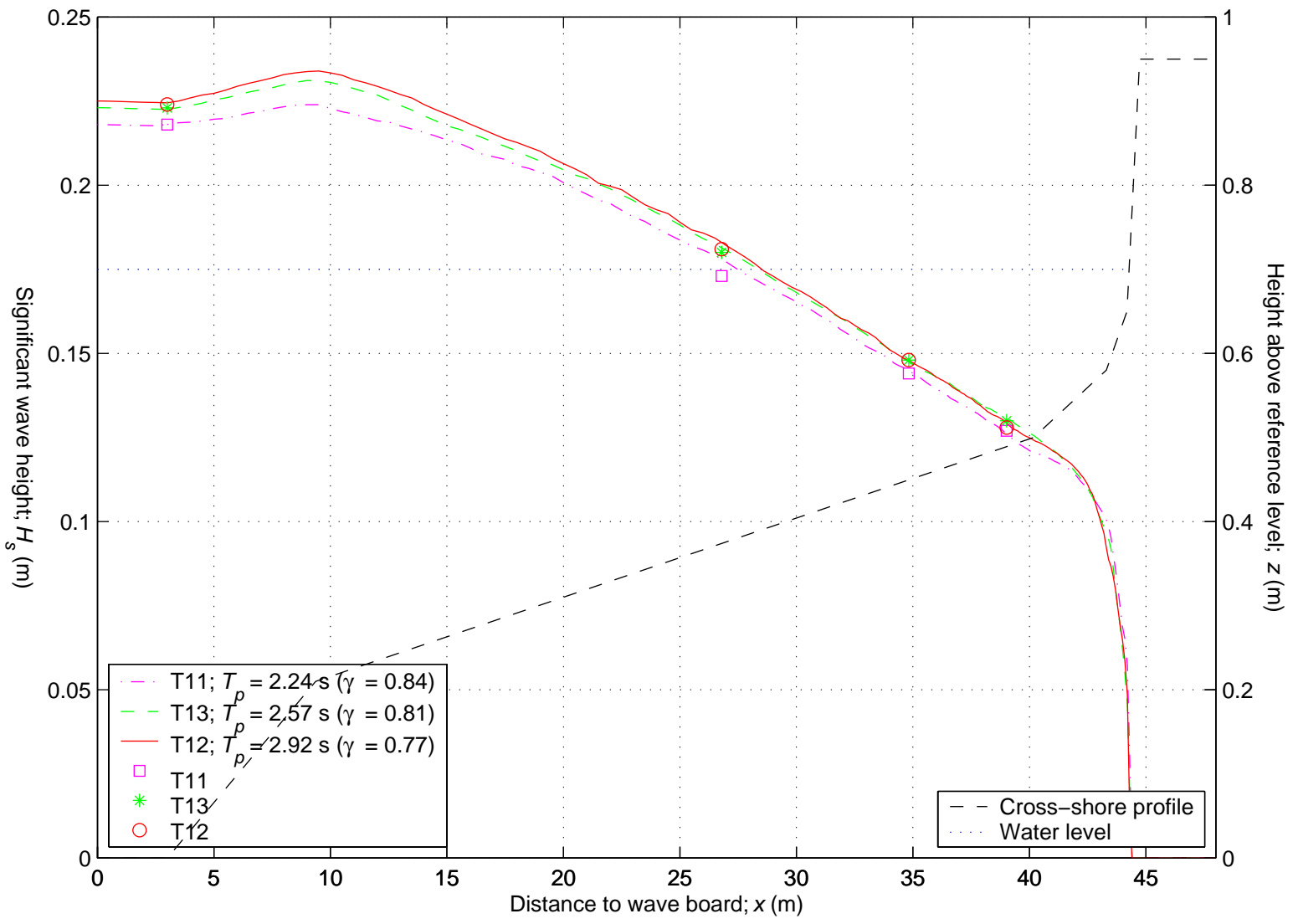


|  |                         |             |
|--|-------------------------|-------------|
| Erosion volume development in time; Tuning by breaker index; | DUROSTA                 |             |
|  | A-series ( $n_d = 30$ ) |             |
| <b>WL   DELFT HYDRAULICS</b>                                 |                         | Figure 4.13 |

Wave propagation;  
Tuning by breaker index  $\gamma$

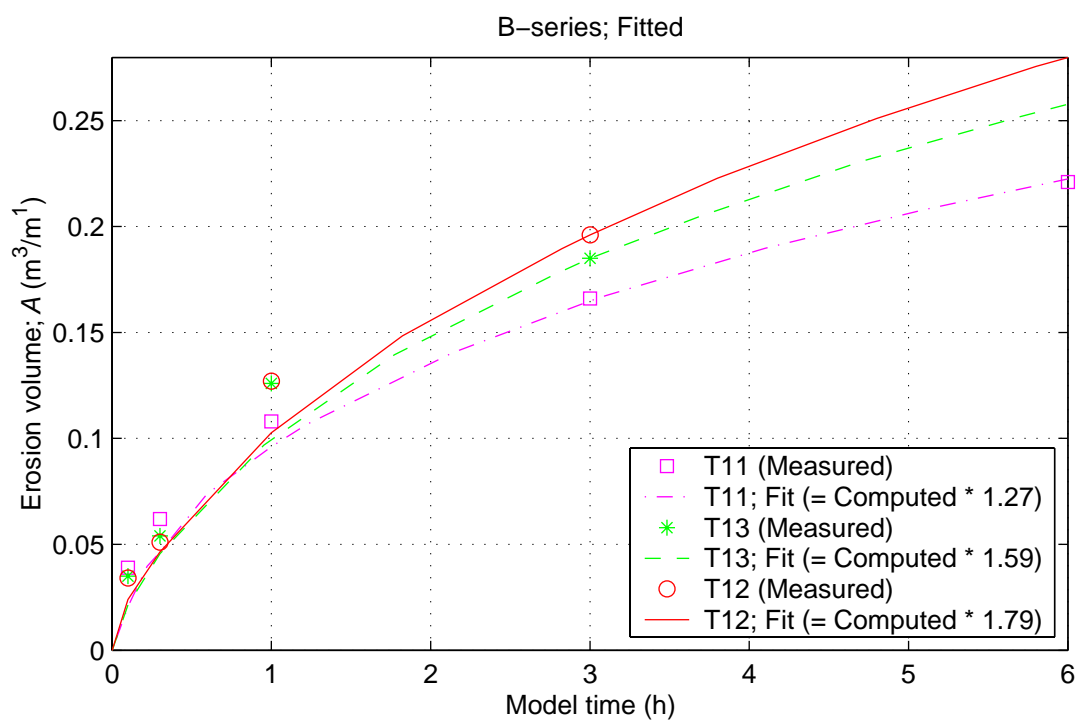
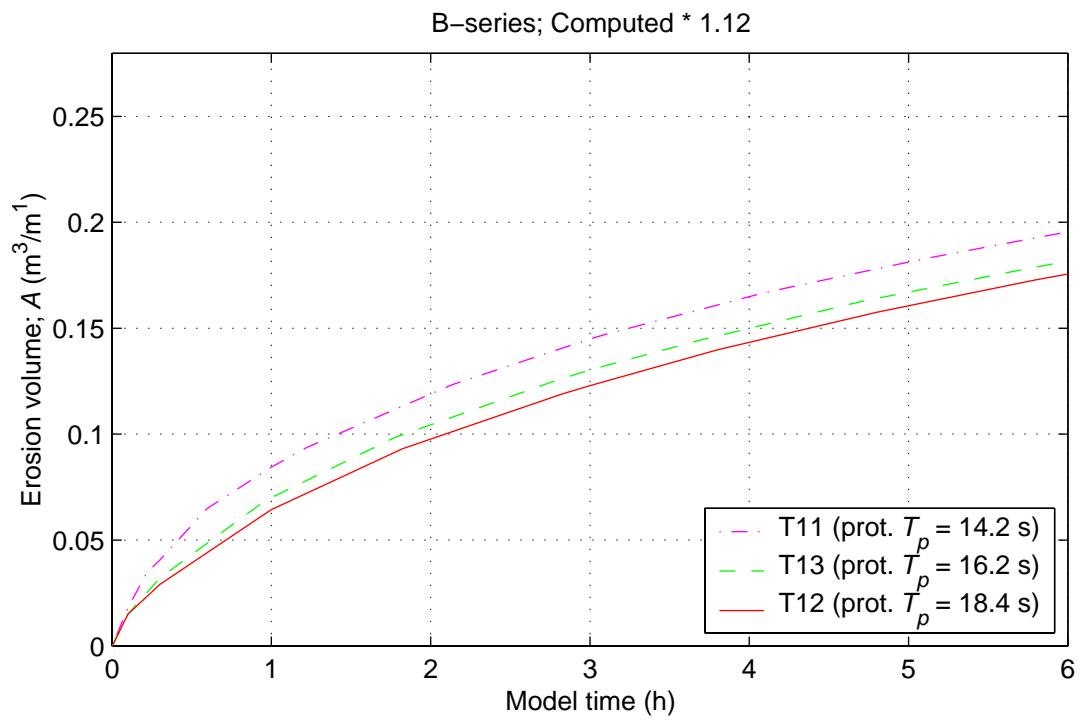
DUROSTA

B-series ( $n_p = 40$ )

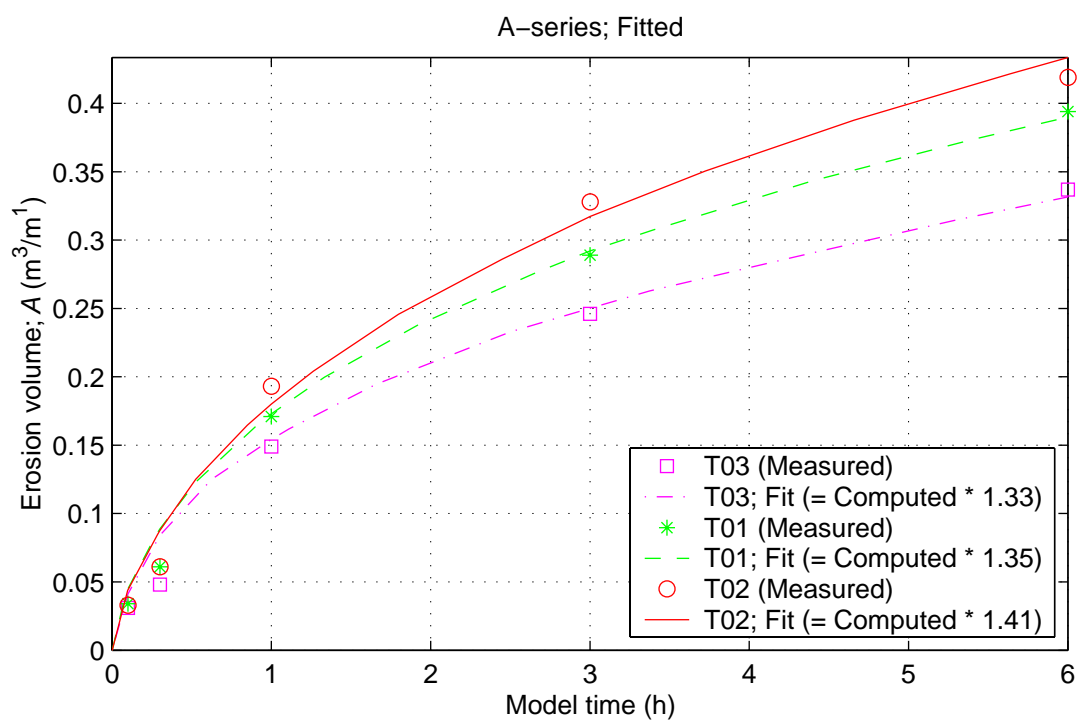
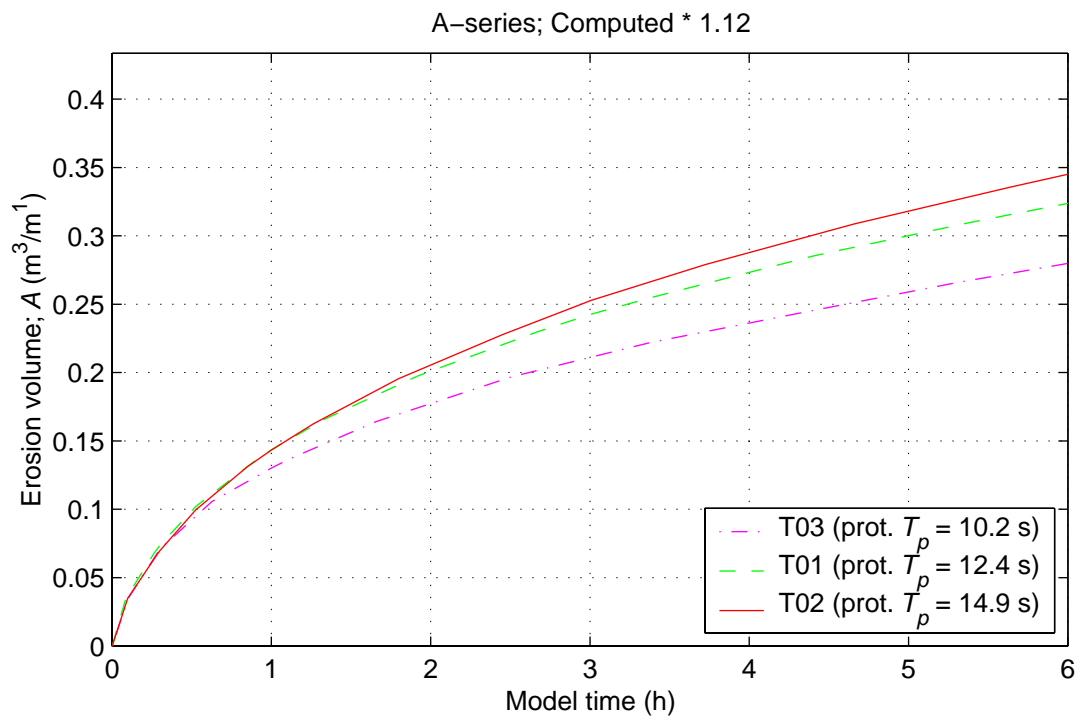


- - T11;  $T_p = 2.24$  s ( $\gamma = 0.84$ )  
- - T13;  $T_p = 2.57$  s ( $\gamma = 0.81$ )  
- - T12;  $T_p = 2.92$  s ( $\gamma = 0.77$ )  
□ T11  
\* T13  
○ T12

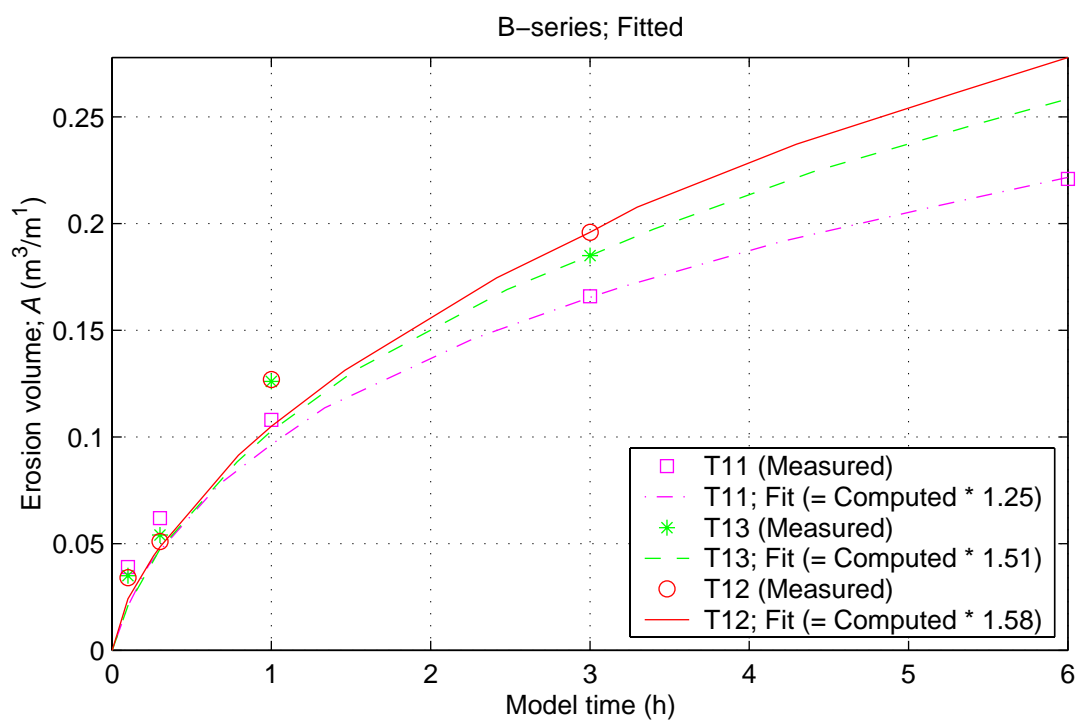
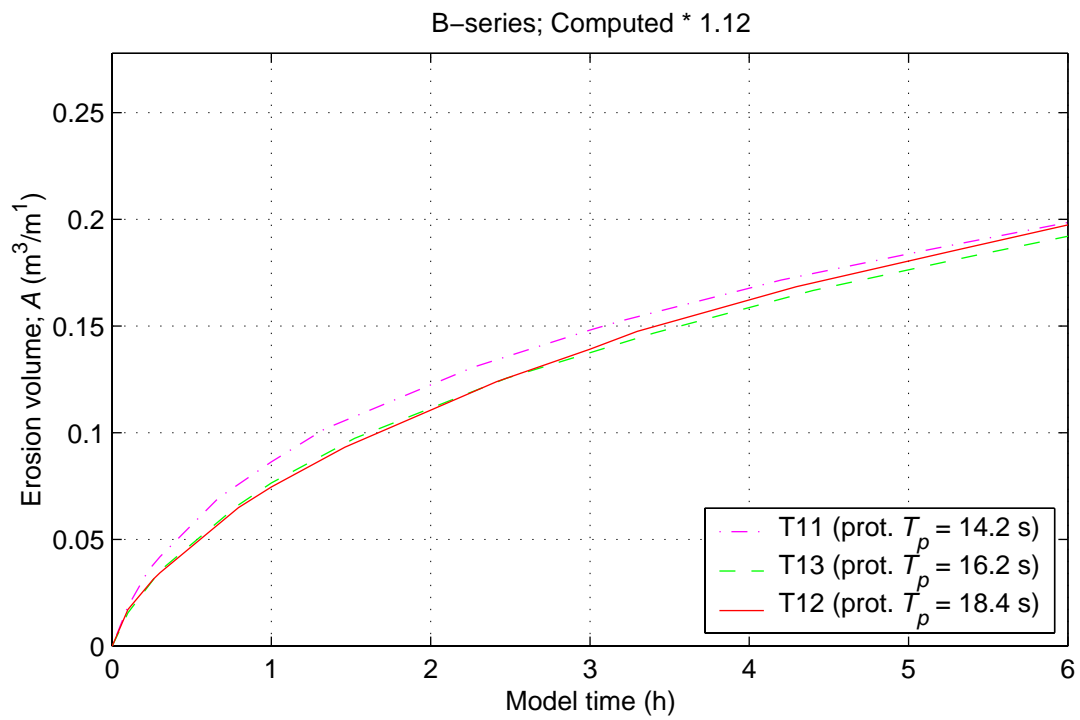
- - Cross-shore profile  
⋯ Water level



|  |                         |             |
|--|-------------------------|-------------|
| Erosion volume development in time; Tuning by breaker index; | DUROSTA                 |             |
|  | B-series ( $n_d = 40$ ) |             |
| <b>WL   DELFT HYDRAULICS</b>                                 |                         | Figure 4.15 |



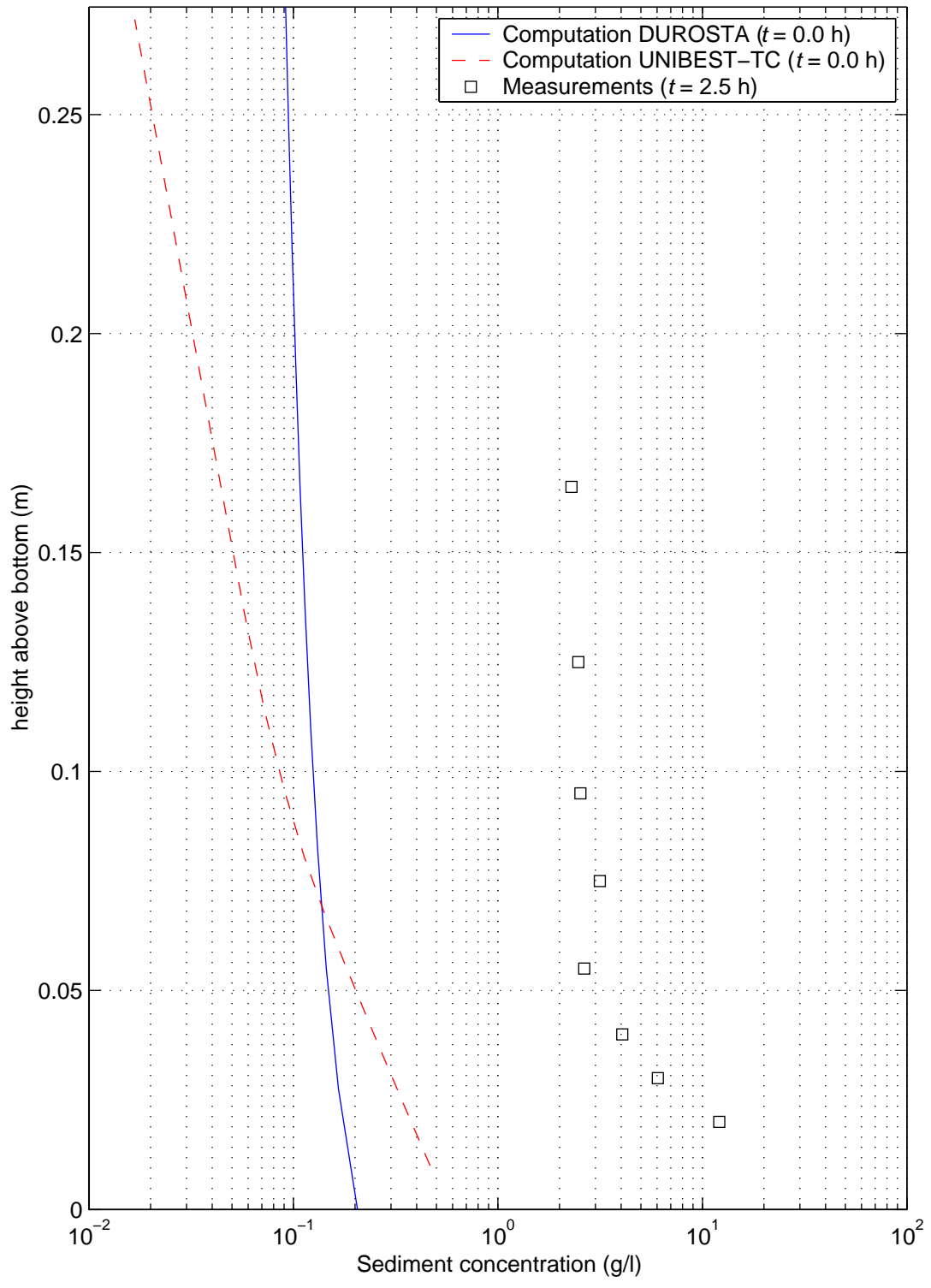
|  |                         |             |
|--|-------------------------|-------------|
| Erosion volume development in time; Tuning by breaker index;<br>$\gamma$ -dependent parameter compensation | DUROSTA                 |             |
|  | A-series ( $n_d = 30$ ) |             |
| <b>WL   DELFT HYDRAULICS</b>   |                         | Figure 4.16 |



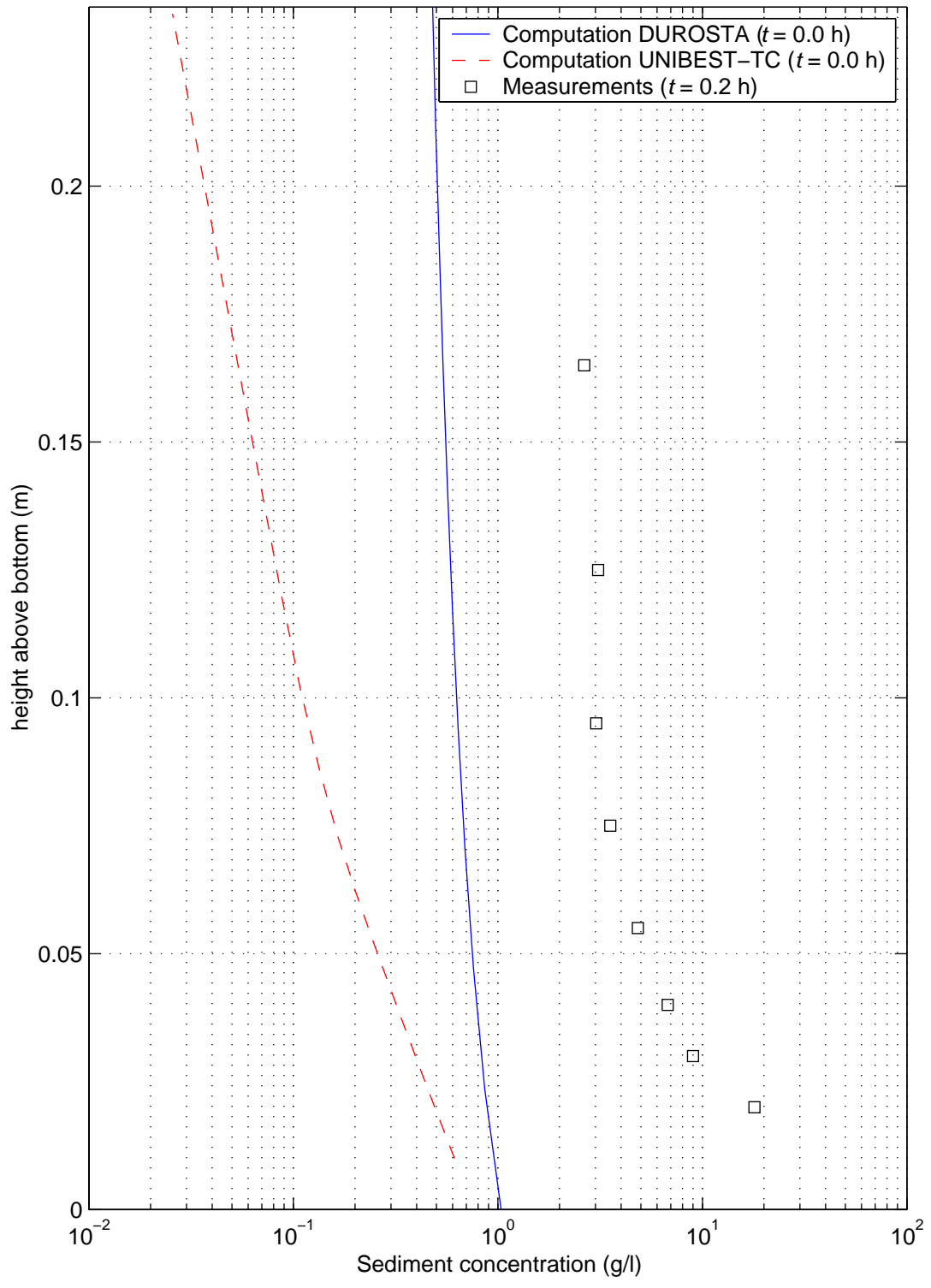
Erosion volume development in time; Tuning by breaker index  $\gamma$ ;  
 $\gamma$ -dependent parameter compensation

DUROSTA

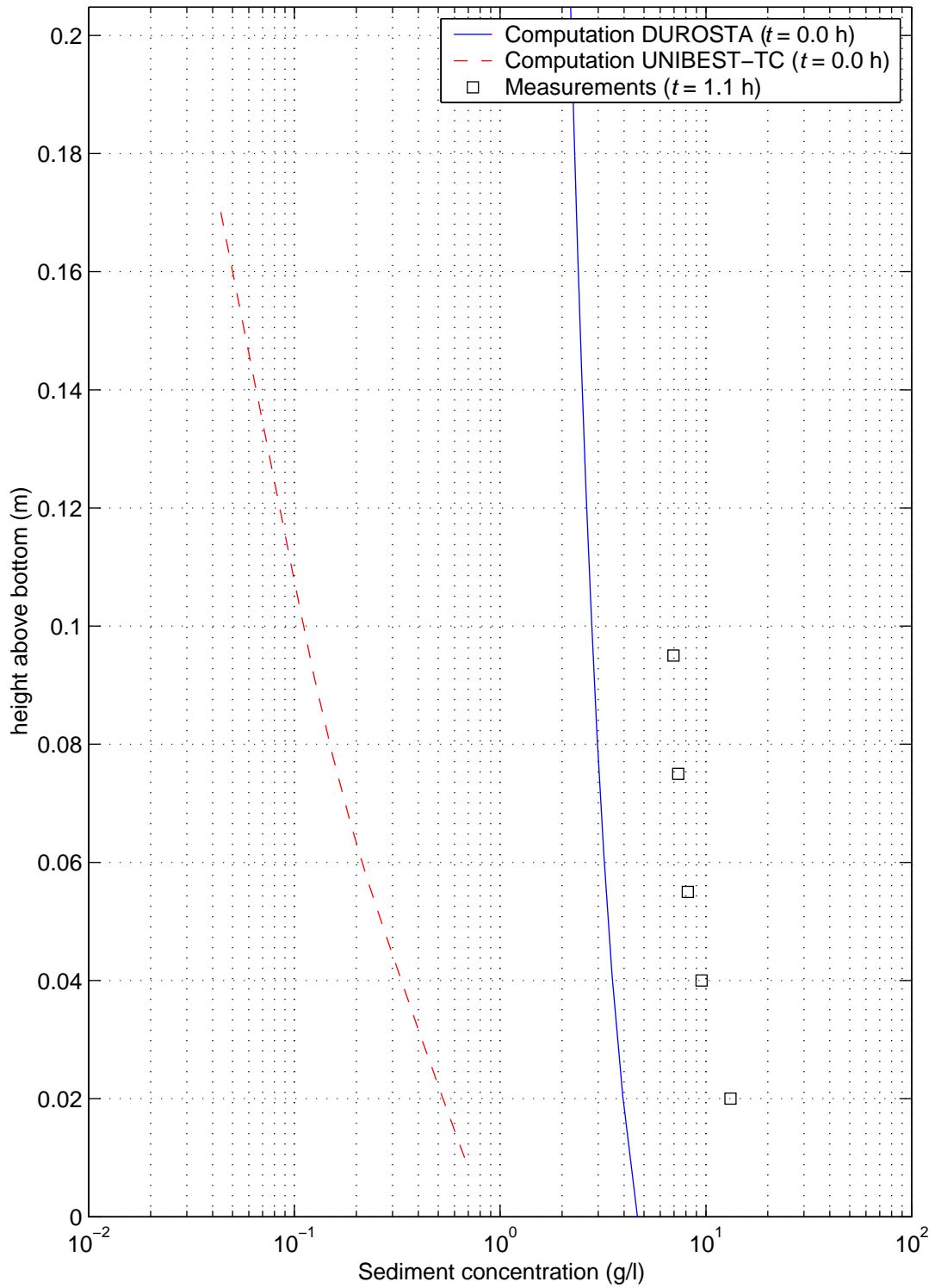
B-series ( $n_d = 40$ )



|   |             |             |
|---|-------------|-------------|
| Comparison sediment concentration<br>computation and measurements Schelde flume | x = 39.13 m | T02         |
|   |             |             |
| <b>WL   DELFT HYDRAULICS</b>  | H4265       | Figure 4.18 |



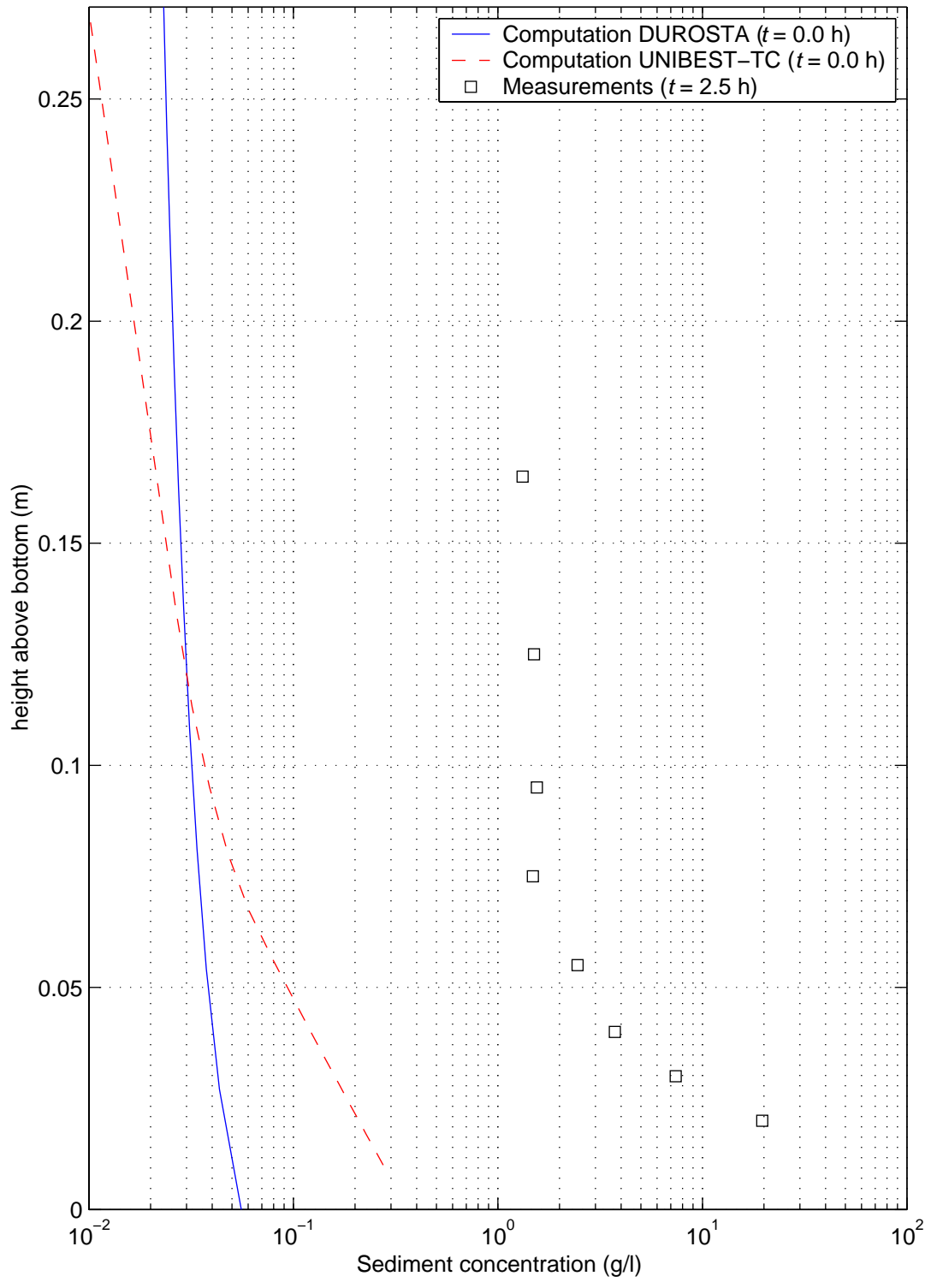
|   |             |             |
|---|-------------|-------------|
| Comparison sediment concentration<br>computation and measurements Schelde flume | x = 40.52 m | T02         |
|   |             |             |
| <b>WL   DELFT HYDRAULICS</b>  | H4265       | Figure 4.19 |



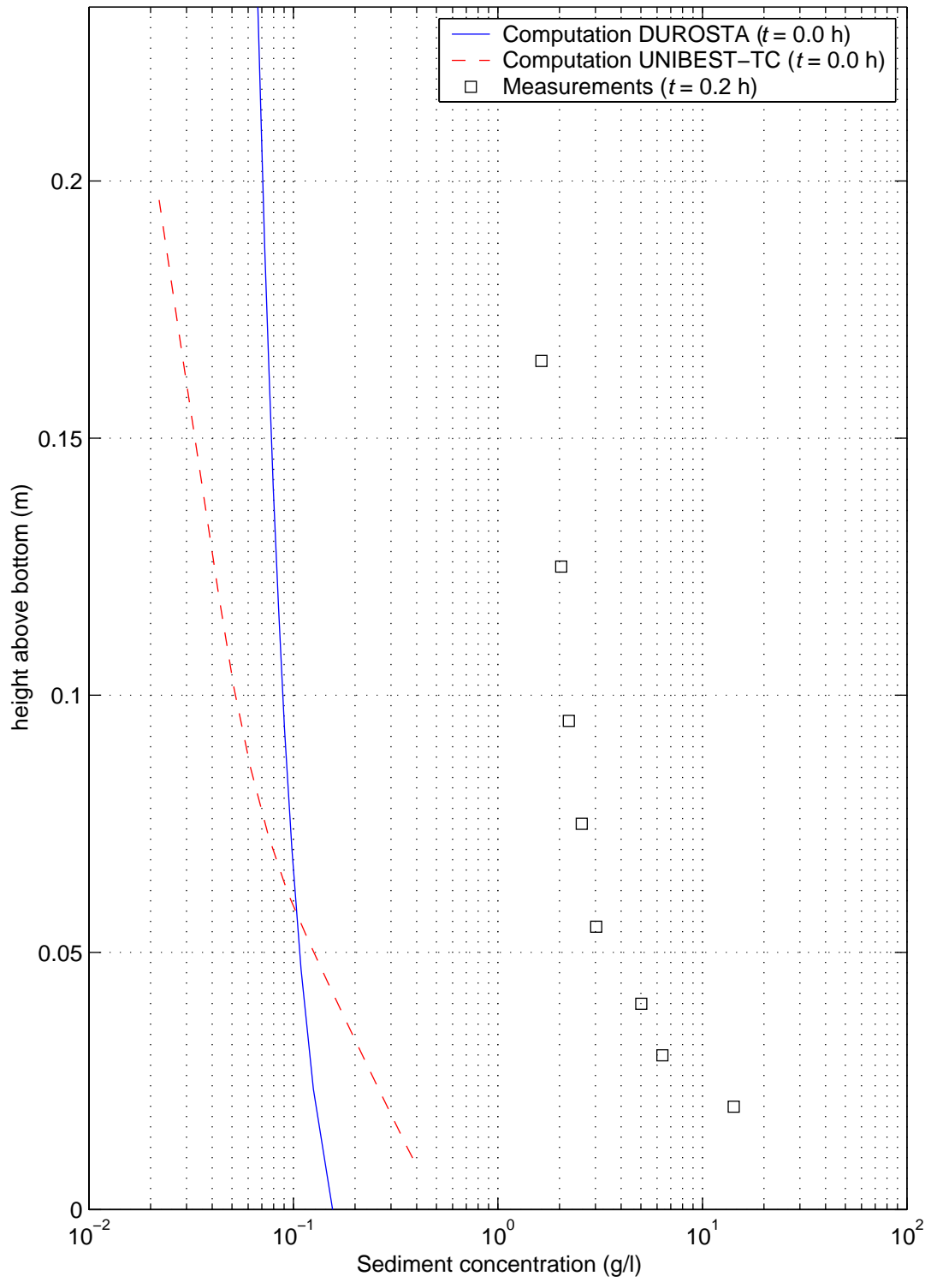
Comparison sediment concentration  
computation and measurements Schelde flume

$x = 41.91 \text{ m}$

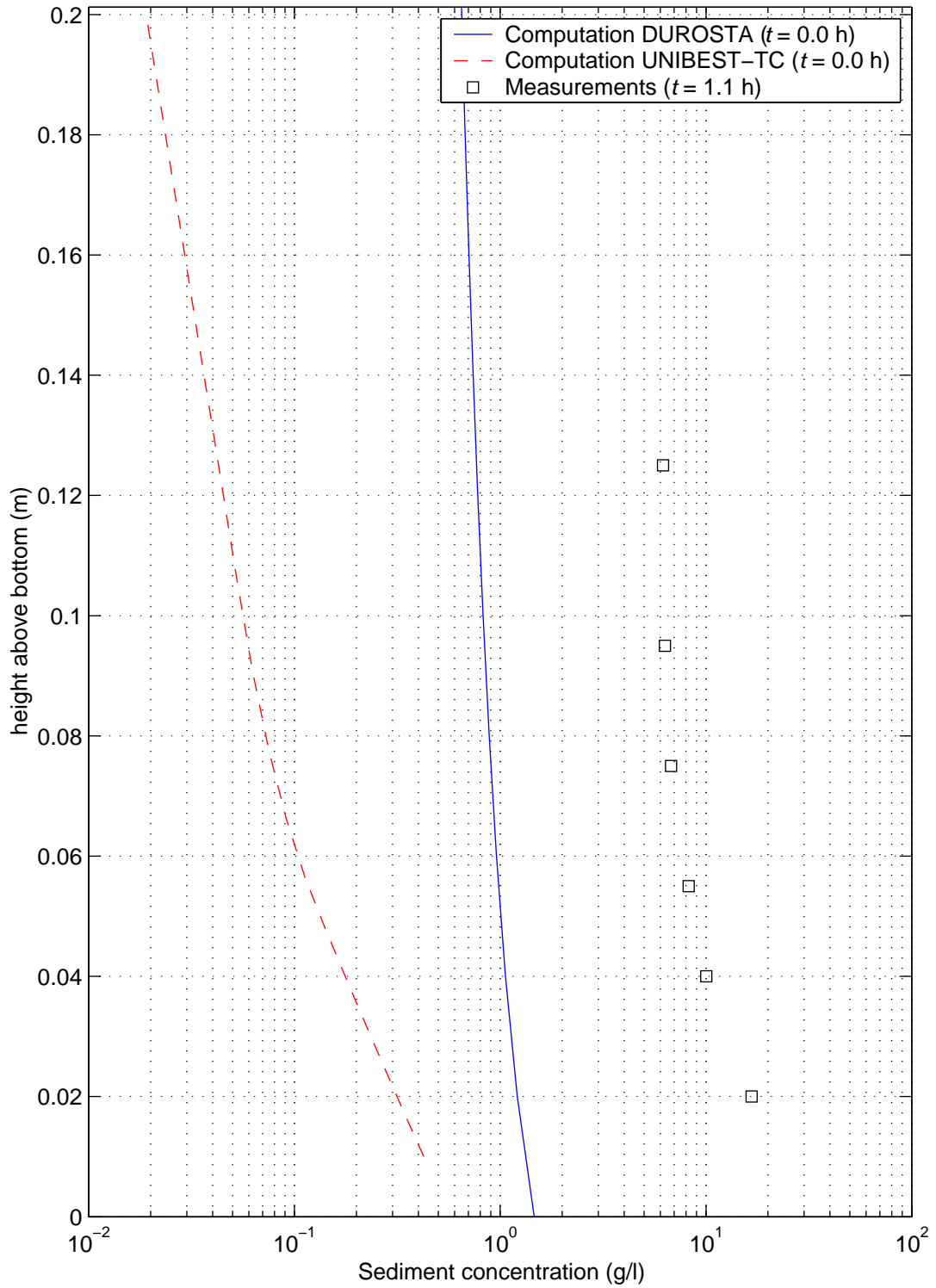
T02



|   |             |             |
|---|-------------|-------------|
| Comparison sediment concentration<br>computation and measurements Schelde flume | x = 39.13 m | T03         |
|   |             |             |
| <b>WL   DELFT HYDRAULICS</b>  | H4265       | Figure 4.21 |



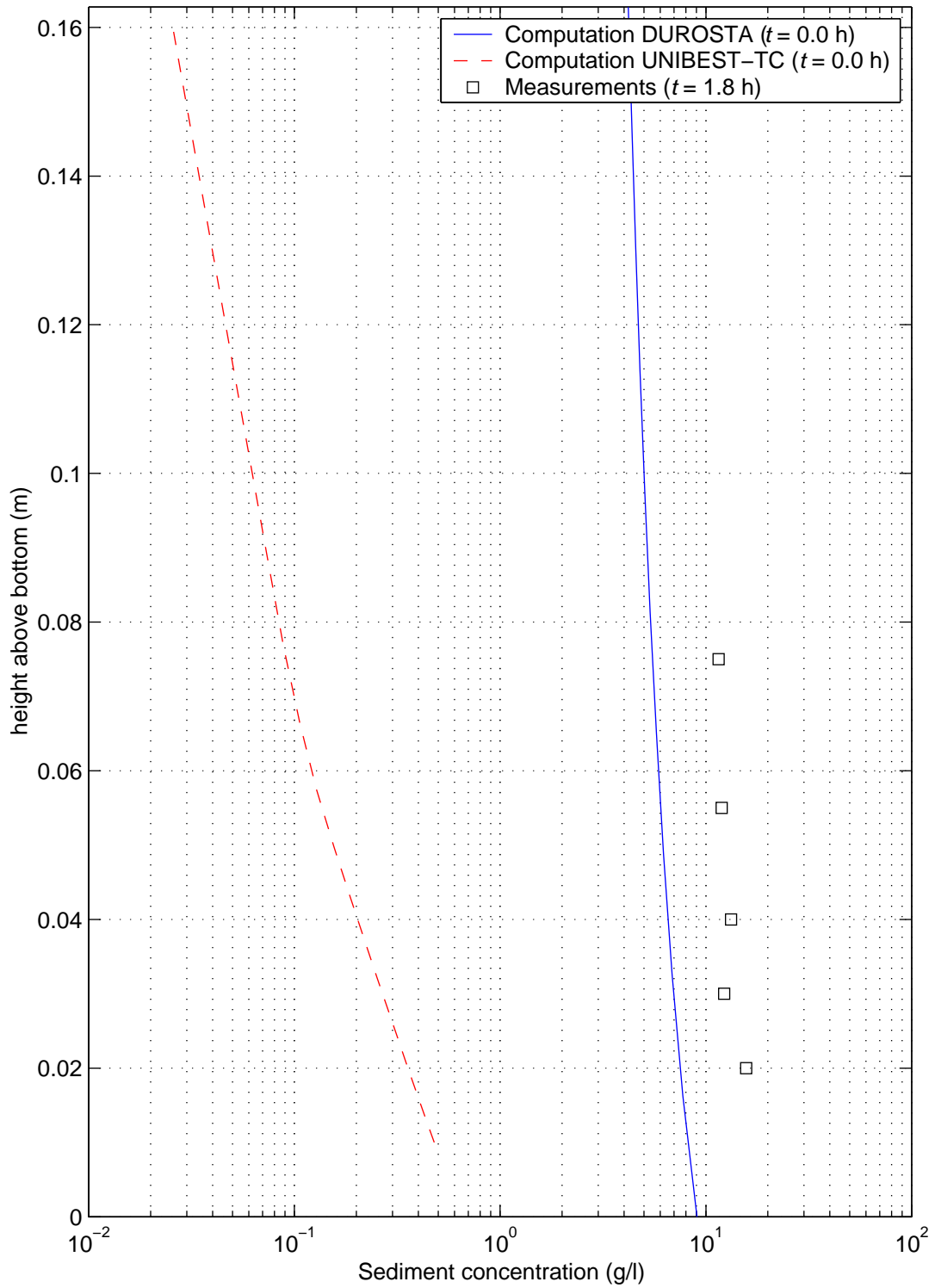
|   |             |             |
|---|-------------|-------------|
| Comparison sediment concentration<br>computation and measurements Schelde flume | x = 40.52 m | T03         |
|   |             |             |
| <b>WL   DELFT HYDRAULICS</b>  | H4265       | Figure 4.22 |



Comparison sediment concentration  
computation and measurements Schelde flume

$x = 41.91 \text{ m}$

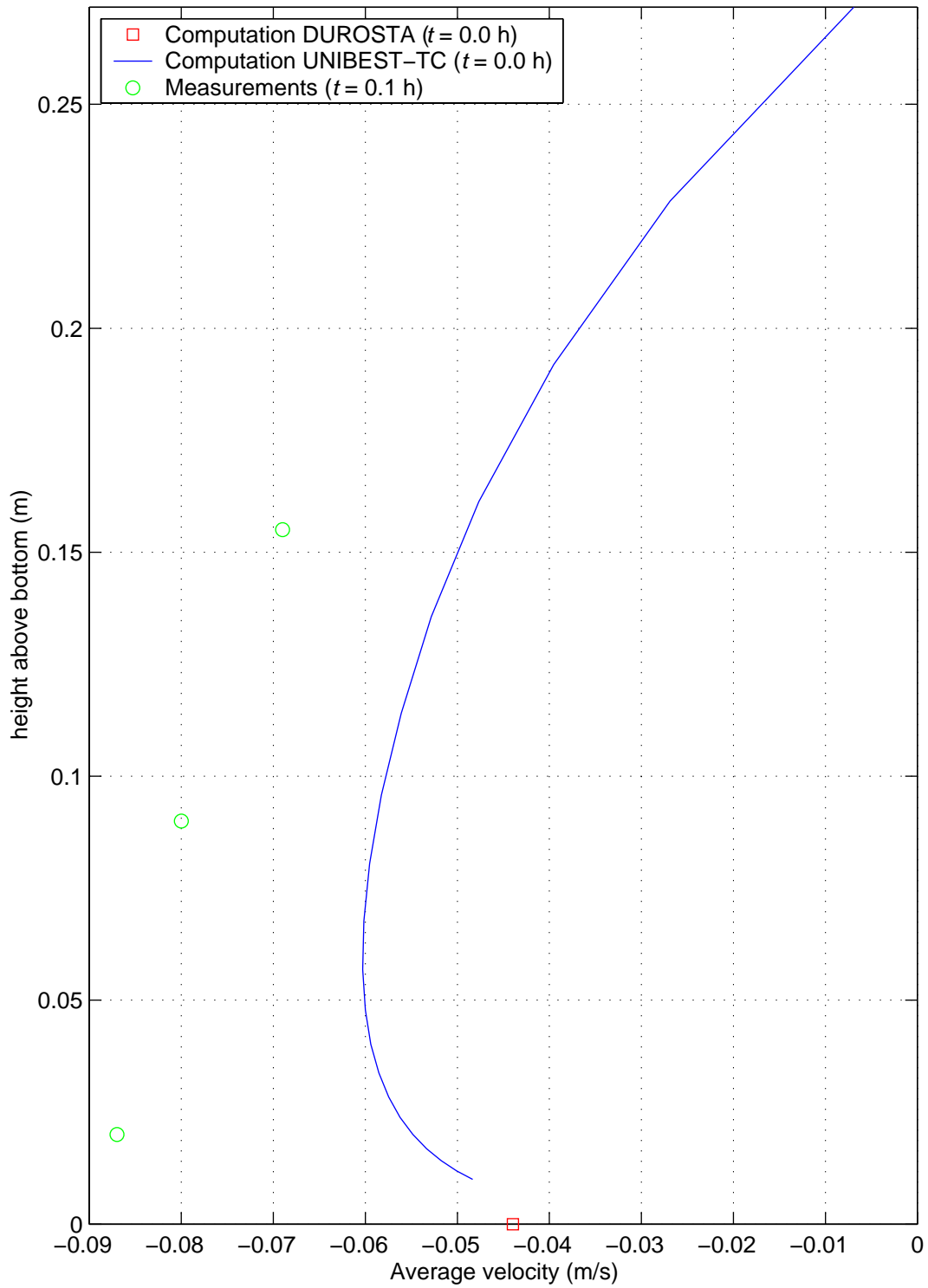
T03



Comparison sediment concentration  
computation and measurements Schelde flume

$x = 43.30$  m

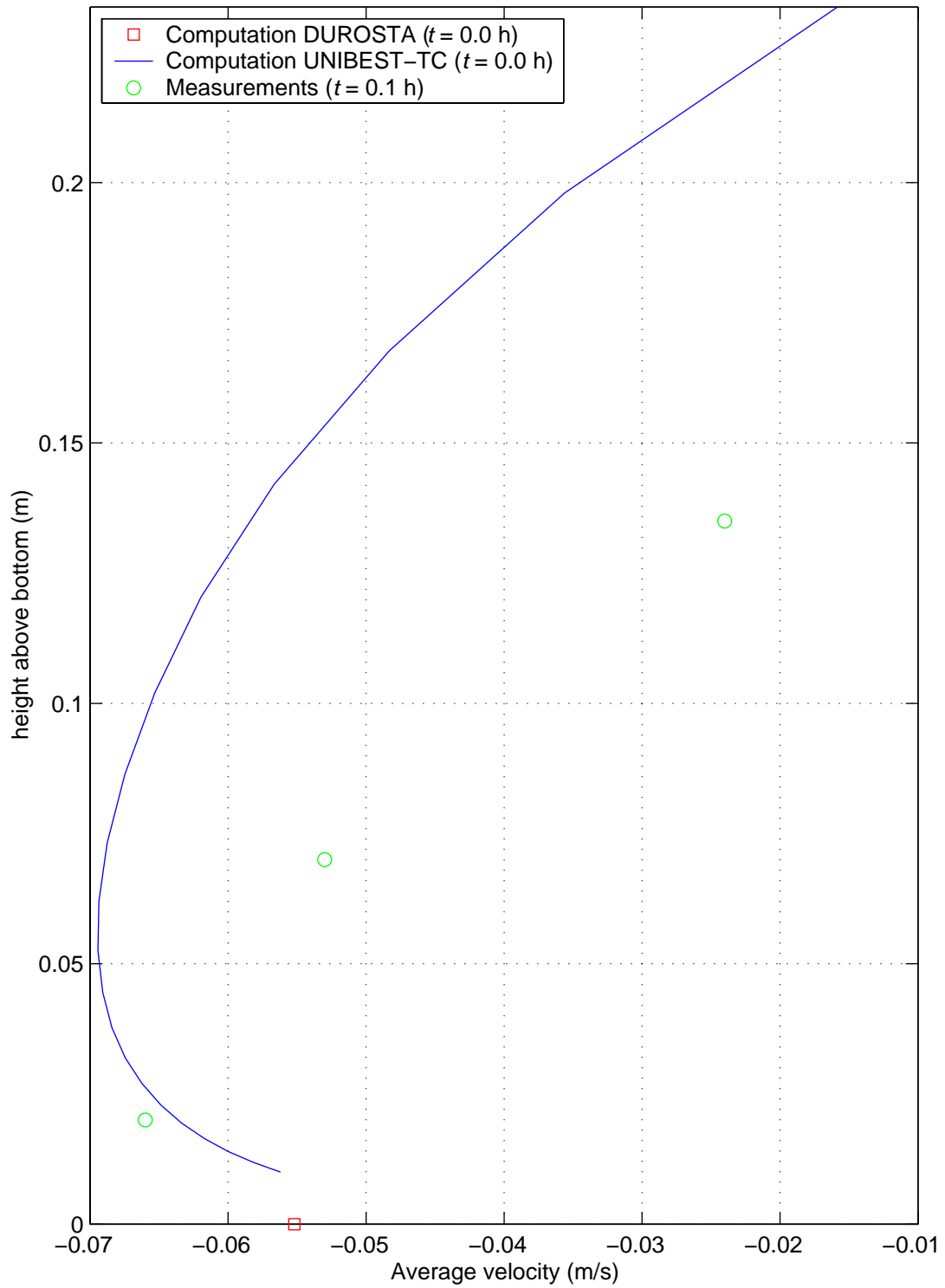
T03



Comparison computed velocities  
and measurements Schelde flume

x = 39.13 m

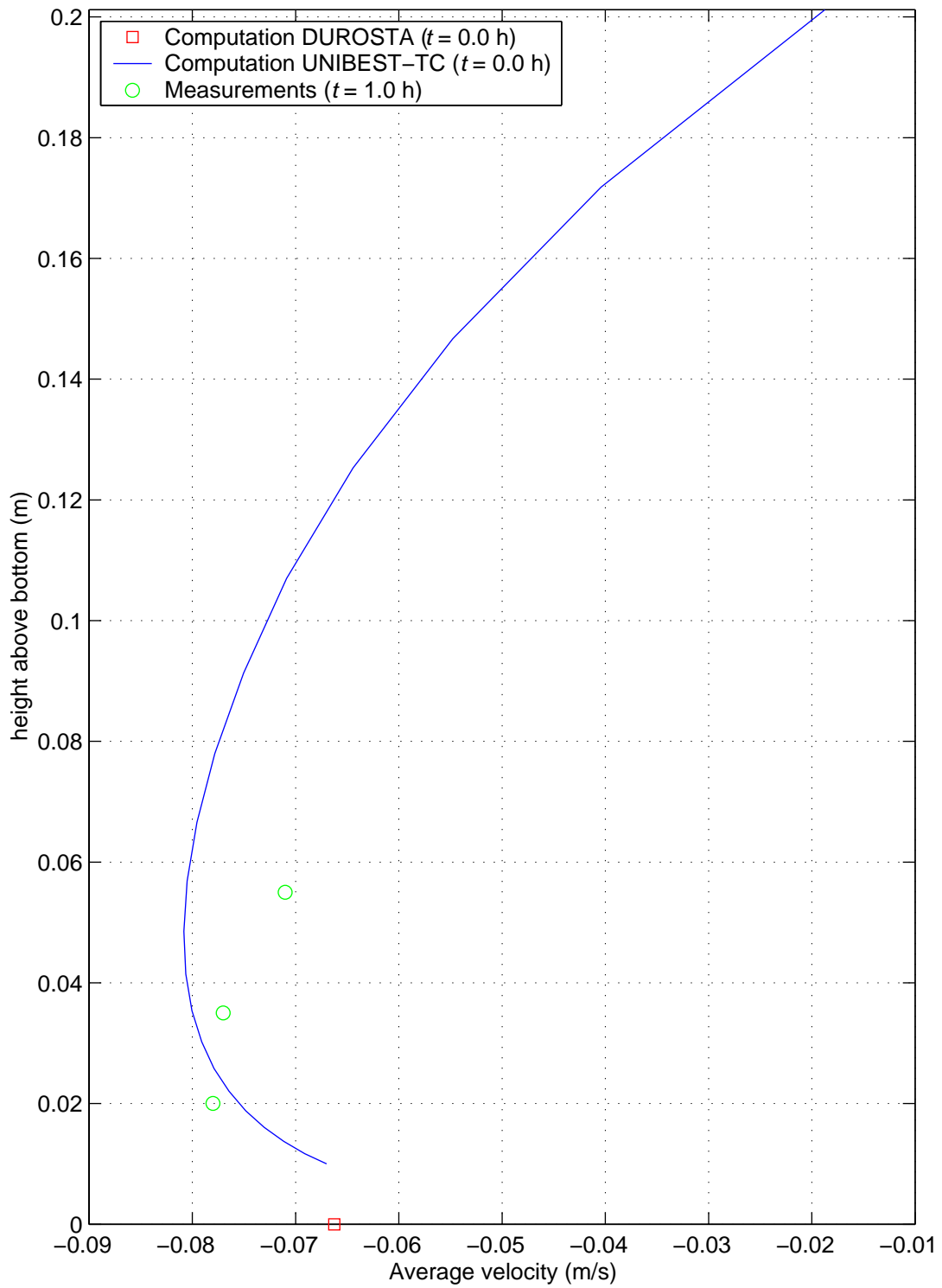
T02



Comparison computed velocities  
and measurements Schelde flume

$x = 40.52$  m

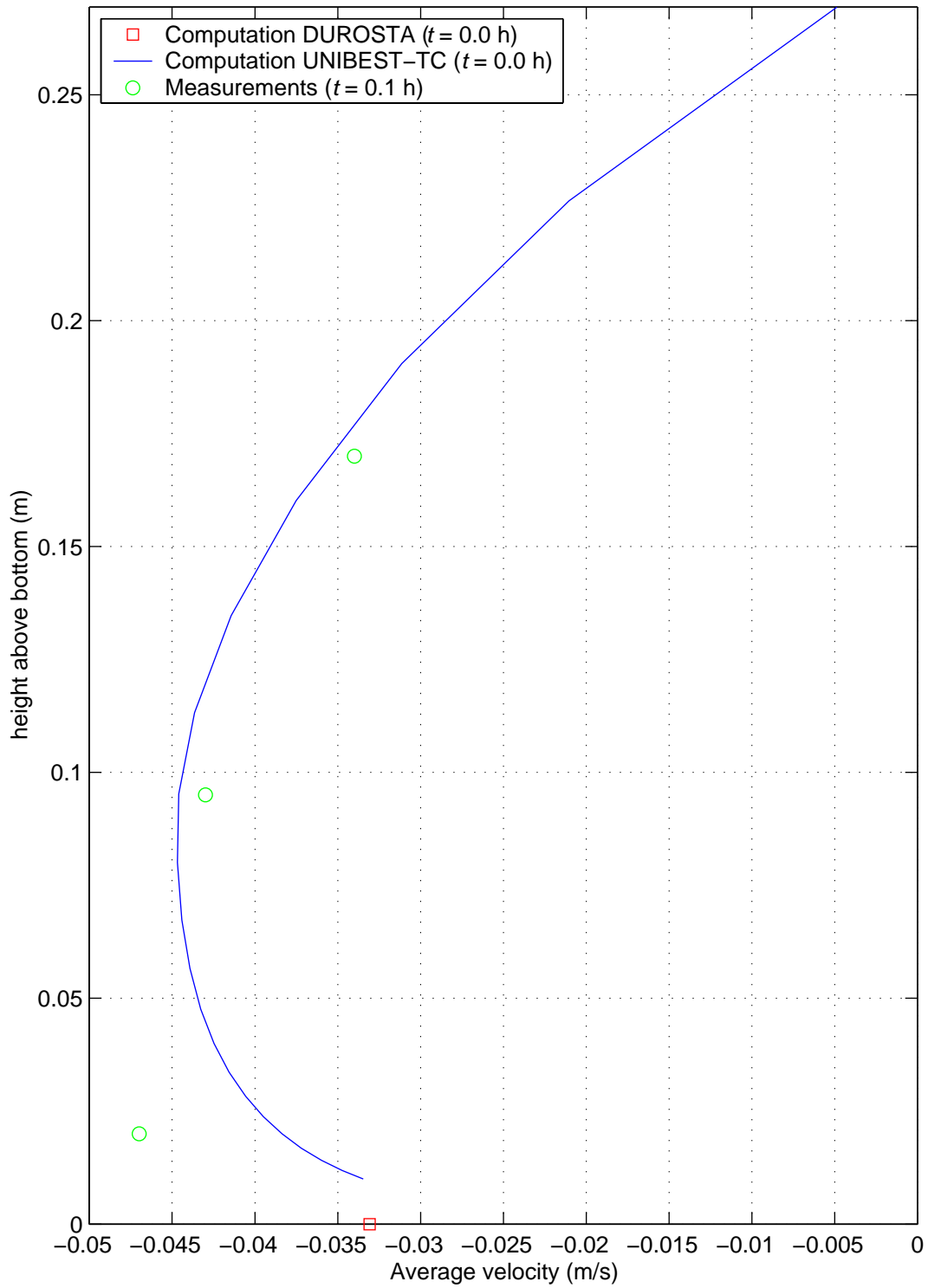
T02



Comparison computed velocities  
and measurements Schelde flume

x = 41.91 m

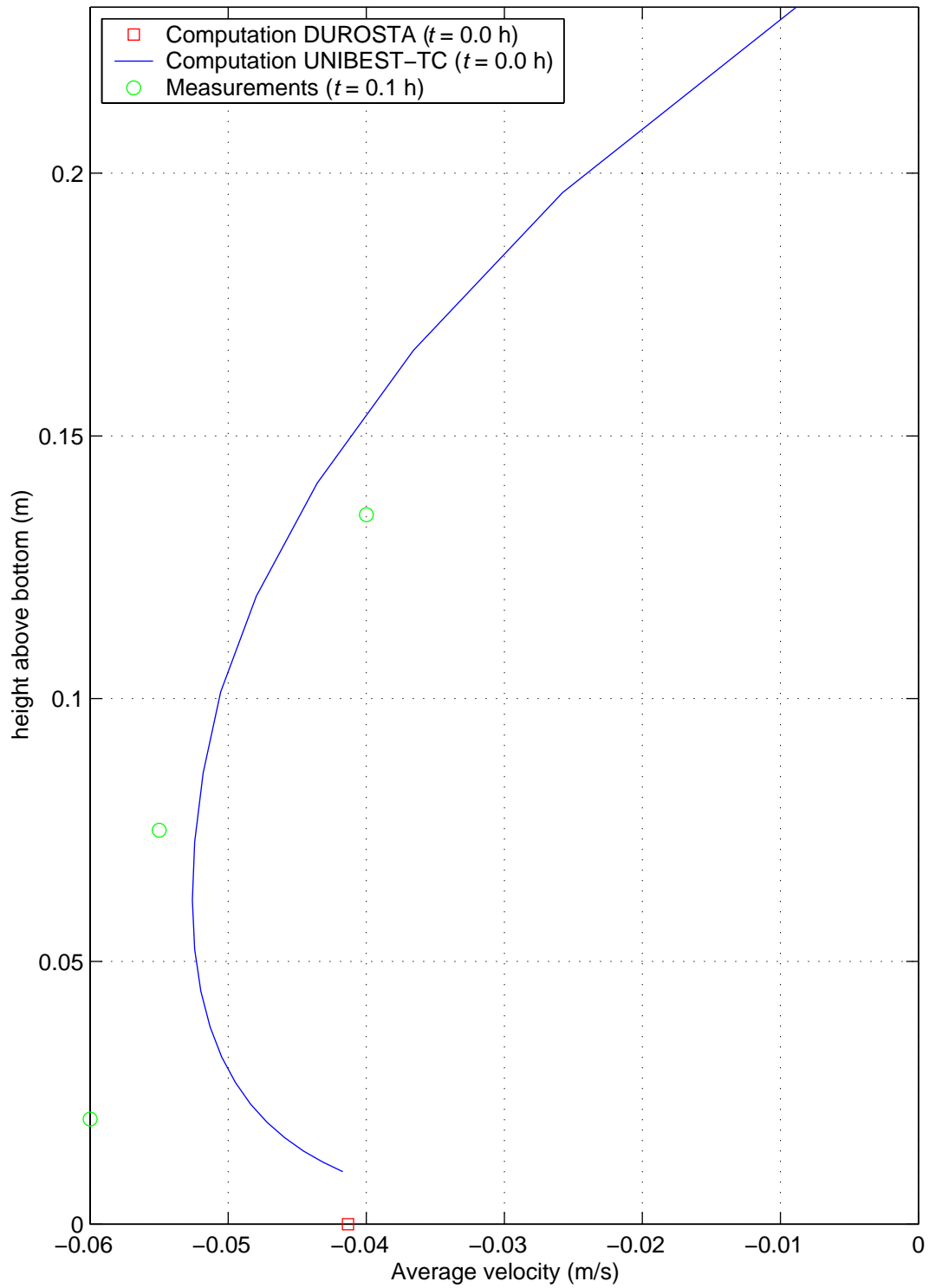
T02



Comparison computed velocities and measurements Schelde flume

$x = 39.13$  m

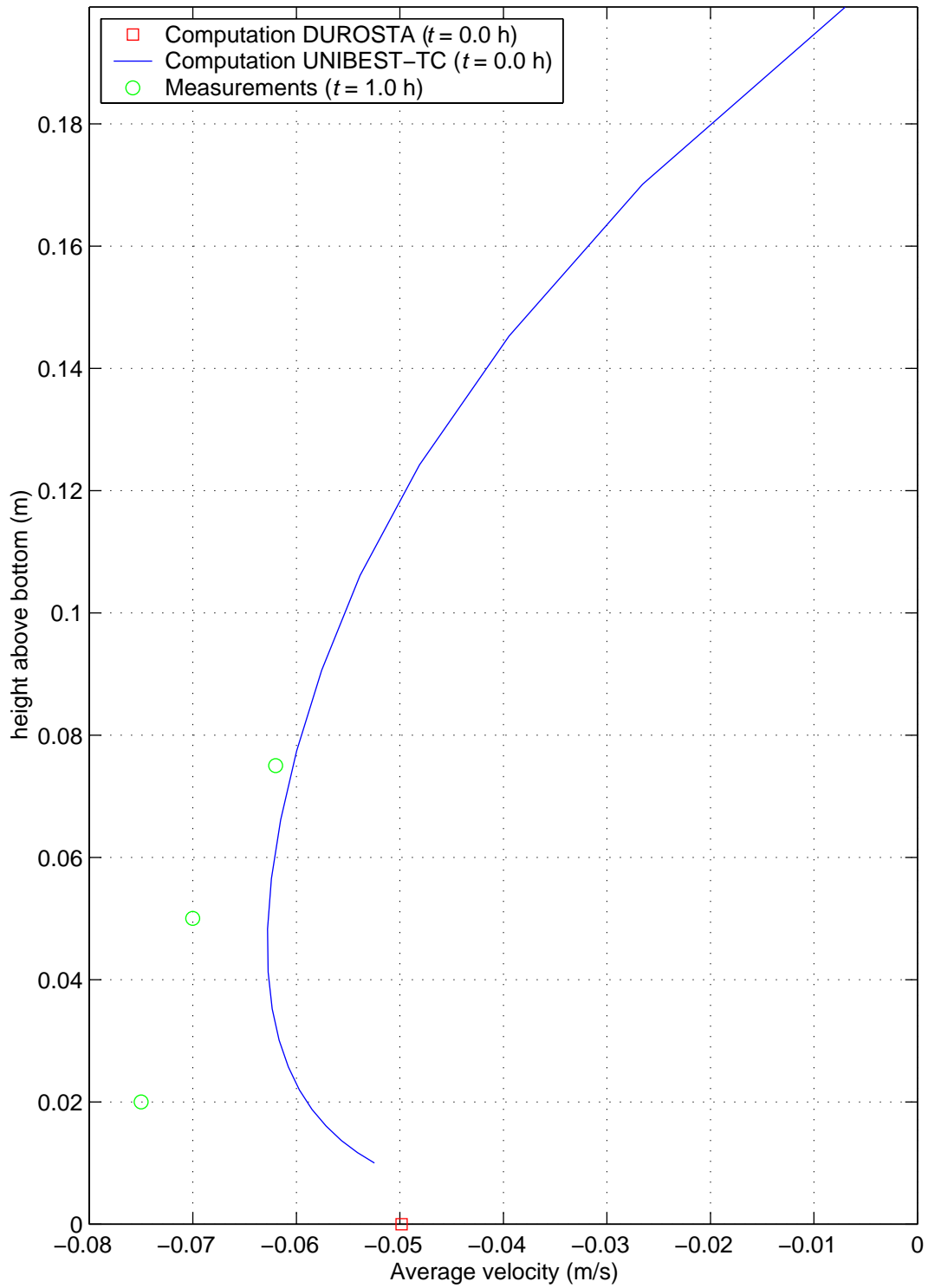
T03



Comparison computed velocities  
and measurements Schelde flume

x = 40.52 m

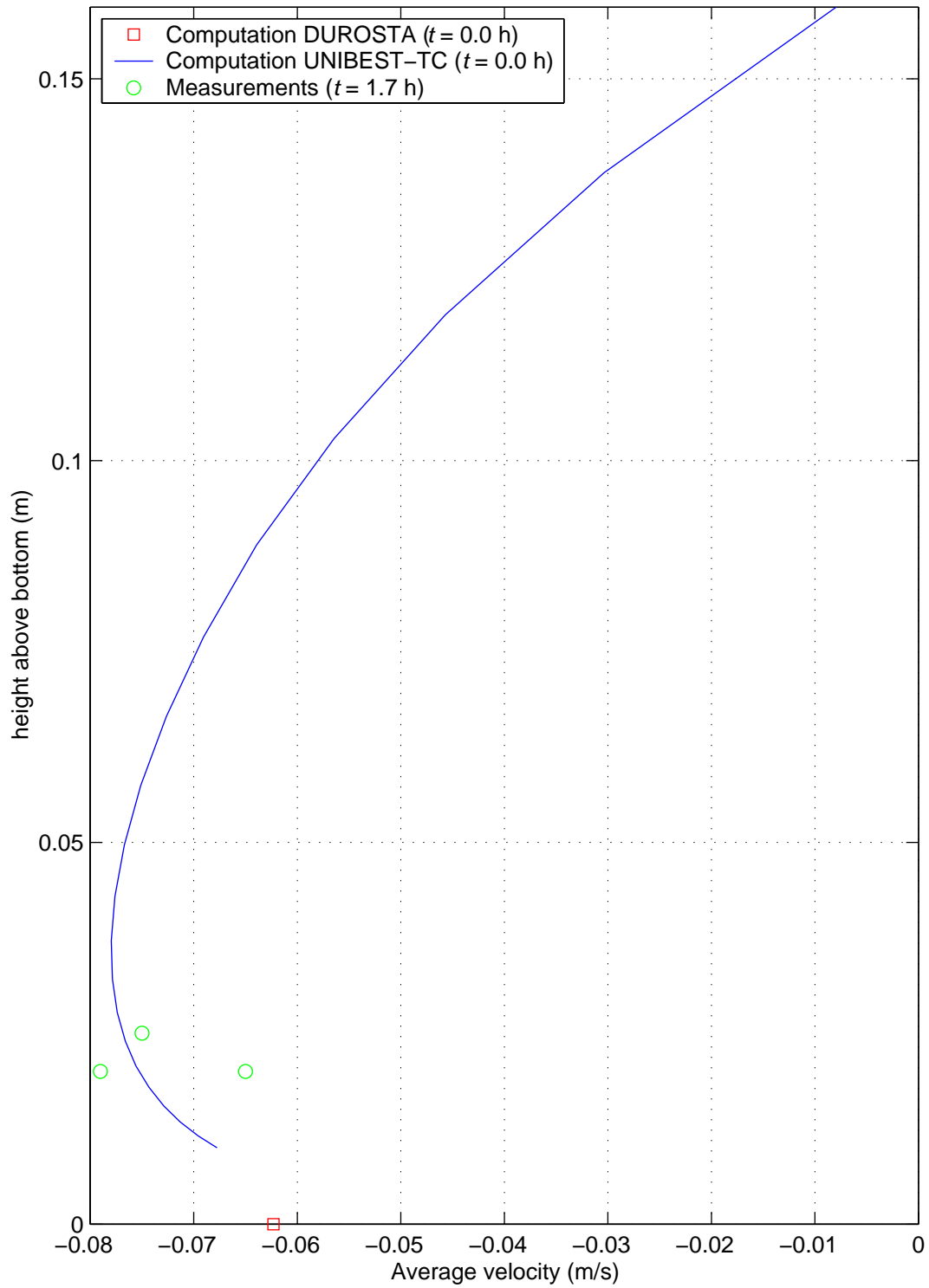
T03



Comparison computed velocities  
and measurements Schelde flume

$x = 41.91$  m

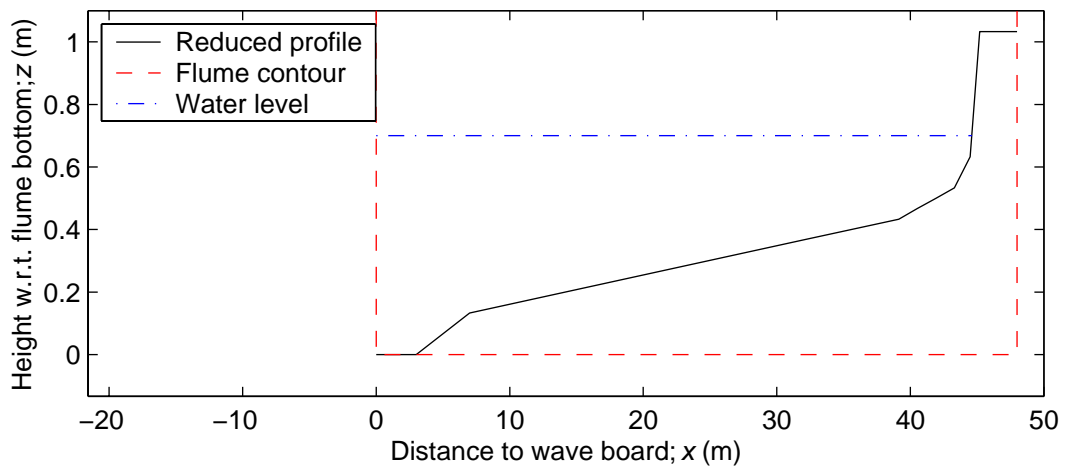
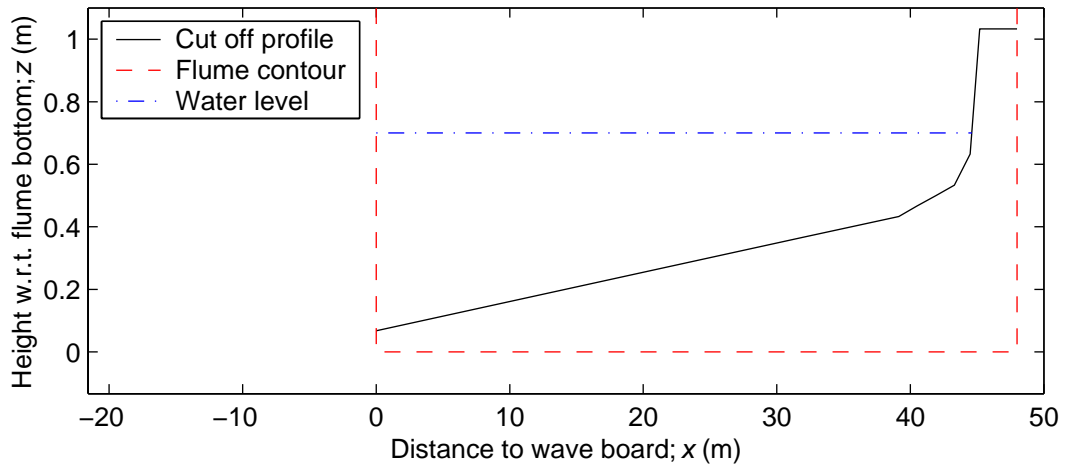
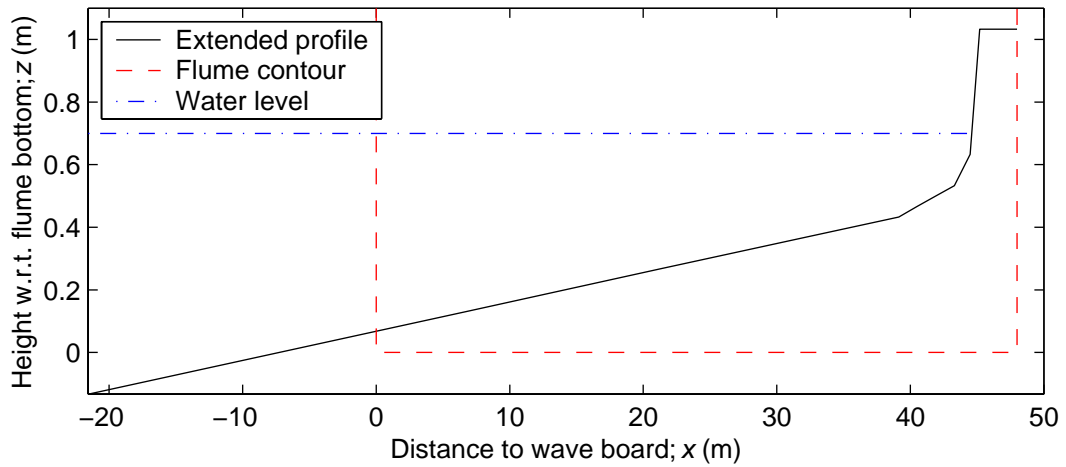
T03



Comparison computed velocities  
and measurements Schelde flume

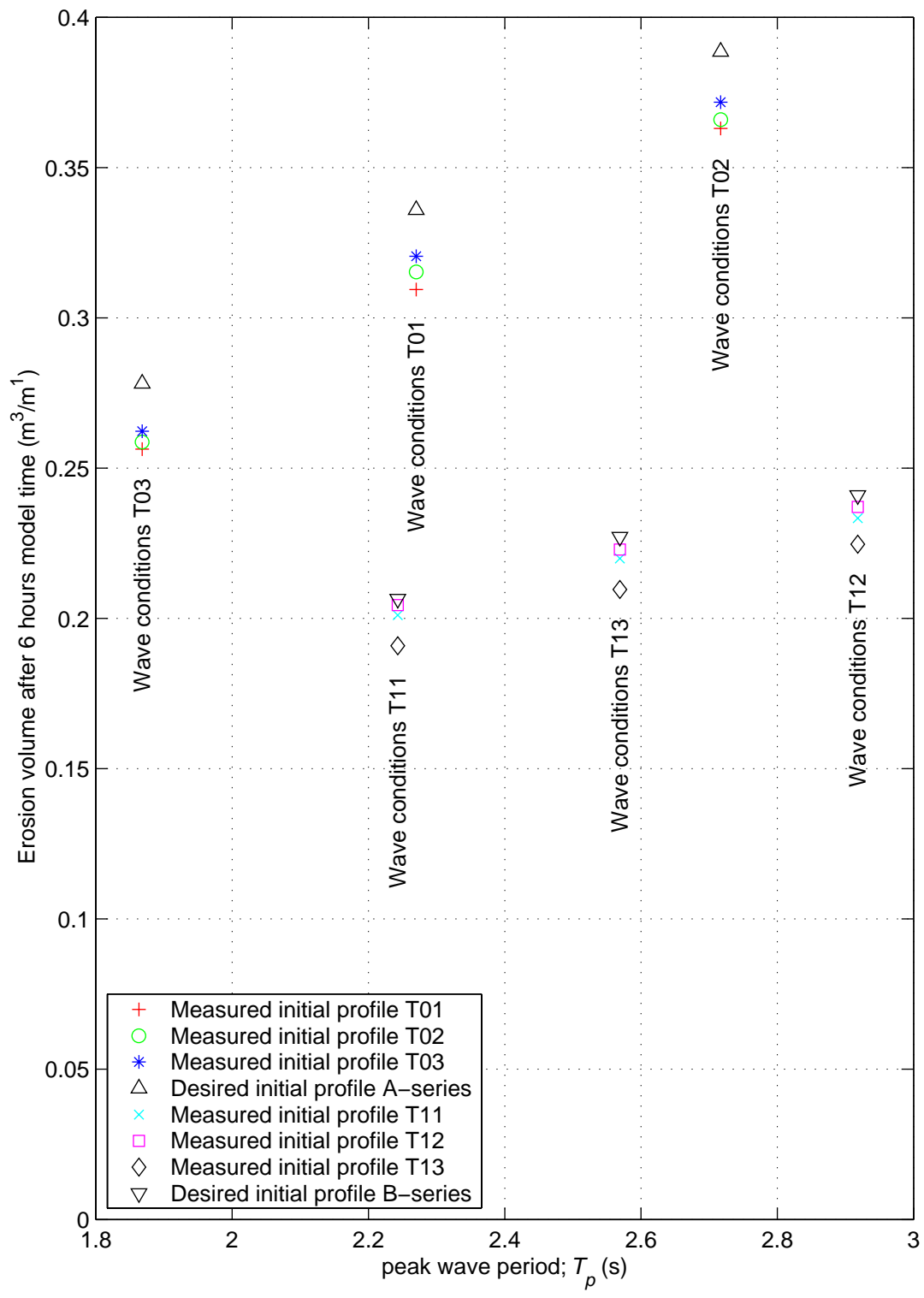
x = 43.30 m

T03



Overview of cross-shore profiles

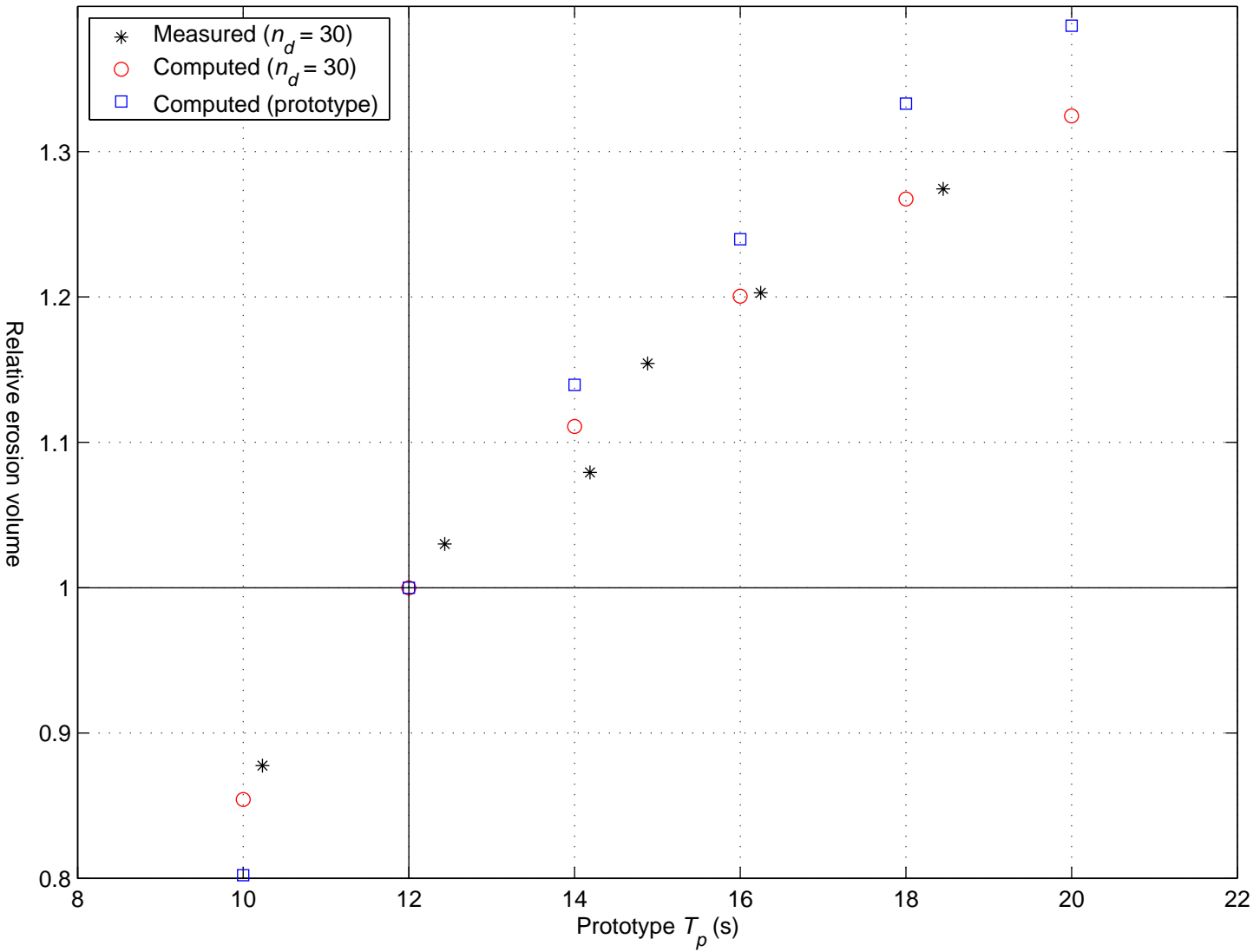
A-series ( $n_d = 30$ )



Sensitivity of erosion volume for slightly different cross-shore profile  
 For each set of wave conditions computations with  
 4 different initial profiles

DUROSTA

Computed \* 1.12

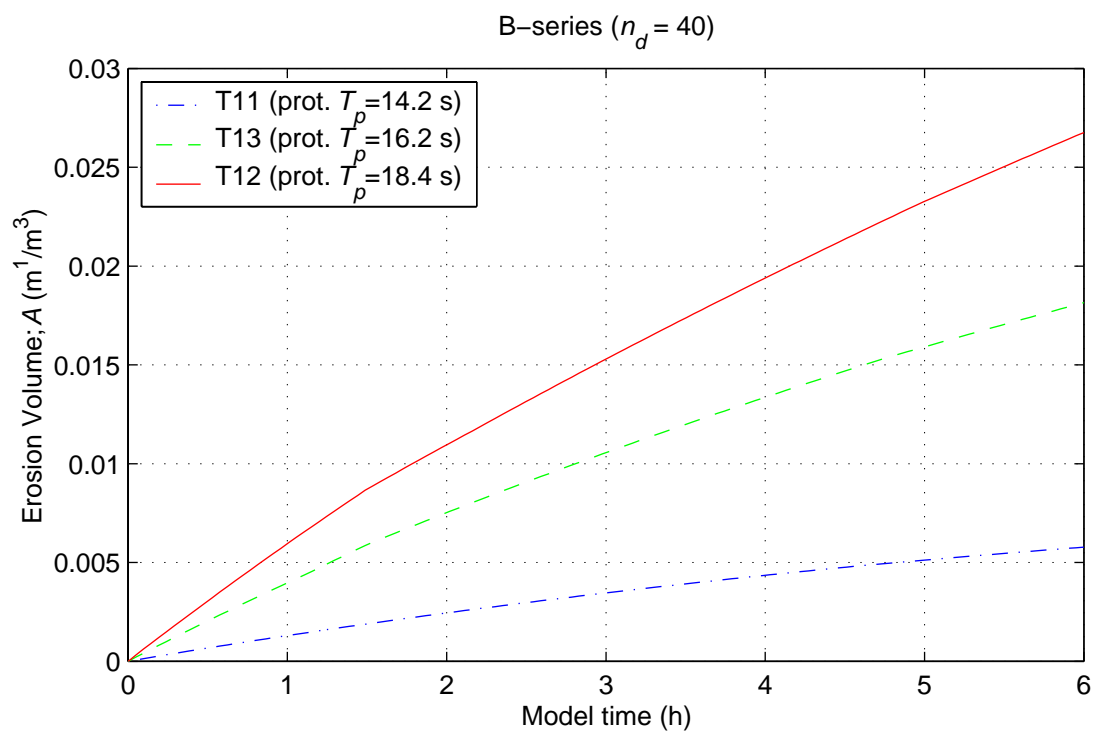
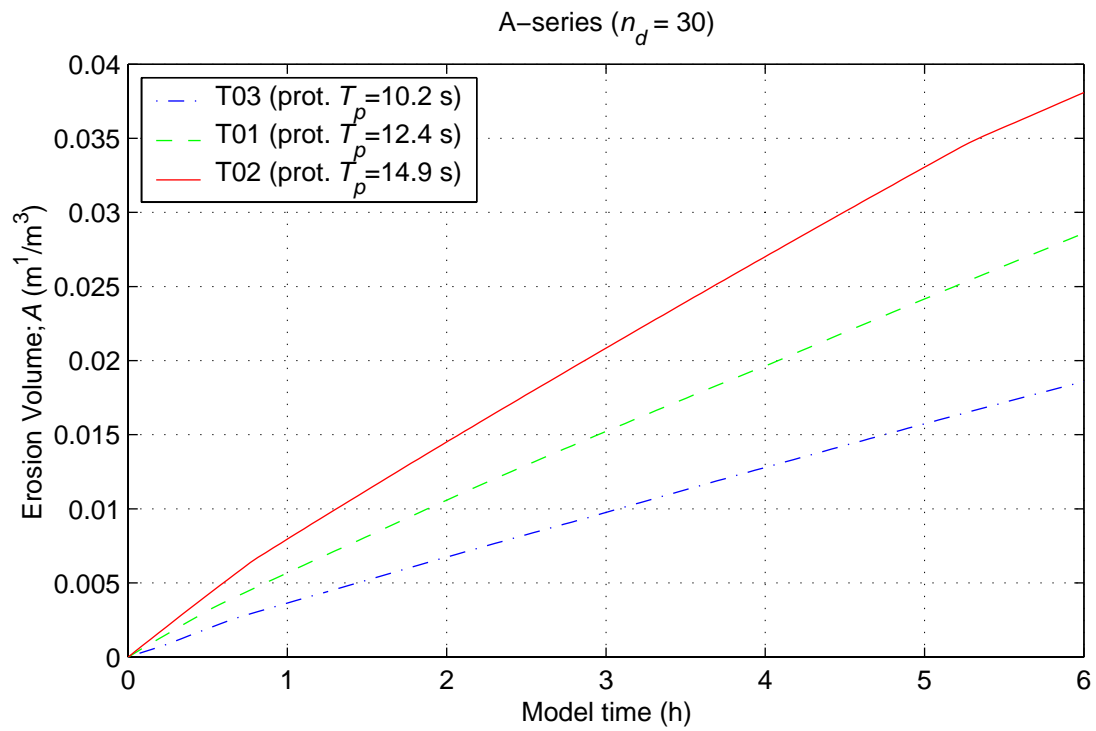


Relative erosion volume w.r.t. prototype  $T_p = 12$  s  
 after 3.5 h model time (19 h prot.) of wave attack

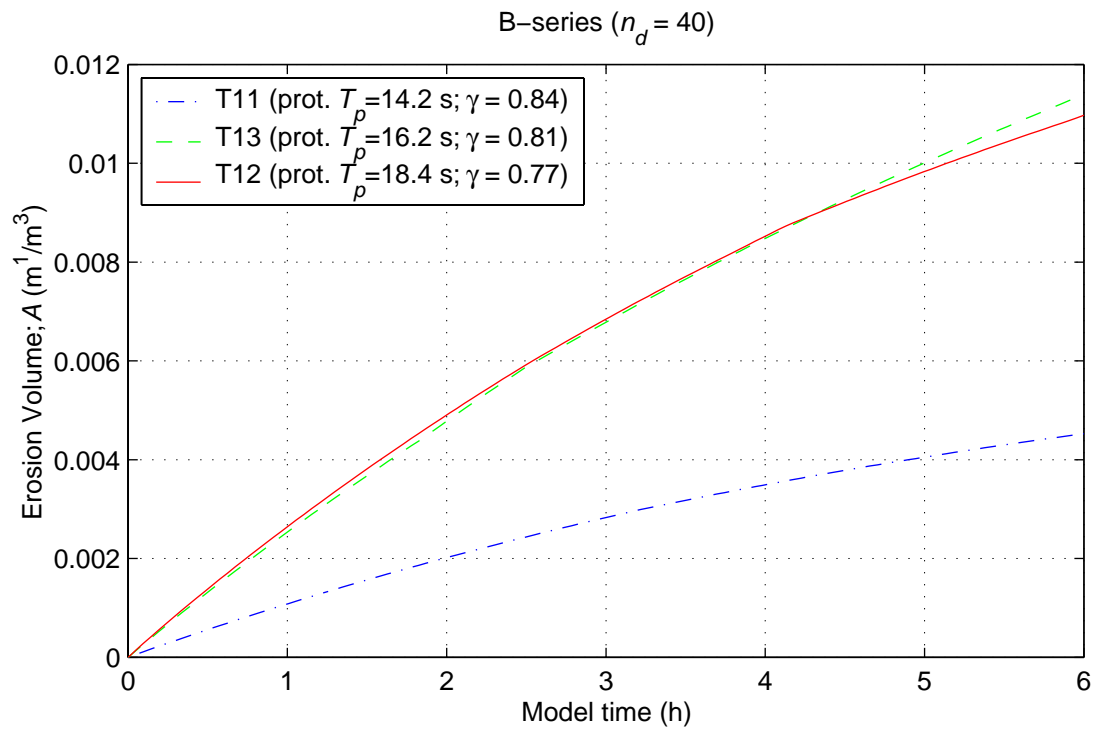
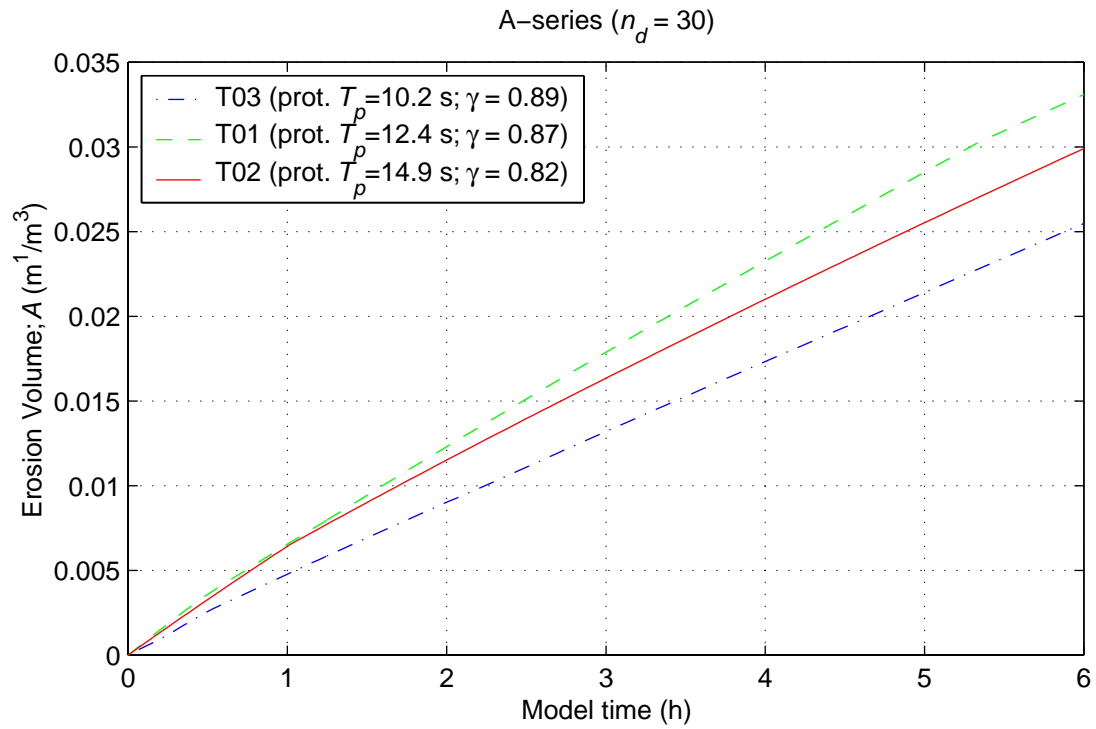
DUROSTA

WL | DELFT HYDRAULICS

Figure 4.34



|   |            |            |
|---|------------|------------|
| Erosion development in time;<br>Tuned near wave board | UNIBEST-TC |            |
| <b>WL   DELFT HYDRAULICS</b>                          |            | Figure 5.1 |



Erosion development in time;  
Tuned by breaker index  $\gamma$

UNIBEST-TC

WL | DELFT HYDRAULICS

Figure 5.2

# Appendices

## A Re-analysis of wave measurement data

The aim is to create one set of wave characteristics out of more successive wave measurements in a particular test. A solution is to combine the signals to one longer signal which can be re-analysed by AUKE-PC (WL | Delft Hydraulics' program to determine wave characteristics out of a measured surface elevation signal).

Just pasting the surface elevation signals behind each other will cause a problem. At the connection of two successive signals originates nearly sure a discontinuity. In AUKE-PC are no possibilities to some kind of smooth discontinuous signals. However, after translating the signals to an ASCII file format other programs can be applied. In this case MATLAB is used.

For each signal a multiplication factor matrix is created, with the same size as the signal, containing almost all ones. Only near a connection the values decrease smoothly but quick to zeros. The beginning of the following matrix starts with zeros and increases with the same shape to ones. By multiplying every original signal by its accompanying multiplication factor matrix a new signal originates which is continuous. Just before every connection the signal dims to zero and just after, it will swell soon to the original signal. Figure A.1 shows as an example for one wave height meter (WHM): the original signals, the multiplication factors, and the smoothed combined signal.

Each of the measurements contains a time axis (first column) which starts from zero. Simply pasting the matrices of the successive measurements behind each other results in a discontinuous time axis which several times starts from zero again. To determine not only the wave heights but also the wave periods it is necessary to make the time axis also continuous. To make that axis continuous the total time, of all the successive signals added, follows from:

$$t_{\max} = \sum_{i=1}^m t_{\max,i} + \sum_{i=1}^{m-1} \frac{t_{\max,i}}{n_i - 1}$$

in which:

|              |   |  |
|--------------|---|--|
| $t_{\max}$   | s | total time of all successive measurements together |
| $m$          | - | number of successive measurements                  |
| $n$          | - | number of rows in a signal matrix                  |
| $t_{\max,i}$ | s | end time (duration) of measurement $i$             |

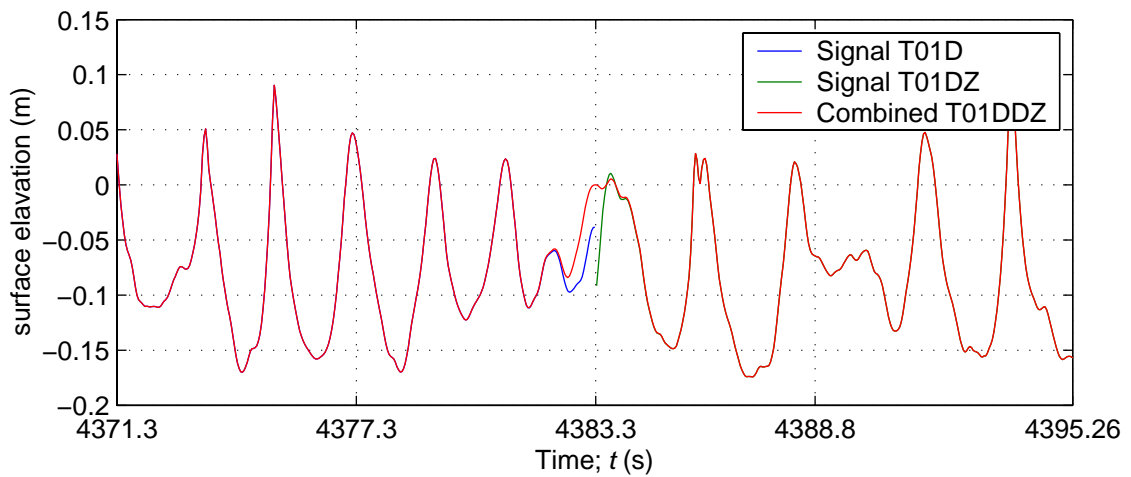
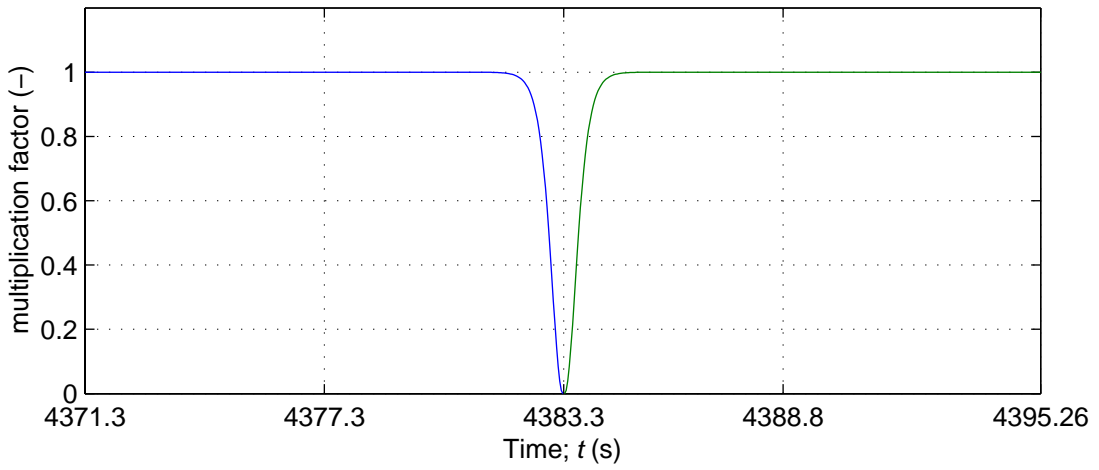
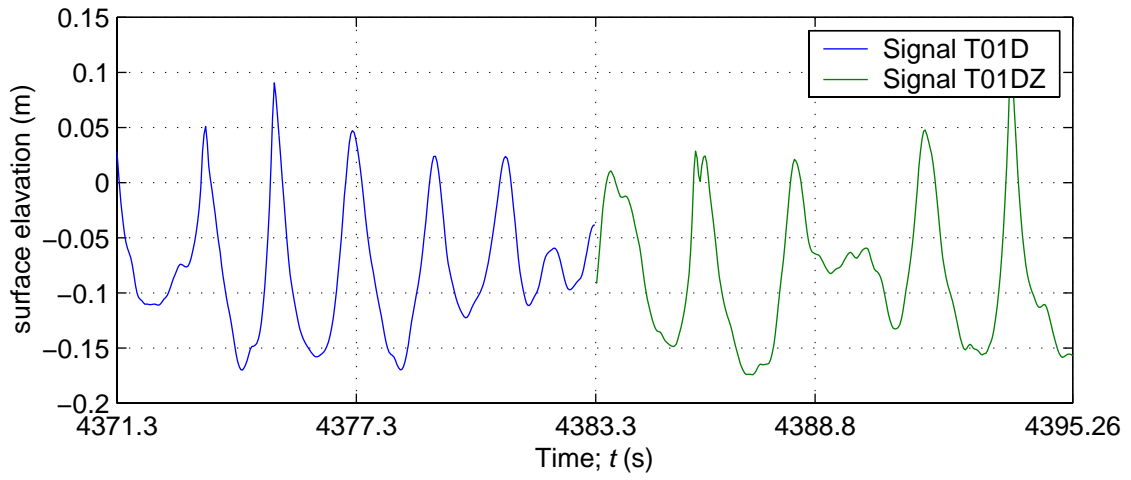
The first term means the sum of all durations of the measurements. The second term is meant to add an extra time step in between each pair of successive measurements since each time axis starts from zero.

The averaged time step can be obtained from the total time divided by the number of time steps (= number of rows minus one):

$$\Delta t = \frac{t_{\max}}{n_{\text{total}} - 1}$$

If the measure frequency for every signal was exactly equal this time step stays still the same (w.r.t. the time step of the separate measurements), otherwise the new time step is indeed averaged. With this time step a new continuous time axis and so a complete new ASCII file can be generated.

By translating the new ASCII file back to an AUKE-PC signal, a problem can appear with the time axis as a consequence of the rounded numbers. Necessary information in the command is the start time ( $t=0$ ), the total time ( $t=t_{max}$ ) and the number of time steps ( $nt$ ). However, the  $t_{max}$  in that command could only be given in 7 significant numbers (in seconds). Finally the number of time steps times the time step ( $nt*dt$ ) has to match exactly with the rounded total time (in this case the time step is obtained from the difference between two successive times, which possibly contains more decimals than the total time). This match is only ensured if the number of decimals of the time step is equal to the rounded total time. As a consequence a longer total time induces a more rounded time axis. In this case a total time of 6 hours, which is approximately 21600 seconds, leaves space for two decimals. After applying the reviewed time axis for this condition the data set is ready for AUKE-PC.



Procedure to connect successive surface elevation signals

WHM 1

## B Input file DUROSTA

```

H4265      Scheldegoot      Gemeten Profiel
1.650000  0.000093  0.006100   0.00   0.00
  0.0000   0.5000
 27.0000   0.4000
 31.0000   0.3000
 34.0000   0.2000
 36.0000   0.1000
 48.0000
  0.0000   0.0100  0.1000   5
  0.1000
  0.3000
  1.0000
  3.0000
  6.0000
BASFUN      1 205
  0.0000   0.0000
  0.5000   0.0000
  1.0000   0.0000
  1.5000   0.0000
  2.0000   0.0000
  2.5000   0.0000
  3.0000   0.0010
  3.5000   0.0240
...
...
...
...
 47.8000   1.0358
 47.9000   1.0346
 48.0000   1.0360
BASFUN      2 2
 -0.0010 -99.9900
  0.0010 -99.9900
BASFUN      3 1
  0.0000   0.7000  0.5330  0.1670
BASFUN      4 1
  0.0000   0.2400
BASFUN      5 1
  0.0000   2.2700
BASFUN      6 1
  0.0000   0.0000
BASFUN      7 1
  0.0000   0.0000
BASFUN      8 1
  0.0000   0.0000

```



## C Input file UNIBEST-TC

RUN IDENTIFICATION - Created by Pre-TC Version 2.10A at: 16:35:27 Monday, 6 September 2004

000

GRID

| XBEGIN | NDX  |
|--------|------|
| 0.00   | 5    |
| NUMBER | DX   |
| 54     | 0.50 |
| 10     | 0.40 |
| 10     | 0.30 |
| 10     | 0.20 |
| 120    | 0.10 |

KEYSECTION

|            |           |
|------------|-----------|
| 'DT '      | 0.000200  |
| 'NT '      | 1250      |
| 'JFR '     | 10        |
| 'K_IJL '   | 0         |
| 'TANPHI1 ' | 0.600000  |
| 'TANPHI2 ' | 0.600000  |
| 'GAMMA '   | 0.850000  |
| 'OPTDRY '  | 2         |
| 'RKVAL '   | 0.005000  |
| 'D50 '     | 0.000093  |
| 'D90 '     | 0.000122  |
| 'DSS '     | 0.000080  |
| 'RC '      | 0.005000  |
| 'ZDRY '    | 3         |
| 'TEMP '    | 15.900000 |
| 'END'      | 0.000000  |

Boundary Conditions

| FUNCTION | CODE | VALUE | COLUMN | FILE      |
|----------|------|-------|--------|-----------|
| 'H0'     | 1    | 0.700 | 1      | 'No File' |
| 'V_TIDE' | 1    | 0.000 | 1      | 'No File' |
| 'A_WAVE' | 1    | 0.000 | 1      | 'No File' |
| 'HRMS'   | 1    | 0.170 | 1      | 'No File' |
| 'T'      | 1    | 2.270 | 1      | 'No File' |
| 'Z'      | 2    | 0.000 | 1      | 'T01.bot' |
| 'Z_FIX'  | 1    | 0.000 | 1      | 'No File' |
| 'V_WIND' | 1    | 0.000 | 1      | 'No File' |
| 'A_WIND' | 1    | 0.000 | 1      | 'No File' |

BASIC FUNCTIONS

X-POINTS FOR TIME FUNCTIONS (COLUMNS ON UTC###.HIS)

| 1      |         |
|--------|---------|
| NUMBER | X-POINT |
| 1      | 0.00    |

NUMBER OF ACTUAL TIME FUNCTIONS  
 0  
 FUNCTIONS(1:29) X1 X2 ETC  
 T-POINTS FOR PLACE FUNCTIONS (BLOCKS ON UTC###.MP@)  
 1  
 NUMBER T-POINT  
 1 0.00  
 NUMBER OF ACTUAL PLACE FUNCTIONS  
 0  
 FUNCTIONS(1:29) @ T1 T2 ETC  
 REFERENCE VOLUMES VERTICAL  
 1  
 X1 X2 Zref  
 0.000 0.000 0.000  
 REFERENCE VOLUMES HORIZONTAL  
 1  
 Z1 Z2 Xref  
 0.000 0.000 0.000  
 VERTICAL FUNCTIONS  
 12  

| X-POINT | T-POINT | F-TYPE |
|---------|---------|--------|
| 39.130  | 0.001   | 3      |
| 39.130  | 0.040   | 3      |
| 39.130  | 0.130   | 3      |
| 40.520  | 0.001   | 3      |
| 40.520  | 0.040   | 3      |
| 40.520  | 0.130   | 3      |
| 41.910  | 0.001   | 3      |
| 41.910  | 0.040   | 3      |
| 41.910  | 0.130   | 3      |
| 43.300  | 0.001   | 3      |
| 43.300  | 0.040   | 3      |
| 43.300  | 0.130   | 3      |

# Verkenning effect van golfperiode op veiligheid duinenkust

Een probabilistische beschouwing



C. den Heijer



Minor M.Sc. Thesis

april 2005



wL | delft hydraulics





# Verkenning effect van golfperiode op veiligheid duinenkust

Een probabilistische beschouwing

C. den Heijer

Minor M.Sc. Thesis

april 2005

Afstudeercommissie:

Prof.dr.ir. M.J.F. Stive

TU Delft

Dr.ir. J. van de Graaff

TU Delft

Dr.ir. A.J.H.M. Reniers

TU Delft

Ir. J.H. de Vroeg

WL | Delft Hydraulics

Dr.ir. H.J. Steetzel

Alkyon

Ir. J.S.M. van Thiel de Vries

TU Delft



## Voorwoord

Dit onderzoek is uitgevoerd als aanvullend (minor) afstudeerwerk in het kader van de studie Civiele Techniek aan de Technische Universiteit Delft. Het huidige programma (Bachelor-Master) biedt de mogelijkheid om naast het gebruikelijke afstudeerwerk een aanvullende afstudeeropdracht uit te voeren.

Aansluitend op mijn afstudeerwerk betreffende ‘*The effect of wave period on dune erosion*’ (Den Heijer, 2005), waarin de Scheldegoot-duinafslagproeven die bij WL | Delft Hydraulics (Coeveld en De Vroeg, 2004) zijn uitgevoerd uitgebreid aan de orde komen, is dit onderzoek uitgevoerd.

Graag wil ik alle leden van mijn afstudeercommissie bedanken voor hun bijdrage aan dit onderzoek. In het bijzonder ben ik dank verschuldigd aan Jan van de Graaff voor zijn inbreng. Verder wil ik Pieter van Gelder bedanken voor zijn nuttige tips en hulp bij de uitvoering van dit onderzoek.

Delft, 12 april 2005

Kees den Heijer



## Inhoud

|  |     |
|--|-----|
| Voorwoord.....                                 | i   |
| Inhoud.....                                    | iii |
| Lijst van figuren .....                        | v   |
| Lijst van tabellen .....                       | vii |
| Samenvatting .....                             | ix  |
| 1 Inleiding.....                               | 1   |
| 1.1 Aanleiding .....                           | 1   |
| 1.2 Probleemstelling.....                      | 1   |
| 1.3 Doelstelling.....                          | 2   |
| 1.4 Aanpak.....                                | 2   |
| 1.5 Leeswijzer.....                            | 2   |
| 2 Vigerende toetsingsmethode.....              | 3   |
| 2.1 DUROS-model .....                          | 3   |
| 2.2 Toetsingsmethode.....                      | 4   |
| 2.3 Beoordeling .....                          | 5   |
| 3 Probabilistische berekeningen .....          | 6   |
| 3.1 Zonder golfperiode invloeden .....         | 6   |
| 3.1.1 Variabelen en gebruikte verdelingen..... | 6   |
| 3.1.2 Numerieke integratie .....               | 7   |
| 3.2 Golfcondities .....                        | 8   |
| 3.2.1 Golfhoogte.....                          | 9   |
| 3.2.2 Golfperiode.....                         | 9   |
| 3.3 Met golfperiode invloed .....              | 10  |
| 3.4 Afsluitende opmerkingen .....              | 11  |
| 4 Conclusies en aanbevelingen.....             | 13  |
| 4.1 Conclusies.....                            | 13  |
| 4.2 Aanbevelingen.....                         | 13  |
| Literatuur .....                               | 14  |
| Figuren  |     |



## Lijst van figuren

|  |   |
|--|---|
| Figuur 2.1 Principe van het DUROS-rekenmodel voor duinafslag.....  | 4 |
| Figuur 3.1 Standaard dwarsprofiel  |   |
| Figuur 3.2 Toegepaste waterstandsverdeling met daarin aangegeven de gebruikte stappen  |   |
| Figuur 3.3 Voorbeeld van afslagberekening met daarin de definities van AF, A en $\Delta A$   |   |
| Figuur 3.4 Overschrijdingskans afslag zonder invloed van golfperiode   |   |
| Figuur 3.5 Waterstand-gemiddelde-golfhoogte verband voor Hoek van Holland volgens<br>Leidraad Duinafslag; Bijbehorende overschrijdingskansen bij een<br>standaardafwijking van $\sigma_{Hs} = 0.6$ m |   |
| Figuur 3.6 Fictief waterstand-golfperiode verband; Bijbehorende overschrijdingskansen bij<br>een standaardafwijking $\sigma_{Tp} = 1.3$ s  |   |
| Figuur 3.7 Relatieve afslag t.o.v. basisgeval $T_p = 12$ s   |   |
| Figuur 3.8 Resultaten van numerieke integratie met volledige correlatie tussen golfhoogte<br>en golfperiode  |   |
| Figuur 3.9 Resultaten van numerieke integratie met volledige onafhankelijkheid tussen<br>golfhoogte en golfperiode   |   |



## Lijst van tabellen

Tabel 3.1 Afgeleide kwantielen golfhoogte vergeleken met kwantielen van Europlatform . 9

Tabel 3.2 Fictieve kwantielen golfperiode vergeleken met de kwantielen van de  
meetstations Schiermonnikoog-Noord en Eierlandse Gat..... 9



## Samenvatting

Bij de beoordeling van de veiligheid van de Nederlandse duinenkust wordt gebruik gemaakt van een rekenmodel dat, voor vastgestelde ontwerpomstandigheden, de mate van duinafslag bepaalt. De kern van dit rekenmodel wordt gevormd door het zogenaamde DUROS-rekenmodel (TAW, 1984).

Op basis van beschikbare informatie en het verwachte bereik van de golfperioden ( $T_p \leq 12$  s) werd, tijdens de ontwikkeling van het DUROS-rekenmodel, de vorm van het afslagprofiel verondersteld onafhankelijk te zijn van de golfperiode. Echter, volgens de huidige inzichten moet er rekening mee gehouden worden dat tijdens extreme omstandigheden veel langere golfperioden voorkomen dan eerder verondersteld werd.

Om een schatting te kunnen maken van de invloed van deze langere golfperioden op de mate van duinafslag zijn kleinschalige proeven uitgevoerd door WL | Delft Hydraulics in de Scheldegoet. Op basis van de analyse van die proeven is enig inzicht verkregen in de gevoeligheid van de mate van duinafslag voor de golfperiode.

Het doel van dit onderzoek is een indicatie te geven van de toename in ontwerpafslag bij de recente inzichten, betreffende de golfperiode, t.o.v. de huidige beoordelingsmethode voor de veiligheid van de duinenkust.

Om een uitspraak te kunnen doen over deze invloed is de probabilistische simulatie (numerieke integratie), die mede te grondslag ligt aan de huidige toetsingsmethode, uitgebreid met het effect van de golfperiode.

Er is een fictieve situatie gecreëerd waarbij voor de golfperiode met een overschrijdingskans van  $10^{-4}$  per jaar een piek-golfperiode van  $T_p = 18.5$  s is gekozen. Voor deze situatie zijn een aantal simulaties uitgevoerd waarbij de relatieve toename van het afslagvolume bij  $T_p = 18.5$  s t.o.v.  $T_p = 12$  s (als de overige factoren gelijk blijven) is gevarieerd van 0 tot 50 %. Deze relatieve toename, welke de gevoeligheid van het afslagvolume voor de golfperiode weergeeft, wordt hier *Scenario* genoemd.

Uit de uitgevoerde numerieke integraties, onder genoemde omstandigheden, kan geconcludeerd worden dat afslagvolume met een overschrijdingskans van  $10^{-5}$  per jaar ongeveer met  $0.8 \cdot \textit{Scenario}$  zal toenemen. Dit betekent dat er voor een *Scenario* van 25 % toename bij  $T_p = 18.5$  s t.o.v.  $T_p = 12$  s rekening gehouden moet worden met  $0.8 \cdot 25\% = 20\%$  extra afslagvolume bij een overschrijdingskans van  $10^{-5}$  per jaar.



# 1 Inleiding

## 1.1 Aanleiding

Bij de beoordeling van de veiligheid van de Nederlandse duinenkust wordt gebruik gemaakt van een rekenmodel dat, voor vastgestelde ontwerpomstandigheden, de mate van duinafslag bepaalt. De kern van dit rekenmodel wordt gevormd door het zogenaamde DUROS-rekenmodel (TAW, 1984).

Op basis van beschikbare informatie en het verwachte bereik van de golfperioden werd, tijdens de ontwikkeling van het DUROS-rekenmodel, de vorm van het afslagprofiel verondersteld onafhankelijk te zijn van de golfperiode.

Momenteel wordt als maatgevende golfperiode, uitgedrukt als piek-golfperiode, de waarde  $T_p = 12.0$  s gebruikt voor de Waddenkust en de Hollandse kust en voor het zuidelijke deel van de Zuid-Hollandse kust en Zeeuwse eilanden de waarde  $T_p = 8.0$  s (DWW, Hydraulische Randvoorwaarden 2001). Echter, volgens de recente inzichten moet er tijdens ontwerpomstandigheden rekening gehouden worden met veel langere golfperioden (De Ronde *et al.*, 1995; Roskam en Hoekema, 1996). Deze toename varieert tussen 30 % (in het zuiden) tot 60 % (in het noorden) ten opzichte van de thans gebruikte maatgevende waarden. Hoewel in 1995/1996 deze 'nieuwe' inzichten betreffende zwaardere golfcondities al bestonden is tijdens de voorbereiding van het Randvoorwaardenboek 2001 en daarna pas meer onderzoek gedaan naar de gevolgen voor de veiligheid van de duinenkust.

Uit recent uitgevoerd verkennend onderzoek (Steetzel, 2002) blijkt, dat de golfperiode toch invloed heeft op de vorm van het afslagprofiel. Ook is er een significante toename in afslagvolume berekend. Echter, de hiervoor toegepaste methode is gevalideerd voor golfperioden  $T_p \leq 12.0$  s.

Eind 2003 heeft WL | Delft Hydraulics (Coeveld en De Vroeg, 2004) kleinschalig fysisch modelonderzoek uitgevoerd (diepteschaal 30 en 40). Dit onderzoek bestond uit zes proeven met verschillende golfperioden (prototype  $T_p$  tussen 10 s en 18.5 s). Uit een eerste analyse van deze kleinschalige proeven (Den Heijer, 2005) blijkt niet alleen dat voor grotere golfperioden significant meer duinafslag verwacht mag worden, maar ook dat met het numerieke model DUROSTA de resultaten van de proeven op deze schaal niet zonder meer 'nagerekend' kunnen worden.

## 1.2 Probleemstelling

Bij de Scheldegoet-proeven (Coeveld en De Vroeg, 2004) en de analyse daarvan (Den Heijer, 2005) is (voorlopig) alleen gekeken naar de invloed van de golfperiode op de mate van duinafslag als de overige afslagbepalende factoren gelijk blijven.

In de recente onderzoeken naar de toename van de mate van duinafslag als gevolg van zwaardere golfcondities is tot nu toe (gemakshalve) aangenomen dat er rekening gehouden moet worden met piek-golfperioden met een overschrijdingskans van  $10^{-4}$  per jaar (hiervoor als ontwerpomstandigheden aangegeven). Om een schatting te kunnen maken van het effect van deze grotere golfperiode (t.o.v.  $T_p = 12$  s) zijn de andere invloedsfactoren (zoals stormvloedpeil, golfhoogte enz.) niet gevarieerd. Echter, om

uiteindelijk een uitspraak te kunnen doen over de veiligheid van de (Nederlandse) kust zijn de volgende punten van belang:

- De hoeveelheid afslag die optreedt bij de ontwerpomstandigheden ( $10^{-5}$  afslag)
- De combinatie van afslagbepalende factoren die tot deze ontwerpafslag leidt met de grootste kans van voorkomen (ontwerppunt)

Op basis daarvan kan meer duidelijkheid verkregen worden over de maatschappelijke implicaties van de huidige inzichten over verzwaarde golfcondities in extreme omstandigheden tegen het licht van onder andere de resultaten van de Scheldegoot-proeven (Coeveld en De Vroeg, 2004).

### **1.3 Doelstelling**

Het doel van dit onderzoek is een indicatie te geven van de toename in ontwerpafslag bij de recente inzichten, betreffende de golfperiode, t.o.v. de huidige beoordelingsmethode voor de veiligheid van de duinenkust.

De vraag betreffende de ligging van het ontwerppunt onder deze omstandigheden wordt hier buiten beschouwing gelaten.

### **1.4 Aanpak**

De huidige toetsingsmethode voor veiligheid van de Nederlandse kust, op basis van het zogenaamde DUROS-model, is gebaseerd op onder andere een numerieke integratie (niveau III probabilistische methode; Van de Graaff, 1984). Daarbij zijn een zevental variabelen in beschouwing genomen. De golfperiode maakte daarvan echter geen deel uit.

In dit onderzoek wordt eerst de bovengenoemde numerieke integratie met 7 variabelen (Van de Graaff, 1984) gereproduceerd om deze daarna uit te breiden met de invloed van de golfperiode.

### **1.5 Leeswijzer**

Aan het begin van dit document is een lijst van figuren, een lijst van tabellen en een samenvatting van het onderzoek weergegeven. Achterin staat een literatuurlijst en zijn tevens de meeste figuren te vinden. De tabellen bevinden zich tussen de tekst. Indien een figuur zich tussen de tekst bevindt dan wordt dat vermeld bij de verwijzingen naar die figuur.

In hoofdstuk 2 wordt de huidige methode voor de beoordeling van de veiligheid van de Nederlandse duinenkust kort samengevat. In hoofdstuk 3 komt eerst een probabilistische berekening aan de orde die mede ten grondslag ligt aan de huidige veiligheidsbeoordeling van de Nederlandse kust. Vervolgens wordt deze berekening uitgebreid met invloed van de golfperiode. Ten slotte komen in hoofdstuk 4 conclusies en aanbevelingen aan de orde.

## 2 Vigerende toetsingsmethode

De vigerende toetsingsmethode voor de beoordeling van de Nederlandse duinenkust op veiligheid is gebaseerd op het DUROS-model (TAW, 1984). Dit model gaat uit van het ontstaan van een bekend verondersteld afslagprofiel tijdens een maatgevende stormvloed. De toelaatbare doorbreekkans is in de Leidraad Duinafslag (TAW, 1984) gesteld op 10 % van de veiligheidsnorm (de veiligheid is gerelateerd aan de overschrijdingskans van de maximale waterstand). Bij een norm van  $10^{-4}$  per jaar betekent dit een toelaatbare kans op doorbraak van  $10^{-5}$  per jaar. In de toetsingsmethode wordt deze kans gerepresenteerd door de keuze van representatieve waarden voor zowel de hydraulische randvoorwaarden als de sterkte.

### 2.1 DUROS-model

Het DUROS-model gaat uit van het ontstaan van een afslagprofiel dat afhangt van de waterstand, significante golfhoogte en de valsnelheid van duinzand in zeewater (gerelateerd aan de korreldiameter).

Het afslagprofiel wordt als volgt samengesteld:

- De duinvoet, het punt waar het steile front van het afgeslagen duin overgaat in het relatief flauwe profiel van het strand, ligt na de storm op het stormvloedpeil.
- De helling van het afgeslagen duintalud bedraagt 1 : 1.
- Zeewaarts van de duinvoet ( $x = 0, y = 0$ ), loodrecht op de kust, verloopt het profiel parabolisch volgens de formule (Vellinga, 1986):

$$\left(\frac{7.6}{H_{0s}}\right)y = 0.4714 \left[ \left(\frac{7.6}{H_{0s}}\right)^{1.28} \cdot \left(\frac{w}{0.0268}\right)^{0.56} x + 18 \right]^{0.5} - 2.00 \quad (2.1)$$

waarin:

|          |       |   |
|----------|-------|---|
| $H_{0s}$ | [m]   | significante golfhoogte op diep water                       |
| $y$      | [m]   | verticale afstand tot stormvloedpeil, positief naar beneden |
| $w$      | [m/s] | valsnelheid van duinzand in zeewater                        |
| $x$      | [m]   | horizontale afstand tot nieuwe duinvoet, positief zeewaarts |

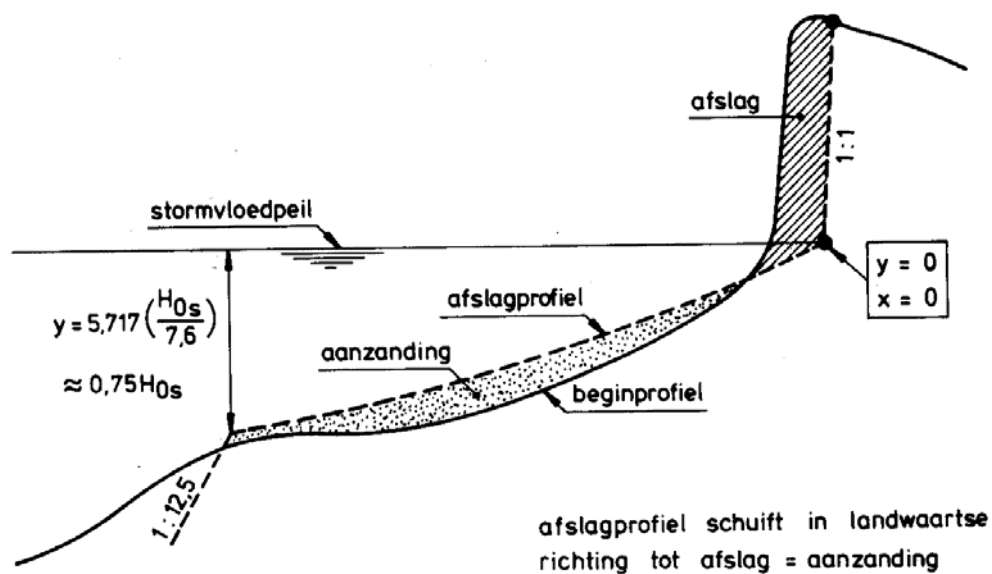
- Zeewaarts van het punt waarvoor geldt

$$x = 250 \left(\frac{H_{0s}}{7.6}\right)^{1.28} \cdot \left(\frac{0.0268}{w}\right)^{0.56} \quad (2.2)$$
$$y = 5.717 \left(\frac{H_{0s}}{7.6}\right)$$

gaat het parabolische profiel over in een rechte lijn onder een helling van 1 : 12.5 tot het oorspronkelijke profiel wordt gesneden.

Vervolgens wordt het afslagprofiel landwaarts verschoven totdat afslag en aanzanding aan elkaar gelijk zijn.

Het principe is weergegeven in Figuur 2.1 (pagina 4).



Figuur 2.1 Principe van het DUROS-rekenmodel voor duinafslag

De mate van duinafslag is in het model sterk afhankelijk van het stormvloedpeil en in mindere mate van de golfhoogte. Het model is afgeregeld voor een golfsteilheid van 0.034 op diep water. Deze golfsteilheid treedt op bij een golfhoogte van  $H_{0s} = 7.6$  m en een golfperiode van  $T_p = 12$  s.

## 2.2 Toetsingsmethode

Tijdens de ontwikkeling van de vigerende toetsingsmethode is ervoor gekozen om de toelaatbare doorbreekkans af te leiden uit berekeningen met representatieve waarden voor zowel de hydraulische randvoorwaarden als de sterkte.

De toetsingsmethode is ontwikkeld op basis van een probabilistische veiligheidsbeschouwing (Van de Graaff, 1984) welke in hoofdstuk 3 aan de orde komt. Hierbij wordt rekening gehouden met de nauwkeurigheid van het rekenmodel en het stochastische karakter van de duinafslagbepalende factoren die toentertijd van belang werden geacht. De volgende zeven variabelen werden in beschouwing genomen:

- Stormvloedpeil
- Significante golfhoogte
- Korreldiameter (valsnelheid in (zee)water)
- Onnauwkeurigheden van het rekenmodel
- Buistoten en bui-oscillaties
- Stormvloedduur
- Profiel fluctuaties

Voor de hydraulische randvoorwaarden wordt een waterstand (rekenpeil) gebruikt die correspondeert met een overschrijdingsfrequentie van  $10^{-4}$  plus  $2/3$  van de decimeringshoogte, en bijbehorende golfhoogte (volgens Van Aalst, 1983).

In de duinvoetverplaatsing tijdens een stormvloed wordt een toeslag opgenomen voor modelonnauwkeurigheid, onzekerheid in het verloop van de stormopzet en voor buistoten en bui-oscillaties.

Voor de korreldiameter, waaruit de valsnelheid in (zee)water wordt afgeleid, wordt een rekenwaarde toegepast afhankelijk van het gemiddelde en de standaardafwijking van het ter plaatse aanwezige duinzand.

Omdat het duinprofiel van jaar tot jaar verschilt wordt bij een duinwaterkering ook gerekend met een in de tijd variërende sterkte. Dit wordt in rekening gebracht door met behulp van regressieanalyse een trendlijn te trekken door een meerjarige reeks afslagpunten (dit is de theoretische duinvoet op rekenpeil na een stormvloed) en een landwaartse marge voor fluctuaties hierin. De trendberekening wordt uitgevoerd over een opgetreden periode van ca. 10 jaar op basis van de jaarlijkse kustmeting (JARKUS).

### 2.3 Beoordeling

Als criterium voor de sterkte wordt een grensprofiel gedefinieerd dat nog minimaal aanwezig moet zijn. Uit de regressieanalyse volgt een representatief afslagpunt. Landwaarts van dit afslagpunt moet zich een profiel bevinden met een buitentalud van 1 : 1 en een kruinhoogte van minimaal

$$\begin{aligned}h_0 &= RP + 0.12T_p\sqrt{H_{0s}} \\h_0 &\geq RP + 2.5\end{aligned}\tag{2.3}$$

waarin:

|       |     |                                  |
|-------|-----|----------------------------------|
| $h_0$ | [m] | kruinhoogte                      |
| $RP$  | [m] | rekenpeil boven NAP              |
| $T_p$ | [s] | piekperiode van het golfspectrum |

Tevens dient de kruinbreedte minimaal 3 m te zijn en moet het binnentalud een helling hebben van 1 : 2 of flauwer.

Indien het bovengenoemde grensprofiel nog aanwezig is in het overgebleven duinmassief dan wordt de desbetreffende raai geacht aan de veiligheidsnorm te voldoen.

### 3 Probabilistische berekeningen

#### 3.1 Zonder golfperiode invloeden

##### 3.1.1 Variabelen en gebruikte verdelingen

De variabelen en verdelingen die worden gehanteerd in de numerieke integratie (niveau III probabilistische methode) zijn gebaseerd op Van de Graaff (1984). Hier volgt een samenvattend overzicht.

- Maximale waterstand
  - Overschrijdskans per jaar (voor Hoek van Holland):

$$P(\underline{h} > h) = 727.86 \exp(-3.01h) \quad \text{voor } h > 2.2 \text{ m} \quad (3.1)$$

waarin:

$h$  [m] maximale waterstand boven NAP

- Significante golfhoogte
  - Gegeven de waterstand  $h$ , een normale verdeling met:
 
$$\mu_{H_s} = 4.82 + 0.6h - (0.0063(7.0 - h)^{3.13}) \quad \text{voor } h < 7 \text{ m} \quad (3.2)$$

$$\mu_{H_s} = 4.82 + 0.6h \quad \text{voor } h \geq 7 \text{ m}$$

$$\sigma_{H_s} = 0.6 \text{ m}$$
  - Deze verdeling is bedoeld in combinatie met vergelijking (3.1) en geldt voor Hoek van Holland (Van Aalst, 1983)
- Profielvariaties
  - Normale verdeling
  - Gemiddeld profiel: standaardprofiel (figuur 3.1)
  - Standaardafwijking van profielvariaties:  $60 \text{ m}^3/\text{m}$
- Korrel diameter
  - Normale verdeling
  - $\mu_{D_{50}} = 225 \text{ } \mu\text{m}$
  - $\sigma_{D_{50}} = 22.5 \text{ } \mu\text{m}$  (= 10 % van  $\mu_{D_{50}}$ )
- Stormvloedduur
  - Normale verdeling
  - Met een DUROS-berekening wordt, gegeven de overige randvoorwaarden de afslag boven de maximale waterstand berekend (volume  $A \text{ m}^3/\text{m}$ )
  - Afslag bij gemiddelde stormvloedduur =  $A \text{ m}^3/\text{m}$
  - Standaardafwijking =  $0.1 * A \text{ m}^3/\text{m}$
- Buistoot en bui-oscilaties
  - Effecten samengenomen. Een buistoot met variërende hoogte.
  - Normale verdeling
  - Gemiddelde buistoothoogte =  $0.40 \text{ m}$
  - Standaardafwijking =  $0.10 \text{ m}$
  - Effect van buistoot met hoogte  $\Delta h$  op afslag boven de waterlijn  $\Delta A = 0.05 A (\Delta h / 0.40)$
  - Daaruit volgt een normale verdeling voor  $\Delta A$

- Gemiddelde =  $0.05A$
- Standaardafwijking =  $0.25 * 0.05A$
- Nauwkeurigheid berekeningsmethode
  - Normale verdeling
  - Gemiddelde: uitkomst DUROS-berekening  $\rightarrow A \text{ m}^3/\text{m}$
  - Standaardafwijking  $\rightarrow (20+0.1*A) \text{ m}^3/\text{m}$

### 3.1.2 Numerieke integratie

Van een standaardgeval is een volledige numerieke integratie uitgevoerd, zij het dat daarbij de stappen tamelijk groot zijn genomen. De volgende schematisaties zijn toegepast.

- Waterstand

Het waterstandsgebied met overschrijdingskansen van  $10^{-2}$  tot  $10^{-7}$  per jaar is in rekening gebracht (NAP + 3.72 m tot NAP + 7.54 m). Elke decade (bijvoorbeeld  $10^{-6}$  tot  $10^{-7}$  overschrijdingskans) is in principe in 5 stappen in de berekening ingevoerd; in totaal dus 25 waterstandsstappen. Elke waterstandsstap vertegenwoordigt een waterstandsinterval van 0.153 m. Daarentegen zijn met de verschillende stappen verschillende kansen gemoeid, variërend van  $5.8*10^{-8}$  tot  $3.7*10^{-3}$ . Als kenmerkende waterstand  $h$  voor elke stap is de waterstand gekozen, die qua overschrijdingskans halverwege de stapgrootte ligt. Dit betekent dat de gebruikte kenmerkende waterstand voor elke stap iets lager ligt dan het gemiddelde van de grenzen van het desbetreffende waterstandsinterval. Eén en ander is ook weergegeven in figuur 3.2.
- Golfhoogte

Bij de kenmerkende waterstand van elke stap, is de significante golfhoogte  $\mu_{H_s}$  met de grootste kansdichtheid met vergelijking (3.2) berekend. In de simulaties zijn voor elke waterstandsstap 5 verschillende golfhoogten in rekening gebracht. Deze zijn afgeleid uit de aangenomen normale verdeling met een standaardafwijking  $\sigma_{H_s} = 0.6 \text{ m}$ . Elke stap heeft een kans van 20 %.
- Korrel diameter duinmateriaal

De normale korrel diameter verdeling is in 20 stappen, met elk een kans van 5 %, verdeeld.
- Ligging beginprofiel

De variatie van de ligging van het beginprofiel (normale verdeling,  $\mu = 0$ ;  $\sigma = 60 \text{ m}^3/\text{m}$ ), is in 5 stappen in de berekening ingevoerd. Om deze variatie in het standaardprofiel te bewerkstelligen is deze verrekend bij het bepalen van de balans tussen afgeslagen en aangezand volume. In principe wordt d.m.v. iteratie *aanzanding - afslag* = 0 benaderd. Door te streven naar *aanzanding - afslag*  $\neq 0$  kan een magerder of juist voller profiel gesimuleerd worden.
- Overige invloeden

Met de variaties in de 4 hiervoor genoemde parameters zijn in totaal  $25 * 5 * 20 * 5 = 12500$  daadwerkelijke duinafslag berekeningen gemaakt. Alle berekeningen resulteren in een bepaalde ligging van het afslagpunt R en een afslagvolume boven de waterlijn van  $A \text{ m}^3/\text{m}$ . De effecten op de afslag ten gevolge van variaties in stormvloedduur, het optreden van buistoten en de nauwkeurigheid van de berekeningsmethode, zijn alle uitgedrukt in het volume A. Voor de 3 genoemde invloeden zijn normale verdelingen aangenomen met als kenmerken:

| <u>invloed</u>             | $\underline{\mu}$ | $\underline{\sigma}$ |
|----------------------------|-------------------|----------------------|
| stormvloedduur             | 0                 | $0.1 * A$            |
| buistoot                   | $0 + 0.05 * A$    | $0.25 * 0.05 * A$    |
| nauwkeurigheid DUROS-model | 0                 | $20 + 0.1 * A$       |

Omdat er in alle gevallen een normale verdeling wordt gebruikt, kunnen deze samen genomen worden. De nieuwe normale verdeling die op basis van deze 3 verdelingen gevormd kan worden heeft de volgende karakteristieken:

$$\begin{aligned}\mu &= 0.05A \\ \sigma &= \sqrt{(0.1A)^2 + (0.25 * 0.05)^2 + (20 + 0.1A)^2}\end{aligned}\quad (3.3)$$

De resulterende verdeling is in 20 stappen onderverdeeld. Er resulteren in principe 20 extra in rekening te brengen afslag volumina ter grootte van:

$$\Delta A = 0.05A + factor * \sigma \quad (3.4)$$

waarin:

|            |           |   |
|------------|-----------|---|
| $\Delta A$ | $[m^3/m]$ | toename afslagvolume boven de waterlijn |
| $factor$   | $[-]$     | uit normale verdeling volgende factor   |

Hierbij moet opgemerkt worden dat het discutabel is of in de waarde  $A$  in vergelijking (3.3) het gemiddelde aangenomen buistoot effect van  $0.05 * A$  dient te worden opgenomen of niet. Er is gekozen om dat niet te doen (Van de Graaff, 1984).

- **Resultaat**

Uitgaande van elk van de eerder genoemde 12500 gevallen, worden 20 nieuwe liggingen van het punt R berekend volgens de normale verdeling van  $\Delta A$ .

Uiteindelijk resulteren er dan  $12500 * 20 = 250000$  gevallen.

Elk van deze gevallen heeft, uitgaande van de onafhankelijkheid van de variabelen, een kans van voorkomen van:

$$\underbrace{\text{kans van voorkomen waterstandsinterval}}_{\text{verschil overschrijdingskansen stapgrenzen}} * \underbrace{\frac{1}{5}}_{H_s} * \underbrace{\frac{1}{20}}_{D_{50}} * \underbrace{\frac{1}{5}}_{\text{Profielfluctuatie}} * \underbrace{\frac{1}{20}}_{\text{Overige invloeden}} \quad (3.5)$$

In figuur 3.3 is de terugschrijding van het duinfront AF aangegeven, welke gedefinieerd is als de horizontale afstand tussen het punt R en de doorsnijding van het niveau NAP + 5 m met het beginprofiel.

In overeenstemming met de resultaten van Van de Graaff (1984) wordt er bij een overschrijdingskans van  $10^{-5}$  een waarde van  $AF = 86.0$  m gevonden. Dit valt ook af te lezen uit figuur 3.4.

### 3.2 Golfcondities

Om de invloed van de golfperiode op duinafslag van uit probabilistisch oogpunt te benaderen moet deze ook als variabele worden meegenomen. Om dit te bewerkstelligen moet, uitgaande van de toelichting in paragraaf 3.1.1, een verband tussen de golfperiode en golfhoogte of tussen golfperiode en waterstand worden aangenomen. In dit onderzoek is ervoor gekozen om de golfperiode aan de waterstand te koppelen. Dit is op vergelijkbare manier gedaan als de koppeling tussen golfhoogte en waterstand. Om die reden wordt

hieronder eerst ingegaan op het gebruikte verband tussen waterstand en golfhoogte. Vervolgens wordt een vergelijkbaar verband voor de golfperiode afgeleid.

### 3.2.1 Golfhoogte

In figuur 3.5 is het verband tussen waterstand en gemiddelde golfhoogte weergegeven zoals dat in paragraaf 3.1.1 gegeven is (voor Hoek van Holland; zie ook: Van de Graaff, 1984). Daarbij kan de kansverdeling voor de waterstand (paragraaf 3.1.1) en de standaardafwijking van de golfhoogte  $\sigma_{H_s} = 0.6$  m in beschouwing worden genomen. Op basis daarvan is het mogelijk om voor een willekeurige golfhoogte de overschrijdingskans te berekenen. In het onderste deel van figuur 3.5 is de resulterende overschrijdingskans van de golfhoogte weergegeven. Tevens zijn in die figuur de  $10^{-1}$ ,  $10^{-2}$ ,  $10^{-3}$  en  $10^{-4}$  kwantielen eenvoudig af te lezen. Ter vergelijking zijn deze kwantielen in onderstaande tabel samen met de waarden van het Europlatform (De Ronde *et al.*, 1995) weergegeven.

| kwantielen       | golfhoogten (m) |           |           |           |
|------------------|-----------------|-----------|-----------|-----------|
|                  | $10^{-1}$       | $10^{-2}$ | $10^{-3}$ | $10^{-4}$ |
| HvH              | 6.52            | 7.35      | 8.04      | 8.66      |
| EUR ( $H_{m0}$ ) | 6.22            | 7.07      | 7.78      | 8.40      |

**Tabel 3.1 Afgeleide kwantielen golfhoogte vergeleken met kwantielen van Europlatform**

Hieruit blijkt dat de hierboven afgeleide kwantielen voor Hoek van Holland (HvH) feitelijk hoger zijn dan waarden bij het Europlatform.

In het rekenrecept van de TAW Leidraad 1984 wordt de bij het rekenpeil behorende gemiddelde golfhoogte aangenomen. Voor Hoek van Holland komt dat neer op een waarde van  $H_s$  van 8.20 m. Het is een misvatting om die waarde als de  $10^{-4}$  per jaar overschrijdingskans op te vatten.

De aanname dat de golfhoogten onderschat zouden zijn bij de toepassing van de TAW Leidraad 1984 berusten dan ook op een misverstand.

### 3.2.2 Golfperiode

Er wordt hieronder een verband tussen waterstand en gemiddelde golfperiode afgeleid voor een fictieve situatie waarbij het  $10^{-4}$ -kwantiel voor de piek-golfperiode 18.5 s is. Dit, in overeenstemming met de langste golfperiode toegepast in de Scheldegoet-proeven (Coeveld en De Vroeg, 2004). De gebruikte kwantielen zijn zodanig lineair geïnterpoleerd tussen de  $T_p$ -waarden van meetstation Schiermonnikoog-Noord en Eierlandse Gat (Roskam en Hoekema, 1996) dat het  $10^{-4}$ -kwantiel inderdaad 18.5 s bedraagt. Dit is weergegeven in onderstaande tabel.

| kwantielen     | piek-golfperioden $T_p$ (s) |             |             |             |
|----------------|-----------------------------|-------------|-------------|-------------|
|                | $10^{-1}$                   | $10^{-2}$   | $10^{-3}$   | $10^{-4}$   |
| SON            | 15.0                        | 16.7        | 18.2        | 19.4        |
| <i>fictief</i> | <i>14.4</i>                 | <i>16.0</i> | <i>17.4</i> | <i>18.5</i> |
| ELD            | 13.4                        | 14.9        | 16.1        | 17.1        |

**Tabel 3.2 Fictieve kwantielen golfperiode vergeleken met de kwantielen van de meetstations Schiermonnikoog-Noord en Eierlandse Gat**

Voor de standaardafwijking van de golfperiode is een waarde van  $\sigma_{T_p} = 1.3$  s gekozen. De keuze van  $\sigma_{T_p}$  is gebaseerd op de verhouding tussen  $\sigma_{H_s}$  en de golfhoogte kwantielen. Hierbij is voor de verhouding tussen  $\sigma_{T_p}$  en de golfperiode kwantielen dezelfde waarde

aangehouden. Dit betekent voor bijvoorbeeld het  $10^{-4}$  kwantiel  $1.3s/18.5s \approx 0.6m/8.66m$  en voor het  $10^{-2}$  kwantiel  $1.3s/16.0s \approx 0.6m/7.35m$ .

Op basis van de bovengenoemde gegevens kan iteratief een verband tussen waterstand en gemiddelde golfperiode bepaald worden. In figuur 3.6 is het resultaat weergegeven. Dit is als volgt tot stand gekomen:

- Een tweede orde polynoom is gefit door de kwantielen in het bovenste deel van figuur 3.6 (zie stippellijn).
- Voor waterstanden hoger dan het  $10^{-4}$ -kwantiel ( $h = 5.25$  m) is de lijn lineair verondersteld met de helling die bij  $h = 5.25$  m gevonden wordt.
- Vervolgens kan de bijbehorende overschrijdingslijn voor de golfperiode worden bepaald, rekening houdend met de standaardafwijking van  $\sigma_{T_p} = 1.3$  s. De methode hiervoor is reeds in paragraaf 3.2.1 voor de golfhoogte kort toegelicht.
- In eerste instantie ligt deze overschrijdingslijn boven de in het onderste deel van figuur 3.6 gemarkeerde kwantielen. Deze verschillen geven echter een aanknopingspunt op basis waarvan de lijn in de bovenste figuur weer bijgesteld kan worden.
- Dit proces kan herhaald worden totdat de weergegeven lijnen ontstaan. Uit de onderste figuur blijkt dat de lijn goed door de opgelegde kwantielen loopt.

### 3.3 Met golfperiode invloed

Uitgaande van de in paragraaf 3.2.2 afgeleide relatie tussen waterstand en gemiddelde golfperiode kan de numerieke integratie van paragraaf 3.1.2 uitgebreid worden met de invloed van de golfperiode.

Ten eerste moet de lijst van variabelen zoals opgesomd in paragraaf 3.1.1 worden uitgebreid met:

- Piek-golfperiode
  - Gegeven de waterstand  $h$ , een normale verdeling met:
 
$$\begin{aligned} \mu_{T_p} &= -0.2136h^2 + 3.0959h + 6.0507 && \text{voor } h < 5.25 \text{ m} \\ \mu_{T_p} &= 11.9375 + 0.8531h && \text{voor } h \geq 5.25 \text{ m} \\ \sigma_{T_p} &= 1.3 \text{ s} \end{aligned} \quad (3.6)$$

Vervolgens moet voor elke golfperiode een correctie op het afslagvolume boven stormvloedpeil worden gehanteerd. Voor deze correctie worden een zestal scenario's gedefinieerd zoals weergegeven in figuur 3.7. Daarbij moge duidelijk zijn dat het '0 %-scenario' per definitie hetzelfde resultaat moet geven als de berekening zonder periode invloed (paragraaf 3.1.2).

De invloed van de golfperiode wordt in het afslagvolume als volgt verwerkt:

$$A = \left[ 1 + \underbrace{\frac{\text{Scenario}}{18.5 - 12} * (T_p - 12)}_{\text{Invloed golfperiode}} \right] * A_{DUROS} \quad (3.7)$$

waarin  $\text{Scenario} = 0, 0.1, 0.2, 0.3, 0.4, \text{ of } 0.5$  (zie figuur 3.7)

De normale verdeling van de piek-golfperiode levert via bovenstaande vergelijking in feite een normaal verdeeld afslagvolume  $A$  op.

De normale verdeling van de golfperiode wordt, evenals die van de golfhoogte, in 5 stappen verdeeld. Daarbij worden de volgende 2 situaties beschouwd:

- Golfhoogte en golfperiode volledig gecorreleerd. Dit betekent dat bij elke golfhoogte slechts één golfperiode 'hoort'.
- Golfhoogte en golfperiode volledig onafhankelijk. Dit betekent dat bij elke golfhoogte alle 5 varianten (stappen) van de golfperiode verdeling worden meegerekend.

### Resultaat

Het grootste deel van de numerieke integratie is gelijk aan de situatie zoals in paragraaf 3.1.2 is beschreven. Het aantal DUROS-berekeningen blijft gelijk (12500 stuks). Op basis van de volledige correlatie dan wel volledige onafhankelijkheid tussen golfhoogte en golfperiode wordt het laatste deel, de overige invloeden, anders.

#### *Golfhoogte en golfperiode volledig gecorreleerd*

Bij deze variant blijft het totale aantal gesimuleerde gevallen gelijk aan de situatie uit paragraaf 3.1.2 ( $12500 * 20 = 250000$ ). Het verschil is dat nu voor elke golfhoogte ook een golfperiode gedefinieerd is. Op basis van deze golfperiode zal het afslagvolume  $A$ , en daarmee dus de terugschrijding van het duinfront (AF), veranderen (in de meeste gevallen toenemen). In figuur 3.8 is het resultaat weergegeven. Hierbij staat op de horizontale as de relatieve verandering van het afslagvolume bij  $T_p = 18.5$  s t.o.v.  $T_p = 12$  s (de scenario's). Op de linker verticale as van de bovenste figuur staan de resultaten van de numerieke integraties bij de 6 scenario's uitgedrukt in AF-waarden. Op de rechter verticale as zijn deze AF-waarden gerelateerd aan het nul-scenario waarbij  $AF = 86$  m. In de onderste figuur zijn dezelfde berekeningsresultaten uitgedrukt in afslagvolume boven NAP + 5 m (links) en eveneens relatief t.o.v. het nul-scenario (rechts).

#### *Golfhoogte en golfperiode volledig onafhankelijk*

Indien de golfperiode toegevoegd wordt als een onafhankelijke variabele neemt het aantal gevallen toe en zal tevens de kans per geval veranderen. Het aantal gesimuleerde gevallen wordt nu  $12500 * 5 * 20 = 1250000$  (uitgaande van een normale verdeling verdeeld in 5 stappen zoals boven genoemd).

$$\underbrace{\text{kans van voorkomen waterstandsinterval}}_{\text{verschil overschrijdingskansen stapgrenzen}} * \underbrace{\frac{1}{5}}_{H_s} * \underbrace{\frac{1}{20}}_{D_{50}} * \underbrace{\frac{1}{5}}_{\text{Profielfluctuatie}} * \underbrace{\frac{1}{5}}_{\text{Golfperiode}} * \underbrace{\frac{1}{20}}_{\text{Overige invloeden}} \quad (3.8)$$

In figuur 3.9 zijn de resultaten weergegeven. In vergelijking met het volledig gecorreleerde geval (figuur 3.8) wordt er slechts een klein verschil gevonden. Het volledig gecorreleerde geval kan worden beschouwd als veilige benadering.

### 3.4 Afsluitende opmerkingen

Volgens Den Heijer (2005) wordt gebaseerd op de Scheldegoot-proeven 25 tot 35 % meer duinafslagvolume bij  $T_p = 18.5$  s t.o.v.  $T_p = 12$  s gevonden. Dit is dan in het geval dat alleen de golfperiode gevarieerd wordt en de overige omstandigheden gelijk blijven. Het toepassen in een numerieke integratie van dit gegeven op een situatie waarbij het  $10^{-4}$  kwantiel van de golfperiode 18.5 s is levert, bij een overschrijdingskans van  $10^{-5}$  per jaar, 20 tot 30 % meer afslagvolume op. Oftewel ongeveer  $0.8 * \text{Scenario}$  waarbij in dit geval het *Scenario* 0.25 tot 0.35 is.

Vergelijkbare simulaties zijn uitgevoerd met andere standaardafwijking  $\sigma_{Tp}$ . Eén en ander blijkt wel gevoelig te zijn voor de keuze van de standaardafwijking  $\sigma_{Tp}$ . Een kleinere standaardafwijking van  $\sigma_{Tp} = 1.0$  s levert een grotere uitkomst op (ongeveer 0.9 \* *Scenario*). Een standaardafwijking van  $\sigma_{Tp} = 1.65$  s levert ongeveer 0.4 \* *Scenario* op.

## 4 Conclusies en aanbevelingen

### 4.1 Conclusies

- Bij een piek-golfperiode van 18.5 s wordt volgens Den Heijer (2005) een 25 tot 35 % groter afslagvolume gevonden dan bij  $T_p = 12$  s. Deze toename is gebaseerd op een geval waarbij, voor zover mogelijk, alleen de golfperiode gevarieerd is en de overige omstandigheden onveranderd zijn gehouden.
- Het toepassen van deze toename in een probabilistische numerieke integratie voor een fictief geval met een  $10^{-4}$  golfperiode kwantiel van 18.5 s resulteert in ongeveer 20 tot 30 % toename van het afslagvolume.

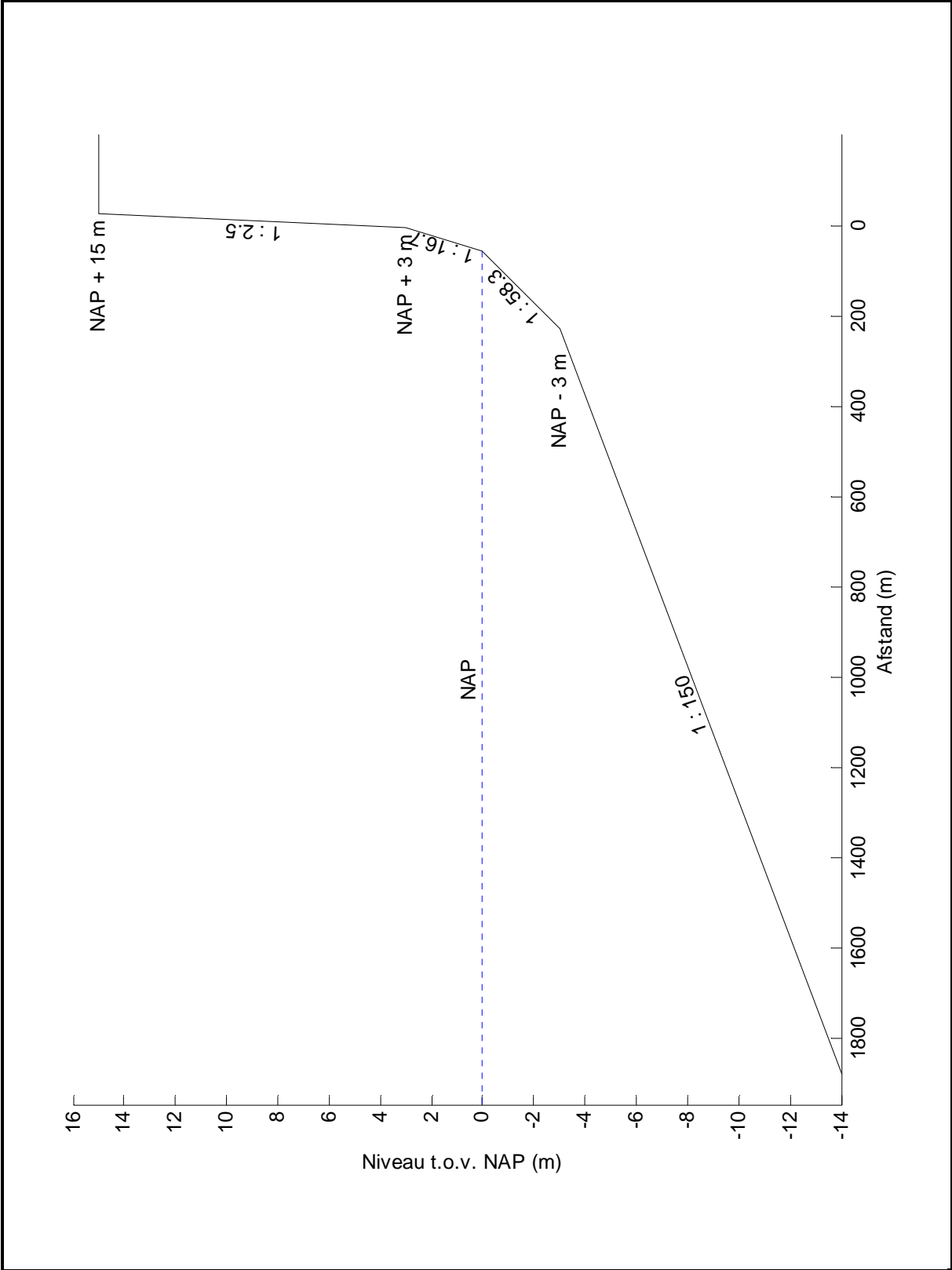
### 4.2 Aanbevelingen

- Het strekt tot aanbeveling om op basis van het probabilistische principe dat in deze studie toegepast is ook andere golfcondities en duinprofielen te beschouwen.
- Het bepalen van het ontwerp punt voor een situatie waarbij de invloed van de golfperiode wordt meegerekend.
- Uit de afleiding van de overschrijdingskans uit de thans gehanteerde golfhoogte-waterstands-relatie bleken voor de vier vergeleken kwantielen grotere golfhoogten te komen dan welke uit de metingen bij het Europlatform afgeleid worden. Dit zou kunnen betekenen dat voor de veiligheidsbeoordeling van de Nederlandse kust kleinere golfhoogten kunnen worden gehanteerd. Het is zeer aan te bevelen om dit verder te onderzoeken.
- Gezien het feit dat de resultaten van de uitgevoerde simulaties gevoelig zijn voor de keuze van de standaardafwijking van de golfperiode is het aan te bevelen om verder onderzoek te doen naar een verantwoorde waarde hiervoor.
- In dit onderzoek zijn de toegepaste golfperioden gekoppeld aan de waterstand en daarmee indirect aan de golfhoogte. Het is aan te bevelen om ook vergelijkbare berekeningen te maken waarbij de golfperiode rechtstreeks aan de golfhoogte gekoppeld is.
- Grootschalige proeven in de Deltagoot zijn dringend gewenst om een goed kwantitatief inzicht in het effect van de golfperiode op de mate van afslag te verkrijgen.

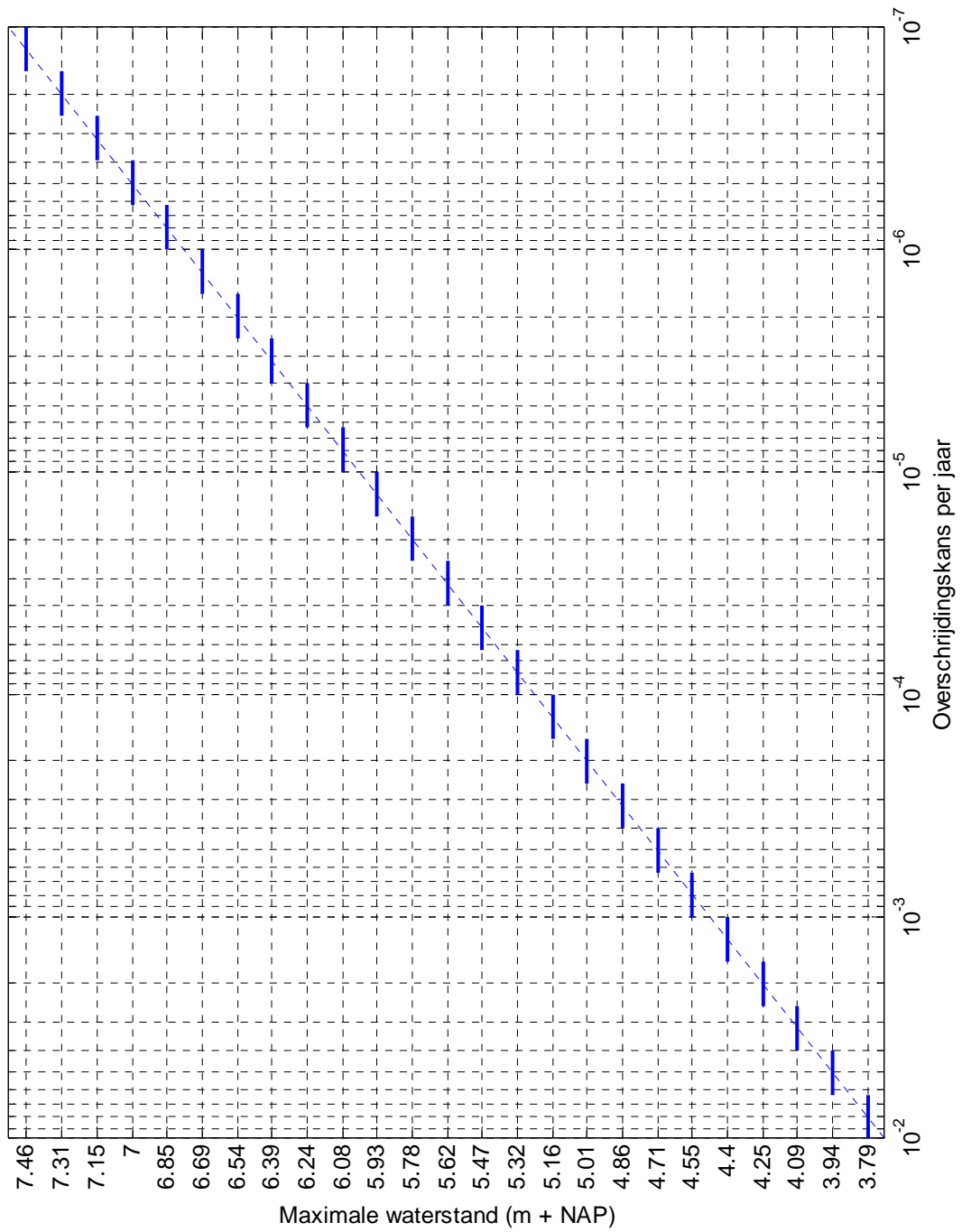
## Literatuur

- Aalst, W. van, 1983**, *Golfhoogte-waterstandsrelaties t.p.v. de NAP-20 m lijn langs de Nederlandse kust*. Rijkswaterstaat notie WWKZ-83G.218, maart 1983.
- Dienst Weg- en Waterbouwkunde / DWW, 2001**, *Hydraulische Randvoorwaarden 2001 voor het toetsen van primaire waterkeringen*, december 2001.
- Coeveld, E.M. & J.H. de Vroeg, 2004**, *Modelonderzoek duinafslag, Meetverslag kleinschalige gidsproeven*. WL | Delft Hydraulics rapport H4265, maart 2004.
- Graaff, J. van de, 1984**, *Probabilistische methoden bij het duinontwerp; Achtergronden van de TAW-Leidraad 'Duinafslag'*. TH Delft, Afdeling Civiele Techniek, Vakgroep Kustwaterbouwkunde, maart 1984.
- Heijer, C. den, 2005**, *Effect of wave period on dune erosion (Effect van golfperiode op duinafslag)*. Afstudeerverslag TU Delft, januari 2005.
- Ministerie van Verkeer & Waterstaat, 2002**, *Naar integraal kustzonebeleid, beleidsagenda voor de kust*, januari 2002.
- Roelse, R., T. Walhout & G.J. Liek, 2002**, *Duinveiligheid bij nieuwe inzichten belasting en sterkte*. Rijkswaterstaat, Rijksinstituut voor Kust en Zee / RIKZ, werkdocument RIKZ/AB/2002.842x, december 2002.
- Ronde, J.G. de, J.G.A. van Marle, A.P. Roskam & J.H. Andorka Gal, 1995**, *Golfrandvoorwaarden langs de Nederlandse kust op relatief diep water*. Rijkswaterstaat, Rijksinstituut voor Kust en Zee / RIKZ, Rapport RIKZ-95.024, december 1995.
- Roskam, A.P. & J. Hoekema, 1996**, *Randvoorwaarden voor golfperioden langs de Nederlandse kust*. Rijkswaterstaat, Rijksinstituut voor Kust en Zee / RIKZ, Rapport RIKZ-96.019, juli 1996.
- Steetzel, H.J., 2002**, *Effect van zwaardere golfcondities op duinenkust. Verkenning effect grotere golfhoogte en langere golfperiode op mate duinafslag en veiligheid duinenkust*. Verslag bureaustudie, Alkyon rapport A963, september 2002.
- Technische Adviescommissie voor de Waterkeringen / TAW, 1984**, *Leidraad voor de beoordeling van de veiligheid van duinen als waterkering*.
- Vellinga, P., 1986**, *Beach and dune erosion during storm surges*. Proefschrift, Technische Universiteit Delft; ook: Publicatie nr. 372 WL | Delft Hydraulics, december 1986.

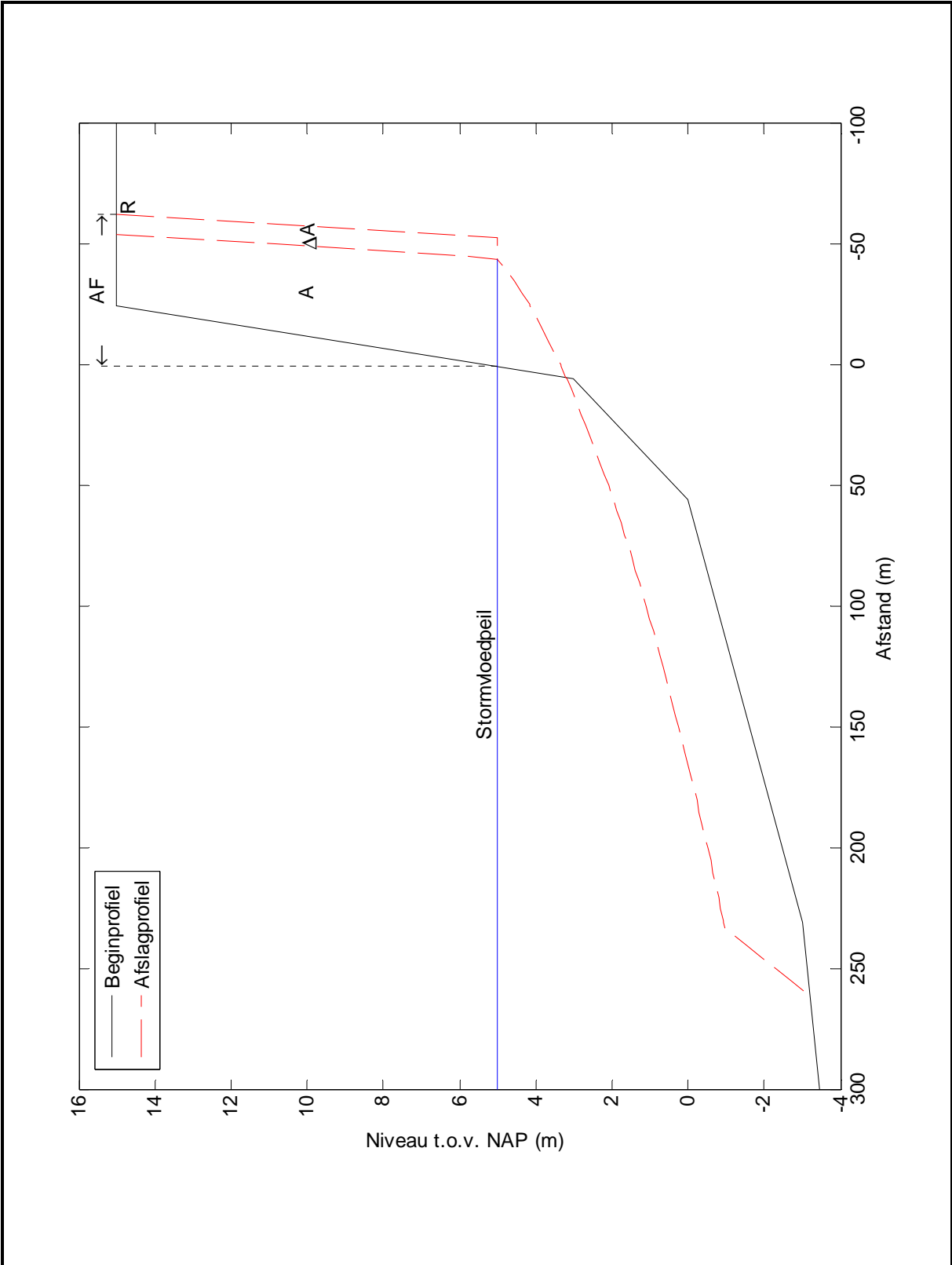
# Figuren



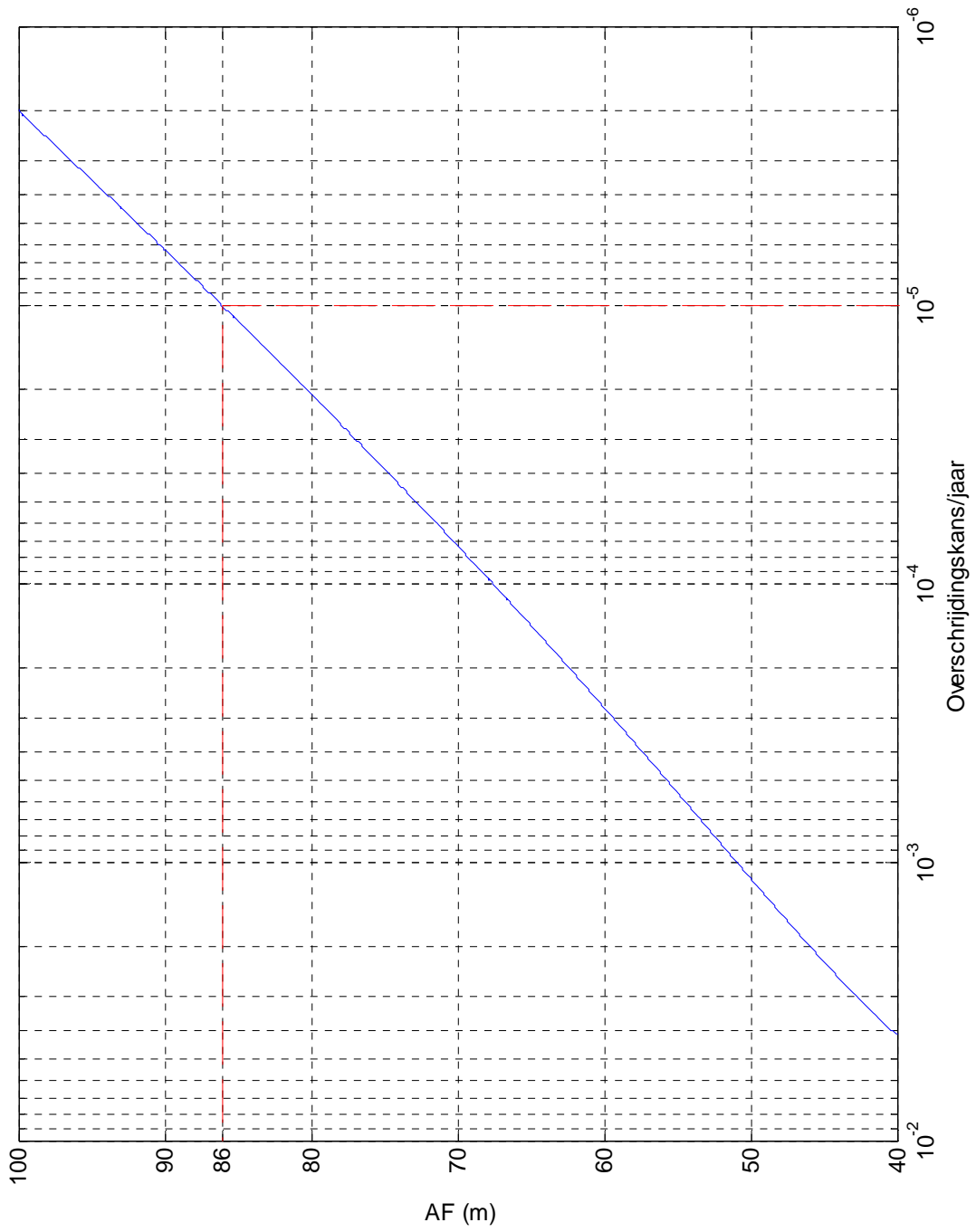
|                        |  |  |            |
|------------------------|--|--|------------|
| Standaard dwarsprofiel |  |  |            |
|                        |  |  |            |
| TU Delft               |  |  | Figuur 3.1 |



Toegepaste waterstandsverdeling met daarin  
aangegeven de gebruikte stappen

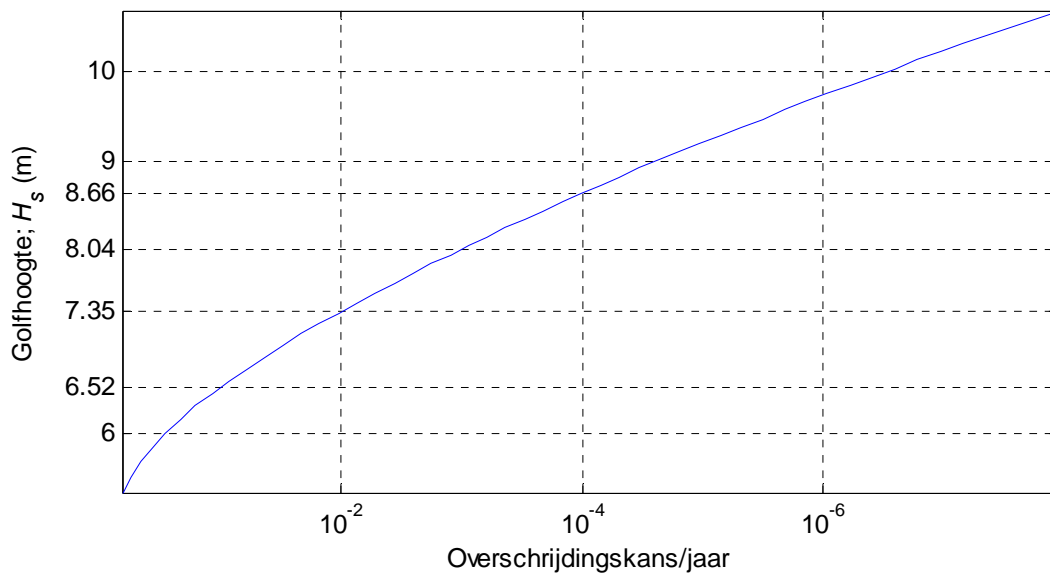
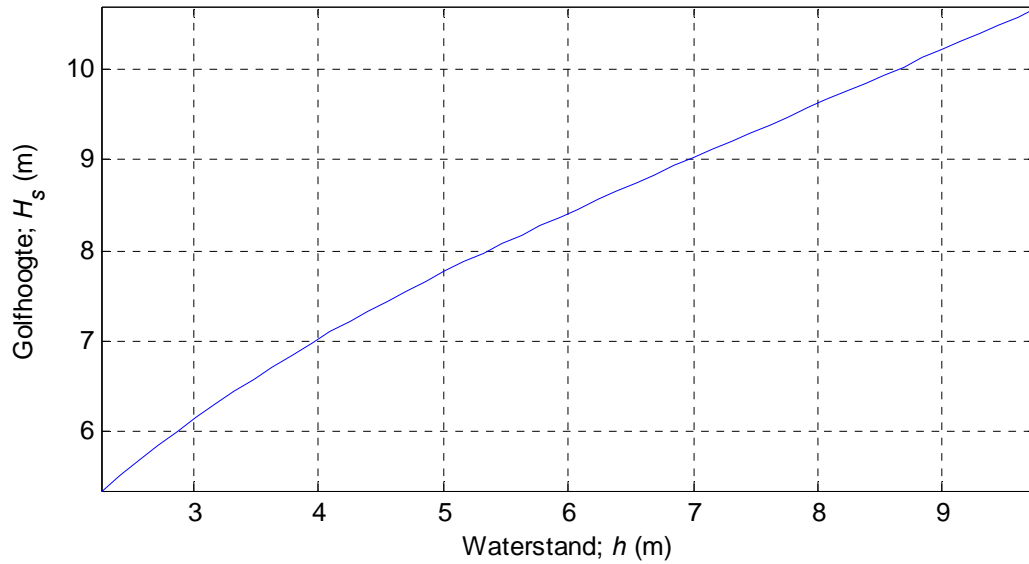


Voorbeeld van aflagberekening met daarin de definities van AF, A en  $\Delta A$

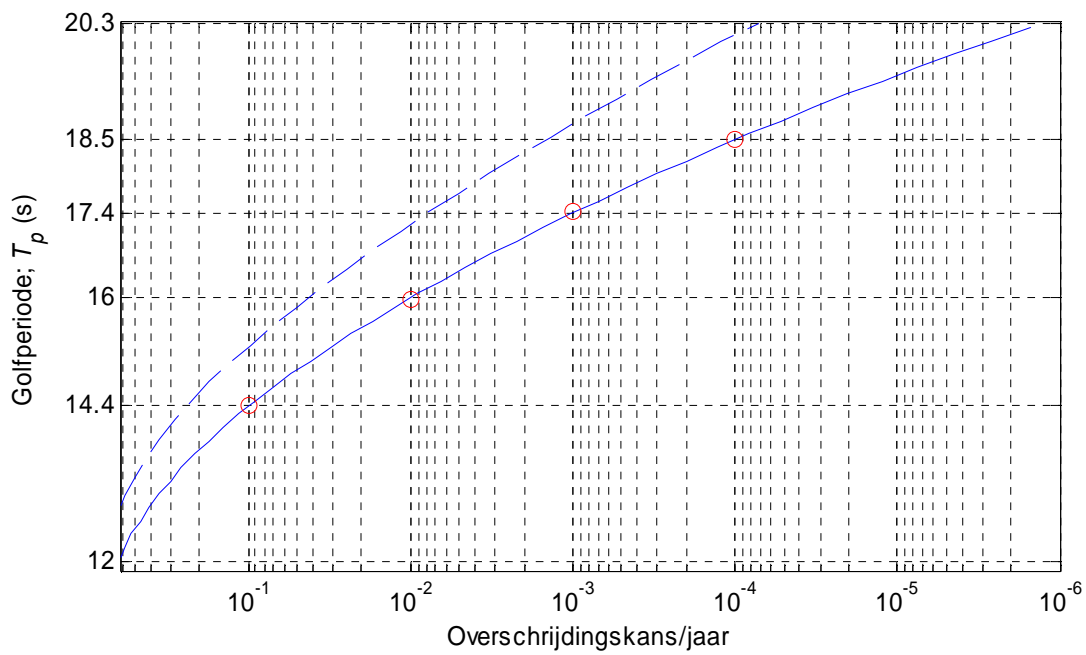
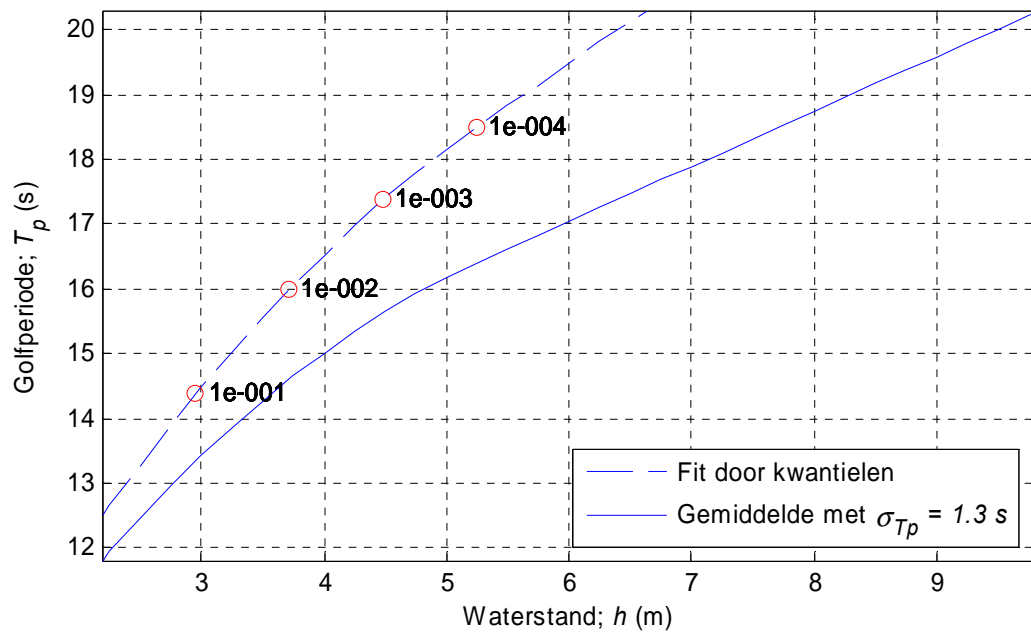


Overschrijdingskans afslag zonder invloed van  
golperiode

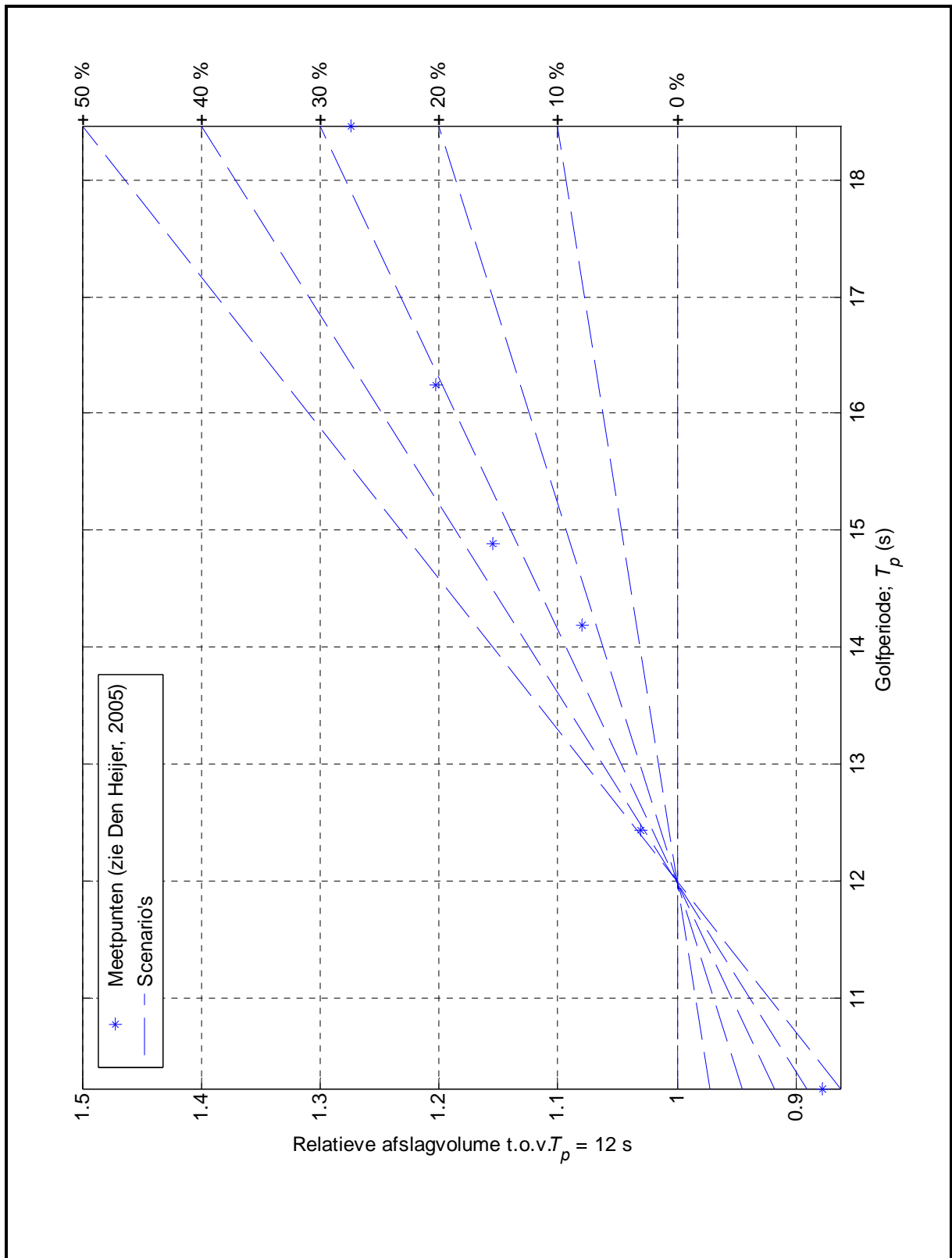
(Van de Graaff, 1984)



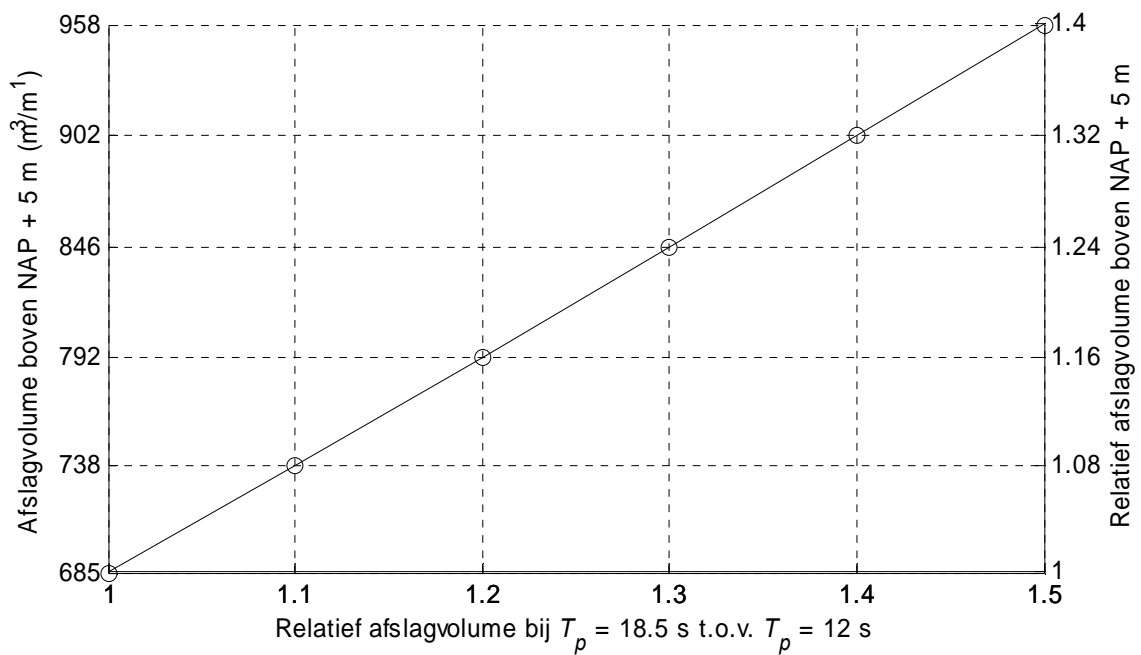
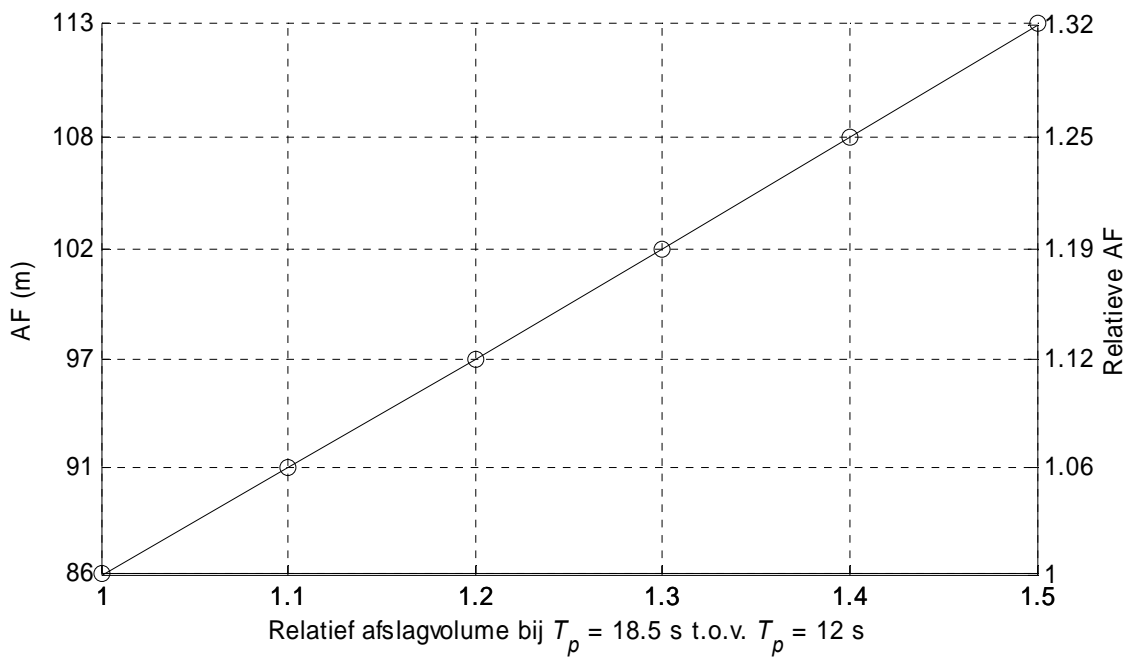
Waterstand-gemiddelde-golfhoogte verband voor Hoek van Holland volgens Leidraad Duinafslag; Bijbehorende overschrijdingskansen bij een standaardafwijking van  $\sigma_{H_s} = 0.6$  m



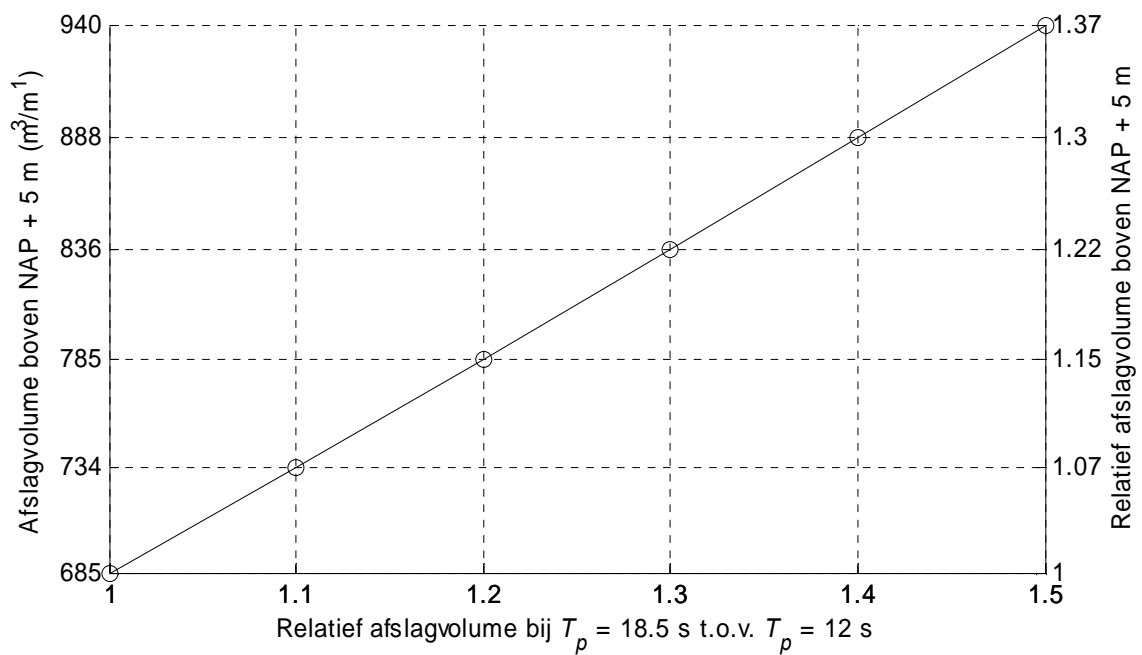
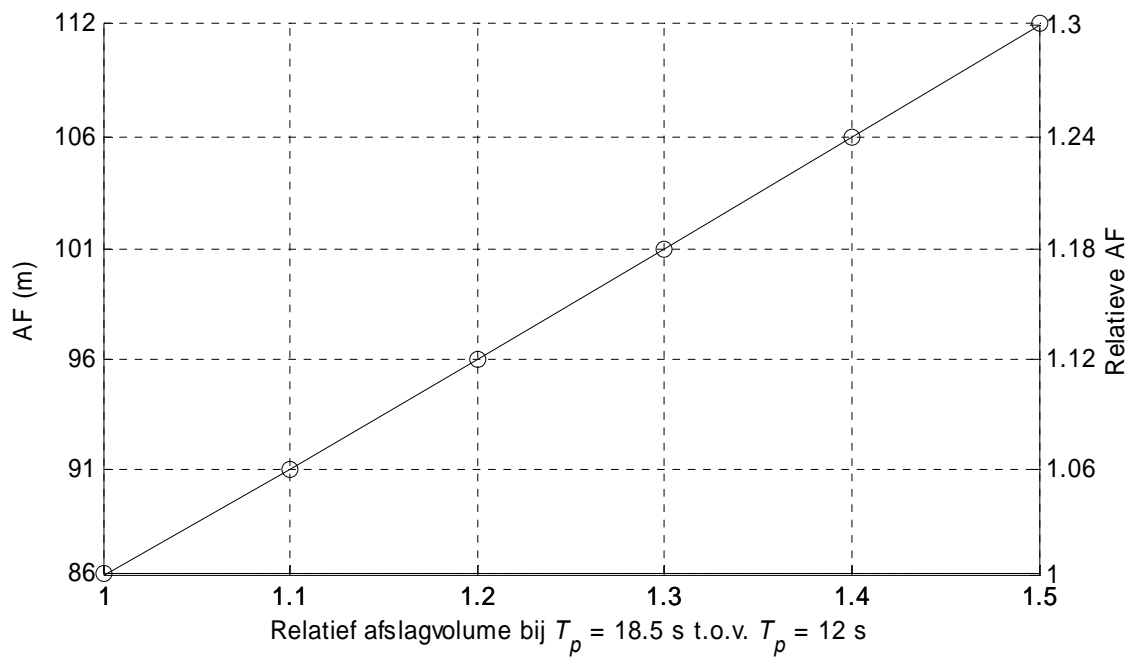
Fictief waterstand-golfperiode verband;  
 Bijbehorende overschrijdingskansen bij een  
 standaardafwijking  $\sigma_{T_p} = 1.3$  s



Relatieve afslag t.o.v. basisgeval  $T_p = 12$  s



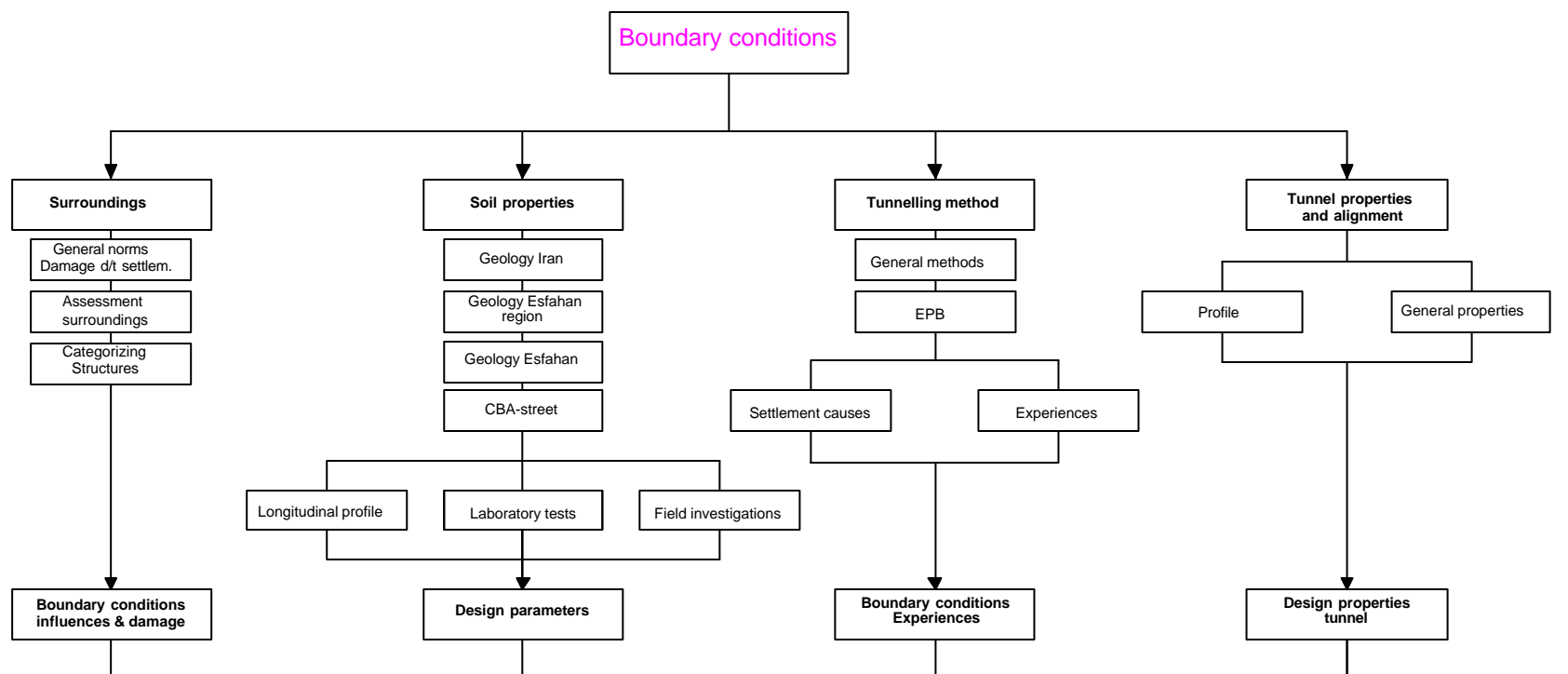
Resultaten van numerieke integratie met volledige correlatie tussen golfhoogte en golfperiode



Resultaten van numerieke integratie met volledige onafhankelijkheid tussen golfhoogte en golfperiode

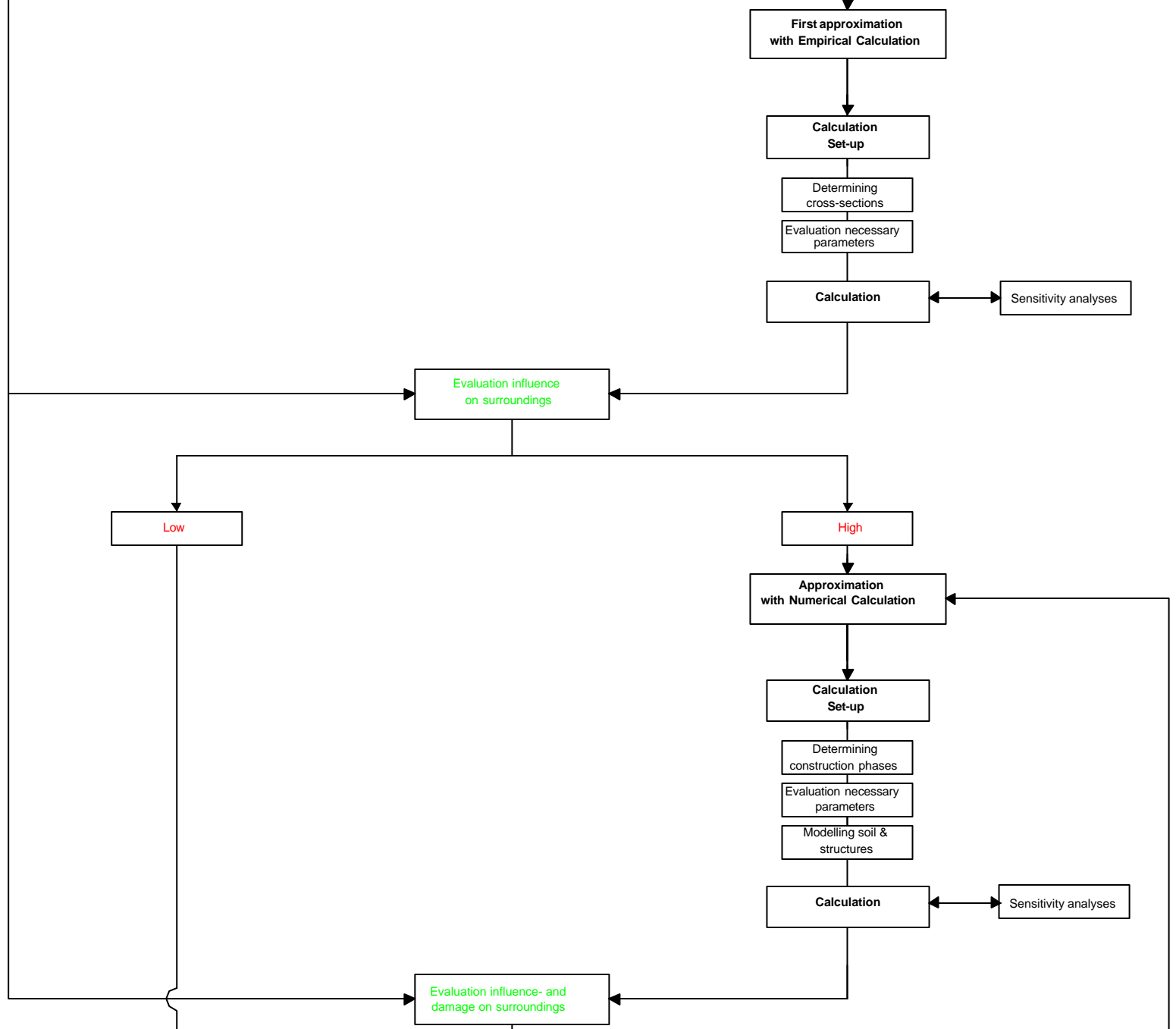


PART I



PART II

Calculations



PART III

